IAEA HUMAN HEALTH SERIES
No. 29

Guided Intraoperative Scintigraphic Tumour Targeting (GOSTT)

Implementing Advanced Hybrid Molecular Imaging and Non-imaging Probes for Advanced Cancer Management

IAEA
International Atomic Energy Agency

GUIDED INTRAOPERATIVE SCINTIGRAPHIC TUMOUR TARGETING (GOSTT)

The following States are Members of the International Atomic Energy Agency:

AFGHANISTAN
ALBANIA
ALGERIA
ANGOLA
ARGENTINA
ARMENIA
AUSTRALIA
AUSTRIA
AZERBAIJAN
BAHAMAS
BAHRAIN
BANGLADESH
BELARUS
BELGIUM
BELIZE
BENIN
BOLIVIA
BOSNIA AND HERZEGOVINA
BOTSWANA
BRAZIL
BRUNEI DARUSSALAM
BULGARIA
BURKINA FASO
BURUNDI
CAMBODIA
CAMEROON
CANADA
CENTRAL AFRICAN REPUBLIC
CHAD
CHILE
CHINA
COLOMBIA
CONGO
COSTA RICA
CÔTE D'IVOIRE
CROATIA
CUBA
CYPRUS
CZECH REPUBLIC
DEMOCRATIC REPUBLIC OF THE CONGO
DENMARK
DOMINICA
DOMINICAN REPUBLIC
ECUADOR
EGYPT
EL SALVADOR
ERITREA
ESTONIA
ETHIOPIA
FIJI
FINLAND
FRANCE
GABON
GEORGIA
GERMANY
GHANA
GREECE
GUATEMALA
HAITI
HOLY SEE
HONDURAS
HUNGARY
ICELAND
INDIA
INDONESIA
IRAN, ISLAMIC REPUBLIC OF
IRAQ
IRELAND
ISRAEL
ITALY
JAMAICA
JAPAN
JORDAN
KAZAKHSTAN
KENYA
KOREA, REPUBLIC OF
KUWAIT
KYRGYZSTAN
LAO PEOPLE'S DEMOCRATIC REPUBLIC
LATVIA
LEBANON
LESOTHO
LIBERIA
LIBYA
LIECHTENSTEIN
LITHUANIA
LUXEMBOURG
MADAGASCAR
MALAWI
MALAYSIA
MALI
MALTA
MARSHALL ISLANDS
MAURITANIA, ISLAMIC REPUBLIC OF
MAURITIUS
MEXICO
MONACO
MONGOLIA
MONTENEGRO
MOROCCO
MOZAMBIQUE
MYANMAR
NAMIBIA
NEPAL
NETHERLANDS
NEW ZEALAND
NICARAGUA
NIGER
NIGERIA
NORWAY
OMAN
PAKISTAN
PALAU
PANAMA
PAPUA NEW GUINEA
PARAGUAY
PERU
PHILIPPINES
POLAND
PORTUGAL
QATAR
REPUBLIC OF MOLDOVA
ROMANIA
RUSSIAN FEDERATION
RWANDA
SAN MARINO
SAUDI ARABIA
SENEGAL
SERBIA
SEYCHELLES
SIERRA LEONE
SINGAPORE
SLOVAKIA
SLOVENIA
SOUTH AFRICA
SPAIN
SRI LANKA
SUDAN
SWAZILAND
SWEDEN
SWITZERLAND
SYRIAN ARAB REPUBLIC
TAJIKISTAN
THAILAND
THE FORMER YUGOSLAV REPUBLIC OF MACEDONIA
TOGO
TRINIDAD AND TOBAGO
TUNISIA
TURKEY
UGANDA
UKRAINE
UNITED ARAB EMIRATES
UNITED KINGDOM OF GREAT BRITAIN AND NORTHERN IRELAND
UNITED REPUBLIC OF TANZANIA
UNITED STATES OF AMERICA
URUGUAY
UZBEKISTAN
VENEZUELA, BOLIVARIAN REPUBLIC OF
VIET NAM
YEMEN
ZAMBIA
ZIMBABWE

The Agency's Statute was approved on 23 October 1956 by the Conference on the Statute of the IAEA held at United Nations Headquarters, New York; it entered into force on 29 July 1957. The Headquarters of the Agency are situated in Vienna. Its principal objective is "to accelerate and enlarge the contribution of atomic energy to peace, health and prosperity throughout the world''.

IAEA HUMAN HEALTH SERIES No. 29

GUIDED INTRAOPERATIVE SCINTIGRAPHIC TUMOUR TARGETING (GOSTT)

IMPLEMENTING ADVANCED HYBRID MOLECULAR IMAGING
AND NON-IMAGING PROBES FOR
ADVANCED CANCER MANAGEMENT

INTERNATIONAL ATOMIC ENERGY AGENCY
VIENNA, 2014

COPYRIGHT NOTICE

Marketing and Sales Unit, Publishing Section
International Atomic Energy Agency
Vienna International Centre
PO Box 100
1400 Vienna, Austria
fax: +43 1 2600 29302
tel.: +43 1 2600 22417
email: sales.publications@iaea.org
http://www.iaea.org/books

Printed by the IAEA in Austria
December 2014
STI/PUB/1648

IAEA Library Cataloguing in Publication Data

Guided intraoperative scintigraphic tumour targeting (GOSTT) : implementing advanced hybrid molecular imaging and non-imaging probes for advanced cancer management. — Vienna : International Atomic Energy Agency, 2014.
p. ; 24 cm. — (IAEA human health series, ISSN 2075–3772 ; no. 29)
STI/PUB/1648
ISBN 978–92–0–102214–1
Includes bibliographical references.

1. Cancer — Diagnosis. 2. Lymph nodes — Cancer 3. Radiopharmaceuticals. 4. Positron-Emission Tomography. I. International Atomic Energy Agency. II. Series.

IAEAL 14–00934

FOREWORD

The aim of this publication is twofold. One objective is to provide an update on the latest advances concerning sentinel lymph node mapping (SLNM) and radioguided sentinel lymph node biopsy (SLNB) for the diagnosis and treatment of patients with cancer. Special emphasis is given to issues under debate, including changing indications. The second objective is to provide a thorough review of the latest experience and literature, and to define procedural recommendations on applications of radioguided surgery other than SLNB.

This publication provides an update on innovations in the use of radiopharmaceuticals for SLNM and SLNB, in combination with vital dyes, when appropriate, to facilitate the detection of sentinel lymph nodes. In addition, advances in the implementation of hybrid imaging technologies for the surgical management of patients with cancer in conjunction with intraoperative regional lymph node mapping are described; the use of small field scintigraphic imaging devices in the operating theatre is also discussed. Advances in computer technology and data processing make it possible to integrate 3-D rendering systems that facilitate intraoperative localization of deep seated lesions, thus allowing for minimal invasive endoscopic procedures using specially designed probes.

The sentinel node procedure has been established for certain indications and shows a promising future in others. This procedure, however, is still associated with some controversies. It has various performance methodologies, and these options depend on the equipment available.

The growing impact of positron emission tomography (PET) imaging on cancer patient management has prompted the development of intraoperative probes for detecting positron emission, thereby enabling the identification of occult tumour lesions intraoperatively, following systemic administration of tumour seeking PET agents.

This publication will therefore contribute to supporting and facilitating both the clinical decision making process and the implementation of minimally invasive surgical procedures; the ultimate aim of both approaches is to improve the standard of health care received by patients with cancer.

The IAEA is grateful to the contributors to this publication for sharing invaluable knowledge, time and effort, in particular to F. Giammarile, G. Mariani, R. Valdés Olmos and S. Vidal-Sicart for compiling the contents. The technical officers responsible for this publication were J.J. Zaknun, D. Paez and M. Dondi of the Division of Human Health.

EDITORIAL NOTE

This report does not address questions of responsibility, legal or otherwise, for acts or omissions on the part of any person.

Although great care has been taken to maintain the accuracy of information contained in this publication, neither the IAEA nor its Member States assume any responsibility for consequences which may arise from its use.

The use of particular designations of countries or territories does not imply any judgement by the publisher, the IAEA, as to the legal status of such countries or territories, of their authorities and institutions or of the delimitation of their boundaries.

The mention of names of specific companies or products (whether or not indicated as registered) does not imply any intention to infringe proprietary rights, nor should it be construed as an endorsement or recommendation on the part of the IAEA.

The authors are responsible for having obtained the necessary permission for the IAEA to reproduce, translate or use material from sources already protected by copyrights.

Material prepared by authors who are in contractual relation with governments is copyrighted by the IAEA, as publisher, only to the extent permitted by the appropriate national regulations.

This publication has been prepared from the original material as submitted by the authors. The views expressed do not necessarily reflect those of the IAEA, the governments of the nominating Member States or the nominating organizations.

The IAEA has no responsibility for the persistence or accuracy of URLs for external or third party Internet web sites referred to in this book and does not guarantee that any content on such web sites is, or will remain, accurate or appropriate.

CONTENTS

1. INTRODUCTION

1.1. BACKGROUND

Radioguided surgery, and especially sentinel lymph node biopsy (SLNB), is now the accepted standard of care for various clinical conditions, in particular for patients with early stage breast cancer and cutaneous melanoma (CM). Despite the established benefits of SLNB as a minimally invasive approach for nodal staging, this procedure is still underutilized in many developing countries. The IAEA convened advisory meetings with panels of multidisciplinary experts from different backgrounds with the task to advise on options for extending current applications of radioguided surgery. Because radioguided surgery is intrinsically a comprehensive team approach, establishing a successful radioguided surgery programme mandates close collaboration and coordination of the different specialties involved; it is in this early phase of coordinated planning that most of the challenges are encountered in both experienced and less experienced centres. In the past 5 years, there has been a momentum in technology and clinical research, thus opening new avenues to novel strategies for radioguided surgery. In this setting, the integration of 'virtual surgery' to clinical practice has increased the applications of 'minimally invasive surgeries'. Indeed, molecular imaging, in particular radionuclide imaging, is becoming essential for optimizing surgical approaches tailored to the disease specific condition encountered. This synergy has fostered growing interactions between surgical specialties and nuclear medicine.

In this new perspective, different medical specialties cooperate to achieve a common goal of improved management and overall benefit for the patients. In this regard, it seems appropriate to introduce a general term that encompasses this entire domain as 'guided intra/perioperative scintigraphic tumour targeting' (GOSTT).

1.2. OBJECTIVE

The objective of this book is to provide an updated source for professionals involved in employing GOSTT procedures. Its contents will therefore contribute to supporting and facilitating both the clinical decision making process and the implementation of minimally invasive surgical procedures; the ultimate aim of both approaches is to improve the standard of health care received by patients with cancer.

1.3. SCOPE

The above considerations highlight the need to make use of new devices and procedures and to expand existing applications of GOSTT in a manner that will ensure the high quality that is necessary to guarantee excellent performance towards positively influencing management of cancer patients. This book is intended to constitute a useful complementary resource to expand professional knowledge of the multidisciplinary teams involved in the implementation of radioguided surgery.

The guidance provided here, describing good practices, represents expert opinion but does not constitute international/Member State consensus recommendations.

1.4. STRUCTURE

This book provides an update on innovations in the use of radiopharmaceuticals for sentinel lymph node mapping (SLNM) and SLNB, in combination with vital dyes when appropriate, to facilitate detection of sentinel lymph nodes (SLNs). In addition, the book provides an update on advances in the implementation of hybrid imaging technologies for the surgical management of patients with cancer in conjunction with intraoperative regional lymph node (LN) mapping. Experience with the use of small field scintigraphic imaging devices in the operating theatre is also presented, considering the growing evidence that these molecular imaging devices may improve the intraoperative identification of SLNs and of occult neoplastic lesions. Advances in computer technology and data processing make it possible to integrate three dimensional (3-D) rendering systems that facilitate intraoperative localization of deep seated lesions, thus allowing for minimally invasive endoscopic procedures using specially designed probes. Finally, the growing impact of positron emission tomography (PET) imaging on cancer patient management has prompted the development of intraoperative probes for localizing tumour foci with high uptake of positron emitting radiopharmaceuticals; while most of these probes are designed to detect high energy annihilation photons (511 keV), some of them enable direct detection of emitted positrons.

2. INSTRUMENTATION

2.1. SPECT/CT

Single photon emission computed tomography (SPECT) is a nuclear medicine technique for in vivo measurement of the local concentration throughout the body of a single photon emitting radioisotope using the computed tomography (CT) imaging technique. Radionuclides that emit a single γ ray as a result of a γ emission of excited nuclei are used in SPECT as a source of signal. SPECT is then an emission imaging technique, i.e. the source of the signal is within the object (body) to be analysed. The line along which the γ ray emission occurs can be determined by measuring the flight direction of the emitted γ ray. The objective of SPECT is to measure the local density of activity of a radioisotope in a 3-D space, ρ(x,y,z). This distribution can be obtained by knowing the line integrals, i.e.:

$$N_\gamma = k \int_L \rho(x,y,z)\, \mathrm{d}l \tag{2.1}$$

where N_γ is the number of γ rays emitted along the line L and is proportional to the number of single photon emitters that are present along the same line. The proportionality factor k includes the effect of the attenuation of the emitted γ ray in the object and the effect of the efficiency of the γ ray detection process.

In single photon emission imaging, there are two different families of acquisition modalities: planar and tomographic. In planar imaging (usually called scintigraphy), the activity distribution is projected along a single direction L. For example, considering the previous equation for N_γ and taking the y direction as the direction of L, the planar projection image can be written as:

$$N_\gamma(x,z) = k \int_L \rho(x,y,z)\mathrm{d}y \tag{2.2}$$

In the tomographic approach (SPECT), different projection images, recorded at different angles, are combined with dedicated algorithms to reconstruct an image of the original activity distribution.

The measurement of the projection image expressed by $N_\gamma(x,z)$ implies the possibility of selecting only the γ rays that are emitted along a well defined

direction. This is the principle of the collimation technique. The most widely used collimator to detector ensemble for single photon emission imaging is the gamma camera.

2.1.1. The gamma camera concept

A gamma camera consists of a collimator, a slab of a scintillating crystal, an assembly of photomultiplier (PMT) tubes optically coupled to the scintillator, and an electronic readout and acquisition system. The active part of the detector is the scintillator, where the energy of the incoming γ ray is converted into a light signal with an intensity proportional to the energy released in the interaction (the full energy of the γ ray in the case of a photoelectric interaction, or part of it in the case of a Compton interaction). The PMT assembly converts the light into an electrical signal that is proportional to the light intensity. The position of the interaction is obtained by a centre of gravity calculation of the signal measured by the PMT tubes reached by the light spot. A typical scintillating material used in a gamma camera is thallium doped sodium iodide, NaI(Tl). This material is particularly suitable for SPECT imaging owing to its relatively high light yield and good efficiency for low to medium energy γ rays. For example, the mass attenuation coefficient for NaI(Tl) at 140 keV is 0.654 cm^2/g, corresponding to an attenuation length of approximately 4.2 mm.

To provide good light detection and a precise light spot localization, the PMT tubes are usually arranged on a hexagonal grid. In modern versions of a gamma camera, the centre of gravity of the light spot, corresponding to the point of interaction of the γ ray, is calculated using statistical calculations.

The sum of all the signals from the PMT tubes involved in a single event is used to calculate the released energy. On the basis of the energy estimation, the events are selected or discarded for image reconstruction. This energy selection is made so that only those γ rays that did not experience any Compton scattering before the detection are selected. In fact, such events would degrade the quality of the image because of their deviation from the line integral model. A good energy resolution is therefore crucial for the selection of good events. The energy resolution is usually expressed as $\Delta E/E$ for a given energy, i.e. as the fluctuation of the measured energy, estimated by the full width at half-maximum (FWHM) of the peak in the energy spectrum. A typical value for the energy resolution of a NaI(Tl) based gamma camera is approximately 0.1, i.e. a percentage energy resolution of 10%.

2.1.2. Collimator geometries

Unlike PET (see Section 2.2), SPECT does not suffer from intrinsic spatial resolution limitations. The main limitation of SPECT lies in finding the optimal compromise between spatial resolution and sensitivity. Both these figures of merit depend on the characteristics of the collimator. For this reason, optimal choice of the collimator type and geometrical parameters of the collimator is a fundamental issue for image quality in SPECT.

Collimators are usually classified in terms of construction material, geometry and shape, and size of the holes. Ideally, a collimator is a binary filter. A γ ray that hits a collimator can reach the detector only if its line of flight obeys the geometrical condition defined by the collimator. This 'selection' should occur through the photoelectric absorption in the collimator material of those γ rays that are not coaxial with the collimator holes. However, some Compton scattering events may occur in the collimator; in addition, the probability of reaching the detector with no interactions in the collimator septa (penetration effect) is not negligible. To maximize the photoelectric probability and to minimize Compton interaction and the penetration effect, high density (ρ) and high atomic number (Z) materials such as lead (ρ = 11.3 g/cm^3, Z = 82), tungsten (ρ = 19.4 g/cm^3, Z = 74) or gold (ρ = 19.3 g/cm^3, Z = 79) are used for the construction of collimators.

Possible geometries of collimators commonly used in SPECT are parallel holes, converging or diverging holes, and pinholes.

Parallel hole collimators are usually built from a solid block of material, with the holes being arranged in a regular pattern. The solid material between the holes is called the septum. Holes are perpendicular to the collimator surface and parallel to each other. This type of collimator is the most widely used in clinical systems because it can provide a large field of view (FOV) and a distortion free, real size projection image. Sensitivity and spatial resolution of this type of collimator are a function of the hole's size and shape, of the hole's length, and the source to collimator distance. In fact, owing to the finite size of the holes, the collimators can accept photons that have an angle of incidence with the collimators that are included in the solid angle defined by a cone of aperture θ_{tot} [2.1]:

$$\theta_{tot} \approx \tan\theta_{tot} = \frac{D}{L} \tag{2.3}$$

where D and L are the diameter (assuming a round hole) and length of the holes, respectively. The geometrical spatial resolution of a parallel hole collimator,

expressed in terms of the FWHM of the point spread function, can be written as [2.1]:

$$R_C = D\frac{(d+L)}{L} \tag{2.4}$$

where d is the source to collimator distance. On the other hand, the geometrical efficiency of a parallel hole collimator is expressed by the relation:

$$\varepsilon_C = K^2\left(\frac{D}{L}\right)^2\frac{D^2}{(D+h)^2} \tag{2.5}$$

where h is the minimum septa thickness and K is a hole shape dependent factor [2.1].

It is important to note that, while the spatial resolution degrades as the source to collimator distance increases, the geometrical efficiency, and therefore the sensitivity of a parallel hole collimator, does not depend on the source to collimator distance. Typical values for the geometrical efficiency of a parallel hole collimator are in the 10^{-4}–10^{-6} range.

The parallel hole collimators used in clinical systems are not classified in terms of hole size and geometry, but simply on the basis of the reported spatial resolution, sensitivity and energy range of usability. This classification simplifies the collimator choice irrespective of construction details and collimator manufacturer. Typical types of parallel hole collimators are: low energy, high resolution (LEHR), low energy all purpose or low energy general purpose; medium energy all purpose or medium energy general purpose; and high energy all purpose or high energy general purpose. The collimators classified as low energy are usually recommended for ^{57}Co (122 keV), ^{123}I (159 keV), ^{99m}Tc (140.5 keV) and ^{201}Tl (69–81 keV); medium energy collimators are used for ^{111}In (172 keV and 247 keV); and high energy collimators are used for ^{131}I (284 keV and 364 keV).

Converging hole collimators and diverging hole collimators are variations of the parallel hole collimator concept. These collimators are used in specific applications, where a higher resolution is needed, or when the required FOV is larger than the detector's size, respectively. However, the use of converging and diverging hole collimators is limited for SPECT imaging, whereas they are more often used for planar scintigraphy.

Recently, there has been a growing interest in the use of pinhole collimators as a solution for ultra-high-resolution SPECT imaging. A pinhole collimator

consists of a single hole shaped like a double cone. These collimators are usually made of high Z materials (e.g. gold) to reduce the radiation penetration at the edge of the hole. For this type of collimator, the FWHM of the spatial resolution is given by [2.1]:

$$R_{\mathrm{C,pinhole}} = D_{\mathrm{e}} \frac{(d+L)}{L} \tag{2.6}$$

where d is the distance between the object and the pinhole and L is the distance between the pinhole and the scintillator. D_{e} represents the effective diameter of the pinhole, which also depends on the attenuation coefficient of the collimator material and on the hole's aperture. Unlike parallel hole collimators, the sensitivity of a pinhole is proportional to $1/d^2$. Thus, the closer the object is to the hole, the higher the sensitivity. By using the intrinsic geometrical magnification of a pinhole collimator, it is therefore possible to obtain high resolution images with an FWHM of the same order of D_{e} ($L > d$) and a good sensitivity (only using small d). Such magnification allows the use of instruments with an intrinsic resolution larger than the system resolution. On the other hand, reducing the pinhole to object distance proportionally reduces the size of the FOV. In clinical practice, the use of pinhole collimators is now limited to high resolution planar imaging for the relatively small FOV offered by pinholes with a single hole. Following the successful use of multipinholes in small animal imaging (to increase sensitivity and FOV size), there is a growing interest in the application of this technology to human imaging, both for tomography and for planar applications [2.2, 2.3].

2.1.3. The SPECT image

Tomographic data to reconstruct volume images are typically acquired by collecting planar images, e.g. of sizes 64 × 64 pixels or 128 × 128 pixels, at multiple angles around the patient. Typical SPECT systems include single head, dual head or triple head gamma cameras, usually equipped with parallel holes. During the tomographic acquisition, detectors rotate around the patient over 360°, usually acquiring 120 views of 3° each. In some cases, the rotation over 360° is somewhat difficult (e.g. in cardiac imaging); in this case, the rotation is limited to 180°.

Raw data consist of information on the coordinates of the 'line of response' (LOR) and the energy detected in each event. The LORs are usually stored in the form of a sinogram, i.e. LORs are classified in terms of inclination (ϕ) and distance from the tomograph axis (s). Typical SPECT data using a parallel hole

collimator are organized in two dimensional (2-D) sinograms, where each slice of the sinogram contains information from a single slice of the body. In this case, the angle ϕ is simply given by the angle of rotation of the SPECT head.

Mathematical algorithms for SPECT image reconstruction can be subdivided into two main classes: analytical and iterative algorithms. The most widely used analytical algorithm is the filtered back projection (FBP) algorithm. FBP is fast, but can produce image artefacts and relatively high noise, especially in low activity FOV regions. Iterative algorithms are based on statistical estimation methods. These are usually slower and computationally more intensive than FBP, but produce better quality images. The most common iterative algorithm is the maximum likelihood expectation maximization (MLEM) algorithm. To improve reconstruction speed, an accelerated version of the MLEM algorithm, called the ordered subset expectation maximization (OSEM) algorithm, is commonly implemented. The larger the number of subsets, the faster the reconstruction; on the other hand, the image quality could be compromised. Hence, the number of subsets is always a compromise between reconstruction speed and image quality.

The choice of the reconstruction algorithm and image postprocessing can have a strong impact on the final image resolution and noise. For example, in iterative reconstruction algorithms, the signal to noise ratio depends on the number of iterations and the number of subsets used for OSEM, as well as on the image smoothing procedures, when applied. A finer spatial resolution is required for tumour targeting to minimize partial volume effects (PVEs). For the same reason, gated acquisitions are recommended for the target definition of tumour masses that can be subject to motion (e.g. patient breathing motion during examination). This function is usually implemented in modern SPECT/CT systems.

2.1.4. SPECT/CT imaging

In single photon imaging, the relatively low energy of the γ rays emitted by the commonly employed radionuclides makes the attenuation of the emitted radiation a very important issue. For example, the 140.5 keV γ rays emitted by ^{99m}Tc have a linear attenuation coefficient in water of approximately 1.53×10^{-1} cm^{-1}, corresponding to a half value thickness of approximately 4.5 cm. This effect is very important in human imaging, e.g. the emitted γ rays are attenuated by a factor of approximately 450 in a 40 cm diameter body. Incorporating the effect of the attenuation in the line integral expression gives:

$$N_\gamma(x,z) = \int_L \rho(x,y,z) \mathrm{e}^{-\int_{L'} \mu(x,z,y')\mathrm{d}y'} \mathrm{d}y \tag{2.7}$$

where L is the line along which the activity is estimated, L' is the actual line that the γ ray, emitted from point (x,z,y), travels through the body along line L, while $\mu(x,z,y,E)$ is the local linear attenuation coefficient for γ rays with energy E (the so called μ map). The underestimation of the line integrals causes not only an underestimation of the overall activity in the body, but also attenuation artefacts in the reconstructed images [2.4].

For this reason, in order to estimate the activity distribution, it is necessary to have an a priori knowledge of the attenuation properties of the body in terms of a μ map. Therefore, more recent SPECT systems are equipped with an X ray CT scanner.

CT is an imaging technique that is able to visualize transversal slices of a body. It is based on the measurement of the transmission properties of an X ray beam through the object under study. Tomographic acquisition is performed by measuring the attenuation of the X ray beam at different angles and then combining this information to obtain a 3-D map of the local linear attenuation coefficients. The resulting image is a high quality image of the body attenuation, and therefore is representative of the body anatomy, which is represented as a greyscale image. To standardize the attenuation values, these are typically converted to CT numbers (Hounsfield units (HUs)) using the attenuation coefficient of water (μ_{water}) as the normalization value with the following formula:

$$\mathrm{HU} = \frac{\mu_{\mathrm{tissue}} - \mu_{\mathrm{water}}}{\mu_{\mathrm{water}}} \times 1000 \tag{2.8}$$

Then, the CT numbers of air and water are −1000 and 0, respectively.

The essential components of a CT scanner are an X ray source and a detector positioned on the opposite side, mounted on a rotating gantry. The X ray source is an X ray tube with a maximum emission in the 80–140 keV range. The detectors are usually based on pixilated scintillators. In a typical CT system, the detector is subdivided into 600–900 columns and 1–64 rows, and each element has a size of approximately 0.6 mm × 1 mm. The number of rows defines the number of slices that can be obtained in a single gantry rotation. Most CT scanners now have more than a single slice, and are therefore called multislice (MS) systems. Most are also capable of spiral scanning around the patient, with advantages of image quality and axial extension of the scan. However, it should be noted that the CT systems integrated in combined SPECT/CT systems might have a lower performance than a stand alone clinical CT system, and are usually optimized for low dose imaging.

Once the areas with abnormal radiopharmaceutical uptake have been detected, it is also important to exactly locate the region to define the proper tumour target for determining the course of therapy or for surgical guidance. The added value of the combined use of the SPECT/CT system is the possibility of visualizing the anatomy of the part of the body under examination with a high spatial resolution and to overlap these morphological images with the relatively low spatial resolution functional images from SPECT.

The integration of the SPECT and the CT techniques is usually obtained by combining the two systems on a single gantry with a common imaging table. SPECT and CT images are then sequentially acquired.

One additional advantage of the integration of SPECT and CT is the possibility to correct the acquired data by the attenuation of the γ rays in the body. This feature is of great importance for reducing attenuation artefacts and for improving the quantitative information in the SPECT measurements.

The attenuation correction procedure for SPECT consists of deriving from the CT acquisition the attenuation correction factors to be applied to the SPECT image. The first step is to derive the attenuation μ map at 140.5 keV. This can be obtained by rescaling in energy the local attenuation coefficient measured by CT; the emission images can thus be corrected for the attenuation effect during the image reconstruction step [2.5]. This is accomplished by using a bilinear model [2.6].

2.2. PET/CT

PET is a nuclear medicine technique for in vivo measurement of the local concentration of a positron emitting radioisotope. As for SPECT imaging (see Section 2.1), PET is an emission imaging technique. The sensitivity of the PET technique is relatively high, of the order of 10^{-11}–10^{-12} mol/L. Typically, a few million cells incorporating the radionuclide can be identified and distinguished from background radioactivity.

PET in combination with CT in integrated multimodality imaging systems now has significant importance, especially in oncology, for a wide range of applications including diagnosis and staging, treatment planning in radiotherapy or hadron therapy, and also for surgical guidance. For example, PET/CT imaging has largely been demonstrated to be more effective for tumour, node, metastasis (TNM) staging than stand alone CT and PET systems [2.7], once all the correction procedures, including attenuation correction of PET data [2.6], have been correctly applied.

The physical processes used to obtain information on the activity distribution comprise positron emission, positron annihilation, interaction of γ rays with matter and γ ray detection.

A positron is a positively charged particle and is the antiparticle of the electron. It is usually called a β^+ particle. Positrons are emitted during the decay of proton rich nuclei, where stability is reached by converting a proton into a neutron because of the emission of a positron and a neutrino, i.e.:

$$ {}_{Z}X \rightarrow {}_{Z-1}X^{*} + \beta^{+} + \nu \tag{2.9} $$

In some cases, the daughter nucleus is produced in an excited state and can reach stability by emitting an additional γ ray. Owing to the presence of the neutrino, the β^+ decay is a three body decay where most of the energy is shared by the two lighter particles, the positron and the neutrino. The positron is emitted with a continuous energy distribution ranging from zero to a characteristic value $E_{\max}$, which depends on the radioisotope and which may have values from a few hundred keV up to a few MeV.

After emission, the positron travels within the surrounding tissue/material and interacts, mainly through Coulomb interactions, with electrons, thus resulting in a random path. When the positron energy is sufficiently low, the positron annihilates with an electron. The distance between the emission point and the annihilation point is called the positron range. For example, the average range for positrons emitted by ^{18}F is 1–2 mm in water.

The positron annihilation can occur in flight or through a positron–electron bound state called a positronium. The most probable result of the annihilation is the emission of a pair of γ rays with an energy of 51 keV. In fact,

$$ E_{\gamma} = (m_{\mathrm{e}}c^2 + m_{\beta}c^2)/2 = (511\ \mathrm{keV} + 511\ \mathrm{keV})/2 = 511\ \mathrm{keV} \tag{2.10} $$

where c is the speed of light in a vacuum and m_{e} and m_{β} are the electron and positron rest masses, respectively. In the positron reference frame, these γ rays are emitted along the same line (at an angle of 180°). However, in the laboratory reference frame, because the positron (or the positronium) is not at complete rest, the two γ rays are emitted at $180° \pm \Delta\theta$ with a magnitude of approximately 0.5° deviation $\Delta\theta$ in water.

The line along which the annihilation occurs can be determined from the electronic time coincidence detection of the two γ rays in the detectors surrounding the radioactive source. As for SPECT, the objective of PET is then

to measure the local density of activity $\rho(x,y,z)$ of a radioisotope. In this case, the line integrals can be rewritten as:

$$N_{\gamma-\gamma} = k \int_L \rho(x,y,z)\mathrm{d}l \tag{2.11}$$

where $N_{\gamma-\gamma}$ is the number of γ pairs emitted along the line L and is proportional to the number of β^+ emitters present along the same line. After tomographic acquisition, dedicated algorithms (similar to those used in SPECT) are employed for image reconstruction.

A PET system consists of instruments that are able to detect the line of flight of a γ ray pair produced by positron annihilation. Therefore, γ rays are detected in 'time coincidence', i.e. identified as an annihilation pair when the two detection times occur within the selected timing window ΔT, typically of the order of 10 ns or less. Such pair detection defines the LOR and then defines the line along which the annihilation occurs (electronic collimation). Once recorded at various angles (tomographic acquisitions), the LORs are processed by reconstruction software, providing the local activity concentration within the object or organ under investigation.

As for SPECT, the emitted photons may interact with the surrounding material via photoelectric or Compton interactions. Because of the higher energy of the γ ray, i.e. 511 keV, the total interaction probability is lower. However, the Compton–photoelectric interaction probability ratio is usually higher, resulting in a higher fraction of events contributing to noise. For example, in water, the linear attenuation coefficient at 511 keV is $\mu_{H2O} = 9.6 \times 10^{-2}$ cm^{-1}, corresponding to a half value thickness ($\lambda_{1/2}$) of approximately 7.2 cm.

2.2.1. PET detectors

The most widely used detector arrangement is the ring geometry where detectors are arranged around the body on a fixed ring. Nowadays, all the clinical PET systems utilize this geometry with one or more rings (multiring) surrounding the patient. In this way, an axial FOV coverage up to approximately 23 cm is now offered.

Each detector is in time coincidence with an opposing sector of detectors. The intersection of all of these angular sectors defines the system FOV. Unlike SPECT, in PET, with this geometry, the collection of LORs at different angles (tomography) occurs without any detector rotation. A detailed discussion on PET design is reported in Ref. [2.8].

A detection system suitable for PET imaging should be able to provide all the information for building the LOR's spatial distribution and then the reconstructed activity distribution. Therefore, PET detectors are required to measure the point of the interaction of γ rays and the energy. This should be repeated for various angles around the object under study, to provide a suitable set of angular LORs to the reconstruction software.

Multiring PET systems are classified as 2-D when coincidences are accepted only when both detectors involved belong to the same ring. Instead, a system is classified as 3-D when coincidences involving detectors belonging to different ring are also accepted. In the 2-D method, image reconstruction is simplified and intrinsically eliminates most of the scatter events when rings are physically separated by lead or tungsten septa.

On the other hand, the 3-D mode has a higher sensitivity (by a factor approximately equal to the number of rings); consequently, with the advent of more powerful computers able to reconstruct large datasets, this has become the most commonly used method. The use of 3-D modality usually improves the signal to noise ratio, but slightly degrades the spatial resolution, especially in the axial direction. For this reason, in some cases it is necessary to limit the maximum distance between the rings to be used for the coincidence detection. The maximum distance is usually called the 'ring difference'.

The ideal detector for PET should be able to provide the position of the interaction of the γ ray, the time of the interaction and the released energy. The most widely used technology to build a PET detector is to use scintillating crystals coupled with photodetectors.

The most common approach for a scintillator based detector for PET is the use of pixilated blocks in the form of the so called block detector. A good scintillator should be dense enough to stop a good fraction of the incoming 511 keV γ rays, and should have a good light yield to facilitate the identification of the position of the interaction and to measure the energy with a good resolution. In its original version, it was composed of a bismuth germanate (BGO) solid block separated by cuts of different depths. The block was then coupled with a 2 × 2 array of PMT tubes able to distinguish the position of the pixel where the interaction occurs via centre of gravity calculations of the electrical signal produced by the four tubes, while the total energy is given by the sum of the four signals. With this kind of detector, it is therefore possible to measure two coordinates only, while the third, i.e. the depth of the interaction, within the scintillator cannot be determined. In more recent versions of the block detector, different materials are used, and BGO has been widely replaced by faster and higher light yield scintillators, such as lutetium oxyorthosilicate (LSO), lutetium-yttrium oxyorthosilicate (LYSO) or gadolinium orthosilicate (GSO). In the new blocks, the pixel elements are completely separated from adjacent ones. In

clinical PET, the smaller pixel sizes available are approximately 4 mm × 4 mm in cross-section.

The acquisition system of a PET scanner can be subdivided into two main parts: the timing section and the energy section. The timing section identifies the occurrence of coincidence detection. For the detection of a γ ray, a timing signal is produced. If a second γ ray is detected within a well defined time window, i.e. with a time delay less than a fixed value (usually approx. 10 ns or less), the two signals are recognized to be a coincidence. The use of faster scintillating materials improves the timing performance of the system, thus making the use of narrower timing windows possible. The timing signals are usually produced by constant fraction discriminators that also discard events with a released energy below a certain threshold.

As for SPECT, raw data are stored in sinograms and consist of information on the coordinates of the LOR and on the energy detected in each event. In addition to the ϕ and s coordinates, a PET sinogram should also include the inclination θ along the axial direction if 3-D mode data acquisition is used. However, the 3-D sinograms are rebinned in 2-D sinograms, thus eliminating the θ coordinate, to facilitate the image reconstruction process. Similar to SPECT, in the 2-D sinograms, each slice corresponds to a slice of the body. Rebinning of 3-D sinograms to 2-D sinograms is performed with interpolation techniques such as MS rebinning [2.9], Fourier rebinning [2.10] or exact Fourier rebinning [2.11] algorithms.

Mathematical algorithms for PET image reconstruction are similar to those described for the SPECT case. In addition, some modern PET systems include full 3-D image reconstruction methods [2.12].

2.2.2. PET performance

The spatial resolution of a PET system is limited both by the physics of the β^+ decay and by technological limitations. The positron travels a certain distance from the emission point before the annihilation. This causes a degradation of the spatial resolution because of the range effect. In addition, the angular deviation of the two γ rays from 180° causes a further degradation of the highest spatial resolution achievable. While the range effect is a constant factor depending on the radioisotope only, the non-collinearity effect becomes more important for large detection separation systems, as follows:

$$\mathrm{FWHM}_{\Delta\theta} \approx \Delta\theta \times \frac{D}{4} = 0.0022D \tag{2.12}$$

where D is the distance between two opposite detectors in metres.

The maximum spatial resolution is also limited by factors connected to the technology used for determining the position of the interaction. When including these factors, the best spatial resolution of a PET system can be expressed as:

$$\mathrm{FWHM} = 1.2\sqrt{\left(\frac{d}{2}\right)^2 + b^2 + (0.0022D)^2 + r^2 + p^2} \tag{2.13}$$

The first factor (d/2) is attributable to the finite dimension of the scintillator pixel elements (of pitch d). Factor b is attributable to the fact that the identification of the pixel where the interaction occurs is not perfect and may be affected by a certain coding error, factor r indicates the positron range and factor p is due to parallax error. This parallax error is caused by a lack of information on the depth of the interaction in the scintillator, and is therefore related to the crystal thickness. In fact, in ring geometry, the lines that do not pass through the tomograph centre are affected by an uncertainty that increases as the distance from the centre increases. The multiplicative factor depends on the reconstruction algorithm used and is approximately 1.2 for FBP. All dimensions in Eq. (2.13) are in m.

The best clinical PET systems now offer a spatial resolution of approximately 4 mm and a maximum sensitivity of approximately 3% at the centre of the FOV.

Performing quantitative PET measurements requires direct proportionality between the number of counts in each voxel of the image and the activity concentration in the same point in the space. Once the image is correctly normalized, one can expect that such proportionality is verified. However, this is true for image details whose sizes are larger than twice the FWHM of the instrument's spatial resolution. For smaller structures, such proportionality is lost because of the PVEs, which causes a loss of contrast for small objects. The correct value for the activity concentration in an object whose size is in the 1–2 spatial resolution FWHM range can be restored using experimentally measured recovery curves, which provide the multiplicative factor to be applied to the measured activity as a function of the detail size.

Another factor reducing image quality, in addition to the spatial resolution degradation, is noise. The major sources of noise in PET are scatter (S) and random (R) counts. An event is defined as true (T) when the two γ rays detected in coincidence arise from the same annihilation event, without any deviation along their path. These are the events that generate good LORs for image reconstruction. On the other hand, an event is defined as an S event when at least one of the two annihilation γ rays experiences a Compton interaction along its path, thus generating a wrong LOR, i.e. the emission point does not lie on the

LOR itself. An estimation of the effect of the S counts on the final image quality is given by the scatter fraction (SF), which is given by the ratio SF = $S/(T + S)$. The sum of the T and S events is usually referred to as the prompt event. It is important to note that the SF does not depend on the count rate. On the other hand, the R count varies with the rate of single counts:

$$R_{ij} = 2\tau C_i C_j \tag{2.14}$$

where R_{ij} is the random count rate in the LOR connecting detectors i and j, C_i and C_j are the single count rates measured by detectors i and j, respectively, and τ is the timing window of the system. It is now clear that a faster scintillator permits the use of a narrower time window, ultimately reducing the R count rate. Count rates cannot be directly measured or identified, but an estimation of the R count rate distribution can be obtained using the delayed coincidence technique.

A measure of the influence of S and R counts on the final image quality as a function of the count rate is given by the noise equivalent count rate (NEC) curve. In practice, the NEC value measures the ability of the system in selecting T counts only. The NEC is usually defined as:

$$\mathrm{NEC} = \frac{T^2}{T + S + kR} \tag{2.15}$$

where k is a factor related to the method used to correct data for R events. The NEC curve usually shows a peak at a certain value of the count rate that corresponds to a certain activity in a typical patient body (peak NEC activity). NEC curves are used to optimize the PET protocols. For example, a common recommendation is to start the acquisition with an activity level that maximizes the NEC value.

2.2.3. Time of flight (TOF) PET

Another source of noise in PET is its relatively poor counting statistics. A method for reducing the image noise is the TOF PET concept, where the time difference in the detection of the two annihilation γ rays is measured. Such timing information can be used to remove the coupling between voxels that are separated by more than the TOF measurement distance. For example, using recently developed fast and high light yield scintillators, it could potentially be possible to achieve a time resolution of 300–500 ps at the FWHM. Such a value corresponds to a net reduction of the background variance, which is equivalent to

an improvement in sensitivity. TOF PET usually requires dedicated reconstruction algorithms to fully exploit the potential advantages of this technique [2.13].

2.2.4. PET/CT

Nowadays, PET/CT systems are replacing stand alone PET systems and creating a new paradigm for cancer imaging [2.14]. A PET/CT system usually comprises a PET scanner and a CT scanner joined together on the same axis and with a common patient imaging table. An important issue in a PET/CT system is the relative position of the two systems, and therefore of the two FOVs that should be overlapped during image processing to obtain fused PET/CT images. For the modern systems, the reported maximum displacement error is approximately 0.5 mm. A possible source of error is, for example, some bending of the imaging table, which is usually characterized by a longer travel range than PET or CT only. For heavy patients, this issue could become relevant, and for this reason, the maximum patient body weight is usually specified by the manufacturer. PET and CT components in an integrated PET/CT system are usually both top end performance scanners, so that they can produce high quality images in each modality. The CT component of a PET/CT system can therefore be used as a diagnostic tool (higher mAs, contrast media). PET/CT systems are usually equipped with the gated acquisition modality.

As for SPECT, the combination of PET and CT yields much more information with respect to separate use of the two instruments. The main advantage lies in the possibility to fuse the morphological information from CT with the functional information from PET. Further advantages of the PET/CT combination are the possibility to use CT information to correct PET data, e.g. in defining the region of interest in the calculation of the standardized uptake values or for correcting the PVEs. On the other hand, the PET image completes the morphological information like a ‘metabolic’ contrast agent, which is very important in, for example, the definition of treatment planning in radiotherapy. As for SPECT, the X ray attenuation properties measured using CT can be used to correct PET images for the attenuation.

To obtain quantitative information from a PET measurement, it is fundamental to correct the acquired data by the attenuation of the γ rays in the object under study (the body). For example, in PET, the attenuation correction factor is 45 for a 40 cm diameter man. From a mathematical point of view, the attenuation procedure is simpler for PET imaging than for SPECT imaging. Because of the presence of the second γ ray, the correction factor for a single LOR does not depend on the position of the emission point along the LOR, but depends on the object thickness only. In fact, considering a uniform object and an LOR intersecting the object in a segment of length L, the probability that at least

one γ ray of the annihilation pair, emitted at a position x along the same LOR, is attenuated in the object is:

$$P = \mathrm{e}^{-\mu x} \times \mathrm{e}^{-\mu(L-x)} \tag{2.16}$$

When considering the local attenuation coefficients along the LOR, the attenuation coefficient factor (ACF) can be expressed as:

$$\mathrm{ACF} = \frac{1}{P} = \mathrm{e}^{\int_L \mu(x)\mathrm{d}x} \tag{2.17}$$

This factor can be evaluated by directly measuring the attenuation map of the object by means of transmission based methods. The transmission images can be obtained either with a positron emitting source (usually ^{68}Ge) rotating around the object by using the PET detectors, or with a CT scanner. Although the PET based method gives a direct measurement of the attenuation coefficient at 511 keV, the CT based method has some advantages in terms of noise properties, thus ultimately resulting in a higher image quality. When using CT, the attenuation coefficients are measured with a continuous X ray spectrum ranging from a few tens of keV to 140 keV. Hence, for any tissue X, the CT energy linear attenuation coefficient ($\mu_{\mathrm{CT},X}$) has to be scaled to the 511 keV value ($\mu_{\mathrm{PET},X}$). For the energy scaling, a linear relation between $\mu_{\mathrm{CT},X}$ and $\mu_{511,X}$ is assumed up to a certain value (all soft tissues stay in this first range). Because this first range includes water, the following equation can be written:

$$\mu_{511,X} = \mu_{\mathrm{CT},X} \times \frac{\mu_{511,\mathrm{water}}}{\mu_{\mathrm{CT,water}}} \tag{2.18}$$

Above a certain value, a lower proportionality factor is assumed, and in some cases, $\mu_{\mathrm{CT},X}$ can also be assumed to be constant. The upper range of materials usually includes bone structures.

2.3. INTRAOPERATIVE DEVICES

The concept of radioguided surgery [2.15] using radiation detection probe systems was first introduced in 1949 by Selverstone et al. [2.16] at Harvard Medical School, where patients suspected of having a brain tumour were injected with ^{32}P, a β^- radiation emitter (14.3 d half-life, 1.71 MeV maximum β energy).

The intraoperative probe was a Geiger–Müller (GM) counter [2.17], and a gas filled radiation detector operated in a breakdown regime to enhance sensitivity of the device. One electron with the maximum energy can penetrate up to 8 mm in tissue (2.8 mm for the average energy). The properties of β radiation match well the technical characteristics of the probe. The short range of the β particle ensures that all the detected radiation comes from the source in contact with the tip of the probe. This means no background from distal parts of the body, and therefore neither collimation nor shielding is required.

The success of the use of gas filled detectors was partially limited because the absorbed dose for ^{32}P is much higher (300–600 times) than that of the current most frequently used radionuclide for nuclear medicine, ^{99m}Tc. Another limiting aspect of the GM tubes is their transparency to γ rays (less than 1% of the 140 keV γ rays from ^{99m}Tc crossing a GM detector are detected).

In 1956, Harris et al. [2.18], at the Oak Ridge Institute of Nuclear Studies Medical Hospital, reported the first radioguided surgery involving gamma detection probe systems. They used a hand-held scintillation detector device to detect γ rays from ^{131}I iodide that had been administered to a patient with differentiated thyroid cancer.

Since the pioneering experiences of Selverstone et al., radioguided surgery, together with the instrumentation involved, has developed tremendously, and it is now a well established discipline within the practice of surgery [2.19–2.38], with parallel technological evolution of the instrumentation.

2.3.1. Non-imaging devices

Intraoperative radiation detectors are subdivided into two general categories: gamma probes and beta probes [2.25]. Gamma probes detect photons, while beta probes detect electrically charged radiation consisting of either positrons or electrons. The latter category includes beta probe systems with γ photon background rejection capabilities [2.38].

The nature of the radiation and its different kinds of interaction in tissues define the requirements for intraoperative probes. Although γ rays undergo exponential attenuation in tissue, they can penetrate large distances before being significantly absorbed. Because collimation has a relevant impact on the final outcome of radioguidance, the thickness and design of the collimation and shield depend on the energy of the radionuclide used. Likewise, γ rays are monoenergetic, and so can be discriminated according to their energy using dedicated processing electronics (thresholding or energy windowing techniques).

Beta particles (positrons and electrons) undergo many inelastic collisions before reaching a complete stop in tissue (a few mm, depending on the beta energy). They are easy to collimate and much less sensitive to background uptake

from surrounding tissues, making the probe more specific than gamma probes. However, the continuous energy distribution spectrum does not allow energy discrimination and the short range of the β particle limits the range of the probe to a few mm under the skin or tissue surface, thus making it difficult to locate deeper tumours.

The most significant parameters defining the performances, especially for gamma probes, consist of: (i) overall sensitivity (efficiency), (ii) spatial resolution (radial and lateral), (iii) energy resolution and (iv) signal to noise ratio [2.15].

The sensitivity is the detected count rate per unit of activity and is determined at the tip of the probe. Radial resolution is the width of the measurement cone where the radiation is detected at a defined distance. With a wider cone, the background signal may overcome the target source. With a narrower cone, the background will be reduced and the detection of the target source will be more accurate. Lateral spatial resolution is the capability to accurately localize the position of a target source and to separate two adjacent sources. Energy resolution is the capacity of the gamma detection system to discriminate between radiations of different energies. This property is essential to distinguish between two simultaneously administered radionuclides that have different energies and to discriminate scattered photons from primary photons. The signal to noise ratio relates to the ability of the probe to discriminate the signal arising from the target with respect to the noise represented by the background radiation within the surrounding tissue.

Detectors for intraoperative probes are subdivided into two categories: the first category includes probes based on scintillation detectors (both crystal and plastic types), while the second category includes semiconductor based probes [2.19, 2.21, 2.23, 2.25, 2.26, 2.31–2.33]. A typical set-up for intraoperative probes, both scintillator or semiconductor, is shown in Fig. 2.1.

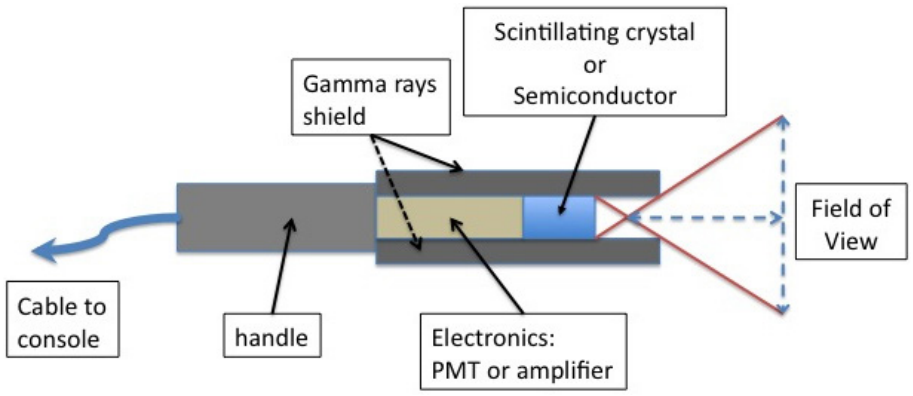

FIG. 2.1. Schematic representation of a typical radiation detection probe design.

The scintillator absorbs the radiation and emits a number of visible photons proportional to the energy absorbed. The visible light is measured using a photon detector, usually a PMT. The crystals used in scintillator detector probes include NaI(Tl), CsI(Tl), cerium activated LSO, BGO and cerium doped GSO.

The high penetration power of γ rays means that background events could come from parts of the patient far away from the target volume. Although a relevant fraction of these events is attenuated within the patient's body, in order to further reduce the background, the gamma probes are equipped with a shield (material such as lead, tungsten, gold or platinum) and collimators (designed with different lengths and apertures for different FOVs) to prevent attenuated radiation from non-target locations (i.e. scattered radiation) from accessing the detector head and thus producing spurious counts. Side shielding and back shielding can be important when there is a localized radiation source (e.g. the injection site of the ^{99m}Tc colloid for radioguided SLNB) in close proximity to the target (the SLN), or for positron emitting radionuclides that produce high energy γ photons through positron–electron annihilation (e.g. ^{18}F). Collimation of the detector head results in a better spatial resolution and higher signal to noise ratio compared to radiation emitted from surrounding tissue. However, strong collimation reduces the sensitivity of the probes by decreasing the detection aperture and lengthening the distance to the actual source position. Furthermore, although a thicker shielding or a longer collimator is needed when detecting higher energy γ rays, this increases the overall weight and size of the probe.

The final elements in the system are the electronics and the readout. Because the scintillator detector provides a signal that is proportional to the deposited energy, it is possible to carry out spectroscopy and to set the sensitive energy range of the probe to select the desired gamma energy and to eliminate part of the scattered radiation. The count rate of the probe is then fed to a ratemeter that also drives an audio output. An increase in loudness or an increase in frequency/pitch of the audio signal provides the surgeon with an acoustic guide to locate the tumour.

Semiconductors are a valid alternative to scintillators as the detector material for intraoperative probes. When radiation is absorbed in a solid state detector, ionization occurs by promoting electrons out of the valence band to the conduction band, where electrons can flow in the crystal lattice. When the electron moves to the conduction band, a positive charge (hole) in the lattice is created, which is free to move in the valence band. If an electric field is applied across the sensitive volume of the detector, the excess of charge (both electrons and holes) is collected by the opposite electrodes, thus providing a signal that is proportional to the energy released in the detector. Crystalline materials that are used in such detectors are cadmium telluride (CdTe), cadmium zinc telluride (CdZnTe) and mercuric iodine (HgI_2).

Scintillation type systems have advantages and disadvantages with respect to semiconductor based systems. In general, scintillator based detectors have a higher sensitivity (because of the higher density and atomic number, they are better suited for medium to high gamma energy detection), but a poorer energy resolution and scatter rejection, owing to the indirect mechanism of the radiation detection: the primary γ ray converts, in the scintillator, into a visible photon, then the light should be conveyed to the PMT to convert from an optical into an electrical signal. Furthermore, scintillation detectors tend to be much bulkier, and are heavy. Instead, semiconductor based probes are direct detectors (the energy released in the material by radiation is directly converted into an electrical charge signal), and they have a higher energy resolution and scatter rejection capability. Semiconductor based probes also tend to have a much more compact probe head design; they can be manufactured in small sizes and they can have a very thin entrance window that enables counting of low energy β and γ rays. Many commercial intraoperative probes are available [2.39].

Several factors determine the choice of a particular intraoperative probe. From the point of view of the surgeon, there are many desirable design features of the detection probe systems that are important [2.15]. In particular, the specific surgical application is an important decision aspect for choice of the appropriate intraoperative probe. Gamma probes for radioguided SLNB require high spatial resolution to allow for a more precise localization of small LNs. On the other hand, gamma probes for radioguided surgical resection of tumours require a high sensitivity to guide the surgeon to the specific site of the target over a relatively large surgical field.

Other features, such as the shape, weight and ergonomic design of an intraoperative probe, are also critical. The audible signal and digital display of the detector control unit are important additional variables for providing critical output information to the surgeon, such as the quick and accurate localization of the radionuclide, without distracting his/her attention from the surgical field. Flexibility and adaptability of the system are also functional to different clinical issues, such as removable side shielding, interchangeable collimators, interchangeable detector probes and adjustable energy windows for different radionuclides. Recent developments of hand-held self-contained gamma detection probes based on wireless technology (bluetooth) eliminate the need for cables connecting the probe to the control unit [2.40, 2.41], which is a possible confounding factor within the surgical field.

The radionuclide used and the energy and quality of radiation emitted are other very important aspects to be considered. Technetium-99m labelled agents have been used almost exclusively for radioguided SLNB. Monoclonal antibodies (MAbs) labelled with various radionuclides, as well as [^{18}F]fluorodeoxyglucose (or [^{18}F]fluoro-2-deoxy-D-glucose ([^{18}F]FDG)) are also suitable for radioguided

surgical resection of tumours. Although most of the probes have a high sensitivity for lower gamma energies (e.g. ^{125}I and ^{99m}Tc), for higher energy emitting radioisotopes (e.g. ^{131}I) or positron emitting radionuclides producing annihilation γ rays (e.g. ^{124}I and ^{18}F); this issue has been the focus of recent developments of probes specifically designed for detection of high energy annihilation γ rays.

PET imaging using [^{18}F]FDG has become an established modality of cancer imaging for different purposes, including initial staging and detecting recurrent disease. Therefore, intraoperative hand-held probes detecting high energy annihilation γ and/or β particles have been developed [2.42, 2.43]. Gulec et al. [2.44] reported encouraging clinical results with high energy gamma probes. In particular, a GSO crystal and a 12.5 mm tungsten shielding probe were used (CareWise Medical, Morgan Hills, USA). Peculiarities of this probe are the associated electronics and the analyser threshold and energy window adjustable around the 511 keV photopeak. Nevertheless, many clinical studies [2.45–2.50] clearly indicate that conventional gamma probes are not clinically useful for the intraoperative detection of [^{18}F]FDG avid tumour sites. The findings of Piert et al. [2.50, 2.51] in vitro and on phantoms demonstrate the superiority of positron probes over high energy gamma probes. The positron probe tested by Piert et al. essentially consists of a silicon detector whose volume is optimized for high β particle sensitivity and low absorption of photons. Other beta probes are based on the LSO scintillating crystal, with diameters ranging from 0.3 mm to 0.6 mm and lengths from 0.5 mm to 2 mm, coupled to optical fibres [2.52] or plastic scintillators [2.34, 2.53]. Despite the high sensitivity of the positron probes, given the short positron range in tissues, tumour sites that are covered with benign tissues may potentially remain unnoticed by positron detection alone. Combined positron/high energy gamma detectors with a reasonably high sensitivity may be the best choice to overcome this limitation.

A number of methods have been proposed to suppress the background from the annihilation radiation. One example is illustrated in Fig. 2.2 [2.54] and is based on the ‘phoswich’ concept [2.55]. A CaF_2:Eu disc, 0.5 mm thick and 1.25 cm in diameter, is coupled with an optical diffuser that is, in turn, coupled with high *Z* scintillating crystal cylinders (GSO), each of which are 2 cm thick and 2 mm in diameter. The optical signal is collected using a multichannel PMT through optical fibres glued to the GSO scintillators. When a positron is absorbed within the CaF_2:Eu disc, the scintillation light passes through the GSO scintillator and down through the optical fibres to give a position signal. The positron also annihilates in the CaF_2:Eu, yielding two 511 keV γ rays at an angle of 180° to each other. The probability that one of these photons interacts in one of the GSO crystals is high. The system requires that both types of detection occur simultaneously for an event to be considered valid. This is achieved by exploiting the different time decay constants of the two scintillators. Other axially oriented

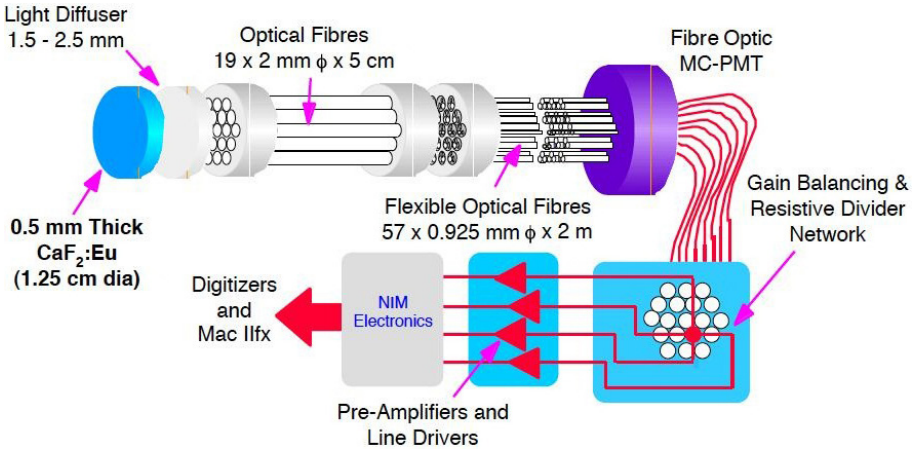

FIG. 2.2. PET probe based on the phoswich concept. A thin CaF_2:Eu scintillator crystal detects positrons from tissues. The resulting scintillation light is coupled, using optical fibres, to a position sensitive PMT tube; Anger logic is used to determine the interaction position. A bundle of BGO scintillator fibres placed between the light diffuser and the transparent optical fibres can be used to reject 511 keV photon interactions in the CaF_2:Eu (reproduced from Ref. [2.54]).

dual detector systems using either phoswich detectors composed of a plastic scintillator and a BGO crystal or an aligned photodiode and a CsI crystal are able to distinguish between β^+ decays and γ quanta from scatter or annihilation [2.56]. The additional use of a collimator was suggested to obtain spatial information at the primary intraoperative orientation.

A new positron emission probe (PEP) that is able to detect high energy gamma as well as positron emission annihilation gammas has been introduced [2.57]. PEP works with electronic collimation using multiple CsI crystals to measure tracer uptake and background activity without shielding (overall weight is 330 g). While target activity is preferably detected by the central crystal, background and scatter quanta are mainly detected by the concentric tapered detector ring. Counts obtained by the central detector and the crystals of the outer ring are compared to obtain spatial information. Electronic collimation allocates target and background activity by special algorithms. Aperture angles for the central detector can be varied via software to optimize the focus for the different applications.

Basic physical properties, such as spatial and angular resolution, of the new preliminary prototype were determined and compared to those of a conventional gamma probe. In contrast to a conventional gamma probe, the spatial resolution of the PEP is almost independent of the source energy, as shown in Table 2.1 [2.58].

TABLE 2.1. COMPARISON OF SPATIAL RESOLUTION OF A PEP AND A CONVENTIONAL GAMMA PROBE *(Adapted from Ref. [2.58])*

Point source	Co-57	Ba-133	Na-22	Cs-137
γ ray energy	122 keV	356 keV	511 keV 1275 keV	662 keV
PEP probe (FWHM)	7 mm	9 mm	9 mm	7 mm
Conventional probe (FWHM)	18 mm	19 mm	27 mm	22 mm

Note: FWHM: full width at half-maximum; PEP: positron emission probe.

2.3.2. 3-D/2-D tracking assisted probes

An interesting development of intraoperative probes is the combination of intraoperative nuclear devices with position and orientation (‘pose’) tracking systems. Wendler et al. introduced tracking of beta probes for activity surface reconstruction, visualization and intraoperative guidance [2.59]. The β radiation considered was emitted from superficial tissue, and consequently, only an activity surface reconstruction was proposed. Benlloch et al. proposed tracking of 2-D gamma cameras and the use of 2-D acquisitions for limited 3-D intraoperative functional imaging [2.60]. In that approach, the 3-D position was reconstructed from two 2-D images taken at an angle close to 90° or three 2-D images at relative angles close to 120°.

Further work by Wendler et al. [2.61] shows a novel approach employing tracked gamma probes and algorithms for 3-D tomographic reconstruction based on gamma readings, and a synchronized 3-D pose of the detector was proposed. Image acquisition was obtained using a standard, collimated gamma probe together with an optical tracking system [2.61, 2.62]. Visualization itself can include the rendering of pre-operative PET/CT images onto the registered image of a camera using 3-D textures, where each voxel is rendered with a colour and transparency as a function of its value. During the scan, the positions of the acquired measurements are also augmented onto the scene as a point cloud (Fig. 2.3, left), and are colour coded according to the measured activity (no activity in green, and red for positions with activity). For better 3-D perception, the points can optionally be displayed as vectors, adding the missing orientation component to the visualization. Afterwards, a volume rendering of the reconstructed volume is overlaid onto the image (Fig. 2.3, right).

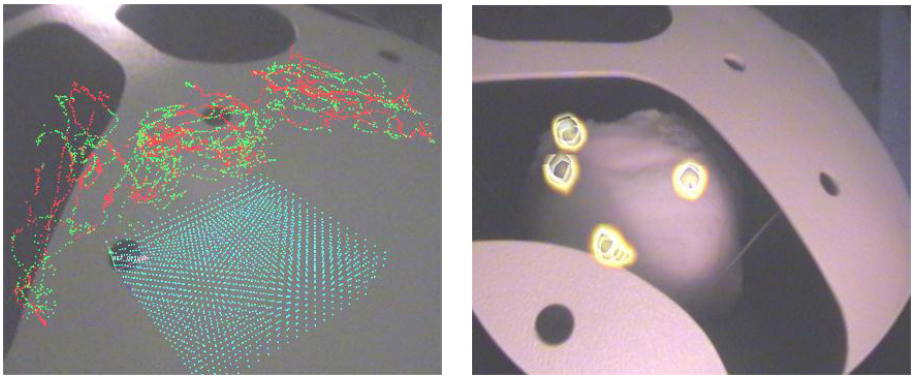

FIG. 2.3. Left: Green and red points mark the acquisition path of the gamma probe (red for active, green for inactive), and the reconstruction grid is marked in cyan. Right: Reconstructed activity distribution marked in yellow (reproduced from Ref. [2.61]).

An interesting solution was proposed by Huh et al. [2.63], where an intraoperative PET probe was equipped with a position tracker and operated in conjunction with a segment of a conventional PET scanner. Surgeons hold the probe and move it around the lesions. The goal is to provide a continuously updated 3-D reconstructed image that is reprojected in real time onto a plane whose orientation is driven by the tracking system. In parallel with ultrasound (US) imaging, this device is able to image the distribution of the radiotracer in the patient.

2.3.3. Small field portable imaging devices

Provided that non-imaging probes are still the standard equipment for detection of radiolabelled tissue in the operating room, they cannot provide further details of the source. The exact localization of a source can only be performed if the tip is under direct contact with the tissue after dissection.

On the other hand, intraoperative real time imaging using portable gamma cameras provides an overview of all radioactive hotspots in the whole surgical field [2.25, 2.64]. For instance, its position can be adjusted to also show SLNs near the injection site, which can easily be overlooked when using a non-imaging probe. Discrimination between a true SLN and a secondary tier node can be achieved using the amount of counts simultaneously recorded with the cameras, and can be related to the pre-operative scintigraphic images. The gamma camera can also be used in conjunction with the gamma probes.

Imaging devices must meet several requirements to be employed in the intraoperative setting. These include a portable and stable design, no delay

between image acquisition and display (real time imaging) and the possibilities for continuous monitoring, spatial orientation on screen, real time quantification and display of the counts recorded. Finally, they should also have adequate spatial resolution, sensitivity and FOV. While the first such cameras were heavy, hand-held devices, new generation portable gamma cameras are lighter, or equipped with stable support systems.

Among the products commercially available, only a few that implement the requirements with different approaches in the radiation detector are mentioned. One of the most widely used devices is the Sentinella 102 manufactured by GEM Imaging, Spain [2.65], which is equipped with a continuous CsI(Na) scintillating crystal readout by position sensitive PMTs and different collimators (pinhole collimators, 2.5 mm and 4 mm in diameter, and divergent). The pinhole collimators enable the visualization of the whole surgical field depending on the distance between the camera and the source. The FOV is 4 cm × 4 cm at 3 cm from the source and 20 cm × 20 cm at 15 cm from the source. This device has been integrated into a mobile and ergonomic support that is easily adjustable. The imaging head is located on one arm, which allows positioning on the specific area. Another approach is based on the use of CdZnTe as the radiation detector. For instance, in the Anzai eZ-SCOPE-Handheld Gamma Camera [2.66], the detector is fabricated using a single tile of CdZnTe, patterned in an array of 16 × 16 pixels at a pitch of 2 mm. The head is equipped with a series of interchangeable parallel hole collimators to achieve different performances in terms of spatial resolution and/or sensitivity, and pseudotomographic visualization. The FOV is 3.2 cm × 3.2 cm and the weight is 800 g.

A further development of the intraoperative gamma camera is the lumaGEM from Gamma Medica Ideas, USA [2.67]. It is still based, as is the eZ-SCOPE, on CdZnTe pixel technology and was originally developed for breast imaging. The FOV is 13 cm × 13 cm and the intrinsic spatial resolution is 2 mm. This camera is also equipped with an exchangeable parallel hole collimator and is integrated on a workstand articulated arm.

In the long run, PMT based systems will be replaced by cameras consisting of scintillators coupled with solid state photodetectors. In these solid state systems, the photodetector will be an array of photodiodes (most likely, silicon PMTs) coupled to a slab or a matrix of crystals designed to be coupled one to one to the photosensors [2.68]. In such a way, the thickness of the detector (including the crystal, photodiodes and electronics) coupled to a shallow collimator could be less than 5 cm, and it would be compact enough to be brought into a surgery room as the intraoperative imaging probe.

REFERENCES TO CHAPTER 2

[2.1] ZAVATTINI, G., DEL GUERRA, A., "Small animal scanners", Ionizing Radiation Detectors for Medical Imaging (DEL GUERRA, A., Ed.), World Scientific (2004) 385–464.

[2.2] GOORDEN, M.C., RENTMEESTER, M.C., BEEKMAN, F.J., Theoretical analysis of full-ring multi-pinhole brain SPECT, Phys. Med. Biol. **54** (2009) 6593–6610.

[2.3] FUNK, T., KIRCH, D.L., KOSS, J.E., BOTVINICK, E., HASEGAWA, B.H., A novel approach to multipinhole SPECT for myocardial perfusion imaging, J. Nucl. Med. **47** (2006) 595–602.

[2.4] FREEDMAN, N., et al., SPECT attenuation artifacts in normal and overweight persons: Insights from a retrospective comparison of Rb-82 positron emission tomography and TI-201 SPECT myocardial perfusion imaging, Clin. Nucl. Med. **25** (2000) 1019–1023.

[2.5] PATTON, J.A., TURKINGTON, T.G., SPECT/CT physical principles and attenuation correction, J. Nucl. Med. Tech. **36** (2008) 1–4.

[2.6] KINAHAN, P., HASEGAWA, B., BEYER, T., X ray based attenuation correction for PET/CT scanners, Semin. Nucl. Med. **33** (2003) 166–179.

[2.7] ANTOCH, G., et al., Accuracy of whole-body PET/CT for tumour staging in solid tumours: Comparison with CT and PET in 260 patients, J. Clin. Oncol. **22** (2004) 4357–4368.

[2.8] TOWNSEND, D.W., From 3-D positron emission tomography to 3-D positron emission tomography/computed tomography: What did we learn? Mol. Imaging Biol. **6** (2004) 275–290.

[2.9] DAUBE-WITHERSPOON, M.E., MUEHLLEHNER, G., Treatment of axial data in three-dimensional PET, J. Nucl. Med. **28** (1987) 1717–1724.

[2.10] DEFRISE, M., et al., Exact and approximate rebinning algorithms for 3D PET data, IEEE Trans. Med. Imaging **16** (1997) 145–158.

[2.11] XUAN, L., et al., Exact rebinning methods for three-dimensional PET, IEEE Trans. Med. Imaging **18** (1999) 657–664.

[2.12] MATEJ, S., et al., Evaluation of task-oriented performance of several fully 3D PET reconstruction algorithms, Phys. Med. Biol. **39** (1994) 355.

[2.13] VANDENBERGHE, S., KARP, J., Rebinning and reconstruction techniques for 3D TOF-PET, Nucl. Inst. Meth. Phys. Res. **569** (2006) 421–424.

[2.14] TOWNSEND, D.W., Multimodality imaging structure and function, Phys. Med. Biol. **53** (2008) 1–39.

[2.15] POVOSKI, S.P., et al., A comprehensive overview of radio-guided surgery using gamma detection probe technology, World J. Surg. Oncol. **7** (2009) 11.

[2.16] SELVERSTONE, B., SWEET, W.H., ROBINSON, C.V., The clinical use of radioactive phosphorus in the surgery of brain tumours, Ann. Surg. **130** (1949) 643–651.

[2.17] GEIGER, H., MÜLLER, W., Elektronenzählrohr zur messung schwächster aktivitäten, Naturwissenschaften **16** (1928) 617–618.

[2.18] HARRIS, C.C., BIGELOW, R.R., FRANCIS, J.E., KELLY, G.G., BELL, P.R., A CsI(Tl)-crystal surgical scintillation probe, Nucleonics **14** (1956) 102–108.

[2.19] WOOLFENDEN, J.M., BARBER, H.B., Radiation detector probes for tumour localization using tumour-seeking radioactive tracers, Am. J. Roentgenol. **153** (1989) 35–39.
[2.20] SCHNEEBAUM, S., et al., Clinical applications of gamma-detection probes — radio-guided surgery, Eur. J. Nucl. Med. **26** (1999) 26–35.
[2.21] BARBER, H.B., et al., Comparison of NaI(Tl), CdTe, and HgI_2 surgical probes: Physical characterization, Med. Phys. **18** (1991) 373–381.
[2.22] KWO, D.P., BARBER, H.B., BARRETT, H.H., HICKERNELL, T.S., WOOLFENDEN, J.M., Comparison of NaI(Tl), CdTe, and HgI_2 surgical probes: Effect of scatter compensation on probe performance, Med. Phys. **18** (1991) 382–389.
[2.23] THURSTON, M.O., "Development of the gamma-detecting probe for radioimmunoguided surgery", Radioimmunoguided Surgery (RIGS) in the Detection and Treatment of Colorectal Cancer, Vol. 1 (MARTIN, E.W., Ed.), Landes (1994) 41–65.
[2.24] TIOURINA, T., et al., Evaluation of surgical gamma probes for radio-guided sentinel node localization, Eur. J. Nucl. Med. **25** (1998) 1224–1231.
[2.25] HOFFMAN, E.J., TORNAI, M.P., JANECEK, M., PATT, B.E., IWANCZYK, J.S., Intra-operative probes and imaging probes, Eur. J. Nucl. Med. **26** (1999) 913–935.
[2.26] MacDONALD L.R., Imaging Research Laboratory Homepage, University Of Washington Radiology (2013), http://depts.washinghton.edu/nucmed/IRL/
[2.27] ZANZONICO, P., HELLER, S., The intra-operative gamma probe: Basic principles and choices available, Semin. Nucl. Med. **30** (2000) 33–48.
[2.28] RICARD, M., Intra-operative detection of radiolabeled compounds using a hand held gamma probe, Nucl. Instrum. Meth. Phys. Res. **458** (2001) 26–33.
[2.29] ZANZONICO, P., "The intra-operative gamma probe: Design, operation, and safety", Sentinel Lymph Node Biopsy, Vol. 1 (CODY, H.S., Ed.), Informa Health Care (2002) 45–68.
[2.30] WENGENMAIR, H., KOPP, J., Gamma Probes for Sentinel Lymph Node Localization: Quality Criteria, Minimal Requirements and Quality of Commercially Available Systems (2005), http://www.sln-kompetenzzentrum.de/gammaprobes.pdf
[2.31] MARIANI, G., VAIANO, A., NIBALE, O., RUBELLO, D., Is the "ideal" gamma-probe for intra-operative radio-guided surgery conceivable? J. Nucl. Med. **46** (2005) 388–390.
[2.32] MOFFAT, F.L., Jr., Targeting gold at the end of the rainbow: Surgical gamma probes in the 21st century, J. Surg. Oncol. **96** (2007) 286–289.
[2.33] SARIKAYA, I., SARIKAYA, A., REBA. R.C., Gamma probes and their use in tumour detection in colorectal cancer, Int. Semin. Surg. Oncol. **5** (2008) 25.
[2.34] DAGHIGHIAN, F., et al., Intra-operative beta probe: A device for detecting tissue labeled with positron or electron emitting isotopes during surgery, Med. Phys. **21** (1994) 153–157.
[2.35] RAYLMAN, R.R., WAHL, R.L., A fiber-optically coupled positron-sensitive surgical probe, J. Nucl. Med. **35** (1994) 909–913.

[2.36] RAYLMAN, R.R., WAHL, R.L., Evaluation of ion-implanted-silicon detectors for use in intra-operative positron-sensitive probes, Med. Phys. **23** (1996) 1889–1895.
[2.37] RAYLMAN, R.R., A solid-state intra-operative beta probe system, IEEE Trans. Nucl. Sci. **47** (2000) 1696–1703.
[2.38] YAMAMOTO, S., et al., An intra-operative positron probe with background rejection capability for FDG-guided surgery, Ann. Nucl. Med. **19** (2005) 23–28.
[2.39] VALDÉS OLMOS, R.A., et al., The GOSTT concept and hybrid mixed/virtual/augmented reality environment radioguided surgery, Q. J. Nucl. Med. Mol. Imaging, **58** 2 (2014) 207–15.
[2.40] W.O.M. WORLD OF MEDICINE AG, Gamma Finder II (2014), http://www.gammafinder.com/en/
[2.41] SCHILLACI, O., PET probes and oncological surgery: A productive new marriage for nuclear medicine? Eur. J. Nucl. Med. Mol. Imaging **34** (2007) 1530–1533.
[2.42] FRANC, B.L., MARI, C., JOHNSON, D., LEONG, S.P., The role of a positron- and high-energy gamma photon probe in intra-operative localization of recurrent melanoma, Clin. Nucl. Med. **30** (2005) 787–791.
[2.43] GULEC, S.A., DAGHIGHIAN, F., ESSNER, R., PET-probe: Evaluation of technical performance and clinical utility of a handheld high-energy gamma probe in oncologic surgery, Ann. Surg. Oncol. (2006) DOI: 10.1245/ASO.2006.05.047.
[2.44] GULEC, S.A., HOENIE, E., HOSTETTER, R., SCHWARTZENTRUBER, D., PET probe-guided surgery: Applications and clinical protocol, World J. Surg. Oncol. **5** (2007) 65.
[2.45] GULEC, S.A., PET probe-guided surgery, J. Surg. Oncol. **96** (2007) 353–357.
[2.46] MELLER, B., et al., Conventional gamma and high energy probe for radio-guided dissection of metastases in a patient with recurrent thyroid carcinoma with ^{99m}Tc-MIBI and ^{18}F-FDG, Nuklearmed. **44** (2005) 23–25.
[2.47] ESSNER, R., et al., Application of an [^{18}F]fluorodeoxyglucose-sensitive probe for the intraoperative detection of malignancy, J. Surg. Res. **96** (2001) 120–126.
[2.48] NWOGU, C., et al., Radio-guided detection of lymph node metastasis in non-small cell lung cancer, Ann. Thor. Surg. **82** (2006) 1815–1820.
[2.49] DESAI, D.C., et al., Positron emission tomography affects surgical management in recurrent colorectal cancer patients, Ann. Surg. Oncol. **10** (2003) 59–64.
[2.50] PIERT, M., et al., Positron detection for the intra-operative localisation of cancer deposits, Eur. J. Nucl. Med. Mol. Imaging **34** (2007) 1534–1544.
[2.51] PIERT, M., CAREY, J., CLINTHORNE, N., Probe-guided localization of cancer deposits using [^{18}F]fluorodeoxyglucose, J. Nucl. Med. Mol. Imaging **52** (2008) 37–49.
[2.52] MARAMRAJU, S.-H., et al., LSO beta microprobe for measurement of input functions in small animal PET, J. Nucl. Med. Meeting Abstracts **47** (2006) 53.
[2.53] STRONG, V.E., et al., Portable PET probes are a novel tool for intraoperative localization of tumour deposits, Ann. Surg. Innov. Res. **3** (2009) 2.
[2.54] MOSES, W.W., Overview of Nuclear Medical Imaging Instrumentation and Techniques (BROSS, A.D., RUCHTI, R.C., WAYNE, M.R., Eds), AIP Conf. Proc. **450** (1998) 450–477.

[2.55] LEVIN, C.S., TORANI, M.P., MacDONALD, L.R., HOFFMAN, E.J., Annihilation gamma-ray background characterization and rejection for a small beta ray camera imaging positron emitters, IEEE Trans. Nucl. Sci. **44** (1997) 1120–1126.

[2.56] BÄRWOLFF, H., GOEBEL, T., HUG, O., LANGE, D., Vorrichtung und Verfahren zur Bestimmung der Position eines Positronenemitters in einem Material, Patent no. DE 10112297 A1.

[2.57] MELLER, B., et al., High energy probe for detecting lymph node metastases with ^{18}F-FDG in patients with head and neck cancer, Nuklearmed. **45** (2006) 153–159.

[2.58] SONDA INTRACHIRURGICA PET, Accessori per Radiologia — Sistemi di Schermature Antix (2014), www.europrotex.com

[2.59] WENDLER, T., TRAUB, J., ZIEGLER, S.I., NAVAB, N., "Navigated three dimensional beta probe for optimal cancer resection", Proc. Medical Image Computing and Computer-Assisted Intervention, Vol. 1 (2006) 565–569.

[2.60] BENLLOCH, J.M., et al., The Gamma Functional Navigator, IEEE Trans. Nucl. Sci. **51** (2004) 682–689.

[2.61] WENDLER, T., et al., Towards intra-operative 3D nuclear imaging: Reconstruction of 3D radioactive distributions using tracked gamma probes, Med. Image Comput. Comput. Assist. Interv. **10** (2007) 909–917.

[2.62] WENDLER, T., et al., "Real-time fusion of ultrasound and gamma probe for navigated localization of liver metastases", Proc. 10th Int. Conf. Medical Image Computing and Computer-Assisted Intervention (MICCAI) (2007) 252–260.

[2.63] HUH, S.S., ROGERS, W.L., CLINTHORNE, N.H., An investigation of an intra-operative PET imaging probe, Nuclear Science Symp. Conf. Record, NSS IEEE (2007) 552–555.

[2.64] VERMEEREN, L., et al., Sentinel node detection in head and neck malignancies: Innovations in radio-guided surgery, J. Oncol. **2009** (2009) 681746.

[2.65] ONCO VISION, Homepage (2014), http://www.gem-imaging.com/

[2.66] MED WOW, Manufacturer Specifications - eZ-SCOPE (2014), http://www.medwow.com/med/gamma-camera-scanning/jrt-associates/ez-scope/28817.model-spec

[2.67] GAMMA MEDICA, The LumaGEM Molecular Breast Imaging System (2013), http://www.gm-ideas.com/

[2.68] HECKATHORNE, E., TIEFER, L., DAGHIGHIAN, F., DAHLBOM, M., Evaluation of arrays of silicon photomultipliers for beta imaging, Nuclear Science Symp. Conf. Record, NSS IEEE (2008) 1626–1631.

3. RADIOPHARMACEUTICALS FOR GOSTT

3.1. GENERAL BACKGROUND

A radiopharmaceutical is a radioactive compound, with peculiar chemical, physical and biological characteristics, that allows the tracing of specific biological interactions resembling those of endogenous ligands. According to its chemical nature, it can therefore provide information about a specific biological process and is typically administered in very small mass amounts (<100 μg), so that it does not induce any physiological responses or pharmacological effects in patients. Evaluating its in vivo distribution (usually by external imaging) therefore allows exploration of the pathophysiological changes occurring in various disease conditions, without disturbing the function of the biological system to be evaluated.

The nuclear medicine equipment commonly employed for diagnostic purposes (based on either single photon detection or coincidence detection of the pair of photons generated by the annihilation event that follows positron emission) elaborates the physical signals to produce functional images that represent the distribution in space and time of the radiopharmaceutical in the different regions of the body. According to their type of emission, radiopharmaceuticals can also be employed for therapeutic purposes, based on deposition of energy in a very short range, as in the case of radionuclides emitting β^- particles or α^{++} particles that deliver a cytocidal radiobiological effect in a specific target tissue, such as a tumour tissue.

In particular, radiations suitable for use in nuclear medicine are represented by emission of γ rays (on which conventional scintigraphic imaging is based, either planar or SPECT), emission of β^- particles (for therapeutic purposes) and emission of β^- particles (on which imaging with PET is based). The use of radionuclides emitting α^{++} particles is also emerging because it shows high potential for therapeutic applications.

The concept of a radiopharmaceutical can be considered as derived from the original definition of ‘radiotracer’ experimentally introduced by the work of George De Hevesy. Initially, β^- emitting radionuclides were used as therapeutic agents (e.g. ^{32}P phosphate for treating polycythaemia vera and leukaemias, or ^{131}I iodide for thyroid disease). After the development of the first scintillation scanner by Benedict Cassen and owing to its associated emission of γ rays, ^{131}I was also introduced as a radiotracer for diagnostic imaging purposes, e.g. ^{131}I labelled human serum albumin for assessing the integrity of the blood–brain barrier, etc. Impetus to the growth of nuclear medicine came after the introduction of the Anger camera and the development of the first ^{99}Mo/^{99m}Tc generator in the late

1950s, introduced into clinical practice in 1963. Thus, the search for the 'ideal radionuclide' became a novel target for radiochemistry and radiopharmacology, in an attempt to identify different substances that could be labelled with ^{99m}Tc and retain their ability to concentrate in different organs and to characterize specific biological processes; this procedure is denoted 'functional imaging'. The recent advent of PET technology, which yields better spatial resolution and, in general, better contrast images than single photon emission imaging, has stimulated the development of a new cluster of β^+ emitting radionuclides. The most widely used PET radionuclides are currently ^{18}F, ^{11}C, ^{13}N and ^{15}O (which are cyclotron produced), and also ^{68}Ga and ^{82}Rb (which are produced by a generator, see below).

Radiopharmaceuticals can be administered by different routes, usually intravenously, less frequently by oral, interstitial, intracavitary or even intra-arterial routes (see Table 3.1). The main parameters that determine the scintigraphic information are the rate of disappearance (or clearance) from blood, and the kinetics of accumulation, retention and washout in a specific tissue/organ of interest. These parameters reflect physiological changes of function or metabolism in specific areas of the body.

TABLE 3.1. MAIN FEATURES OF RADIOPHARMACEUTICALS USED FOR GOSTT PROCEDURES

Route of administration	Radiopharmaceutical	Indication(s)
Local		
Interstitial	Tc-99m nanocolloid	Lymphoscintigraphic mapping for radioguided sentinel node biopsy
—	Tc-99m MAA	ROLL for breast cancer and other tumours
Intra-arterial	Tc-99m MAA	Radiodosimetry estimates for radioembolization of liver tumours
—	I-131/Tc-99m albumin	Systemic leakage during isolated limb perfusion for anticancer therapy
—	Tc-99m PYP erythrocytes	Systemic leakage during isolated limb perfusion for anticancer therapy

TABLE 3.1. MAIN FEATURES OF RADIOPHARMACEUTICALS USED FOR GOSTT PROCEDURES (cont.)

Route of administration	Radiopharmaceutical	Indication(s)
Systemic		
—	Tc-99m sestamibi	Pre-operative localization and radioguided surgery of parathyroid tumours
—	In-111 pentetreotide	Radioguided surgery of NETs and other SSTR expressing tumours
—	[I-123]MIBG	Radioguided surgery of NETs
—	I-131/I-123 iodide	Radioguided surgery of local recurrences from differentiated thyroid cancer
—	Tc-99m diphosphonate	Radioguided biopsy of isolated bone metastasis from unknown primaries
—	[F-18]FDG	Radioguided surgery of occult tumour lesions
—	Ga-68 DOTA TOC/NOC	Radioguided surgery of NETs and other SSTR expressing tumours

DOTA NOC: 1-NAI3-octreotide; DOTA TOC: Tyr3-octreotide; FDG: fluorodeoxyglucose; GOSTT: guided intraoperative scintigraphic tumour targeting; MAA: macroaggregate of human albumin; MIBG: metaiodobenzylguanidine; NET: neuroendocrine tumour; PYP: pyrophosphate; ROLL: radioguided occult lesion localization; SSTR: somatostatin receptor.

The radiolabelling process consists of a chemical reaction through which the radionuclide is linked or incorporated into the carrier molecule of biological interest. The availability and suitability of radiopharmaceuticals to target specific biological functions and/or structures depend on the feasibility of radiolabelling for any given compound of biological interest; at the same time, the radiolabelling process should be designed so as not to alter interactions of the molecule with its target in tissues/organs.

The radiopharmaceuticals most widely employed in nuclear medicine can be classified on the basis of their mechanism of localization, such as capillary blockade, phagocytosis, ion exchange and chemiabsorption, membrane transport (simple, facilitated and active transport), enzyme mediated intracellular trapping, competitive substrates, receptor mediated probes or immune mediated binding.

The most important radionuclides used in nuclear medicine (both for single photon and for PET imaging) and their main physical characteristics are summarized in Table 3.2.

TABLE 3.2. MAIN PHYSICAL CHARACTERISTICS OF THE MOST COMMONLY EMPLOYED RADIONUCLIDES FOR DIAGNOSTIC NUCLEAR MEDICINE APPLICATIONS

Radionuclide	Half-life	Energy (keV)	Emission
Tc-99m	6.06 h	142	γ
I-131	196.8 h	284, 364, 637 810	γ β^-
I-123 [a]	12.8 h	159	γ Auger β^-
In-111 [a]	67.9 h	172, 245	γ Auger β^-
Tl-201 [a]	72 h	135–167 69–83	γ X ray
Ga-67 [a]	78.3 h	93, 185, 296	γ
F-18	109.8 min	634	β^+
C-11	20.4 min	1982	β^+
Ga-68	68.3 min	770, 1880	β^+
I-124	4.18 d	603, 2130	β^+, γ

[a] Decays also with electron capture and secondary emission of a characteristic X ray.

3.2. RADIONUCLIDES MOST COMMONLY EMPLOYED FOR SINGLE PHOTON EMISSION IMAGING IN ONCOLOGY

3.2.1. Technetium-99m

Technetium-99m is obtained directly by elution from a $^{99}Mo/^{99m}Tc$ generator in the chemical form of pertechnetate, which can be used either as a radiopharmaceutical by itself (e.g. thyroid scintigraphy, salivary scintigraphy and scintigraphic localization of ectopic gastric mucosa) or for radiolabelling more complex molecules to form new radiopharmaceuticals.

Technetium-99m is currently employed for over 85% of diagnostic nuclear medicine applications, owing to its especially favourable physical and biochemical characteristics. It emits γ rays at an energy that is suitable for imaging with today's gamma cameras (140 keV), it has a short physical half-life (6 h), its cost is low and it causes minimal problems for radioactive waste management; a generator can supply as much radioactivity as is necessary for a day in a nuclear medicine centre.

Upon elution from the $^{99}Mo/^{99m}Tc$ generator with physiological saline, ^{99m}Tc is obtained as pertechnetate anion ($[^{99m}TcO_4]$); this stable coordination compound has a very compact structure with the highest possible oxidation state. By using a reducing agent (generally a stannous ion), it is possible to remove the oxygen atoms bound to the metal and to replace them with new ligand coordinated atoms or a chelating agent (e.g. diethylene triamine pentaacetic acid (DTPA)) that has been preattached to the biological molecule to be labelled.

Technetium-99m pertechnetate could be used as a radiopharmaceutical. In fact, following intravenous administration, the pertechnetate ions accumulate in the thyroid, stomach, salivary glands, intestine, choroid plexus, mucous membranes in general (especially in the presence of exocrine glands) and kidneys, where most of the excretion takes place.

It is commonly used for thyroid imaging because of its similarity to the iodide ion in terms of mass, size and charge density. The $[^{99m}TcO_4]$ enters the thyroid follicular cells through the sodium iodide symporter (NIS), which is a transmembrane protein with an active transport mechanism located in the basolateral membrane that is able to transport simultaneously sodium and iodide from the extracellular space. The extraction of iodine from plasma takes place against an electrochemical gradient (the intracellular concentration of iodine is 20–40 times higher than in plasma) and requires energy that is ensured by the Na/K dependent ATPase system. Unlike the iodide ion, once inside the thyroid cell $[^{99m}TcO_4]$ does not undergo subsequent organification as iodide does to initiate the synthesis of thyroid hormones.

The injected activity is approximately 185 MBq, and generally static acquisitions with a pinhole collimator usually start 20 min after intravenous administration.

3.2.2. Radioiodine

There are several nuclear medicine agents labelled with radioiodine, and the availability of different iodine radioisotopes with different characteristics has contributed to this wide spectrum of clinical applications. The radioiodine isotopes most commonly used in clinical practice are:

— Iodine-131 (γ and β^- emitter), which is historically one of the first radionuclides used for both conventional diagnostic imaging and for therapeutic applications;
— Iodine-123 (γ emitter), which is used especially for conventional diagnostic imaging owing to a low dosimetry burden to patients because of either its short physical half-life (12.8 h) and its emission of γ photons with relatively low energy (159 keV) that are optimal for gamma camera imaging;
— Iodine-125 (emitter of γ photons and Auger β− particles), which is widely employed for laboratory applications and for in vitro investigations (e.g. radioimmunological techniques) because of its very low energy γ photons (35 keV) that are not suitable for imaging; it is also used for biodistribution studies in animal models of disease and for early stage trials in humans.

In addition to these single photon emitting radioisotopes of iodine, the availability of ^{124}I (β^+ emitter) has opened new avenues to the use of radioiodine, by combining the advantages of advanced PET imaging technology with the advantages derived from the biochemical knowledge gained with conventional radioisotopes of iodine (see below).

Both ^{123}I and ^{131}I can be used in the simple chemical form of sodium iodide for investigations and/or treatment of patients with thyroid diseases, or linked to more complex molecules through chemical reactions (nucleophilic or electrophilic substitution); each one of the radiopharmaceuticals so obtained exhibits a specific biodistribution pattern dictated by the chemical structure of the radioiodinated molecule.

When administered in the chemical form of iodide, the ^{123}I or ^{131}I ions are transported into the thyroid cells by the NIS system. Once inside the thyroid cell, iodine is oxidized by the enzyme peroxidase; this reaction starts the organification process that enables incorporation of iodine (either native or radioactive) into tyrosine, which is an amino acid contained in the thyroglobulin

molecules produced by the endoplasmic reticulum and the Golgi apparatus. Molecules of monoiodotyrosine and diiodotyrosine are thus formed. These two chemical species are then combined to produce the thyroid hormones thyroxine and triiodothyronine. Thyroid hormones are finally secreted into the circulation by pinocytosis, following stimulation by thyroid stimulating hormone (TSH). Because of this organification, radioiodine still represents the optimal physiological agent for thyroid imaging, in particular, ^{123}I iodide has ideal characteristics for this purpose, with a high thyroidal uptake over the background (activity injected in a 70 kg adult patient is 12–15 MBq, and images are acquired 3–6 h after administration). However, limited availability and high costs restrict the use of ^{123}I iodide to a few clinical conditions, while ^{99m}Tc pertechnetate is used in thyroid scintigraphy in the majority of cases with benign thyroid disease, and ^{131}I iodide for cancer thyroid studies. In the latter case, ^{131}I iodide is currently used for measuring uptake as a preliminary phase prior to therapy (both for hyperthyroidism and for differentiated thyroid cancer); uptake is measured after administering only 1.85 MBq, while an activity of 185 MBq is administered during follow-up of patients with differentiated thyroid cancer for total body scintigraphy. In both cases, the radiopharmaceutical is generally administered orally as a capsule, while in paediatric patients or in patients with swallowing problems, a liquid formulation is also available, to be administered either orally or intravenously.

The most important radioiodinated radiopharmaceutical in oncology is metaiodobenzylguanidine (MIBG), labelled with either ^{123}I (for diagnostic applications) or ^{131}I (mostly for therapeutic applications (see below)).

3.2.3. Indium-111

The radiometal ^{111}In is produced using a cyclotron. Indium-111 has a physical half-life of 2.83 d and emits γ rays with energies of 172 keV and 247 keV (in addition to a 23–26 keV X ray emission). In conventional nuclear medicine, it is used to radiolabel specific target molecules, usually based on the use of chelating molecules such as DTPA or DOTA. The most important radiopharmaceutical labelled with ^{111}In used in oncology is ^{111}In pentetreotide, which is employed for imaging neuroendocrine tumours (NETs) (see below).

3.2.4. Thallium-201

The monovalent cation Tl^+ has biochemical characteristics similar to the K^+ ion. Thallium-201 decays by electron capture with a physical half-life of 73.1 h and emission of X rays with 68–80 keV energy. In addition to its original application for myocardial perfusion imaging, ^{201}Tl ions tend to accumulate also

in all metabolic active cells, including cancer cells. For this reason, ^{201}Tl chloride is still used in tumour imaging as an indicator of cell viability, particularly to discriminate viable tumour tissue from non-tumour tissue after therapy (surgery or external radiation), especially in cerebral tumours (gliomas).

3.2.5. Gallium-67

The biodistribution properties of ^{67}Ga citrate were initially identified in the late 1960s, while searching for a bone seeking agent. Following its introduction into clinical practice in 1969, ^{67}Ga citrate has had a well defined role in staging, prognosis and evaluation of residual disease in lymphoma and soft tissue sarcoma, in inflammatory diseases and fevers of unknown origins. Nowadays, while many of the conventional uses of scintigraphy with ^{67}Ga citrate have been replaced by the introduction of PET techniques using new radiopharmaceuticals, some non-oncological specific indications are still valid, particularly for assessing the degree of sarcoid activity, and to visualize infective foci at specific locations, such as vertebral osteomyelitis.

3.3. MAIN RADIOPHARMACEUTICALS EMPLOYED FOR GOSTT APPLICATIONS

3.3.1. Technetium-99m radiocolloids

Originally introduced to perform hepatosplenic and bone marrow scintigraphy following intravenous administration, radiolabelled colloids are used nowadays for imaging SLNs in radioguided surgery (following interstitial administration). The definition of ‘colloid’ includes a wide class of particles, both organic and inorganic, with sizes between 1 nm and approximately 4 μm and are generally removed by macrophages through phagocytosis. Although macrophages are ubiquitous cells, they are concentrated mostly in the reticuloendothelial system, especially in the liver, spleen, bone marrow and LNs.

There are different kinds of radiocolloids, and the most frequently used consist of ^{99m}Tc labelled albumin based colloids ranging in size between 30 nm and 1000 nm (i.e. 0.03–1 μm). From the site of interstitial injection, radiocolloids migrate through the lymphatic system; in fact, their size prevents them from entering the venous blood capillaries and therefore they drain through the lymphatic route and reach LNs, the first of which is called the ‘sentinel lymph node’. Once inside such LNs, the radiocolloids are engulfed by macrophages lining the sinusoidal spaces, thus allowing subsequent imaging and/or detection using a hand-held intraoperative gamma probe.

If the injection is performed at the site (or near the site) of a tumour, it is reasonable to assume that the SLN is the lymphatic station that tumour cells would first reach in case of lymph nodal metastasis draining from that specific tumour region. Radioguided biopsy of SLN(s) in breast cancer and melanoma patients, which is now routinely performed worldwide, is based on this mechanism.

The ideal radiopharmaceutical for radioguided SLNB should allow for easy visualization of the first LN draining from the tumour/injection site, possibly without further migration to higher echelon nodes. Radiocolloids with relatively large particles (200–300 nm) possess efficient retention in the first LN encountered along the migration route, with very little progression to higher echelon nodes; however, they migrate too slowly to obtain good scintigraphic imaging in a relatively short time. Because the speed of migration of radiocolloids injected interstitially is inversely related to particle size, some compromise must be found between the speed of lymphatic migration and the degree of phagocytosis of the colloidal particles in LNs.

The radiocolloid most frequently used in Europe (^{99m}Tc albumin nanocolloid) is made up of particles mostly smaller than 80 nm in size, and represents a good compromise between speed of migration and degree of LN retention. Other radiocolloids (mostly inorganic) have been developed and are commercially available, such as ^{99m}Tc sulphur rhenium colloid, with particle sizes ranging from 100 nm to 1000 nm (used mostly in the USA), and ^{99m}Tc sulphur colloids, with particle sizes ranging between 3 nm and 30 nm (used mostly in Canada).

According to the specific application and time elapsed between lymphoscintigraphy and surgery, the administered activities, number of injected aliquots and site of injection could vary both in melanoma and in breast cancer.

3.3.2. Technetium-99m MAAs

Radiolabelled macroaggregates of human albumin (MAAs) were first introduced into clinical practice in the 1960s (labelled initially with ^{131}I), and were primarily used for lung perfusion scintigraphy following systemic intravenous injection for the diagnosis of pulmonary embolism. They consist of human albumin particles of irregular sizes that range between 10 μm and 90 μm (with no particles larger than 150 μm). After systemic intravenous injection, they are trapped in the pulmonary capillaries that have a smaller diameter than the size of the MAAs themselves. This microembolization involves approximately 0.1% of all the pulmonary capillary bed, a negligible fraction of pulmonary circulation that does not pose any risk to the patient from the clinical point of

view. The particles lodged in the pulmonary capillary bed are then removed with an effective half-life of 2–3 h through enzymatic degradation and fragmentation into smaller particles because of the mechanical movement of the lung. After this fragmentation, they are then ingested by macrophages of the reticuloendothelial system and removed through the lymphatic vessels, resulting in the radioactivity finally being excreted in the urine.

Because of their relatively large size, upon interstitial injection, ^{99m}Tc MAAs do not migrate through lymphatic drainage as radiocolloids do. Instead, they are retained virtually indefinitely at the site of interstitial administration. For this reason, a further indication for the use of ^{99m}Tc MAA is represented by radioguided surgery for radioguided occult lesion localization (ROLL). Application of this technique is continuously increasing in clinical practice, after its original introduction specifically for breast cancer. In fact, following interstitial administration, this radiopharmaceutical is able to remain inside the site of injection (e.g. a tumour or a suspected lesion), therefore representing, for several hours after administration, a 'radiomarker' that the surgeon can follow in the operating theatre with the help of an intraoperative gamma probe or a portable mini gamma camera. Intralesional administration is, in general, performed under US or CT guidance, especially in those very small tumours that could not be directly recognized by the surgeon (e.g. non-palpable microcalcification in breast cancer or metastatic small LNs in thyroid cancer).

The MAAs are produced industrially simply by heating a solution of human serum albumin at a temperature of 80–90°C for 30 min. The number of particles varies from 1 million to 16 million particles per milligram of aggregated albumin. Commercial kits contain MAAs in lyophilized form and tin tartrate or chloride dihydrate and hydrochloric acid or sodium hydroxide to balance the pH, and labelling is simply performed by adding ^{99m}Tc pertechnetate and leaving to incubate at room temperature for a few minutes. This preparation is stable for several hours, but before withdrawing each aliquot for injection, the vial should be gently shaken.

3.3.3. Technetium-99m sestamibi

Technetium-99m hexakis methoxy isobutyl isonitrile (^{99m}Tc sestamibi) is a positively charged lipophilic radiopharmaceutical whose chemical structure consists of a central atom of technetium linked to six octahedral ligands (see Fig. 3.1). Formation of ^{99m}Tc sestamibi occurs through the reaction of ^{99}Tc pertechnetate with isonitrile ligands, in the presence of stannous ions.

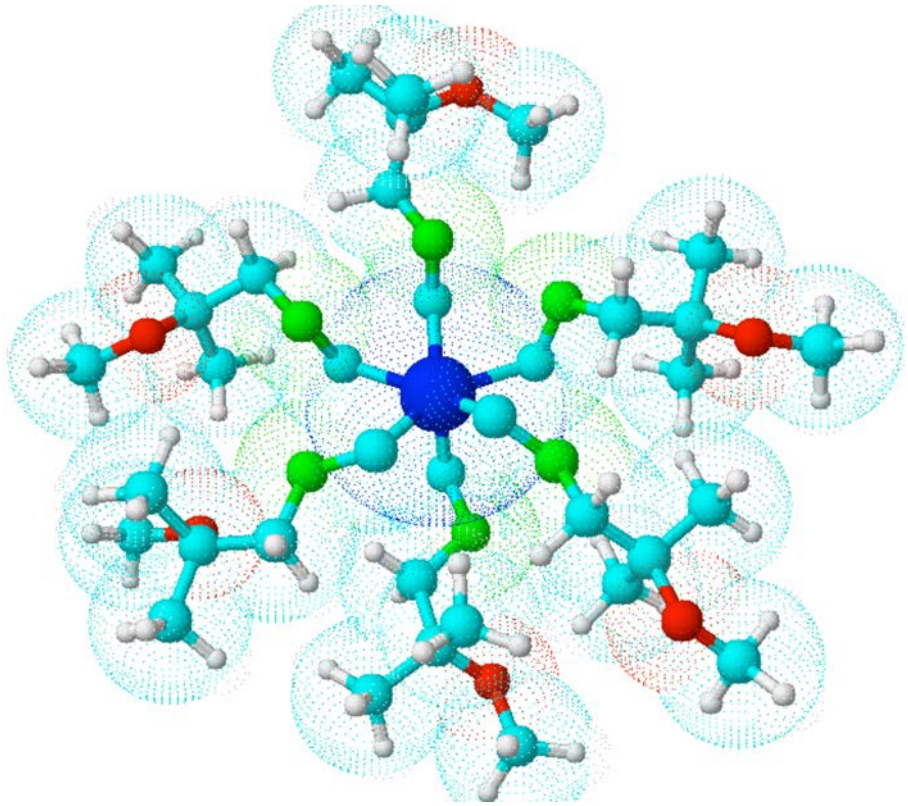

FIG. 3.1. 3-D representation of the chemical structure of ^{99m}Tc sestamibi. The blue atom at the centre of the 3-D structure represents ^{99m}Tc. Other elements are represented with the following colour codes: red = O; white = H; light blue = C; green = N.

This radiopharmaceutical was originally introduced into clinical routine for myocardial perfusion scintigraphy and still represents, together with ^{99m}Tc tetrofosmin, the radiopharmaceutical of choice for myocardial perfusion scintigraphy. After intravenous administration, ^{99m}Tc sestamibi diffuses rapidly in the extracellular spaces, then crosses cell membranes by passive diffusion (because of its lipophilicity) following a concentration gradient with subsequent trapping by mitochondria as a result of the interaction of its positive charge with the mitochondrial membrane negative electrical gradient. Its uptake and retention depends on regional blood flow, cell viability, cell density, cell membrane potential, metabolic activity and mitochondrial density/activity. In fact, intracellular retention of ^{99m}Tc sestamibi occurs via active accumulation in the mitochondria, subcellular organelles that are particularly abundant in cells with high energy demand, as myocardiocytes and tumour cells typically are, in general. Further

clinical diagnostic applications of ^{99m}Tc sestamibi emerged following occasional observations of high uptake in various solid tumours. The use of ^{99m}Tc sestamibi has therefore been approved also for mammoscintigraphy, performed with the aim of evaluating suspicious breast masses. Furthermore, it is also employed for scintigraphic evaluation of the degree of bone marrow infiltration in patients with multiple myeloma. Finally, this agent is the radiopharmaceutical of choice for parathyroid scintigraphy owing to its different washout kinetics from the thyroid and from the hyperfunctioning parathyroid tissue.

After intravenous administration, ^{99m}Tc sestamibi undergoes a rapid blood clearance, so that only 8% of the administered activity remains in the circulation 5 min post-injection. It is then excreted through both the hepatobiliary system (33% at 48 h) and the urine (27% at 24 h).

3.3.4. MIBG

Radioiodinated MIBG (or iobenguane) is a catecholamine analogue in which the iodinated benzyl group of bretylium is combined with the guanidine group of guanethidine (see Fig. 3.2). It was developed in the early 1980s to visualize tumours of the adrenal medulla, and it can be labelled either with ^{123}I (for diagnostic use only) or with ^{131}I (for use in either diagnostic or therapeutic applications).

Because of its structural analogy with catecholamines, MIBG is taken up by chromaffin cells through an active uptake mechanism physiologically via the ephinephrine transporter used for non-adrenaline accumulation in neurosecretory granules. MIBG is then secreted through an exocytosis mechanism following depolarization induced by a high transmembrane flux of calcium ions. This accumulation process is abundantly expressed in the sympathetic ganglia, in the adrenal medulla and in all tissues with high adrenergic innervations (myocardium, salivary glands). Scintigraphic visualization of the thyroid is possible due to free radioactive I^- that is released during in vivo degradation of the radiopharmaceutical. For this reason, a thyroid blocking agent (either supersaturated potassium iodide solution or a similar preparation) is usually administered to patients, especially when using [^{131}I]MIBG rather than [^{123}I]MIBG.

The intensity of MIBG uptake in pathological tissues depends on the extent of accumulation and on local turnover of the radiopharmaceutical. In fact, MIBG does not bind to postsynaptic adrenergic receptors and is not degraded by the enzymes normally degrading catecholamines, i.e. monoamino oxidase and catecholamine-O-methyltransferase. Background activity seen in the scintigraphic images is derived from non-specific passive diffusion of MIBG throughout all tissues and fluids, and also from the binding of MIBG to circulating platelets (early post-administration).

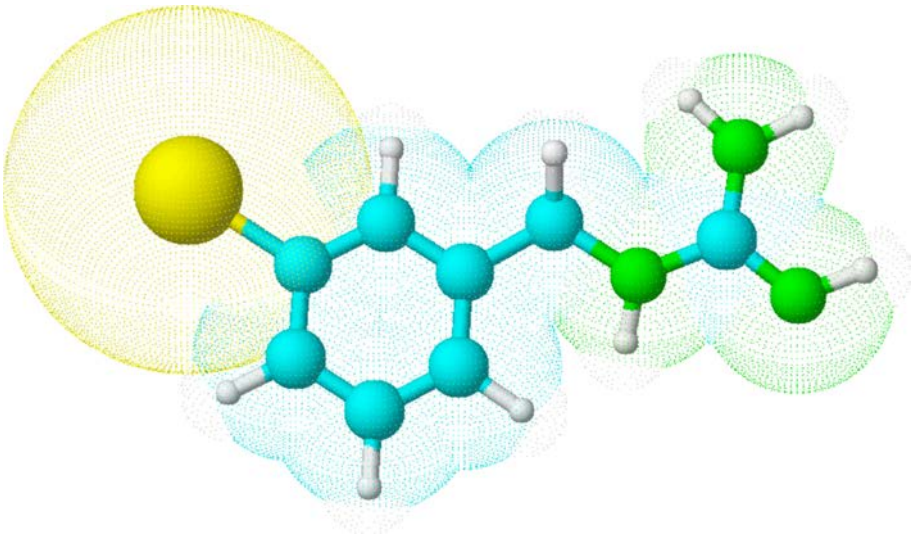

FIG. 3.2. 3-D representation of the chemical structure of MIBG. The yellow atom at the left of the 3-D structure represents radioiodine. Other elements are represented with the following colour codes: white = H; light blue = C; green = N.

Tumours that typically accumulate this radiopharmaceutical are NETs originating from the neural crest. The main clinical applications of MIBG scintigraphy are therefore detection, localization, staging, follow-up and response to therapy of NETs and their metastases, particularly in those of the sympathoadrenal system such as pheochromocytoma, paraganglioma and neuroblastoma. Nevertheless, other NETs, such as medullary thyroid carcinoma and carcinoids, can also be visualized. MIBG scintigraphy is also crucial to assess the extent of uptake by tumour lesions when planning treatment with high activities of [^{131}I]MIBG, as well as to assess the response to therapy.

[Iodine-123]MIBG is the radiopharmaceutical of choice for diagnostic applications (especially in paediatric patients), both because of its more favourable radiation dosimetry and because of the more favourable imaging properties compared to [^{131}I]MIBG.

The radiopharmaceutical is usually administered through intravenous injection. Approximately half of the administered activity is excreted into the urine within the first day, with 70%–90% of the activity being cumulatively excreted within 2 d, so that kidneys, the bladder and the excretory system can be intensely visualized, even in delayed scans. Approximately 3% of MIBG excretion occurs via the gastrointestinal tract.

Radiopharmaceutical administration must be performed very slowly (over 1–5 min in the case of a diagnostic procedure, over 1–4 h after dilution

in 50 mL of saline in the case of therapy) because it may induce the release into circulation of catecholamines previously accumulated in neurosecretory granules, with possible pharmacological effects (e.g. tachycardia and hypertensive crisis).

Free radioiodine produced during in vivo MIBG degradation can accumulate in the thyroid (if the patient has not been adequately prepared with a thyroid blockade) and the gastrointestinal tract. In 15% of cases, low tracer accumulation can be visualized in normal adrenal glands in images acquired 48–72 h after injection.

The standard activity administered to adult patients is 40–80 MBq for [^{131}I] MIBG and 370 MBq for [^{123}I]MIBG. In paediatric patients, the administered activities must be reduced according to body weight. Moreover, because many drugs can interfere with MIBG uptake, attention should be paid to ensure that treatment with these drugs is discontinued for an appropriate period before MIBG administration.

3.3.5. Indium-11 pentetreotide

NETs are characterized by the presence of peptide receptors at the cell membrane, particularly the somatostatin receptors (SSTRs). Somatostatin (SST) is a 14 amino acid peptide produced in different organs and/or tissues with different physiological functions, including inhibition of secretion of various hormones (e.g. insulin and glucagon) and also inhibition of cell growth in general.

Because native SST has a very short biological half-life (approx. 3 min), which limits its use as a therapeutic drug in vivo, different SST analogues have been radiolabelled with diagnostic radionuclides as well as with particle emitters for targeted radionuclide therapy. Five specific SSTR subtypes (SSTR1–SSTR5) with different tissue distributions and affinities for SST analogues have been identified and cloned. They are also expressed in peritumoural vessels and in inflammatory and immune cells, which can account for visualization of those tumours whose cells do not express the receptors (i.e. non-small-cell lung cancer). The most commonly used SST analogue (with a biological half-life much longer than that of native SST) is octreotide, which has a high affinity to SSTR2 and SSTR5, expressed on the cell membrane of many tumours of different origins, especially of NETs.

The presence of a chelating group (DTPA) in DTPA D-Phe^{1}-octreotide (pentetreotide) makes radiolabelling with ^{111}In possible (see Fig. 3.3). The radiopharmaceutical ^{111}In pentetreotide has the commercial name OctreoScan.

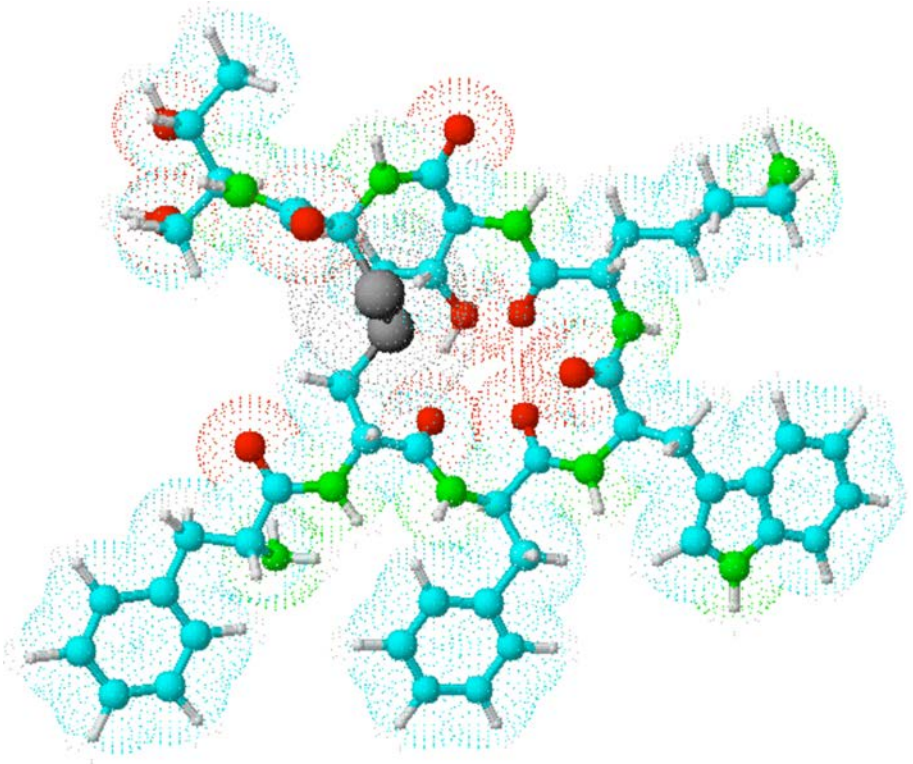

FIG. 3.3. 3-D representation of the chemical structure of pentetreotide. The radionuclide chelated to DTPA (lower left part of the 3-D structure) is not represented here. Other elements are represented with the following colour codes: red = O; white = H; light blue = C; green = N; grey = S.

OctreoScan scintigraphy is employed primarily in patients with NETs (especially gastroenteropancreatic and carcinoid tumours) for localization, staging and follow-up of lesions expressing SSTRs. Increased expression of SSTRs occurs also in tumours originating from the neural crest (paragangliomas, neuroblastomas, pheochromocytomas, medullary thyroid carcinomas) as well as in pituitary tumours and in meningiomas. Varying degrees of SSTR expression are also observed in non-neuroendocrine tumours, such as breast cancer and some lymphomas (both Hodgkin's and non-Hodgkin's lymphomas). Finally, increased SSTR expression occurs even in non-neoplastic disorders, especially in subacute and chronic inflammation (mainly of the granulomatous type, as in sarcoidosis).

OctreoScan mainly undergoes renal excretion, while approximately 2% of the administered activity is excreted through the hepatobiliary system. Scintigraphic images show physiological uptake in the spleen, liver, kidneys, thyroid, pituitary gland and intestine.

The standard injected activity into an adult patient is 110–220 MBq. In paediatric patients, the administered activity is reduced according to body weight or body surface area.

3.4. RADIOPHARMACEUTICALS EMPLOYED FOR PET IMAGING

PET is based on the detection of the pair of 511 keV γ rays (travelling in opposite directions at 180°) produced in the annihilation process that takes place when a β^- particle (the negative electron) in the surrounding matter combines with a β^+ particle (the positive electron, or positron) emitted during nuclear decay of a positron emitting radionuclide. Neutron deficient nuclei reduce their proton surplus by emitting positrons; the atomic mass of these elements is usually one unit smaller than the most common form of the stable isotope (e.g. the positron emitting ^{15}O, ^{13}N and ^{11}C versus stable ^{16}O, ^{14}N and ^{12}C). The annihilation event between a β^+ particle and a β^- particle, which occurs at a certain distance in the matter from the decay point (positron range) over which the positron loses part of its energy, creates two 511 keV γ rays travelling in opposite directions. Some of the positron emitting radionuclides are low atomic mass elements (e.g. C, N and O) that can be used to directly label molecules of interest with minor impacts on their biological activity. The maximum positron energy varies considerably for the different radionuclides, from approximately 0.635 MeV for ^{18}F to 3.35 MeV for ^{82}Rb. Typical specific activities of PET imaging agents (radioactivity per unit mass/mole of labelled compound) are of the order of 50–500 GBq/mmol and generally low amounts of compound are administered, typically of the order of submicrograms. The half-life of the radionuclide used for a PET investigation should be commensurate with the timescale of the biological process to be explored.

PET is one of the most important technologies in medical imaging, with many different applications especially in oncology, cardiology, neurology and infection/inflammation. Over the past 30 years, advances in radiotracer chemistry have permitted development and evaluation in preclinical and clinical studies of many radiotracers with adequate specificity and kinetic characteristics for molecular imaging.

3.5. MAIN POSITRON EMITTERS EMPLOYED FOR PET IMAGING WITH POSSIBLE USE FOR GOSTT

3.5.1. Fluorine-18

Fluorine-18 is the most widely used radionuclide for clinical PET investigations. Fluroine-18 (which decays to stable ^{18}O with 97% positron emission) can be produced either by the $^{20}Ne(d,a)^{18}F$ or by the $^{18}O(p,n)^{18}F$ nuclear reactions. The former reaction leads to the formation of $[^{18}F]F_2$ (molecular fluorine), while the latter results in the formation of $[^{18}F]F^-$ (fluoride ion). The short range of positrons emitted by ^{18}F in tissues (maximum range of 2.3 mm in water) yields high resolution images. The relatively long half-life of this radionuclide (110 min) permits multistep labelling reactions for the synthesis of relatively complex molecules (with radiolabelling yields as high as 20%–40%), and also allows for transport from the production site to peripheral PET centres. Fluorine reacts with many organic and inorganic chemicals because it is the most electronegative of all the elements. The synthetic procedures most widely employed for incorporating ^{18}F into organic molecules are nucleophilic substitution and electrophilic substitution. Because the electrophilic labelling approach (which uses $[^{18}F]F_2$) results in molecules with low specific activities, the nucleophilic approach (based on the use of $[^{18}F]F^-$) is most frequently employed, not only because of the higher specific radioactivity compounds so produced, but also because of greater selectivity of the radiolabelling reactions. The most frequently used radiopharmaceuticals labelled with ^{18}F are $[^{18}F]$FDG, L-3,4-dihydroxy-6-[^{18}F]fluorophenylalanine ($[^{18}F]$DOPA) and ^{18}F fluorocholine.

3.5.2. Gallium-68

Gallium-68 (half-life 68.3 min, maximum positron energy 1.9 MeV) is eluted from a $^{68}Ge/^{68}Ga$ radionuclide generator system, with a concept similar to that of the $^{99}Mo/^{99m}Tc$ generator. Germanium-68 decays by electron capture with a physical half-life of 271 d. A single generator therefore allows continuous production of ^{68}Ga over almost 1 year. Gallium-68 is an excellent positron emitter (89% of decay), with a low associated photon emission (1.077 keV, 3.22%). This metallic radionuclide is used mostly for labelling peptides, such as SST analogues, and yields compounds with high radiochemical purity. The clinical use of PET imaging with ^{68}Ga labelled SST analogues is committed to the study of NETs.

3.5.3. Iodine-124

Iodine-124 is produced using either the $^{124}Te(p,n)^{124}I$ or the $^{124}Te(d,2n)^{124}I$ nuclear reactions. It decays with a physical half-life of 4.2 d, according to a complex decay scheme that includes emission of several high energy γ rays in addition to positron emission (which represents only approximately 23% of the decay). The maximum range in water of the high energy positrons emitted by ^{124}I is approximately 10 mm. Despite these relatively unfavourable characteristics for PET imaging, ^{124}I is an attractive radionuclide that can be used simply as ^{124}I iodide (in patients with thyroid cancer, mostly for quantitative measurements that enable accurate dosimetric estimation) or employed to radiolabel more complex molecules (e.g. MAbs directed against specific tumour associated antigens), relying on the well known radiochemistry of iodine.

3.6. MAIN RADIOPHARMACEUTICALS EMPLOYED FOR PET IMAGING WITH POSSIBLE USE FOR GOSTT

3.6.1. [Fluorine-18]FDG

The glucose analogue [^{18}F]FDG (see Fig. 3.4) is the most important radiopharmaceutical used in PET imaging. 2-Deoxy-D-glucose was first developed in 1960 as a chemotherapeutic agent, under the assumption that it would inhibit glucose consumption by cancer cells. In 1976, the synthesis of [^{18}F]FDG to assess cerebral glucose metabolism was developed; the first [^{18}F]FDG PET brain imaging studies were performed in 1977 at the University of California, USA.

[Fluorine-18]FDG is transported through the cell membrane via the glucose transport proteins (GLUTs) and is then phosphorylated by hexokinase to form [^{18}F]FDG-6-PO4. [Fluorine-18]FDG-6-PO4 is not a substrate for the subsequent enzymatic conversion to fructose-6-phosphate by phosphohexose, and thus does not further participate in the glycolytic pathway and becomes trapped in the cell (see Fig. 3.5). The low activity of the reverse enzyme, glucose-6-phophatase leads to tumour cell accumulation of FDG-6-phosphate. [Fluorine-18]FDG uptake is directly correlated with glucose metabolism, and the most intense activity is present in the brain (9% within 80–100 min), at the sites of inflammation and infection, and in tumour cells. Uptake of [^{18}F]FDG in the myocardium is variable because myocardiocytes rely mostly on fatty acids for their energy supplies.

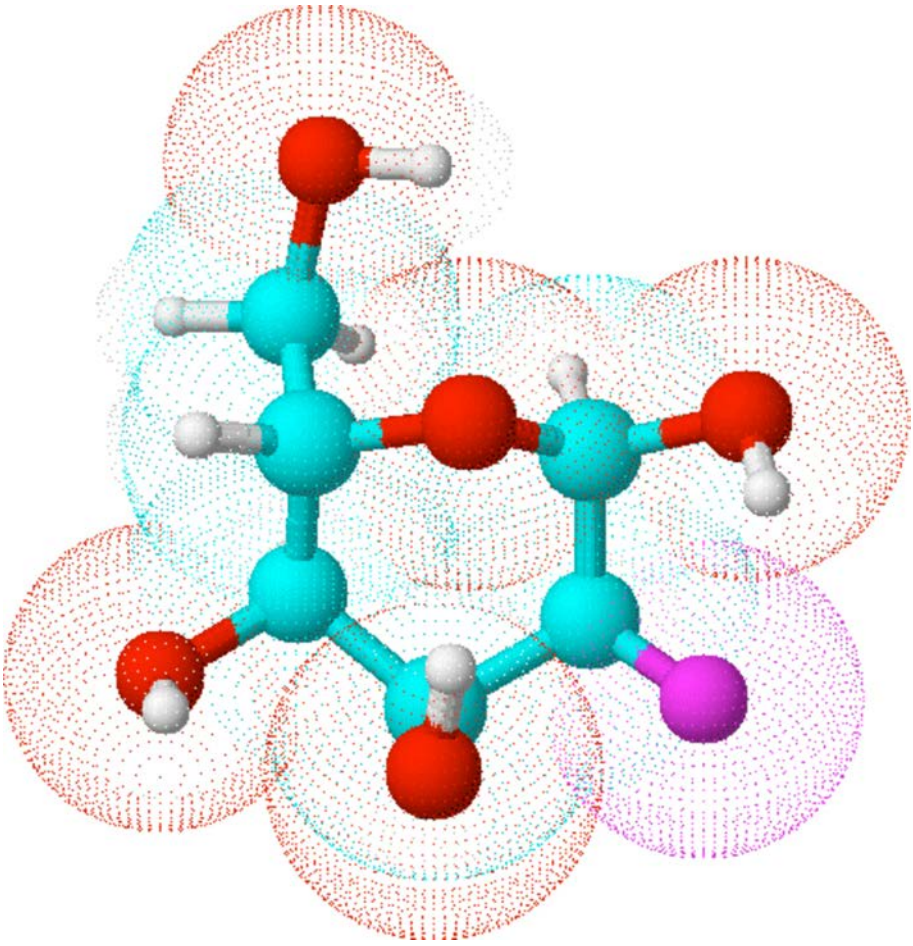

FIG. 3.4. 3-D representation of the chemical structure of [^{18}F]FDG. The fuchsia in the lower right portion of the 3-D structure represents ^{18}F. Other elements are represented with the following colour codes: red = O; white = H; light blue = C.

Physical activity occurring shortly preceding or during [^{18}F]FDG administration increases the accumulation of the radiopharmaceutical in the skeletal muscles. Cancer cells exhibit high rates of metabolism with increased glucose metabolism (Warburg effect). Gene mediated regulation of GLUTs and hexokinase activity contributes to the increased accumulation of [^{18}F] FDG in tumour cells relative to normal tissues. Nevertheless, the time course of [^{18}F]FDG accumulation in malignancy may be different from that in benign lesions and inflammatory processes. The mechanisms and reasons for elevated glucose metabolism in cancers are multifactorial and include tumour related

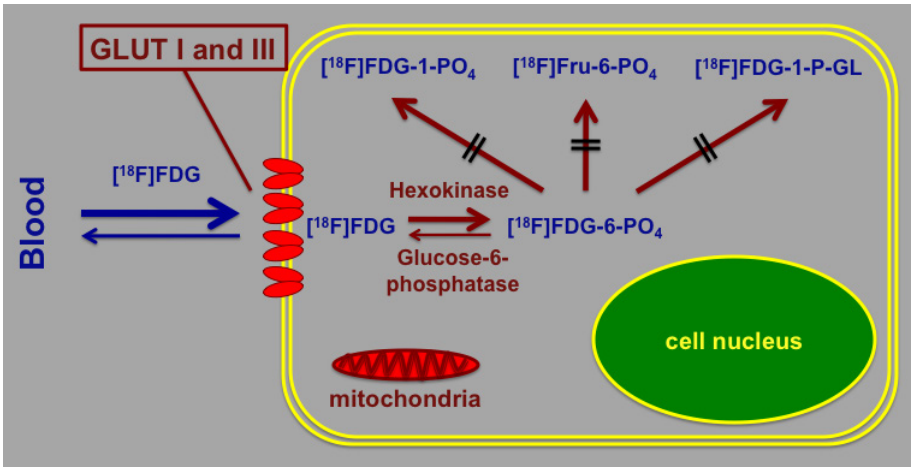

FIG. 3.5. Schematic representation of the mechanism of intracellular accumulation and retention of the radiopharmaceutical [^{18}F]FDG. After entering into the cells through the glucose transport systems (especially GLUT I and GLUT III), the radiolabelled glucose analogue undergoes activity of the enzyme hexokinase (which does not recognize this compound as different from native glucose), thus being transformed into [^{18}F]FDG-6-phosphate (the first metabolic step for intracellular glucose). However, subsequent enzymatic pathways that glucose-6-phosphate normally undergo are precluded to [^{18}F]FDG-6-phosphate, which then becomes trapped intracellularly; this compound is in fact very slowly transformed back to [^{18}F]FDG by glucose-6-phosphatases, the enzyme that reverses the activity of hexokinase.

components, biochemical and molecular alterations (e.g. glucose metabolic pathway, hypoxia), and non-tumour-related constituents (e.g. inflammation). [Fluorine-18]FDG is excreted through the kidneys, and approximately 20% of injected activity is excreted in the urine within 2 h after administration. The uptake of [^{18}F]FDG by tumour tissue competes with endogenous glucose in blood. In the case of high blood glucose levels (as well as low insulin levels), the uptake of [^{18}F]FDG is reduced, and some drugs that modify glucose levels (e.g. valproic acid, glucocorticoids or carbamazepine) can also alter radiotracer uptake. Many other factors (e.g. chemotherapy, radiation therapy or recent administration of granulocyte colony stimulating factor) interfere with [^{18}F]FDG uptake, thus possibly resulting in either false positive or false negative imaging data.

3.6.2. Fluorine-18 fluorocholine

The biosynthesis of cell membranes is enhanced in neoplastic tissues, reflecting indirectly a measure of cell proliferation. Choline is an essential element of phospholipids in the cell membrane and is transported into cells and

phosphorylated by choline kinase before being incorporated into the phospholipid membrane. Tumour cells have also demonstrated elevated levels of choline kinase.

[Carbon-11]Choline (see Fig. 3.6) was developed for imaging prostate tumours, non-small-cell lung cancer, bladder tumours and brain tumours. The increased incorporation in prostate cancer involves phosphatidylcholine production, phospholipid synthesis and upregulation of choline kinase and other enzymes. With regard to particular possible applications for GOSTT procedures, ^{18}F fluorocholine and its analogues, including ^{18}F fluoroethylcholine and ^{18}F fluoromethylcholine, show similar biodistributions to [^{11}C]choline, but with a higher urinary excretion. Normal bowel and liver uptake is observed with radiolabelled choline, thus making this agent unsuitable for exploring these tissues.

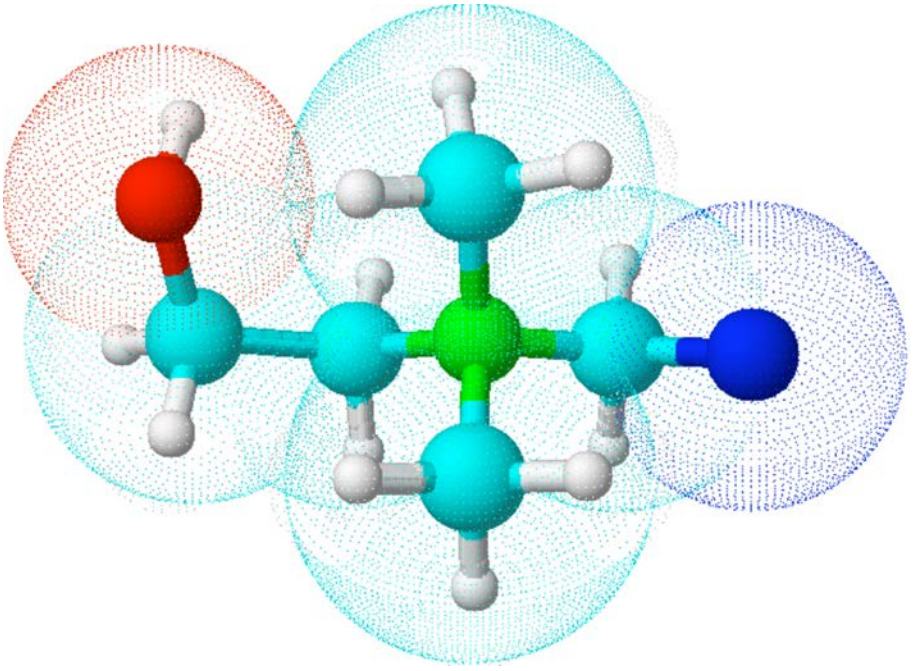

FIG. 3.6. 3-D representation of the chemical structure of [^{11}C]choline. The deep blue atom in the 3-D structure represents ^{11}C. Other elements are represented with the following colour codes: red = O; white = H; light blue = native C; green = N.

3.6.3. [Fluorine-18]DOPA

Amine precursor uptake and decarboxylation is a feature common to peptide producing endocrine cells, including NETs, and indicate a common embryological origin in the neural crest. NETs accumulate and decarboxylate the amino acid L-dihydroxyphenylalanine (L-DOPA) owing to increased activity of L-DOPA decarboxylase. [Fluorine-18]DOPA (see Fig. 3.7), which is an analogue of L-DOPA used in the evaluation of brain dopaminergic metabolism, can be useful for PET imaging of NETs, medullary thyroid carcinomas and pheochromocytomas.

3.6.4. Gallium-68 DOTA TOC/DOTA NOC

Recently, new, different PET tracers for the study of NETs have been introduced. They are the SST analogues ^{68}Ga DOTA NOC (DOTA 1-Nal^3-octreotide) and ^{68}Ga DOTA TOC (DOTA Tyr^3-octreotide, see Fig. 3.8). Uptake of these compounds is based on a receptor mechanism, with high affinities of ^{68}Ga DOTA NOC for SSTR2 and SSTR5, and of ^{68}Ga DOTA TOC for SSTR2, SSTR3 and SSTR5. DOTA is a chelating agent that is able to form stable complexes with the metal radionuclides of interest. The time required to process the generator eluate, synthesize and purify ^{68}Ga labelled DOTA conjugated

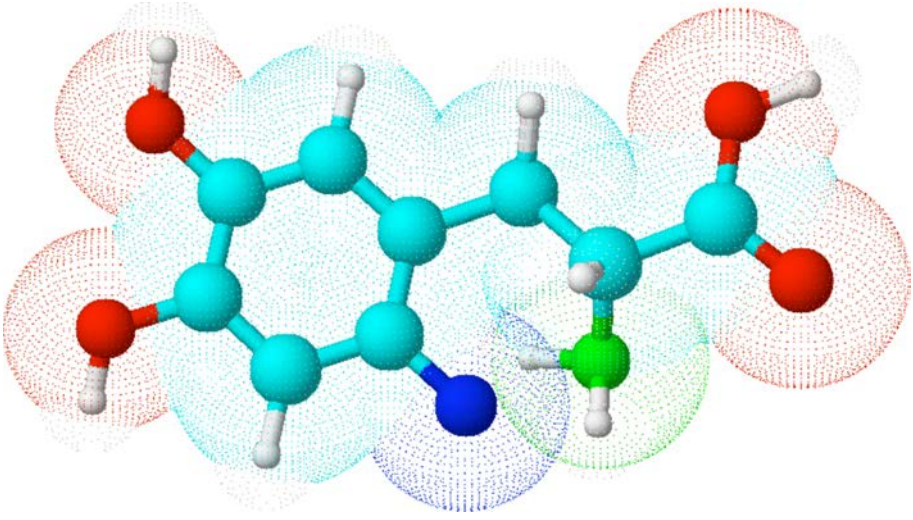

FIG. 3.7. 3-D representation of the chemical structure of [^{18}F]DOPA. The deep blue atom in the 3-D structure represents ^{18}F. Other elements are represented with the following colour codes: red = O; white = H; light blue = C; green = N.

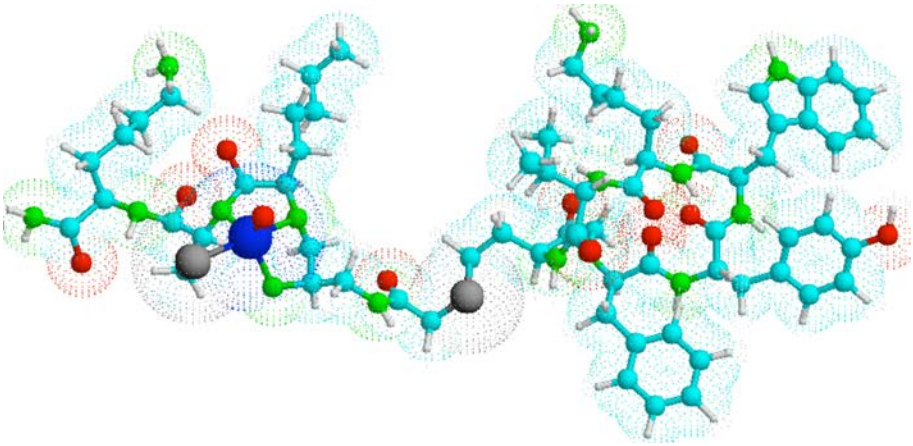

FIG. 3.8. 3-D representation of the chemical structure of ^{68}Ga DOTA TOC. The deep blue atom in the left portion of the 3-D structure (at the centre of the chelating group, DOTA) represents ^{68}Ga. Other elements are represented with the following colour codes: red = O; white = H; light blue = C; green = N; grey = S.

peptides is less than 20 min, resulting in simple and chemically efficient processing. Gallium-68 DOTA TOC has fast pharmacokinetics (80% of activity is cleared from the blood by 10 min post-injection) with kidney excretion and rapid tumour accumulation (maximum after 70 ± 20 min post-injection), thus allowing for PET imaging as early as 1 h after radiotracer administration. Its accumulation in tissues that do not express SSTRs is very low. Particular attention is necessary in imaging interpretation concerning the sites of physiological accumulation such as the spleen, liver, adrenal glands, urinary tract and pituitary gland.

BIBLIOGRAPHY FOR CHAPTER 3

ELL, P.J., GAMBHIR, S.S., Nuclear Medicine in Clinical Diagnosis and Treatment, 3rd Edn, Churchill Livingstone, Edinburgh (2004).

HERBERT, J.C., ECKELMAN, W.C., NEUMANN, R.D., Nuclear Medicine: Diagnosis and Therapy, Thieme Medical Publishers, Stuttgart (1996).

VALLABHAJOSULA, S., Molecular Imaging — Radiopharmaceuticals for PET and SPECT, Springer, Berlin (2009).

4. QUALITY PARAMETERS IN PLANAR AND TOMOGRAPHIC IMAGING FOR GOSTT

4.1. INTRODUCTION

Since the introduction of the procedure in 1992, lymphoscintigraphy has been an essential component for pre-operative SLN identification in melanoma and breast cancer [4.1, 4.2].

With the new generation of hybrid imaging systems, SPECT/CT imaging has been incorporated into the SLN procedure. The functional information from SPECT imaging can be combined with the morphological information from CT imaging by applying both techniques in one session [4.3]. The resulting fused SPECT/CT images depict SLNs in an anatomical landscape, thus providing a helpful road map for surgeons. SPECT/CT imaging has also been used in melanoma and breast cancer patients with unusual or complex drainage [4.4]. This is the case in melanomas of the neck or the upper part of the trunk and in breast cancer in patients with drainage outside the axilla. SPECT/CT imaging may also visualize SLNs in the axilla when no LNs are visualized on planar images [4.4, 4.5]. Furthermore, SPECT/CT imaging is becoming essential to localize SLNs in locations such as the pelvis, retroperitoneum and upper abdomen in gastrointestinal, gynaecological and urological malignancies.

Based on these considerations, it is necessary to define the role of SPECT/CT in relation to planar imaging for the identification of SLNs. On the other hand, the pre-operative anatomical information obtained using SPECT/CT imaging appears to lead to a more optimal use of portable devices for sentinel localization in the operating room (see below).

4.2. IMPORTANT CONCEPTS FOR THE SLN PROCEDURE

The SLN procedure is based on a hypothesis of the existence of an orderly and predictable pattern of lymphatic drainage to a regional LN basin, and on the functioning of LNs on a direct drainage pathway as effective filters for tumour cells [4.1]. This leads to considering as SLNs all LNs with direct drainage from the primary tumour. The SLN is not necessarily the hottest or the nearest node, although this is often the case.

It should also be considered that the SLN procedure is a multidisciplinary modality based on a combination of pre-operative imaging, intraoperative detection and refined histopathological analysis. For pre-operative imaging, colloid particles labelled with ^{99m}Tc are currently used. Radioactive colloid

particles are incorporated into the macrophages by phagocytosis, enabling prolonged LN retention. This leads to an adequate detection window that enables not only delayed planar imaging and SPECT/CT imaging, but also intraoperative SLN localization using portable devices based on γ ray detection.

SLNM is oriented to the identification of LNs as possible sites of metastasis in patients without clinical evidence of regional metastases. When pre-operative evaluation detects palpable LNs at clinical examination, such suspected LNs are further evaluated using US or CT guidance, or by cytological aspiration. In cases of confirmed LN metastasis, primary surgery usually includes de novo locoregional lymphadenectomy (LDN), whereas the SLN procedure is principally oriented to the identification of LNs as possible sites of subclinical metastasis.

Finally, as already recognized in the TNM classification [4.2], upon completion of pathological analysis, the SLN procedure is able to differentiate between macrometastases (>2 mm), micrometastases (>0.2 mm and <2 mm) and submicrometastases (<0.2 mm). This is made possible by a more detailed histopathological examination focused on the fewer nodes resected (versus the larger number resected during de novo LDN) using more histological sections per LN and more sensitive techniques (immunohistochemistry in addition to haematoxylin and eosin staining).

4.3. IMAGE GENERATION USING SPECT/CT

SPECT/CT imaging is principally oriented to accurate anatomical localization of SLNs depicted during lymphoscintigraphy. This is the principal reason why SPECT/CT images are acquired using low dose CT. The use of diagnostic high dose CT, with or without intravenous contrast, is not necessary in principle because the sentinel procedure is primarily aimed at identifying normal size LNs as possible sites of subclinical metastasis.

However, for accurate SLN localization, the CT component of SPECT/CT imaging must be able to give optimal anatomical information. While, for superficial areas such as the groin and the axilla, 5 mm sections are recommended, for more complex anatomical areas (head/neck, pelvis or abdomen), 2 mm sections may be necessary.

CT image acquisition is also used to correct the SPECT signal for tissue attenuation and scattering. After these corrections, SPECT images are fused with CT images [4.3]. A grey scale is generally used to display the morphology in the background image (CT), whereas a colour scale is used to display the lymphoscintigraphic acquisition in the foreground image (SPECT).

The display of SPECT/CT imaging is similar to that of conventional tomography. Multiplanar reconstruction enables 2-D display of fusion images in

relation to CT and SPECT. The use of cross-reference lines allows navigation between axial, coronal and sagittal views. At the same time, this tool leads to correlation of radioactive SLNs seen on fused SPECT/CT images with LNs seen on CT images (Fig. 4.1(A), (B)). This information may be helpful for the intraoperative procedure and postexcision control using portable gamma cameras or probes.

Fused SPECT/CT images may also be displayed using maximum intensity projection (MIP). This tool enables 3-D display by addition of various slices improving anatomical SLN localization and recognition by the surgeon (Fig. 4.1(C)).

When using volume rendering for 3-D display, different colours can be assigned to anatomical structures such as muscle, bone and skin. This leads to obtaining better anatomical reference points and incorporating an additional dimension in the recognition of SLNs (Fig. 4.1(D)).

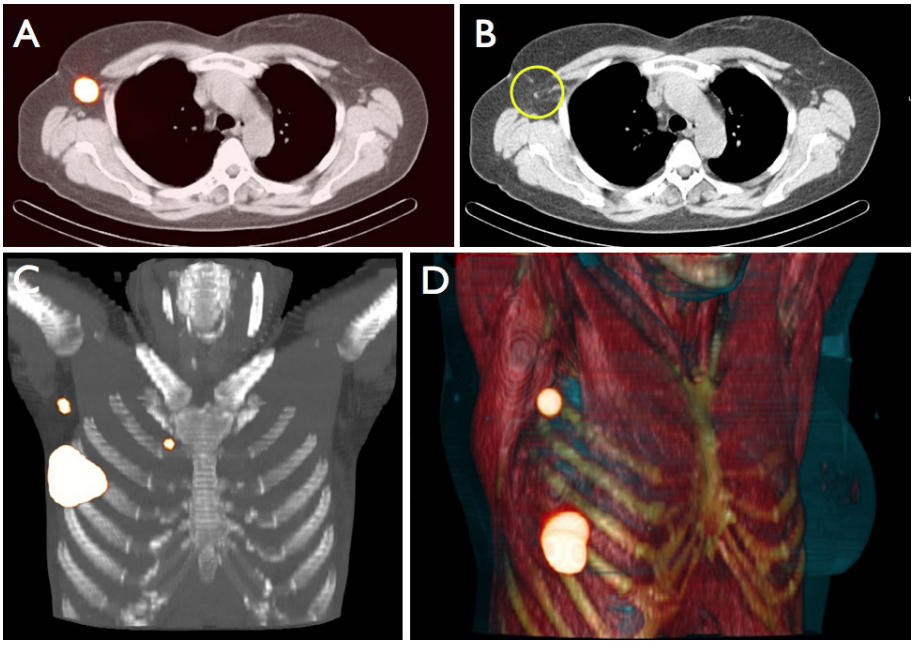

FIG. 4.1. Fused axial SPECT/CT image (A) showing an SLN in the right axilla corresponding to a small LN (circle) on the axial CT image (B). Coronal fused SPECT/CT image (C) displayed with MIP showing an SLN in the right axilla and an internal mammary SLN in the second right intercostal space. SPECT/CT image with volume rendering for 3-D display (D) shows an SLN in the right axilla.

4.4. GENERAL INDICATIONS OF SPECT/CT IMAGING IN SLNM

Indications may depend on the type of malignancy and the complexity of lymphatic drainage. It will also depend on the criteria adopted by surgeons and nuclear physicians in the different hospitals.

In general, some indications for SPECT/CT imaging for SLNM are as follows:

— Detection of SLNs in cases of non-visualization at planar imaging [4.4]. Owing to the correction for tissue attenuation, SPECT/CT imaging is usually more sensitive than planar imaging and may be particularly useful in obese patients (Fig. 4.2).
— Localization of SLNs in areas with complex anatomy and a high number of nodes such as the head and neck, or in cases with unexpected lymphatic drainage (e.g. between the pectoral muscles, internal mammary chain, levels II or III of the axilla, in the vicinity of the scapula) at planar imaging (Fig. 4.3).

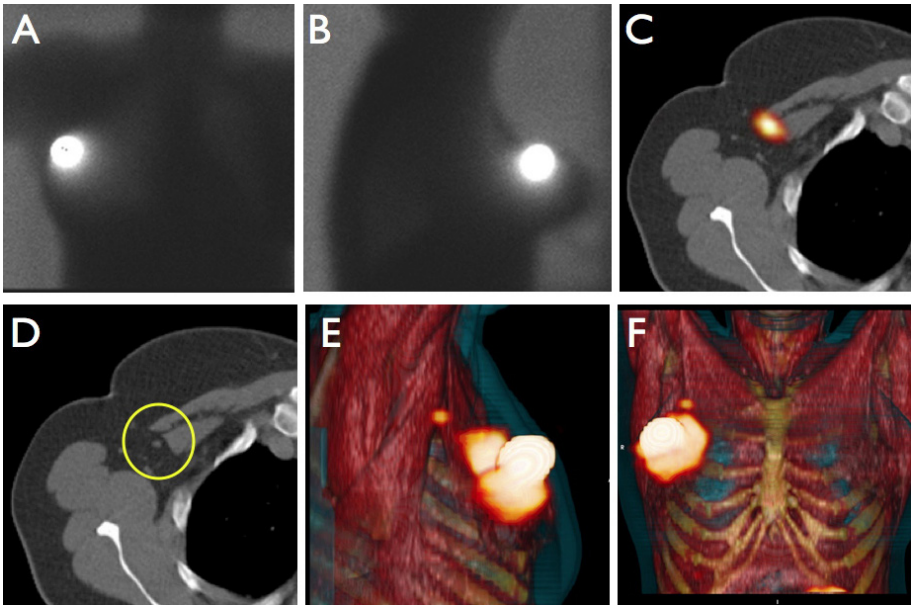

FIG. 4.2. Anterior (A) and lateral (B) planar images showing no drainage of the radiocolloid from the injection site. By contrast, on axial fused SPECT/CT image (C) showing an SLN, corresponding to a single LN on a CT image (circle in D), is seen at the border of the pectoral muscle. This SLN is displayed using 3-D volume rendering for better anatomical recognition (E, F).

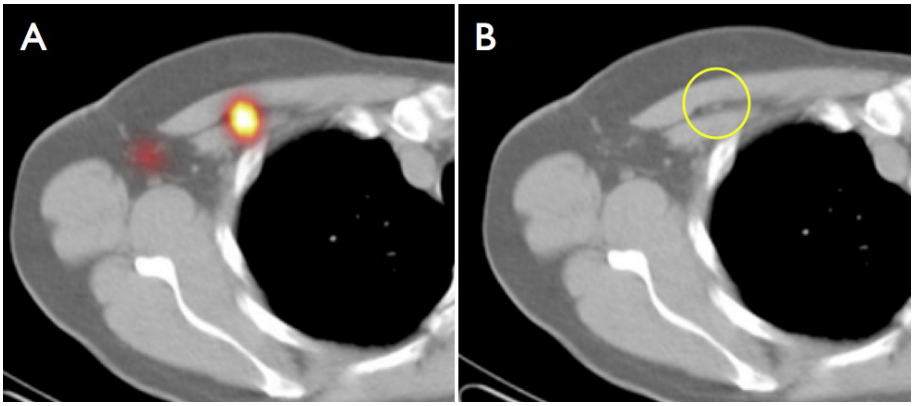

FIG. 4.3. Axial fused SPECT/CT image (A) showing an SLN between the pectoral muscles. This SLN corresponds to a single LN on the CT image (circle in B).

— Anatomical localization and detection of additional SLNs in areas of deep lymphatic drainage such as the pelvis, abdomen or mediastinum [4.5].

4.5. CRITERIA FOR SLN IDENTIFICATION USING SPECT/CT AND PLANAR IMAGING

It should be emphasized that SPECT/CT imaging is not intended to replace planar lymphoscintigraphy, but rather it must be considered as a complementary modality. In fact, in general, SPECT/CT imaging is aimed at anatomic localization of SLNs already visualized on planar imaging (Fig. 4.4). Nevertheless, in some cases, SPECT/CT imaging may detect additional SLNs not seen on planar imaging.

To fully clarify the combined use of SPECT/CT imaging during lymphoscintigraphy, some important issues must be elucidated. First, by acquiring early and delayed planar images, lymphoscintigraphy is able to identify SLNs in most cases. In current protocols, SPECT/CT imaging is performed following delayed planar images (mostly 2–4 h after radiocolloid administration). This sequential acquisition is helpful to clarify the role of both modalities. Nevertheless, it is necessary to specify some criteria for SLN identification on pre-operative imaging. Major criteria to identify LNs as SLNs are the visualization of lymphatic ducts, the time of appearance, the LN basin and the

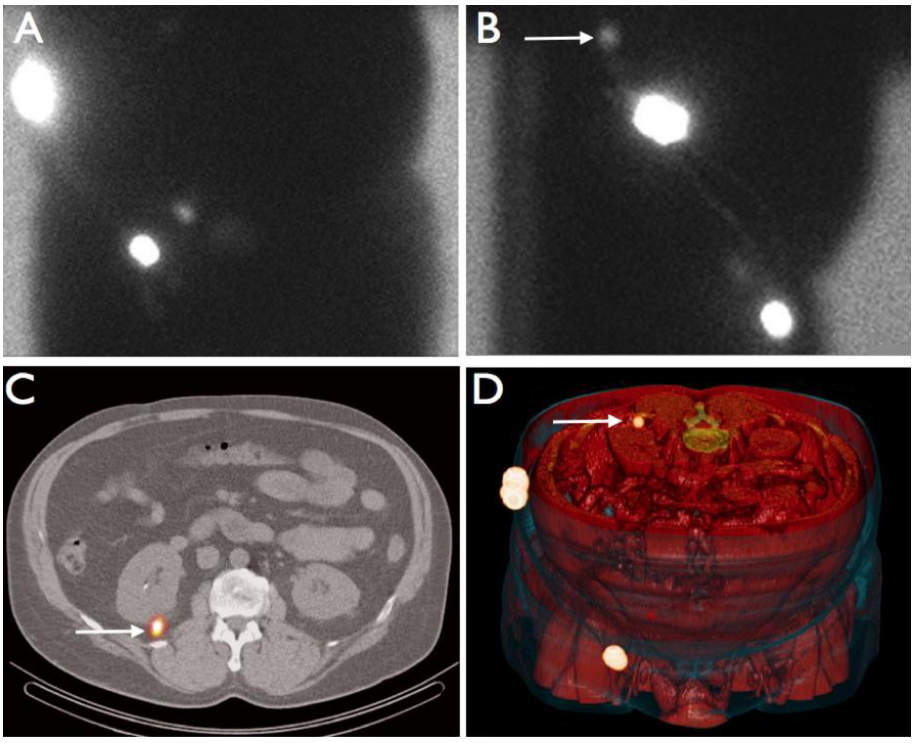

FIG. 4.4. Planar anterior (A) and lateral (B) images showing drainage of the radiocolloid from the injection site to the right groin in a patient with melanoma of the right side of the trunk. Drainage to a cranially located LN (arrow) is also observed. Axial (C) and volume rendering (D) SPECT/CT images show the cranially located SLN to be located in the retroperitoneal area of the abdomen (arrow).

intensity of LN uptake [4.6]. Following these criteria, the visualized radioactive LNs may be classified as:

— Definitively SLNs: This category concerns all LNs draining from the site of the primary tumour through their own lymphatic vessel, or a single radioactive LN in an LN basin [4.7].
— High probability SLNs: This category includes LNs appearing between the injection site and a first draining LN, or nodes with increasing uptake appearing in other LN stations.
— Low probability SLNs: All higher echelon nodes may be included in this category.

Early planar images are essential to identify first draining LNs as SLNs by visualization of lymphatic ducts (Fig. 4.5). These LNs (category A) can be distinguished from secondary LNs (category C), which mostly appear on delayed planar images.

In other cases, a single LN is seen on early and/or delayed imaging. This node is also considered a definitive SLN (category A). However, in some cases, SPECT/CT imaging can detect additional LNs in other basins (Fig. 4.6). These nodes may be considered definitive (category A) or highly probable SLNs (category B). Less frequently, a radioactive LN may appear between the injection site and a first draining node (Fig. 4.5); its increasing uptake may confirm this node as a highly probable SLN (category B) and it helps to differentiate this LN from prolonged valve activity in a lymphatic duct.

4.6. IDENTIFYING SLNs FOR LOCALIZATION IN THE OPERATING ROOM

The use of the scintigraphic categories described above [4.6] to characterize radioactive LNs is also helpful for clinical decision making. LNs of the first two categories (definitive or highly probable SLNs) are the LNs recognized by the nuclear physician that must be removed by the surgeon. Low probability SLNs may sometimes be removed, depending on the amount of remaining radioactivity measured by the gamma probe or by the portable gamma camera during final control of the surgical excision bed [4.8].

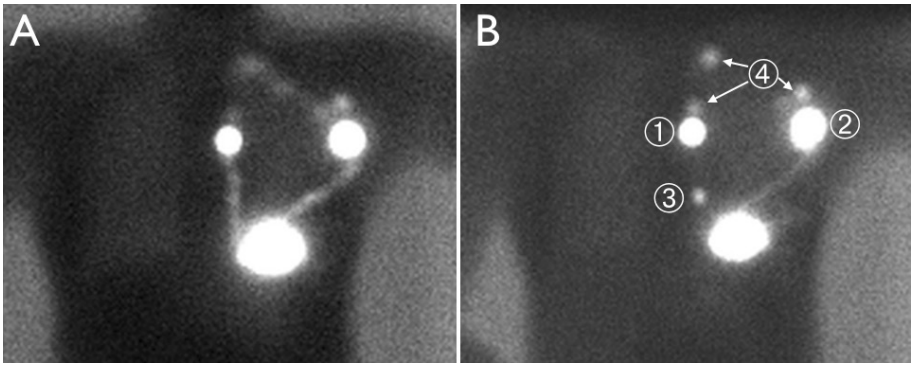

FIG. 4.5. Anterior early (A) and delayed (B) planar images showing drainage of the radiocolloid to the left axilla and to the internal mammary chain. The two LNs with their own lymphatic vessel (1, 2) are considered definitive SLNs, whereas a delayed appearing node (3) is considered a high probability SLN. The higher located LNs (4) are considered as low probability SLNs.

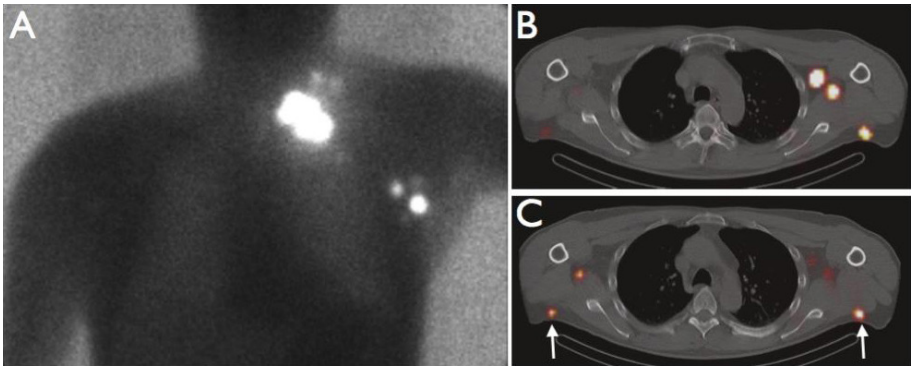

FIG. 4.6. Planar anterior image (A) showing radiocolloid drainage from the injection site to the left supraclavicular area and to the left axilla in a patient with melanoma of the upper back. Axial fused SPECT/CT images (B, C) showing additional LNs in both periscapular areas (arrows) and in the right axilla. These nodes are also considered to be SLNs.

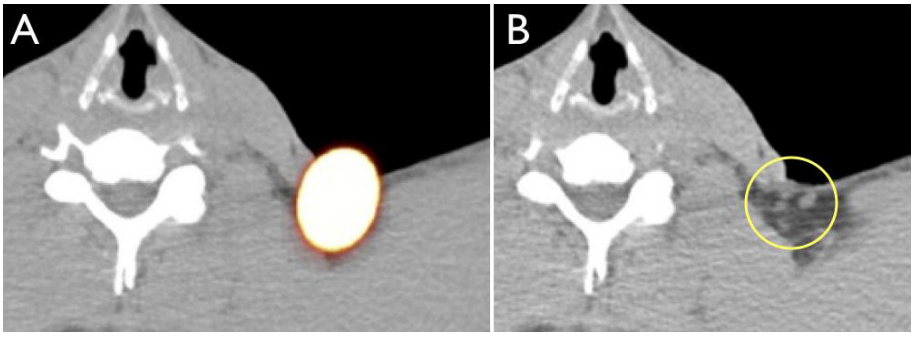

FIG. 4.7. Axial SPECT/CT image (A) showing a radioactive node in the left supraclavicular area. This radioactive accumulation corresponds to a cluster of LNs on the CT image (circle in B).

Another important issue is the necessity to correlate findings of fused SPECT/CT images with those of CT images. In many cases, radioactive SLNs correspond to single LNs. However, in some cases, radioactivity on SPECT/CT images may correspond to a cluster of LNs on the CT image. This pre-operative information may lead to a stringent postexcision control after removal of the first radioactive LN by the surgeon, particularly for areas such as the pelvis and head/neck (Fig. 4.7).

4.7. COMBINING EXISTING TECHNOLOGIES WITH NEW MODALITIES

SPECT/CT imaging is a recent technology that has been fully integrated into the pre-operative approach for a better anatomical baseline, more accurate depiction of SLNs or of tumour lesions and for decision making during surgery. Intraoperative guidance, although taking into account the information provided by SPECT/CT imaging, is generally achieved using conventional hand-held gamma probes, while, more recently, portable gamma cameras have been introduced into this field. This interaction is intended to refine the methodology and final outcome of radioguided surgery.

There are currently new possibilities to explore and possibly integrate into this issue. One is the freehand SPECT based device that integrates a positioning system attached to the conventional gamma probe and permits a virtual reconstruction in a 3-D environment [4.9]. This 3-D information may be further used for precise intraoperative localization and targeting of radioactive SLNs and tumour lesions, thus implementing a radioguided navigation system. The device can ensure permanent assistance and transparent documentation of soft tissue removal during the intervention (Fig. 4.8).

On the other hand, the possibility to combine current radiotracers with other agents opens a new field of exploration. In this regard, a nanocolloid radiotracer has been combined with indocyanine green (a fluorescent agent) for SLN detection during robot assisted LDN [4.10]. In contrast to single fluorescent agents [4.11], this bimodal tracer may allow the surgeons to integrate the standard approach based on radioguided detection using a portable gamma camera with a new optical modality based on fluorescent signal detection. This approach is being successfully applied in various malignancies (Fig. 4.9).

For all these new intraoperative modalities, pre-operative SPECT/CT imaging remains essential as the starting point for surgical planning.

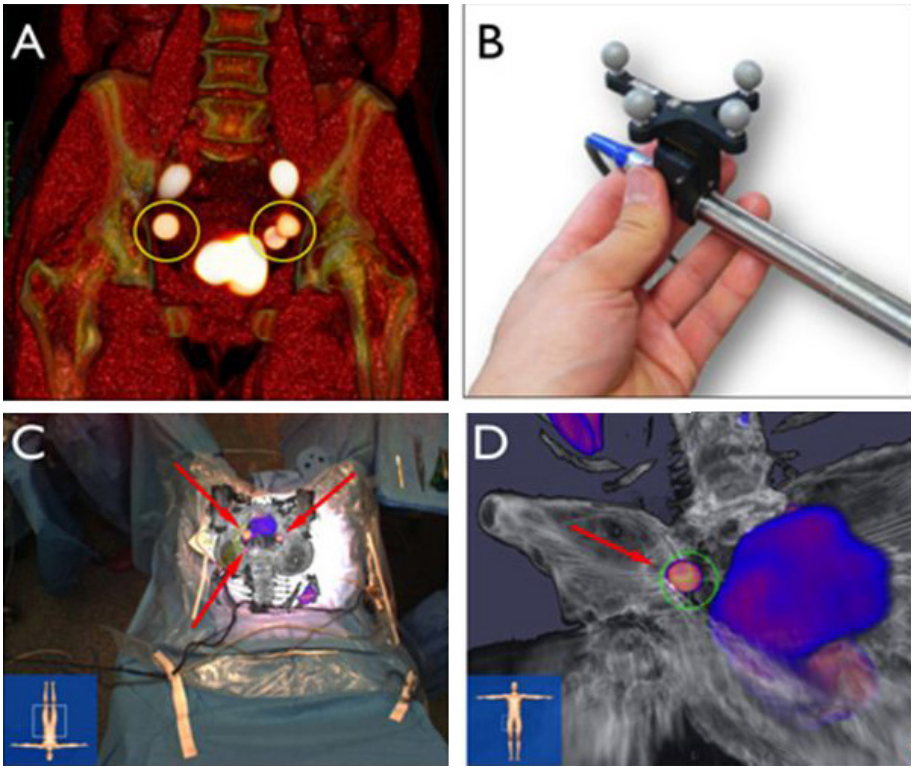

FIG. 4.8. 3-D volume rendering SPECT/CT images showing the lymphatic drainage pattern in a patient with prostate cancer. The SLNs are shown in yellow circles (A). Tracking device attached to a gamma probe to generate freehand SPECT data (B). By integrating pre-operative SPECT/CT data, it is possible to overlay the generated 3-D image onto the patient's body with simultaneous display of the SLNs (red arrows) located very close to the site of the radiocolloid injection in the prostate, depicted in blue (C, D).

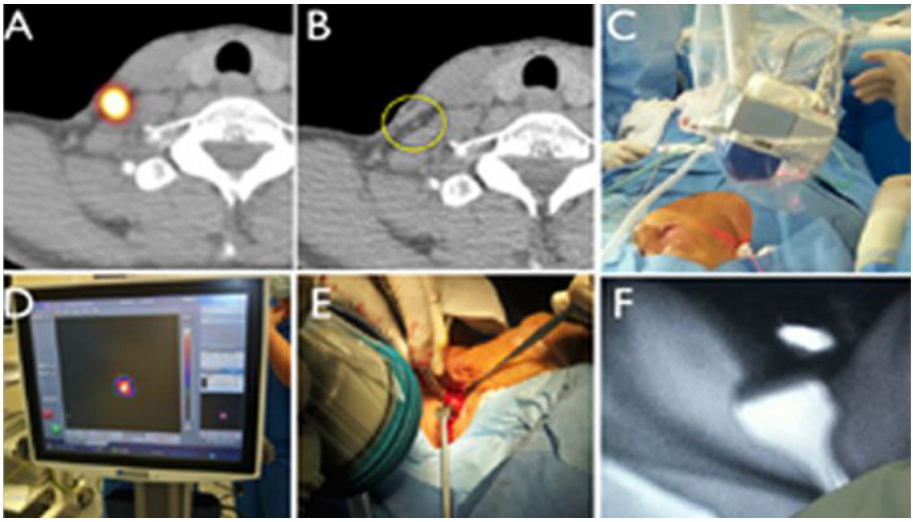

FIG. 4.9. Axial fused SPECT/CT images (A) showing a radioactive SLN in the right cervical area. This radioactive accumulation corresponds to a single LN on the CT image (circle in B). The use of a portable gamma camera permits the surgeon to select the most adequate site for incision (C) and also to monitor the procedure with intraoperative imaging guidance (D). The recent introduction of bimodal tracers for simultaneous radioguided and fluorescent detection involves the additional use of a fluorescence camera (E) to better distinguish the SLN in anatomically complex areas (F).

REFERENCES TO CHAPTER 4

[4.1] MORTON, D.L., et al., Technical details of intraoperative lymphatic mapping for early stage melanoma, Arch. Surg. **127** (1992) 392–399.

[4.2] SOBIN, L.H., TNM, sixth edition: New developments in general concepts and rules, Semin. Surg. Oncol. **21** (2003) 19–22.

[4.3] DELBEKE, D., et al., Procedure guidelines for SPECT/CT imaging, J. Nucl. Med. **47** (2006) 1227–1234.

[4.4] VAN DER PLOEG, I.M., et al., The additional value of SPECT/CT in lymphatic mapping in breast cancer and melanoma, J. Nucl. Med. **48** (2007) 1756–1760.

[4.5] VERMEEREN, L., et al., SPECT/CT for preoperative sentinel node localization, J. Surg. Oncol. **101** (2010) 184–190.

[4.6] NIEWEG, O.E., ESTOURGIE, S., VALDÉS OLMOS, R.A., "Lymphatic mapping and sentinel node biopsy", Nuclear Medicine in Clinical Diagnosis and Treatment, Vol. 3 (ELL, P.J., GAMBHIR, S.S., Eds), (2004) 229–260.

[4.7] ALAZRAKI, N., et al., Procedure guideline for lymphoscintigraphy and the use of intraoperative gamma probe for sentinel lymph node localization in melanoma of intermediate thickness 1.0, J. Nucl. Med. **43** (2002) 1414–1418.
[4.8] VERMEEREN, L., VALDÉS OLMOS, R.A., KLOP, W.M., BALM, A.J., VAN DEN BREKEL, M., A portable gamma-camera for intraoperative detection of sentinel nodes in the head and neck region, J. Nucl. Med. **51** (2010) 700–703.
[4.9] WENDLER, T., et al., First demonstration of 3-D lymphatic mapping in breast cancer using freehand SPECT, Eur. J. Nucl. Med. Mol. Imaging **37** (2010) 1452–1461.
[4.10] VAN DER POEL, T., BUCKLE, T., BROUWER, O.R., VALDÉS OLMOS, R.A., VAN LEEUWEN, F.W., Intraoperative laparoscopic fluorescence guidance to the sentinel lymph node in prostate cancer patients: Clinical proof of concept of an integrated functional imaging approach using a multimodal tracer, Eur. Urol. **60** (2011) 826–833.
[4.11] KEEREWEER, S., et al., Optical image-guided surgery—Where do we stand? Mol. Imaging Biol. **13** (2011) 199–207.

5. GOSTT IN BREAST CANCER

5.1. INTRODUCTION

Soon after publication of the method of SLNB by Cabanas in 1992 [5.1], SLNM and SLNB began to also be applied in patients with breast cancer. Over the last few years, SLNM and SLNB have expanded at an unprecedented rate and have now become a routine technique in breast cancer surgery, contributing to rendering the surgical procedure as minimally invasive as possible. As in other solid epithelial cancers, in breast cancer, the SLN(s) are those LNs that receive direct lymphatic drainage from the breast tumour. Usually, there are one or two SLNs, but occasionally more LNs can be identified during lymphoscintigraphy. Nowadays, the techniques for SLNM and SLNB are routinely employed in most centres with a minimal number of breast cancer surgeries [5.2–5.17].

Accurate LN staging is essential for both prognosis and treatment in patients with breast cancer. As no imaging modality is able to accurately detect microscopic metastasis, SLNB is considered the only reliable method for identifying micrometastatic disease in regional LNs.

5.1.1. Update on emerging evidence in breast cancer

Breast cancer is the most frequent type of cancer diagnosed in women worldwide. In the USA, more than 209 000 new cases were diagnosed in 2009, with more than 40 000 deaths from this malignancy [5.18].

LN status is a major prognostic factor in early stage disease, and this information is paramount for tailoring therapy [5.19]. Axillary LN status is useful for assessing regional control of the disease, as well as for prognostic purposes regarding the expected survival of the patient. Depending on the axilla status, the oncologist will apply different treatment strategies, such as surgery and adjuvant chemotherapy, radiotherapy and hormone therapy. Clinical examination (i.e. palpation) is not accurate enough for assessing the axillary status, and pre-operative modalities include PET/CT imaging with [^{18}F]FDG (>95% specificity, but low sensitivity and high cost) and US imaging (the most widely employed technique owing to its relatively high sensitivity, feasibility and low cost). In patients with non-palpable axillary LNs, US imaging has 56%–72% sensitivity and 70%–90% specificity. Furthermore, US imaging can direct fine needle aspiration (FNA) [5.20], although core needle biopsy [5.21] can also yield excellent results.

Because pre-operative imaging techniques have limited sensitivity, the axillary lymphatic basin must be explored surgically, and the traditional staging approach requires axillary LN dissection. However, routine axillary LN dissection carries the risk of lymphoedema, sensory/motor impairment and pain. SLNB is a less invasive method of assessing for nodal involvement, based on the assumption of orderly progression of malignant cells from one LN to the next. Then, if the SLN does not bear metastasis, the entire basin is assumed to be free from metastasis. The main objective of SLNM and SLNB in breast cancer patients is axillary staging. The technique is validated if SLNs are found in more than 95% of the cases, with less than 5% of false negative results. In this regard, the current gold standard for axillary LN staging is the long term follow-up; nowadays, there is enough experience to compare the axilla disease free survival time after SLNB and after LDN [5.22].

Several international meetings have contributed to standardization of the technique [5.15–5.17]. The consensus conference of Philadelphia in 2002 [5.23] confirmed the effectiveness of selective SLNB in early breast cancer. The American Society of Clinical Oncology (ASCO) defined, in 2005 [5.24], some basic recommendations for SLNB in early stage breast cancer: patients should be selected, the diagnostic imaging study of the axilla must be negative and must include fine needle aspiration cytology (FNAC) in case of suspicious LNs; SLNM can be carried out using blue dye, radiocolloid or both; and a trained multidisciplinary team is required (surgeon, pathologist and nuclear physician) to reduce the number of LDNs and the associated morbidity. According to the National Comprehensive Cancer Network (NCCN) guidelines issued in 2010 [5.25], SLNB experience should be considered in the multidisciplinary team of surgeons, radiologists, nuclear physicians and pathologists, and the incorporation of clinical oncologists and radiotherapists should be encouraged.

The majority of these issues has also been discussed by several European societies. For instance, the Spanish Society of Senology and Breast Pathology suggests a supervised learning process by experienced groups. These groups should have performed more than 300 cases of SLNB during the clinical application phase, with at least a 95% rate of SLN identification and a false negative rate of 5% or less [5.26]. After completing such a learning phase, the results markedly improve.

After a mean follow-up of 5 years, Veronesi et al. described, in 2003 [5.22], a similar incidence of axillary metastases after axillary LN dissection in patients not submitted to axillary dissection because of a negative SLNB. In 2005, the same team reported a percentage of axillary recurrences even lower than expected (0.3%) in patients not undergoing axillary LN dissection because of a negative SLNB [5.27].The survival benefit of SLN was also addressed in the National Surgical Adjuvant Breast and Bowel Project (NSABP) trial B-32 that

randomized 5611 women to SLNB only versus SLNB plus axillary LDN. After a mean follow-up of 95.6 months, the SLNB arm showed a 90.3% 8 year survival rate versus 91.8% in the axillary LDN arm (statistically non-significant) [5.28].

A further step forwards is now being considered. The results of a multicentric randomized American College of Surgeons Oncology Group Z0011 study suggested that axillary LN dissection may not be warranted for women with T1–T2 breast cancer and haematoxylin and eosin detected metastases in the SLN (treated with breast conserving surgery, whole breast irradiation and adjuvant systemic therapy). The results showed that SLNB offers an excellent regional control in early breast cancer patients without axillary LDN, as well as providing enough information for performing adjuvant treatment. The recurrence rate was 2.5% in the SLNB only group versus 3.6% in the axillary LDN group, without significant differences in overall survival rates. Thus, when only isolated tumour cells or micrometastases are present, axillary LDN may be avoided [5.29].

5.2. APPLICATION OF SLNs IN BREAST CANCER

SLNs are those LNs that directly drain the lymph from the primary tumour (Fig. 5.1). Therefore, SLNs are the first LNs to potentially receive the seeding of lymph borne metastatic cells [5.30]. In other words, when breast cancer metastasizes to regional LNs, it most frequently goes to the SLN. If the SLN is free from micrometastasis according to both haematoxylin and eosin and immunohistochemical staining, the probability of detecting tumour cells in non-SLNs is less than 5%. Lymphoscintigraphy allows the surgeon to identify and biopsy the SLN, thus employing a novel approach that has been demonstrated to be safe and accurate for screening axillary LNs [5.22, 5.31].

Important issues to be considered for SLNB include the following:

— The success rate of SLNM. When lymphatic mapping is not successful, full axillary LDN is generally necessary to assess the status of the nodes.
— The false negative rate represents the proportion of patients with negative findings on SLNB who are subsequently found to have disease in the axillary LNs, either upon axillary LDN or during follow-up. An intraoperative false negative finding represents an SLN that is found to be negative for disease on intraoperative evaluation by frozen section or touch preparation, but metastasis is detected by definitive histology on permanent sections [5.32].
— The negative predictive value (NPV) is the proportion of individuals with negative SLNB, but in whom no metastatic involvement of the axillary LNs is found on axillary LDN.

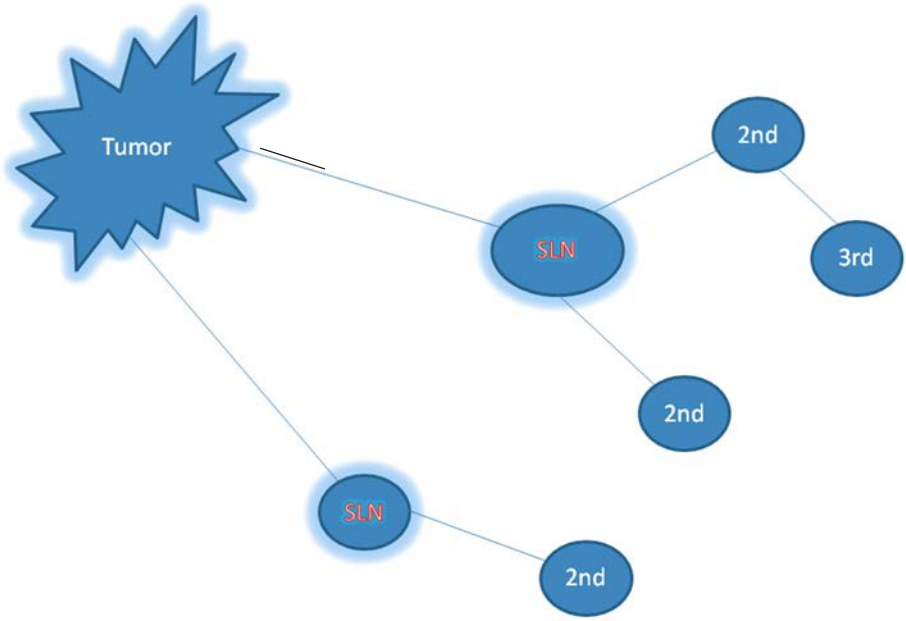

FIG. 5.1. Schematic representation of the SLN concept.

— Accuracy is the proportion of all patients (positive or negative SLNB findings) for whom SLNB correctly predicts the results of axillary LN dissection.

The rate of identification of SLNs generally exceeds 95%, and the reported false negative rates have not been too high so far. In determining the rate of false negative results, the mistake of calculating the rate over the entire group of patients, both those who are axilla positive and those who are axilla negative, must be avoided. The false negative rate should be calculated over the entire group of axilla positive patients, as follows:

$$FN_{rate} = \frac{FN_{procedures}}{FN_{procedures} + TP_{procedures}} \times 100$$

where FN is false negative and TP is true positive.

5.3. ELIGIBILITY

SLNB is an appropriate alternative to routine LN dissection for axillary staging in patients with early stage breast cancer with clinically negative axillary nodes. Complete axillary LN dissection remains the standard treatment for patients with axillary metastases identified during SLNB. Appropriately identified patients with negative SLNB do not need to undergo axillary LN dissection. Isolated cancer cells detected by pathological examination of the SLN with the use of specialized techniques (immunohistochemistry and/or molecular biology analysis) are currently of unknown clinical significance [5.24].

Currently, the SLNB procedure is recognized as the standard treatment for stages I and II breast cancer patients [5.22–5.24, 5.33–5.38]. In these stages, the results presented by the NSABP B-32 [5.36] and by Veronesi et al. [5.22, 5.27] showed that SLNB has a positive LN rate similar to that observed after LDN, yet with a significant reduction in morbidity [5.39] and similar axillary LN recurrence rates at 5 years [5.40]. False negative rates are higher in grade 3 lesions and in cases with a single SLN, compared to cases with multiple SLNs [5.41]. In the case of negative SLNB, the latest results on survival from the NSABP B-32 study suggest no significant differences in disease free survival, overall survival and local control of disease [5.36].

The ASCO guidelines emphasize that, despite the widespread application of SLNB for early stage breast cancer, there is a wide variation in the reported performance parameters; such differences may depend on the size of the patient population, the mapping technique and the proportion of successful mappings. The wide range of false negative rates and SLN identification emphasizes some variability of this procedure in different centres, which is most likely linked to technical factors. Nevertheless, once a multidisciplinary team is experienced with the procedure, reasonable levels of accuracy are achieved, with reported identification rates more than 95%. For patients who have a positive SLNB and for patients in whom an SLN is not identified intraoperatively, axillary LDN should be considered to be standard practice. Patients with a negative SLNB do not require an axillary LDN.

5.3.1. Clinical recommendations for SLNB in breast cancer

SLNM and SLNB should be considered in women who have a biopsy proven carcinoma of the breast in whom definitive surgery and axillary node clearance is planned and in whom there are no palpable axillary LNs [5.42].

The recommendations of the ASCO [5.24] are generally followed worldwide in the treatment of early breast cancer. Several consensus meetings, both national and international, have confirmed these indications and contraindications,

although the emergence of molecular biology and new techniques in imaging raise new challenges in SLNB [5.43]. In 2009, at the 11th International St. Gallen Breast Cancer Conference [5.44], several meta-analyses and guidelines were presented on the application of SLNB after neoadjuvant therapy and in cases of micrometastases. In 2010, an international expert consensus on the current recommendations of locoregional treatment in breast cancer elaborated on several recommendations regarding the assessment of axillary LNs [5.45].

The indications and recommendations for SLNB are summarized in Table 5.1 [5.24].

5.3.2. Controversial indications

Some studies maintain that previous plastic surgery does not contraindicate SLNB. Plastic surgery with breast augmentation or reduction requires major tissue movements, but the SLN is consistently identified also in these patients, irrespective of the technique used [5.46]. Current data indicate that SLNB should be considered to be standard in patients who have undergone previous breast surgery, with accuracies comparable to the results obtained in the general population of breast cancer patients. Indeed, the lymph drainage pattern may change in patients who have undergone prior procedures, as non-axillary drainage has been identified more often in reoperative SLNB than in primary SLNB. In 73% of such patients, radiocolloid migration to the regional nodal drainage basins has been noted in ipsilateral axillary, supraclavicular, internal mammary, interpectoral and contralateral axillary nodes [5.47].

Multifocal breast cancer is defined as separate foci of ductal carcinoma more than 2 cm apart within the same quadrant, while multicentric breast cancer indicates the presence of separate independent foci of carcinoma in different quadrants [5.48]. Until recently, SLNB was contraindicated in patients with multicentric and multifocal breast cancer because it was believed that it was difficult to localize the true SLN, and a negative SLNB would not exclude the possibility of positive LN metastasis in basins draining from other regions of the breast. However, most of the mammary gland can actually be considered as a single unit with lymph drainage to only a few designated LNs in the axilla [5.49, 5.50]. In this regard, the efficacy of SLNB in patients with multifocal/multicentric cancer has been shown to be equal to that in patients with unicentric breast cancer. Nevertheless, it should be noted that the presence of nodal metastasis is significantly higher in SLNs as well as in non-SLNs in patients with multicentric breast cancer; however, sensitivity, false negative rate and overall accuracy of SLNB are similar in both situations, although with some discordant results among different groups of investigators [5.51–5.53].

TABLE 5.1. RECOMMENDATIONS FOR SLNB
(adapted from Ref. [5.24])

Clinical circumstance	Use of SLNB
T1 or T2 tumours	Acceptable
T3 or T4 tumours	Not recommended
Multicentric tumours	Acceptable
Inflammatory breast cancer	Not recommended
DCIS with mastectomy	Acceptable
DCIS without mastectomy	Not recommended except for large DCIS (>5 cm) on core biopsy or with suspected or proven microinvasion
Suspicious, palpable axillary nodes	Not recommended
Older age	Acceptable
Obesity	Acceptable
Male breast cancer	Acceptable
Pregnancy	Not recommended
Evaluation of internal mammary LNs	Acceptable
Prior diagnostic or excisional breast biopsy	Acceptable
Prior axillary surgery	Not recommended
Prior non-oncological breast surgery	Not recommended
After pre-operative systemic therapy	Not recommended
Before pre-operative systemic therapy	Acceptable

Note: DCIS: ductal carcinoma in situ; LN: lymph node; SLNB: sentinel lymph node biopsy.

Early studies showed great variation in the frequency of lymphoscintigraphic visualization of the internal mammary chain during SLNM. It was later found that the internal mammary SLN detection rate is significantly affected by the depth of the radiocolloid injection. It is generally recognized that mapping of the internal mammary node (IMN) requires deep radiocolloid injection, either peritumoural or intratumoural [5.54–5.56]. Nevertheless, the rates of detection and intraoperative harvesting of IMN LNs are much lower than those for axillary LNs. Visualization of the IMN LNs has been detected in approximately one third of patients with breast cancer, of which approximately 63%–92% could be harvested during surgery; 11%–27% of these SLNs had metastases [5.55–5.58]. However, the significance of IMN SLNB is still being debated. There is evidence that IMN mapping leads to upstage migration and modification of treatment planning with respect to radiotherapy and systemic therapy, but evidence does not support that IMN mapping will improve the outcome of treatment and overall survival [5.59]. Debate is ongoing on whether SLNB is accurate enough after neoadjuvant chemotherapy, or whether it should be performed before starting neoadjuvant chemotherapy. Performing SLNB before or after primary systemic treatment has advantages and disadvantages in both cases. Before neoadjuvant chemotherapy (accepted in ASCO guidelines), SLNB yields a more precise axillary staging, with useful information about possible LN metastasis. Nevertheless, the procedure can delay the beginning of the treatment, and two operations can be necessary. On the other hand, SLNB performed after primary chemotherapy can assess the response at lymphatic level in the axilla, but may lead to underestimation of the initial stage [5.60]. After neoadjuvant chemotherapy, the SLN detection rate decreases, the false negative rate increases and the long term local recurrence rate in patients in which LDN has not been performed has not yet been determined. This group of patients was previously regarded as ineligible for SLNB because the lymph drainage pattern evaluated after chemotherapy may not represent the lymph drainage in the tumour basin before chemotherapy, therefore possibly leading to false negative results. Available data show that there are no significant differences in the success rate of SLNB according to clinical tumour size or clinical nodal status, and that the false negative rate is not affected by tumour response to chemotherapy. In particular, a systematic review of 24 clinical trials of SLNB in patients with breast carcinoma after neoadjuvant chemotherapy was undertaken. Metastatic LN involvement was found in 37% of patients, the global SLN identification rate was 89.6% and the overall false negative rate was 8.4% [5.61–5.63].

Until approximately ten years ago, pregnancy was considered to be a contraindication to performing SLNB; however, the radiation dosimetry burden to patients is very low and the overall benefit should be considered in those patients presenting early lesions. Pregnant patients with early lesions and clinically/US

negative axilla should therefore be offered the possibility of performing a 1 d procedure including SLNB (with a low amount of radiotracer) and breast surgery. In this regard, SLNB can be applied safely and successfully in pregnant women with breast cancer, with minimal risk to the fetus [5.64, 5.65]. The radiation exposure of the fetus from radiocolloids is very low and does not increase the risk of prenatal death, congenital malformation or mental impairment. On the other hand, blue dyes should not be used in pregnant patients [5.42].

Finally, some conditions that were previously considered to be formal contraindications to SLNB have changed to possible applications, on a patient to patient basis [5.43–5.45]. These conditions include large or locally advanced invasive breast cancers (T3), in situ ductal carcinoma, prior non-oncological breast surgery or axillary surgery, and the presence of suspicious palpable axillary LNs.

5.4. PROCEDURES FOR SLNM

Generally, the procedure for SLNM and SLNB involves radiocolloid (recommended) and/or blue dye injection, pre-operative scintigraphic imaging and intraoperative gamma probe localization for surgical removal of the detected LNs. However, there is no consensus regarding how the procedure should be performed. Controversies exist with regard to the selection of agents (vital dyes or radiocolloid), the radiocolloid particle size, the optimal route for interstitial injection, time to scintigraphy and intraoperative detection, and whether or not extra-axillary LNs should also be considered for harvesting and analysis. However, pre-operative lymphoscintigraphic mapping should be employed whenever possible because of the added benefit in identifying all potential sites of drainage and in providing the surgeon with a map of SLNs. Thus, pre-operative lymphatic mapping has the potential to both improve accuracy and reduce morbidity relative to the use of hand-held gamma probes alone [5.10, 5.11, 5.42].

5.4.1. Tracers and injection techniques

5.4.1.1. Radiotracers

The ideal radiocolloid should show rapid transit towards SLNs with persistent retention in the nodes. In general, the drainage, distribution and clearance of radioactive colloids by the lymphatic system vary, depending on the particle sizes. Small particles are drained and cleared first, while large particles are drained and cleared last and may be retained at the injection site. Worldwide, numerous ^{99m}Tc based agents have been utilized for radioguided SLNB for

breast cancer. These include ^{99m}Tc sulphur colloid, ^{99m}Tc antimony trisulphide colloid, ^{99m}Tc colloidal human albumin (i.e. ^{99m}Tc nanocolloid), ^{99m}Tc tin colloid, ^{99m}Tc labelled dextran, ^{99m}Tc hydroxylethyl starch and ^{99m}Tc stannous phytate (for a discussion of radiocolloids, see Chapter 3). However, the success rate in the identification of axillary SLNs is not significantly affected by the particle size of the radiocolloid used [5.66–5.68]. Therefore, selection of the radiocolloid is based more on local availability than on differences in SLN detection. New tracers have been developed in recent years. One of them is Lymphoseek, which is composed of a dextran backbone with multiple glucose and mannose residues attached to DTPA for ^{99m}Tc labelling. With a particle size of 7 nm, it binds to the mannose binding protein on the surface of reticuloendothelial cells. Compared with filtered ^{99m}Tc sulphur colloid, Lymphoseek has a faster clearance from the injection site, an equivalent primary SLN uptake and a lower mean number of SLNs detected per study [5.69]. However, it is not yet widely used.

The amount of radiocolloid to be administered varies considerably, and values have been reported as low as 3.7 MBq (0.1 mCi) [5.70] and as high as 370 MBq (10 mCi) [5.71]. In current practice, a single aliquot of 3.7–37 MBq (depending on the elapsed time between scintigraphy and surgery) of radiocolloid in 0.2–0.5 mL is generally considered sufficient for surgery planned the same day; in deep seated lesions, a slightly larger volume (0.5 mL) may be used. Prior day radiocolloid injection has been shown to be technically feasible by adequately increasing the amount of radioactivity injected (up to 148 MBq) [5.72].

European guidelines state that injection of large volumes of radiocolloid may disrupt local lymphatics; therefore, small volumes should be injected. Moreover, the syringe should also contain a similar amount of air to clear any dead space within the syringe and the needle.

5.4.1.2. Injection procedure

Radiocolloid administration for SLNB in breast cancer surgery has been described with numerous variants regarding the injection route, including deep (intratumoural and peritumoural) and superficial (intradermal, subdermal, subareolar and periareolar) injection (see Fig. 5.2). In the USA, the three predominant injection routes are intraparenchymal, intradermal and subareolar. A clinical trial comparing the intraparenchymal, intradermal and subareolar injection routes was conducted among 400 breast cancers, utilizing approximately 14.8 MBq (0.4 mCi) of ^{99m}Tc sulphur colloid. This study demonstrated superior intraoperative gamma probe localization of the axillary SLNs for the intradermal route (100%) compared to the subareolar route (95%) and the intraparenchymal route (90%) [5.73].

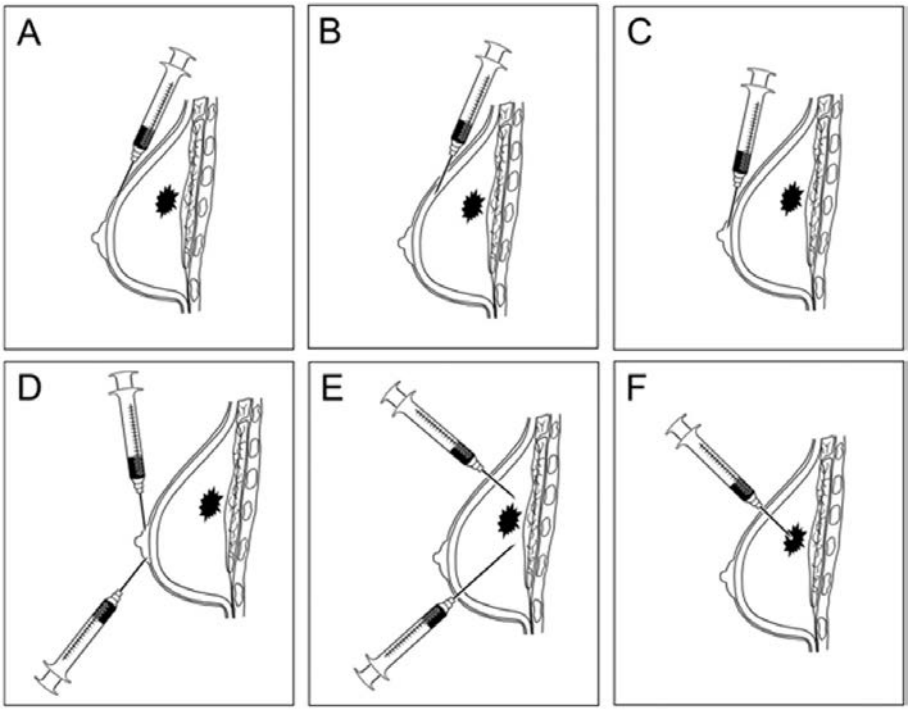

FIG. 5.2. Modalities of interstitial radiocolloid injection for SLNM in breast cancer. Superficial injections (A–D) and deep injections (E, F). Intradermal (A), subcutaneous (B), subareolar (C), periareolar (D), peritumoural (E) and intratumoural (F). Courtesy of R. Valdés Olmos, the Netherlands Cancer Institute.

Although the optimal injection approach has been the subject of active debate, tumour satisfactory results of SLNM and SLNB have generally been reported for all of the different injection approaches. In most cases, the SLNs detected by deep or superficial injections are the same. In this regard, multiple studies support the notion that the injection route does not significantly affect SLN identification. It appears that there is preferential drainage to the same few axillary SLNs for most of the breast tissue and its overlying skin, after merging initially to the retroareolar Sappey plexus; therefore, accurate SLNM of the axilla is not affected by the injection route. Furthermore, the superficial injection route, including intradermal or perisubareolar injections, has the highest SLN detection rate [5.74, 5.75].

One major advantage of superficial radiocolloid injection is that it is easy to perform and results in less interference with scintigraphic imaging. Thus, periareolar injection can be used particularly in upper quadrant tumours to avoid possible cross-talk owing to the short distance between the peritumoural depot and

the axillary SLNs. This approach has the advantage of demanding less experience; in addition, US guidance is not needed for the injection, even in patients with non-palpable breast cancer. However, intradermal or subdermal injection is more painful than intraparechymal injection; the addition of pH balanced 1% lidocaine to the radiocolloid solution has been reported to improve patient comfort without compromising SLN identification [5.42].

Deep injections may be difficult to perform if the tumour is non-palpable, and US or stereotaxic guidance may be needed. For tumours in the upper outer quadrant, radiocolloid injection may cause a shinethrough effect that interferes with SLN detection on pre-operative scintigraphy. An important advantage of deep injection is the improved detection of extra-axillary SLNs (Fig. 5.3) [5.76]. Nevertheless, the combination of both injection routes (either intratumoural or peritumoural and dermal or areolar injections) may improve detection accuracy and decrease the false negative rate. An anatomic study on breast lymphatics showed that, in some cases, alternative lymphatic drainage exists in the breast, although the majority of the superficial lymph vessels of the breast drain to only one SLN. It was also found that separate lymphatic networks exist in the ventral and in the dorsal part of the breast, which drain to the axilla and to the IMN, respectively, apparently without connections between the two lymphatic systems [5.77].

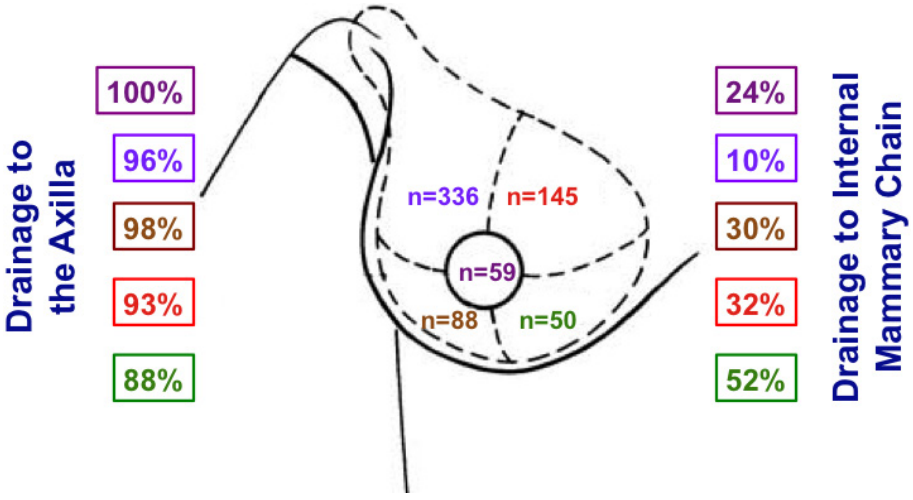

FIG. 5.3. Lymphatic drainage depending on tumour location using intratumoural radiocolloid injection. The reported percentage values correspond to the proportions of patients in whom lymphatic drainage was observed to either the axillary and/or the IMN LNs; sum values of the two lymphatic basins for each tumour location are therefore higher than 100%. Redrawn from data based on Ref. [5.76].

Regarding the use of blue dye for optical guidance during surgery, there is general agreement that combined administration of radiocolloid and blue dye using both superficial injection and deep injection enhances SLN detection. The site of injection can be gently massaged after the administration or if drainage of activity from the injection site is delayed at any time during the study [5.74, 5.75].

5.4.2. Pre-operative imaging and reporting

5.4.2.1. Image acquisition

Lymphoscintigraphic imaging is strongly recommended before any operative procedure because there is some variability in breast lymphatic drainage into the axilla and extra-axillary nodes, and more than one SLN can be visualized in a majority of the procedures.

The gamma camera should be equipped with an LEHR collimator. The energy window should be 15% (±5%) centred over the 140 keV photopeak of ^{99m}Tc. The patient lies supine for imaging on the gamma camera imaging table, although there are other possibilities (prone with hanging breast or upright). Anterior, 45° anterior oblique and lateral imaging can be obtained (at least two of them). During imaging, the arm on the side of the cancer is extended laterally to 90°, in the same position as during surgery.

Generally, a dynamic lymphoscintigraphic acquisition is not performed in SLNM for breast cancer. The images should be acquired within 15–30 min after the injection and 2–4 h or up to 16–18 h thereafter. Delayed images are helpful for detecting SLNs close to the primary tumour site, which may have been obscured on the initial views because of proximity to the radiocolloid injection site, and for detecting drainage to multiple nodal basins (Fig. 5.4).

Planar images are acquired for 3–5 min using a 256 × 256 matrix with a zoom of 1, although every facility can use its own protocol. A ^{57}Co or ^{99m}Tc flood source can be used for better delineation of the patient's body contour. Otherwise, this contour can be achieved by drawing it with a ^{57}Co or ^{99m}Tc source (pointer or syringe needle) (Fig. 5.5). The site of any suspected SLN can be localized on the overlying skin, preferably on the 45° anterior oblique image using a pointer, and the skin is marked with a small spot of indelible ink.

Although conventional planar imaging certainly enables identification of the draining pattern to SLNs, it does not provide the exact anatomic location of the detected nodes, which is information that is very useful intraoperatively. Combining functional and anatomic information, fused SPECT/CT images were introduced into clinical practice approximately ten years ago, to allow for precise anatomic localization of even small hot spots. Several reports have shown that

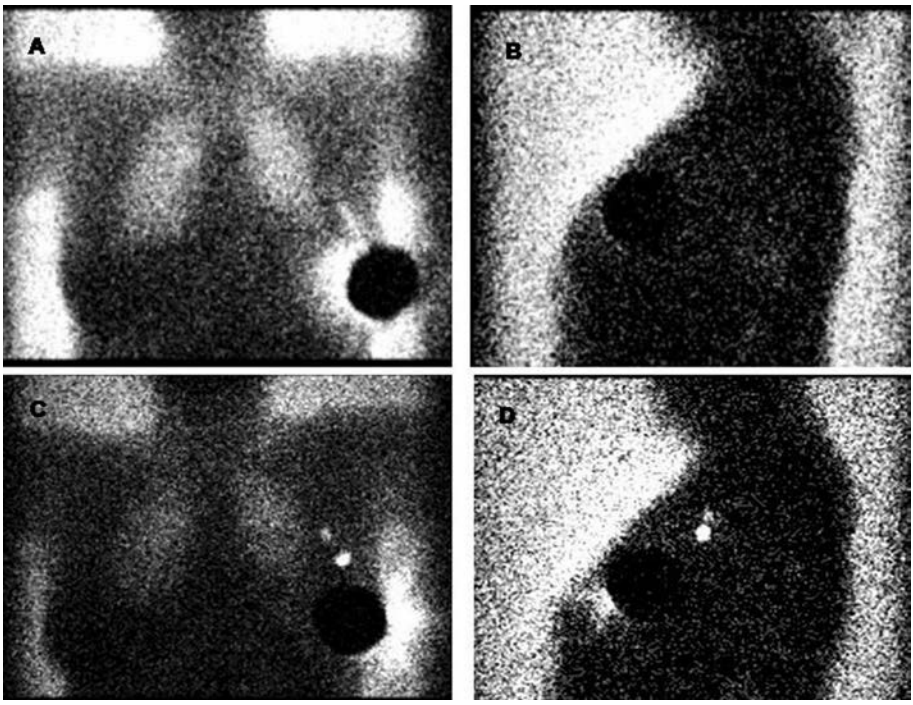

FIG. 5.4. Lymphoscintigraphic images of a 48 year old woman with a palpable cancer in her left breast. After injecting 111 MBq of ^{99m}Tc nanocolloid, early (A, B: anterior and lateral views, respectively) and delayed (C, D) planar images were acquired. The scatter effect in (A) avoids adequate SLN detection. Delayed images show two SLNs clearly detected in both the anterior and the lateral views.

advantages of SPECT/CT images relative to planar images can be seen, especially in obese patients, in deep located SLNs and in cases of lack of radiocolloid drainage visualization. SPECT/CT imaging provides significant information in the large majority of patients, with useful pre-operative complimentary information to the surgeons: better location (axilla, detailed extra-axillary location), reduced surgical time and greater confidence of the surgeons with the technique [5.78] (Fig. 5.6). In general, SPECT acquisition parameters for SLNM may be performed using a 128 × 128 matrix, 180° for each detector and a 3–6° angle step with a 20–25 s/frame acquisition time. CT image acquisition can provide sufficient anatomical details using low dose CT, with 5 mm slices.

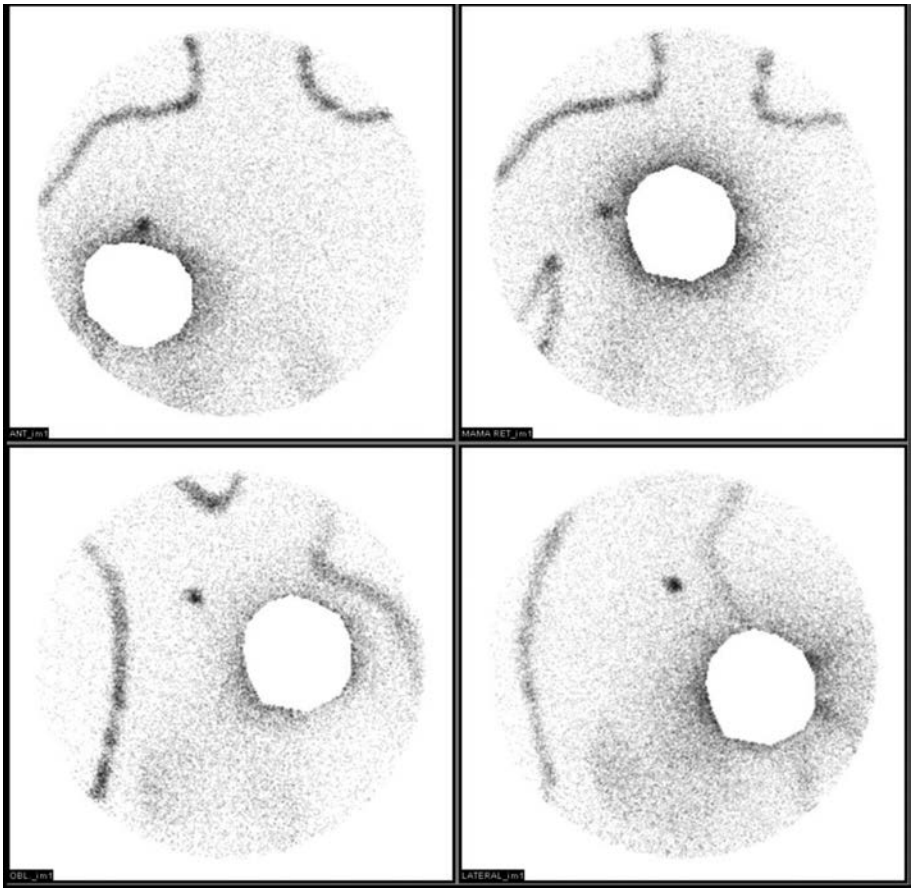

FIG. 5.5. Upper panel: Anterior and anterior with medially displaced breast views. Lower panel: Oblique and lateral views. All images were obtained in a patient with a right breast cancer. Images were acquired 2 h after injecting 105 MBq of ^{99m}Tc nanocolloid intratumourally. The silhouette of the patient was drawn using the remaining activity in the cone of the syringe. The injection site was covered with a lead shield to improve SLN visualization.

5.4.2.2. Interpretation criteria

Early and delayed lymphoscintigraphic planar images identify SLNs in most cases. Major criteria to identify LNs as SLNs are the visualization of lymphatic ducts, the time of appearance, the LN basin and the intensity of LN uptake [5.79]. By adopting these criteria, the visualized radioactive LNs can be classified as definitively SLNs, high probability SLNs and low probability SLNs (Fig. 5.7) (see also Chapter 4).

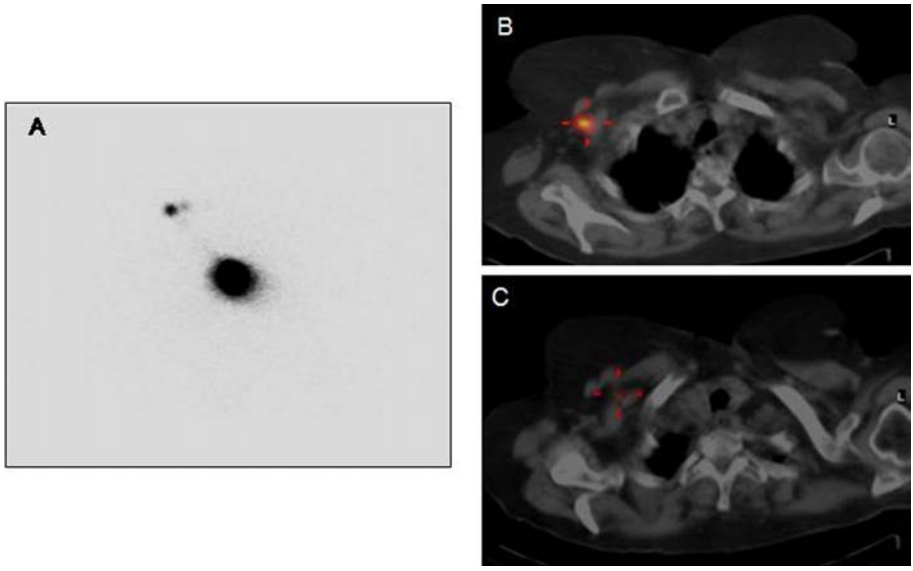

FIG. 5.6. Lymphoscintigraphy of a patient with cancer in the right breast. After injecting 111 MBq of ^{99m}Tc nanocolloid, one definitive SLN is depicted, with another focus of faint uptake nearby (A). The SPECT/CT image performed 2 h after radiocolloid injection provides superior anatomic localization of the SLNs, with impacts on surgical planning (B, C). The SPECT/CT image located on one of these nodes is in the anatomical Berg level 1, and the other is in Berg level 2.

Sequential planar images are essential for identification of the earliest draining LNs as SLNs, by visualizing the afferent lymphatic ducts or the first appearing LNs on lymphoscintigraphy. These nodes can be distinguished from secondary LNs, which mostly appear in the delayed planar images.

In some cases, SPECT/CT imaging can detect additional LNs in other basins. These LNs may, in turn, be considered as definitively or highly probable SLNs. Less frequently, a radioactive LN may appear between the injection site and a first draining node; its time dependent increase in uptake may confirm this node as a highly probable SLN and help to differentiate this node from a lymphatic lake or a lymphatic duct.

The SLN is not necessarily the hottest node, although this is often the case. Separate lymphatic channels that drain to different LNs identify each of those as distinct SLNs, even though they may be located in the same anatomic region. When drainage to more than one anatomic region is seen, each of those regions must have at least one SLN (Fig. 5.8).

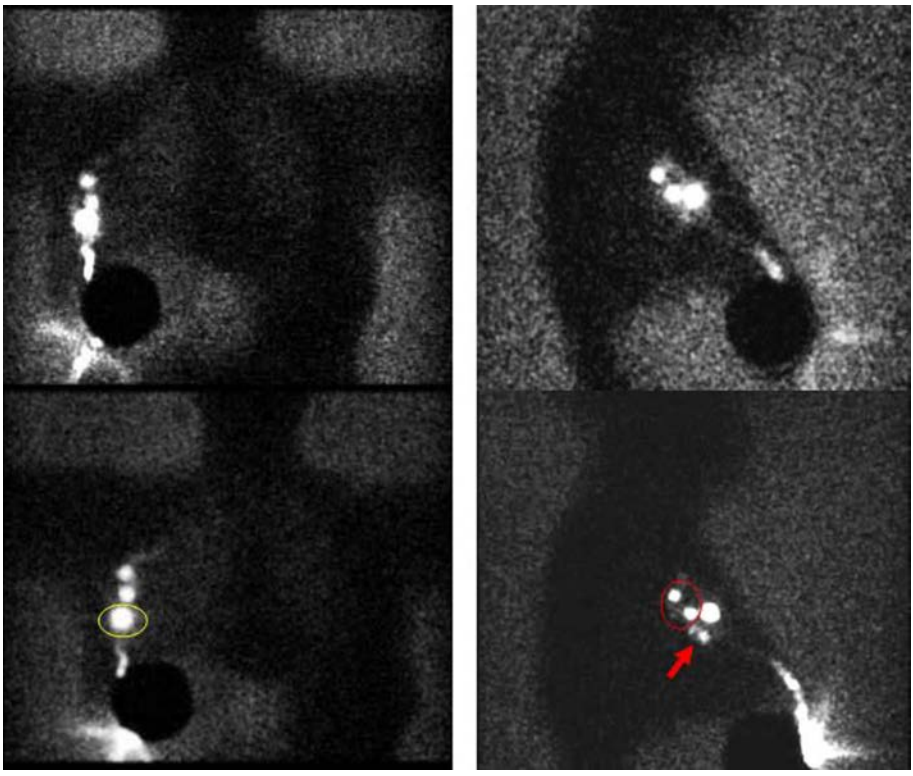

FIG. 5.7. Lymphoscintigraphic images of a 37 year old woman with a palpable cancer in her right breast. After injecting 111 MBq of ^{99m}Tc nanocolloid, early (upper panel) and delayed (lower panel) planar images were acquired. A definitive SLN (yellow circle) and three other high probability SLNs (red circle and arrow) are depicted.

5.4.3. Surgical procedures

Blue dye can be injected around the primary tumour or scar (in a similar way to how the radiocolloid was injected when adopting the peritumoural route) 10–20 min prior to the operation in a volume of 0.5–1 mL. The injection should be performed after the patient is anaesthetized to avoid a painful injection. Five minutes of gentle massage at the injection site enhances movement of the dye through the lymphatics to the SLN. Within 5–15 min, the SLN is coloured, with washout occurring after approximately 45 min. Currently, the most commonly used dyes are patent blue V, isosulfan blue and methylene blue.

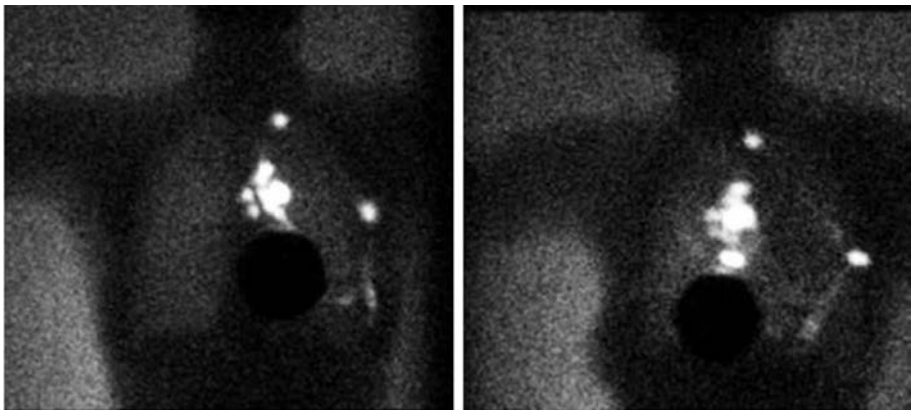

FIG. 5.8. A 29 year old patient with inferior medial quadrant cancer in her left breast. Early images (anterior and oblique) show two separate lymphatic drainage pathways, respectively, to the axilla and to the internal mammary chain. When drainage to more than one anatomic region is seen, each of those regions must have at least one SLN.

Multiple studies have validated the use of blue dyes as markers for SLNs with high detection rates (ranging from 75% to 95%), although these are slightly lower than the rates achieved by radiocolloids. In most cases, the same SLNs are detected by blue dyes as are detected by radiocolloids. A notable disadvantage of using blue dyes instead of radiotracers is that blue dyes are not helpful if extra-axillary nodes (IMN or supraclavicular) are to be evaluated [5.80, 5.81].

There are some contraindications to the use of blue dyes. Blue dyes may interfere with pulse oximetry readings, so in certain patients, they should be used with caution. Furthermore, blue dye is contraindicated in pregnancy (because of the risk of an anaphylactic reaction), in patients with earlier allergic reactions to blue dye and in severe renal impairment (methylene blue) [5.82]. On the other hand, hypersensitivity reactions to radiocolloids are rare, but have also been reported.

Gamma detection probes must be able to detect the SLN within the exposed surgical cavity as well as from outside the skin surface. In fact, the first step of the procedure consists of confirming with external measurements the location of the SLN before making the surgical incision; this task requires the sensitivity of the detector to be sufficient to identify a weakly active SLN when attenuated by, typically, up to 5 cm of soft tissue. Discriminating activity counts within the SLN from those originating from nearby sites requires the probe to be well collimated with a small angle of view. Using the images and skin markings as guides, the probe (placed over the regions of highest counts) can be used to select the optimum location for incision. The probe is placed in a sterile

bag for intraoperative use in the surgical field. The surgeon uses the probe to guide dissection to the hot node(s) and places the probe in the surgical bed after node excision to confirm removal of the hot node(s). When working with the probe, it is important to direct the probe away from activity at the injection sites. Counts are recorded per unit time with the probe in the surgical field, over the node before excision (in vivo) and after excision (ex vivo). A background tissue count is also recorded with the probe pointing away from the injection site, nodal activity or other physiological accumulation sites (i.e. liver) [5.42].

Deeply located SLNs are difficult to detect because of tissue attenuation; furthermore, the large amount of radioactivity retained at the injection site may cause SLNs located nearby to be missed. This is frequently observed when the tumour is located in the upper outer quadrants, or in cases of IMN sentinel nodes when the tumour is located in the inner quadrants. In the latter instance, it is advisable to use thinner probes (e.g. 10 mm diameter) in the intercostal area to better depict the activity spot in an area with reduced surgical space.

5.4.3.1. Interpretation criteria

LNs of the first two categories defined in Section 4.5. (definitively or highly probable SLNs as identified during lymphoscintigraphy) must be removed for analysis. Low probability SLNs may sometimes be removed, depending on the amount of remaining radioactivity measured by the gamma probe. An SLN usually has at least ten times the background count, taken at a location remote from the injection site. Various probe criteria have been employed for identification of the SLN (e.g. counts per second recorded for the presumed SLN have been compared with non-SLNs in vivo, ex vivo or with background counts in vivo, considering as SLNs all those nodes with a count rate higher than 10% of the count rate of the hottest SLN).

When a hot SLN has been removed, the surgical bed should be checked for remaining activity. Even when one hot SLN is clearly noted on lymphoscintigraphy, this scintigraphic appearance could actually represent two close SLNs erroneously detected as one, owing to the limited spatial resolution of the gamma camera. LNs closer than approximately 15–20 mm may well appear as one single node, so in some cases, another hot node may still be present at a close location after removal of the hottest SLN. In this regard, the current use of SPECT/CT imaging is very helpful because it may provide information about the actual presence of a cluster of LNs rather than a single SLN. When other sources of activity are found in the lymphatic basin, the decision of whether to remove them will depend upon the report from lymphoscintigraphy and the working definition of ‘nodes to remove’ (e.g. see below for the ‘10% rule’).

If blue dye is used, it can be a useful adjunct for aiding SLN localization and harvesting. Blue dye presents a lower SLN detection rate than radiotracers, but it can be used in addition to radiocolloids. Following injection, the blue dye drains to the SLNs, staining the channels, which can be followed to the first echelon nodes. Direct visualization and dissection of these channels facilitates SLN localization (Fig. 5.9).

FIG. 5.9. Methylene blue dye (1 mL) was injected periareolarly in a 44 year old woman with left breast cancer 10 min prior to the operation. After axillary surgical incision and tissue dissection, a blue stained SLN is clearly seen.

In practice, any LNs that have increased radioactive uptake or vital dye uptake are localized, and more often than not, multiple nodes are detected. The issue of how many SLNs should be biopsied when multiple nodes are found is still being debated. In this regard, while removing too few nodes may miss potential metastases in regional LNs, indiscriminate removal of axillary nodes may cause morbidity similar to that experienced after conventional axillary LDN (in addition to the unnecessarily increased burden for histopathological analysis).

5.4.3.2. SLN non-visualization or failed intraoperative detection

The majority of patients with pre-operative lymphoscintigraphic non-visualization will have at least one SLN detected intraoperatively, either by a gamma probe alone or by a gamma probe combined with blue dye. Otherwise, a second radiocolloid injection may be useful to depict the previous non-visualized SLN. In approximately 1%–2% of the patients, the SLN will not be detected intraoperatively, and the status of axillary LNs cannot be determined. Old age, obesity, tumour location other than in the upper outer quadrant and non-visualization of SLNs on pre-operative lymphoscintigraphy may be associated with failed SLN localization [5.83]. The significance of pre-operative scintigraphic SLN non-visualization is not yet known. Some studies have suggested that patients with unsuccessful axillary mapping may have an increased risk of metastatic axillary involvement [5.84]. Current standards of care recommend axillary LN dissection in cases of non-intraoperative SLN identification.

5.4.3.3. Histopathology of SLNs

Detailed histopathological analysis of the SLN is the standard procedure on which to base selection of the postoperative management strategy of breast cancer patients. However, protocols for SLN analysis have not yet been standardized; therefore, high variability in procedures still exists among different centres. Different procedures for intraoperative SLN analysis have been developed, including the touch imprint of one or more slices (relatively low sensitivity, but very high specificity), staining of one or several intraoperative frozen sections and even immunohistochemistry for cytokeratins as the most exhaustive method. Immunohistochemistry considerably improves sensitivity by identifying micrometastases and even isolated tumour cells (which are generally missed with conventional haematoxylin and eosin staining alone). Nevertheless, it is still difficult to compare results among different centres, particularly in studies involving detection of micrometastases and isolated tumour cells [5.85].

Molecular biology methods, such as those based on the reverse transcription polymerase chain reaction, are also being used for SLN analysis, although they are generally characterized by relatively poor reproducibility, longer time for intraoperative analysis and their inability to analyse the whole of the LNs. The recently developed one step nucleic acid amplification method is currently being validated in many centres [5.86].

5.5. ADDED VALUE OF INTRAOPERATIVE PORTABLE GAMMA CAMERAS

During the last decade, portable gamma cameras have become available for clinical practice; while some of these portable gamma cameras are not specifically designed for radioguided surgery, other models are focused on SLN procedures [5.87, 5.88] (see Fig. 5.10 for a representative system designed for radioguided surgical procedures).

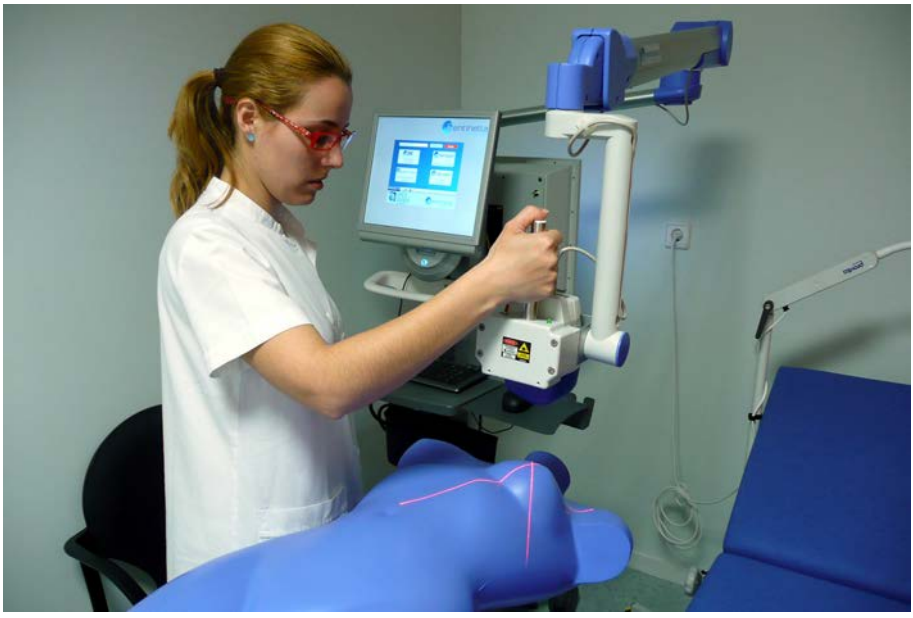

FIG. 5.10. Sentinella 102 (Oncovision, Valencia, Spain) is a portable gamma camera fitted with a pinhole collimator designed for intraoperative use. A laser pointer centres the target image on the screen.

There is no consensus on the need for intraoperative imaging to help SLN detection in breast cancer patients. Some authors believe that intraoperative imaging using a portable gamma camera is useful only when no conventional gamma camera is available, in particular in cases with extra-axillary drainage [5.89]. Difficult situations can be encountered in cases of intramammary or IMN SLNs, or when the SLN is located very close to the injection site. Although the large majority of these cases can be solved using the presurgical information provided by SPECT/CT, real time images acquired using a portable gamma camera can also be useful. Moreover, the use of point sources (e.g. ^{133}Ba or ^{125}I) facilitates SLN localization, as these sources can be depicted separately on the screen of the portable gamma camera, thus functioning as a pointer in the search for the SLNs. Appropriate use of a portable or a hand-held mini gamma camera enhances the reliability of the gamma probe by adding a clear image of the surgical field. Use of an intraoperative imaging device implies the possibility to better plan the surgical approach, to monitor the lymphatic basin before and after removal of the hot nodes, and to verify the correct SLN excision. For difficult to retrieve SLNs, real time imaging with this portable gamma camera in combination with the use of a traditional gamma counting probe results in higher intraoperative detection and localization of SLNs, especially when the injection site is close to the lymphatic basin, as in the case of intramammary and IMN SLNs [5.90] (Fig. 5.11).

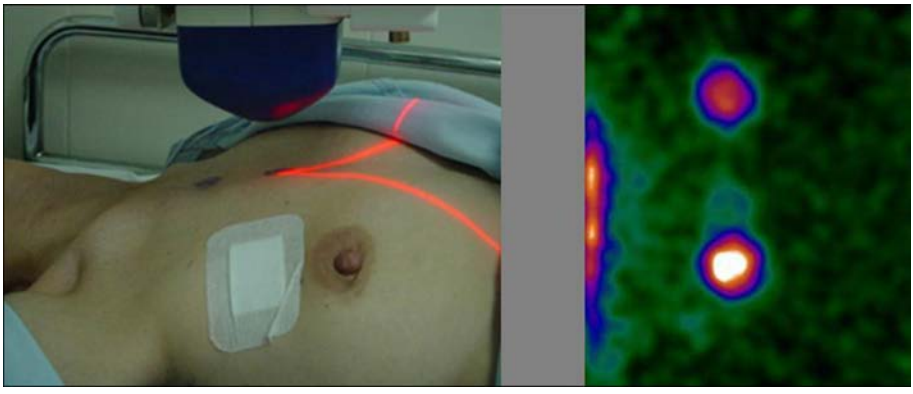

FIG. 5.11. Pre-operative imaging using a portable gamma camera in a 42 year old patient with a T1 breast cancer in her right upper quadrant. Left: After injecting 111 MBq of ^{99m}Tc nanocolloid, a scintigraphic anterior view is acquired by placing the portable gamma camera at previously marked points on the skin (internal mammary chain). Right: Image clearly shows two separate SLNs in this area, of which only the more caudal SLN had been visualized by planar imaging with a conventional gamma camera.

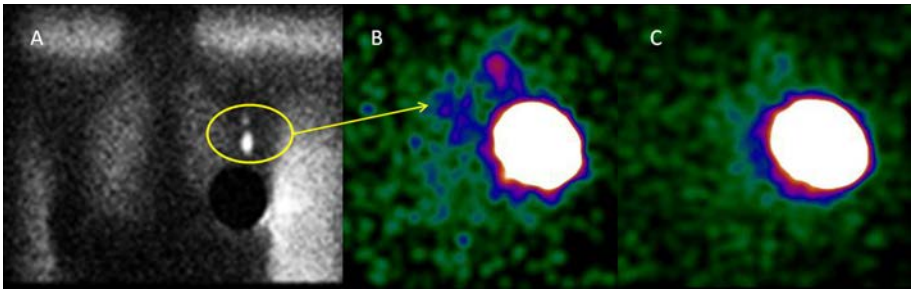

FIG. 5.12. A 57 year old patient with a breast cancer in her left upper outer quadrant. Lymphoscintigraphic images acquired 2 h after intratumoural injection of 111 MBq of ^{99m}Tc nanocolloid, showing two SLNs (yellow circle) (A). Image obtained using a portable gamma camera in the operating room before starting the SLN procedure, showing a similar scintigraphic pattern (yellow arrow) (B). Image acquired using the portable gamma camera after SLN excision, showing completeness of SLN removal (the residual large area of radioactivity accumulation corresponds to retention of the radiocolloid at the intratumoural injection site) (C).

After excision of each hot LN, a new image is acquired and compared with the image acquired before excision (Fig. 5.12). If focal radioactivity remains at the same location, it is concluded that another possible SLN is still in place.

Portable gamma cameras have also been used with promising results in other GOSTT environments regarding breast cancer, such as in the ROLL procedure, to check for tumour involvement of the resection margin [5.91] (Fig. 5.13).

New technological possibilities include a spatial localization system and two tracking targets to be fixed on the gamma probe, with the traditional acoustic signal of the gamma probe thus being combined with a real time 3-D visualization system available for the surgeon in the operating theatre (see Fig. 5.14). This feature, together with the real time depth information that the system may provide, would expand its application in SLN procedures in oncology, particularly for malignancies with deep lymphatic drainage [5.92].

5.6. ROLL AND OTHER PRIMARY LOCALIZING TECHNIQUES

5.6.1. ROLL

Screening programmes for breast cancer have led to an increase in detection of non-palpable breast tumours. Current approaches to breast cancer surgery aim at removing the lesion with an adequate clearance margin while, at the same

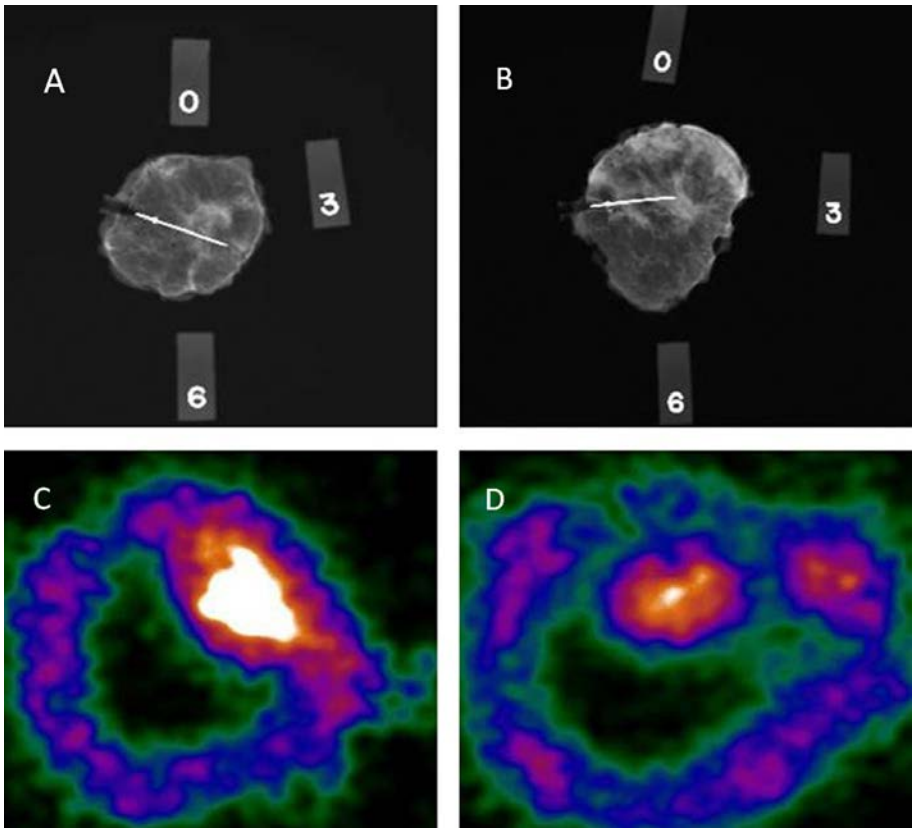

FIG. 5.13. The ROLL technique. After injecting 37 MBq in 0.2 mL of ^{99m}Tc MAA into the breast lesion (guided by ultrasonography), the surgeon performed tumour resection under guidance using the hand-held gamma probe. X ray lateral view of the specimen with the reference needle attached to the lesion (A). X ray anterior view of the same specimen (numbers indicate the specimen orientation in clockwise form) (B). Images of the surgical bed and the tumoural specimen were acquired by means of a portable gamma camera, fitted with a pinhole collimator (C, D). A ^{99m}Tc pointer was used to draw an outline image around the specimen in the same situation as in the X ray views. Potential involvement of the upper outer margins is suggested, as the injected radiotracer is closer to those margins.

time, accurately assessing the risk of distant metastases. Effective localization procedures are required to ensure complete excision of small non-palpable lesions detected on either symptomatic mammography or screening mammography. Several localization techniques have been developed for this purpose.

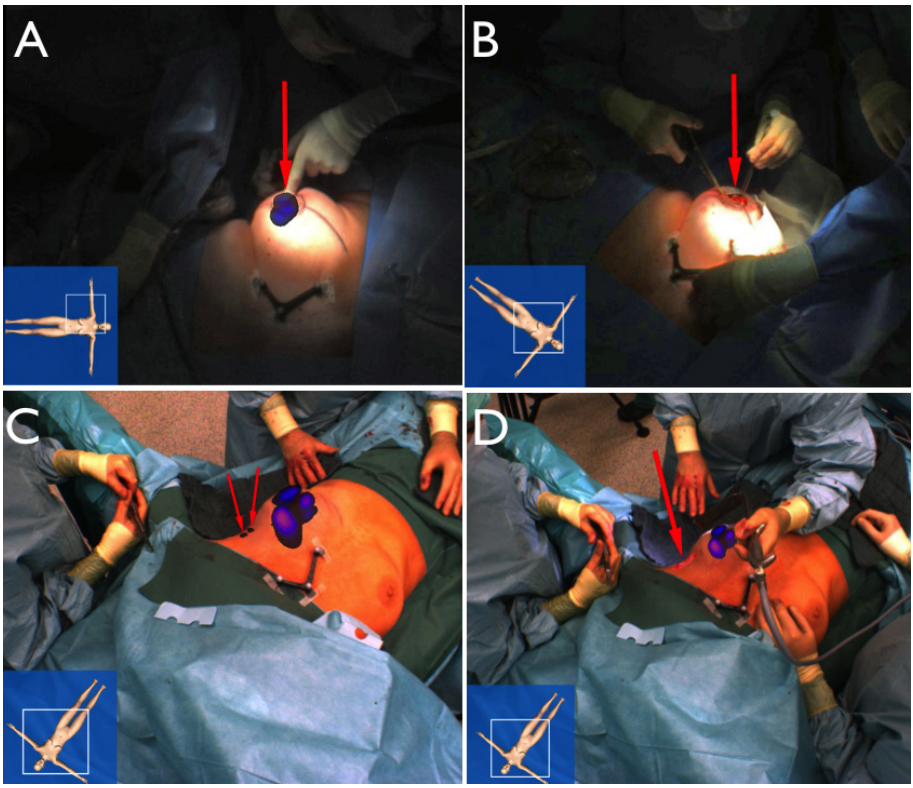

FIG. 5.14. Freehand SPECT based device system used for radioguided surgery in a patient with non-palpable breast cancer. (A) Overlay of freehand SPECT 3-D image on the video display shows high retention of radiocolloid at the intratumoural injection site. (B) After tumour removal, the absence of radioactivity accumulation in the surgical field confirms complete excision of the tumour. (C, D) A similar approach is used to guide the surgeon for complete removal of SLNs (red arrows).

Wire localization of non-palpable lesions has been the most widely used pre-operative technique for many years. Although this is a reasonably effective technique, it involves a number of disadvantages. First, the entry site of the wire is often not at the ideal location for surgical incision at the time of operation. This may lead to additional unnecessary dissection and suboptimal cosmetic results. In addition, the wire must be placed on the day of the operation, necessitating the coordination of radiology and operative schedules. The most important disadvantage, however, is the inaccuracy of localizing the target lesion percutaneously and during dissection. This results in high rates of reoperation for tissue margins involved in carcinoma.

Intraoperative US imaging without pre-operative wire localization has been used to map excision of non-palpable breast lesions; however, this technique has limitations, as the breast lesion must be visible during the US imaging [5.93–5.95].

The ROLL approach has gained popularity for non-palpable tumour lesions, including breast cancer. ROLL involves the injection into the centre of the lesion of a small amount of radioactive tracer that does not migrate from the site of interstitial injection, typically ^{99m}Tc MAA. Injection is performed on the same day or on the day before surgery, under mammographic or US guidance; activity injected ranges from 1.8 MBq (0.05 mCi) to 148 MBq (4 mCi). Surgeons identify the lesion intraoperatively as a hot spot by using a hand-held gamma probe, which allows accurate lesion localization and removal with minimal excision of healthy tissue (Fig. 5.15). After specimen resection, residual activity in the surgical field must be checked to avoid the possibility of missing some residual involved tissue [5.96–5.98]. This technique enables a good cosmetic outcome.

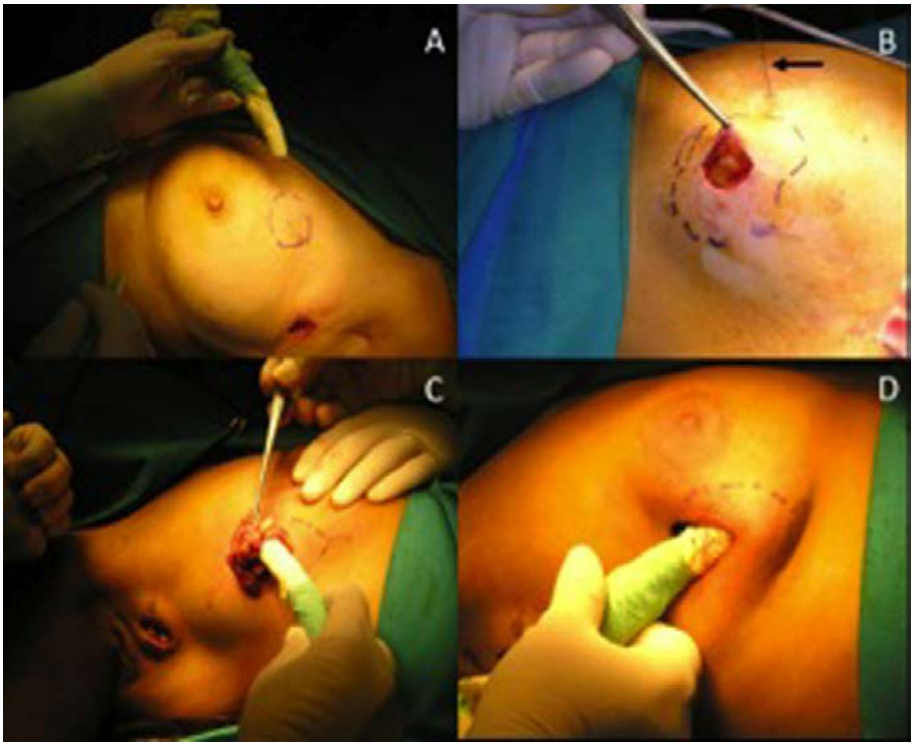

FIG. 5.15. The ROLL surgical technique. (A) The probe assesses the highest activity area. (B) The ROLL technique does not interfere with the surgical approach (skin incision) as the hookwire approach does (black arrow). (C) The surgeon resects the specimen using gamma probe guidance. (D) After resection, the surgical bed is checked again for any residual activity.

Additional advantages of ROLL versus prior techniques include better lesion concentricity into the resected specimen, better free margins and ease of the entire procedure. However, some potential pitfalls have been described; these are related to possible radiotracer spillage, contamination of the skin or the injection path or ductal diffusion, as well as the presence of microcalcifications or ductal carcinoma in situ [5.99, 5.100].

A systematic review of the ROLL technique concluded that this approach compares favourably with conventional wire localization for non-palpable breast lesions (Table 5.2) [5.101–5.108]. On the other hand, radiation doses at the injection site, and patient and staff absorbed doses are maintained well within the recommended limits established by the International Commission on Radiological Protection (ICRP) [5.103, 5.109, 5.110]. Finally, the possibility of performing ROLL after systemic intravenous administration of ^{99m}Tc sestamibi (as a non-specific, tumour seeking agent) on the day of surgery has also been described [5.111].

TABLE 5.2. SUMMARY OF THE STUDIES COMPARING ROLL VERSUS THE HOOKWIRE TECHNIQUE

Reference	*n* (ROLL–hookwire)	Detection (%)	Free margins (ROLL versus hookwire) (%)	*p*
Gallegos [5.101]	132 (65–67)	100	83 versus 64	0.014
Macmillan et al. [5.102]	95 (48–47)	100	61 versus 72	NS
Nadeem et al. [5.103]	130 (65–65)	100	83 versus 57	0.001
Thind et al. [5.104]	140 (70–70)	100	84 versus 60	0.002
Zgajnar et al. [5.105]	143 (51–92)	100	70 versus 44	—
Rönkä et al. [5.106]	78 (64–14)	100	89 versus 79	0.05
Fraile et al. [5.107]	233 (65–168)	100	80 versus 70	NS
Strnad et al. [5.108]	33 (21–12)	100	Hookwire < ROLL	NS

ROLL: radioguided occult lesion localization.

Reported advantages of the ROLL technique include:

— Precise intraoperative localization of the breast lesion;
— Complete lesion resection, with free margins and reduced need for second operations;
— An increased capacity to centre the lesion within the specimen;
— A surgical approach (skin incision) that is independent from the intralesional radiotracer injection procedure.

5.6.2. Combined SLNB and ROLL procedures

As ROLL is an excellent technique to remove small breast cancers, it is very important to simultaneously perform SLNB without compromising oncological safety and the SLN detection rate. Different techniques have been described to identify the SLNs in combination with ROLL (SNOLL). De Cicco et al. [5.112] obtained a high sensitivity when combining an intratumoural injection of ^{99m}Tc MAA for ROLL of a tumour with a subdermal injection of ^{99m}Tc nanocolloid for SLNM and SLNB. When the lesions are located near to the areola, intraoperative interference between the ROLL tracer and SLNM tracer could be avoided by elevation of the dermis and the subdermal area after skin incision. Other investigators have successfully used a single intratumoural injection for both ROLL and SNOLL in the same session. In the largest retrospective series to date, 959 patients with proven breast cancer underwent ROLL plus radioguided SLNB, with successful breast lesion localization in 99.6% of the cases and negative surgical margins in 91.6% of the cases [5.112, 5.113]. The majority of the studies published so far with this technique show a high percentage of successful tumour resection and intraoperative SLN localization with reduced failure [5.114–5.116].

5.6.3. Radioactive seeds

Alternatives to hookwire localization of occult breast lesions include carbon trace and US guided resection, as well as the use of sealed radioactive seeds. The seed technique was described initially in 2001 by Grey et al. [5.117], based on placement of an ^{125}I titanium seed in the centre of the lesion under mammographic or ultrasonographic guidance. Subsequently, excision of the lesion is guided by a hand-held gamma probe. The seeds are essentially the same as the seeds used in brachytherapy for cancer of the prostate. The ^{125}I radioactive seed is composed of a 4.5–0.8 mm titanium capsule containing a ceramic cylinder enriched with radioiodine. Iodine-125 has a long decay time (half-life of 59.4 d), emitting low energy photons (27 keV). The use of one or two seeds with this low

photon energy has a negligible effect on the surrounding tissue. The non-palpable lesion is visualized by mammography or ultrasonography. The radioactive seed is placed in the breast lesion using an 18 G needle fixed in a needle holder. After successful positioning, the exact location is confirmed by mammography. If a SNOLL technique is scheduled, the ^{99m}Tc colloid is injected around the tumour. Thus, the hand-held gamma probe can be switched between the 27 keV energy window of the ^{125}I source and the 140 keV of the ^{99m}Tc, allowing discrimination between these two isotope sources. As in the ROLL technique, the skin incision is made at the site with highest counts, or at a site suitable for oncoplastic breast surgery. Seed removal is verified by the absence of ^{125}I activity in the breast and its presence in the specimen. X rays of the surgical specimen confirm the presence of the seed and the relation of the lesion to the resection margins.

In a study involving 325 patients with non-palpable breast cancer lesions, complete resection was achieved in 95% of the cases [5.118]. The same technique was compared with classical hookwire localization. A second operation was required in 8% of the seed's group to achieve negative margins, versus 25% in the hookwire group [5.119]. Therefore, radioguided seed localization in non-palpable breast lesions is at least equivalent to the hookwire technique in terms of ease of procedure, removing the target lesion, volume of breast tissue excised, obtaining negative margins, avoiding a second operative intervention and allowing for simultaneous axillary staging [5.120, 5.121].

5.7. ADDED VALUE OF SPECT/CT IMAGING IN SLNB

The recently introduced hybrid gamma cameras with integrated CT imaging (SPECT/CT) fuse tomographic lymphoscintigrams with anatomical data from CT. SPECT/CT imaging provides better contrast and resolution than planar imaging and has the possibility to correct for attenuation and scatter. This combination of imaging properties results in a clear depiction of the SLN within an anatomical landscape, thus providing a valuable surgical road map [5.122].

There are limited data on the use of hybrid SPECT/CT images for lymphatic mapping in patients with breast cancer. Mapping of all direct tumour draining LNs requires knowledge of the number and location of these SLNs, which will be provided by SPECT/CT in addition to planar images. The first large study on SPECT/CT imaging in breast cancer reported improved pre-operative localization of hot nodes [5.123]. It has been shown that SPECT/CT images can detect additional SLNs not visualized on planar images and is especially useful in visualization of SLNs outside the axilla or of SLNs close to the injection site.

Non-nodal sites of tracer accumulation, typically owing to contamination, can also be correctly identified, thereby avoiding surgical exploration to pursue a non-existing SLN. While SLNs near the injection area are easily missed with conventional imaging, SPECT/CT imaging can discern such nodes and also identify SLNs in a substantial number of patients in whom the conventional images do not show enough uptake [5.124] (Fig. 5.16).

In a recent review of the use of SPECT/CT imaging for SLNM in breast cancer patients, timing of the SPECT/CT images varied from 30 min up to 18 h after radiocolloid injection, and the SLN visualization rates were better with SPECT/CT imaging (89%–92%) than with conventional imaging (63%–88%) in all comparative studies. SPECT/CT imaging appeared to be of particular value in obese patients. Conventional imaging failed to visualize SLNs in 28% of obese patients, while non-visualization was 13% using SPECT/CT imaging. The visualization rate using conventional imaging decreased with increasing body mass index, while the SPECT/CT results remained relatively stable [5.125].

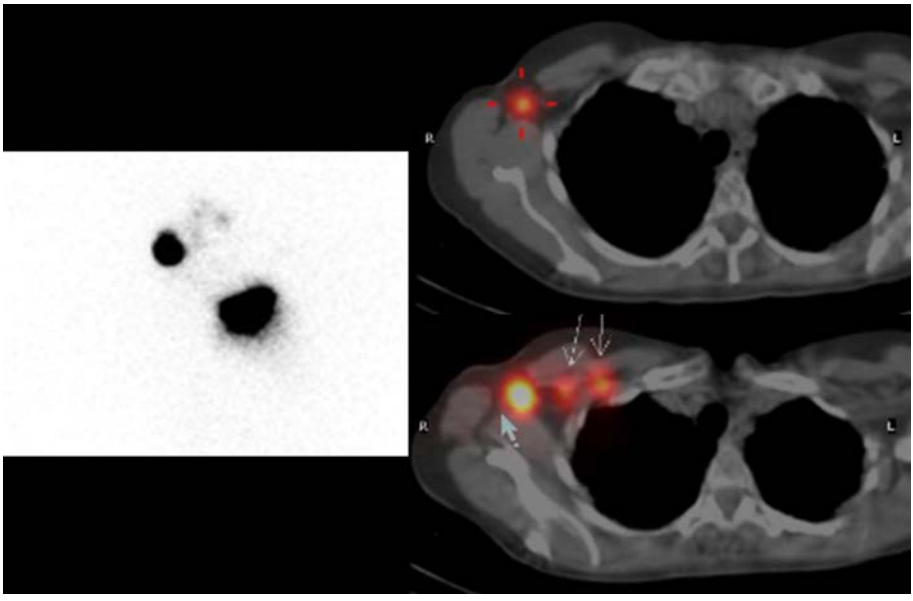

FIG. 5.16. Left: Planar image (anterior view) obtained of a 40 year old woman with a tumour in her right breast. A high uptake is observed in the homolateral axilla, with faint diffuse activity upstream. Right: Fused SPECT/CT images depict a greater number of SLNs than planar images. This issue has a definite surgical impact because SPECT/CT imaging located one of these SLNs in axilla Berg level 1, and three SLNs in levels 2 and 3.

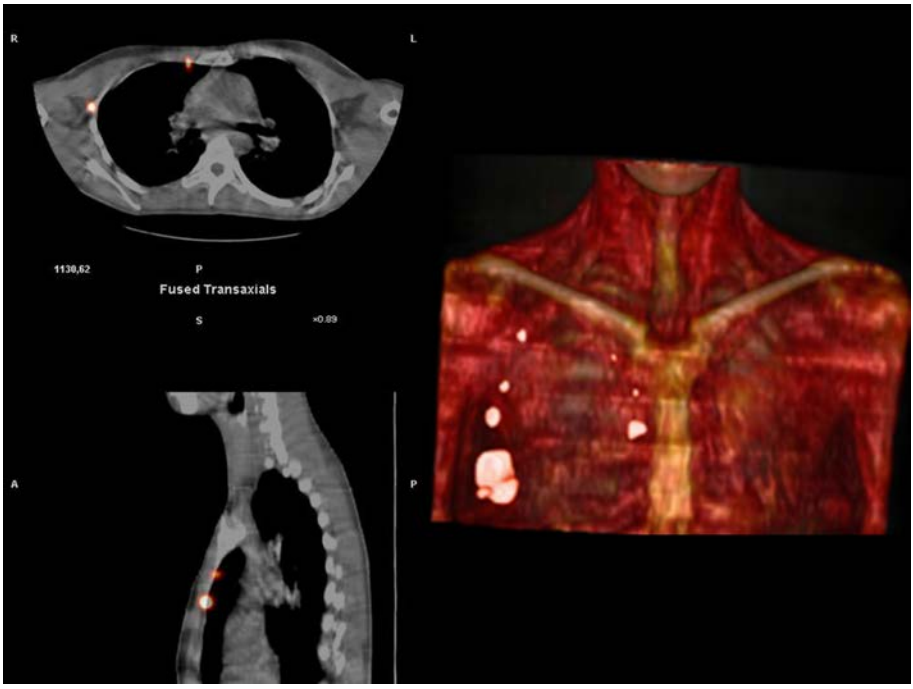

FIG. 5.17. Images obtained of a 38 year old woman with a tumour in her right lower outer quadrant. After injection of 111 MBq of ^{99m}Tc nanocolloid, planar images were acquired at 30 min and 2 h. Subsequently, SPECT/CT acquisition was started. Fused SPECT/CT images (left panel) in the axial and sagittal axes are depicted, showing uptake in IMN and in the axilla. Volume rendering reconstruction (right panel) provides a precise overview of the location of every SLN with reference to the anatomical background.

The value of SPECT/CT imaging for the surgical approach has also been explored, showing that in 15% of all SLN positive patients, the involved SLNs were depicted only on the SPECT/CT images. The initially planned surgical incision was changed on the basis of the anatomical information provided by SPECT/CT imaging in 42% of the patients. The location of the incision was more precise in 36%, an extra incision was made in 4% and an incision was omitted in 1.5% of cases [5.126]. In patients with an SLN located in the IMN, the incision can be placed more precisely because SPECT/CT imaging shows the exact intercostal space that should be explored or a location underneath a rib or behind the sternum (Fig. 5.17). In nearly half of the series, the surgeons found the fused images useful or very useful because they diminish the surgical time. In the majority of cases, the surgical team felt comfortable with the anatomic information provided by the fused SPECT/CT images. In cases of more than

one SLN, the relationship between the SLN counts in the SPECT/CT images is reproduced by the surgical probe and helps to ensure that all SLNs have been identified and removed [5.126].

However, because the current conventional approach based on combined radiocolloid and blue dye injection, pre-operative planar scintigraphic imaging and intraoperative gamma probe counting has proven very successful (with SLN detection rates over 95%), the added value of SPECT/CT imaging seems to be limited to a rather small fraction of the patients undergoing SLNB. Moreover, the introduction of hybrid SPECT/CT into daily practice is associated with additional costs and requires extra time. For these reasons, specific indications for the use of SPECT/CT imaging should be defined, so that the majority of patients who will not benefit from this imaging technique are spared unnecessary costs and inconvenience. Current recognized indications for SPECT/CT imaging in breast cancer patients are represented by non-visualization of SLNs with conventional imaging, obesity, and presence of extra-axillary SLNs or otherwise unusual drainage (e.g. in cases of previous breast surgery). SPECT/CT imaging might also be performed if the conventional images are difficult to interpret (e.g. if contamination is suspected or an SLN is located near to the injection area) [5.127].

5.8. CONCLUDING REMARKS

Current data indicate that the combined use of radioactive tracers and blue dyes is more effective in detecting SLNs than either modality used alone, and is therefore recommended for routine use. Most injection modalities of the radiocolloid provide satisfactory results. The combined radiocolloid injection approach (both superficial and deep injections) results in a higher identification rate of SLNs. Routine pre-operative scintigraphic imaging helps the intraoperative search for SLNs, and is vital for detecting extra-axillary or aberrant SLNs, as well as in patients who have had prior core breast biopsy or surgery. SPECT/CT imaging, in addition to conventional lymphoscintigraphy, leads to improved pre-operative visualization and localization of SLNs, especially if performed for specific indications. Sequential conventional images remain useful to distinguish true SLNs from secondary echelon nodes. In breast cancer, SPECT/CT imaging can depict SLNs that are not visible in conventional imaging. Depiction of the exact location of extra-axillary nodes using SPECT/CT facilitates planning and execution of the operation.

Intraoperative imaging with portable gamma cameras is being increasingly employed, enhancing the reliability of the gamma probe by adding clear imaging of the surgical fields. Use of an intraoperative imaging device implies

the possibilities of improving the planning of the surgical procedure and of monitoring the lymphatic basin before and after removal of the hot SLNs, to verify the completeness of the SLN excision. For difficult to retrieve SLNs, real time imaging with portable gamma cameras in combination with the use of a traditional gamma counting probe results in higher intraoperative detection and localization of SLNs, especially when the injection site is close to the lymphatic basin and intramammary or IMN SLNs are depicted. Portable gamma cameras can also be useful during ROLL procedures in patients with non-palpable breast lesions.

REFERENCES TO CHAPTER 5

[5.1] CABANAS, R.M., Anatomy and biopsy of sentinel lymph nodes, Urol. Clin. North. Am. **19** (1992) 267–276.

[5.2] KRAG, D.N., WEAVER, D., ALEX, J.C., FAIRBANK, J.T., Surgical resection and radiolocalization of sentinel lymph node in breast cancer using a gamma probe, Surg. Oncol. **2** (1993) 335–339.

[5.3] GIULIANO, A.E., KIRGAN, D., GUENTHER, J.M., Lymphatic mapping and sentinel lymphadenectomy for breast cancer, Ann. Surg. **220** (1994) 391–401.

[5.4] GIULIANO, A.E., et al., Improved axillary staging of breast cancer with sentinel lymphadenectomy, Ann. Surg. **222** (1995) 394–401.

[5.5] ALEX, J.C., KRAG, D.N., The gamma-probe-guided resection of radiolabeled primary lymph nodes, Surg. Oncol. Clin. North Am. **5** (1996) 33–41.

[5.6] NOGUCHI, M., KATEV, N., MIYAZAKI, I., Diagnosis of axillary lymph node metastases in patients with breast cancer, Breast Cancer Res. Treat. **40** (1996) 283–293.

[5.7] TAYLOR, A., Jr., MURRAY, D., HERDA, S., VANSANT, J., ALAZRAKI, N., Dynamic lymphoscintigraphy to identify the sentinel and satellite nodes, Clin. Nucl. Med. **21** (1996) 755–758.

[5.8] MEIJER, S., COLLET, G.J., PIJPERS, H.J., VAN HATTUM, L., HOEKSTRA, O.S., Less axillary dissection necessary due to sentinel node biopsy in patients with breast carcinoma, Ned Tijdschr Geneeskd **140** (1996) 2239–2243.

[5.9] ALBERTINI, J.J., et al., Lymphatic mapping and sentinel node biopsy in the patient with breast cancer, JAMA **276** (1996) 1818–1822.

[5.10] ALAZRAKI, N.P., et al., Lymphoscintigraphy, the sentinel node concept, and the intraoperative gamma probe in melanoma, breast cancer, and other potential cancers, Semin. Nucl. Med. **27** (1997) 55–67.

[5.11] PIJPERS, R., et al., Impact of lymphoscintigraphy on sentinel node identification with technetium-99m-colloidal albumin in breast cancer, J. Nucl. Med. **38** (1997) 366–368.

[5.12] GIULIANO, A.E., Lymphatic mapping and sentinel node biopsy in breast cancer, JAMA **277** (1997) 791–792.

[5.13] REINTGEN, D., et al., The role of selective lymphadenectomy in breast cancer, Cancer Control **4** (1997) 211–219.
[5.14] VERONESI, U., et al., Sentinel-node biopsy to avoid axillary dissection in breast cancer with clinically negative lymph-nodes, Lancet **349** (1997)1864–1847.
[5.15] BENSON, J.R., DELLA ROVERE, G.Q., AXILLA MANAGEMENT CONSENSUS GROUP, Management of the axilla in women with breast cancer, Lancet Oncol. **8** (2007) 331–348.
[5.16] INTERNATIONAL BREAST CANCER CONSENSUS CONFERENCE, Image-detected breast cancer: State of the art diagnosis and treatment, Breast J. **8** (2002) 70–76.
[5.17] INTERNATIONAL BREAST CANCER CONSENSUS CONFERENCE, Image-detected breast cancer: State of the art diagnosis and treatment, J. Am. Coll. Surg. **193** (2001) 297–302.
[5.18] JEMAL, A., SIGEL, R., XU, J., WARD, E., Cancer statistics, 2010, CA Cancer J. Clin. **60** (2010) 277–300.
[5.19] CARLSON, R.W., et al., Breast cancer: Clinical practice guidelines in oncology, J. Natl. Compr. Canc. Netw. **7** (2009) 122–192.
[5.20] BONNEMA, J., et al., Ultrasound guided aspiration biopsy for detection of non palpable axillary node metastases in breast cancer patients: New diagnostic method, World J. Surg. **21** (1997) 270–274.
[5.21] ABE, H., et al., Axillary lymph nodes suspicious for breast cancer metastasis: Sampling with US-guided 14-gauge core-needle biopsy—Clinical experience in 100 patients, Radiology **1** (2009) 41–49.
[5.22] VERONESI, U., et al., A randomized comparison of sentinel-node biopsy with routine axillary dissection in breast cancer, N. Engl. J. Med. **349** (2003) 546–553.
[5.23] SCHWARTZ, G.F., GIULIANO, A.E., VERONESI, U., CONSENSUS CONFERENCE COMMITTEE, Proceedings of the consensus conference on the role of sentinel lymph node biopsy in carcinoma of the breast April 19–22, 2001, Philadelphia, PA, USA, The Breast **11** (2002) 362–373.
[5.24] LYMAN, G.H., et al., American Society of Clinical Oncology guideline recommendations for sentinel lymph node biopsy in early-stage breast cancer, J. Clin. Oncol. **23** (2005) 7703–7720.
[5.25] NATIONAL COMPREHENSIVE CANCER NETWORK, Clinical Practice Guidelines in Oncology, Breast Cancer (2010), www.nccn.org
[5.26] PIÑERO, A., et al., Consensus meeting on sentinel lymph node biopsy in breast cancer, Spanish society of mastology and breast disease, Rev. Esp. Med. Nucl. **26** (2007) 176–180.
[5.27] VERONESI, U., et al., Sentinel node biopsy in breast cancer: Early results in 953 patients with negative sentinel node biopsy and no axillary dissection, Eur. J. Cancer **41** (2005) 231–237.
[5.28] KRAG, D.N., et al., Sentinel lymph node resection compared with conventional axillary-lymph-node dissection in clinically node-negative patients with breast

cancer: Overall survival findings from the NSABP B-32 randomised phase 3 trial, Lancet Oncol. **11** (2010) 927–933.
[5.29] GIULIANO, A.E., et al., Axillary dissection vs no axillary dissection in women with invasive breast cancer and sentinel node metastasis: A randomized clinical trial, JAMA **305** (2011) 569–575.
[5.30] KESHTGAR, M.R.S., ELL, P.J., Sentinel lymph node detection and imaging, Eur. J. Nucl. Med. **26** (1999) 57–67.
[5.31] VERONESI, U., et al., Sentinel-lymph-node biopsy as a staging procedure in breast cancer: Update of a randomized controlled study, Lancet Oncol. **7** (2006) 983–992.
[5.32] ESTOURGIE, S.H., et al., What is a false-negative result for sentinel node procedures in breast cancer? J. Surg. Oncol. **82** (2003) 141–142.
[5.33] PEPELS, M.J., et al., Safety of avoiding routine use of axillary dissection in early stage breast cancer: A systematic review, Breast Cancer Res. Treat. **125** (2011) 301–313.
[5.34] GALIMBERTI, V., ZURRIDA, S., ZUCALI, P., LUINI, A., Can sentinel node biopsy avoid axillary dissection in clinically node-negative breast cancer patients? Breast **7** (1998) 8–10.
[5.35] ZAVAGNO, G., et al., Sentinel node biopsy in breast cancer, Breast **9** (2000) 139–143.
[5.36] KRAG, D.N., et al., National Surgical Adjuvant Breast and Bowel Project, Technical outcomes of sentinel-lymph node resection and conventional axillary lymph-node dissection in patients with node-negative breast cancer: Results from the NSABP B32 randomised phase III trial, Lancet Oncol. **8** (2007) 881–888.
[5.37] KESHTGAR, M., et al., Implementing sentinel lymph node biopsy programs in developing countries: Challenges and opportunities, World J. Surg. **35** (2011) 1159–1168.
[5.38] MANSEL, R.E., et al., Randomized multicenter trial of sentinel node biopsy versus standard axillary treatment in operable breast cancer: The ALMANAC trial, J. Nat. Cancer Inst. **98** (2006) 599–609.
[5.39] PURUSHOTHAM, A.D., et al., Morbidity after sentinel node biopsy in primary breast cancer: Results from a randomized controlled trial, J. Clin. Oncol. **23** (2005) 4312–4321.
[5.40] VAN DER PLOEG, I.M., NIEWEG, O.E., VAN RIJK, M.C., VALDÉS OLMOS, R.A., KROON, B.B., Axillary recurrence after a tumour-negative sentinel node biopsy in breast cancer patients: A systematic review and meta-analysis of the literature, Eur. J. Surg. Oncol. **34** (2008) 1277–1284.
[5.41] GOYAL, A., NEWCOMBE, R.G., CHABRA, A., MANSEL, R.E., ALMANAC TRIALISTS GROUP, Factors affecting failed localization and false-negative rates of sentinel node biopsy in breast cancer-results of the ALMANAC validation phase, Breast Cancer Res. Treat. **99** (2006) 203–208.
[5.42] BUSCOMBE, J., et al., Sentinel node in breast cancer procedural guidelines, Eur. J. Nucl. Med. Mol. Imaging **34** (2007) 2154–2159.
[5.43] EDGE, S.B., et al. (Eds), AJCC Cancer Staging Manual, 7th edn, Springer (2010).

[5.44] GOLDHIRSCH, A., et al., Thresholds for therapies: Highlights of the St Gallen international expert consensus on the primary therapy of early breast cancer, Ann. Oncol. **20** (2009) 1219–1229.
[5.45] KAUFMANN, M., Locoregional treatment of primary breast cancer, Cancer **116** (2010) 1184–1191.
[5.46] RODRIGUEZ-FERNANDEZ, J., et al., Sentinel node biopsy in patients with previous breast aesthetic surgery, Ann. Surg. Oncol. **16** (2009) 989–992.
[5.47] TABACK, B., et al., Sentinel lymph node biopsy for local recurrence of breast cancer after breast-conserving therapy, Ann. Surg. Oncol. **13** (2006) 1099–1104.
[5.48] KUMAR, R., et al., Retrospective analysis of sentinel node localization in multifocal, multicentric, palpable, or nonpalpable breast cancer, J. Nucl. Med. **44** (2003) 7–10.
[5.49] KLIMBERG, V.S., et al., Subareolar versus peritumoural injection for location of the sentinel lymph node, Ann. Surg. **229** (1999) 860–864.
[5.50] NIEWEG, O.E., ESTOURGIE, S.H., VAN RIJK, M.C., KROON, B.B., Rationale for superficial injection techniques in lymphatic mapping in breast cancer patients, J. Surg. Oncol. **87** (2004) 153–156.
[5.51] KNAUER, M., et al., Multicentric breast cancer: A new indication for sentinel node biopsy – a multi-institutional validation study, J. Clin. Oncol. **24** (2006) 3374–3380.
[5.52] GOYAL, A., et al., Sentinel lymph node biopsy in patients with multifocal breast cancer, Eur. J. Surg. Oncol. **30** (2004) 475–479.
[5.53] GIARD, S., et al., Feasibility of sentinel lymph node biopsy in multiple unilateral synchronous breast cancer: Results of a French prospective multi-institutional study (IGASSU 0502), Ann. Oncol. **21** (2010) 1630–1635.
[5.54] KRYNYCKYI, B.R., et al., Factors affecting visualization rates of internal mammary sentinel nodes during lymphoscintigraphy, J. Nucl. Med. **44** (2003) 1387–1393.
[5.55] PAREDES, P., et al., Clinical relevance of sentinel lymph nodes in the internal mammary chain in breast cancer patients, Eur. J. Nucl. Med. Mol. Imaging **32** (2005) 1283–1287.
[5.56] ESTOURGIE, S.H., et al., Should the hunt for internal mammary chain sentinel nodes begin? An evaluation of 150 breast cancer patients, Ann. Surg. Oncol. **10** (2003) 935–941.
[5.57] VAN DER ENT, F.W., et al., Halsted revisited: Internal mammary sentinel lymph node biopsy in breast cancer, Ann. Surg. **234** (2001) 79–84.
[5.58] BOURRE, J.C., et al., Can the sentinel lymph node technique affect decisions to offer internal mammary chain irradiation? Eur. J. Nucl. Med. Mol. Imaging **36** (2009) 758–764.
[5.59] VERONESI, U., MARUBINI, E., MARIANI, L., VALAGUSSA, P., ZUCALI, R., The dissection of internal mammary nodes does not improve the survival of breast cancer patients. 30-year results of a randomised trial, Eur. J. Cancer **35** (1999) 1320–1325.
[5.60] VERONESI, P., GENTILINI, O., RODRÍGUEZ-FERNANDEZ, J., MAGNONI, F., Breast conservation and sentinel lymph node after neoadjuvant systemic therapy, Breast **18** (2009) 590–592.

[5.61] MAMOUNAS, E.P., et al., Sentinel node biopsy after neoadjuvant chemotherapy in breast cancer: Results from National Surgical Adjuvant Breast and Bowel Project Protocol B-27, J. Clin. Oncol. **23** (2005) 2694–2702.
[5.62] KELLY, A.M., DWAMENA, B., CRONIN, P., CARLOS, R.C., Breast cancer sentinel node identification and classification after neoadjuvant chemotherapy — systematic review and metaanalysis, Acad. Radiol. **16** (2009) 551–563.
[5.63] PIÑERO, A., GIMENEZ, J., VIDAL-SICART, S., INTRA, M., Selective sentinel lymph node biopsy and primary systemic therapy in breast cancer, Tumouri **96** (2010) 17–23.
[5.64] GENTILINI, O., et al., Sentinel lymph node biopsy in pregnant patients with breast cancer, Eur. J. Nucl. Med. Mol. Imaging **37** (2010) 78–83.
[5.65] KHERA, S.Y., et al., Pregnancy-associated breast cancer patients can safely undergo lymphatic mapping, Breast J. **14** (2008) 250–254.
[5.66] BURAK, W.E., AGNESE, D.M., POVOSKI, S.P., Advances in the surgical management of early stage invasive breast cancer, Curr. Probl. Surg. **41** (2004) 877–936.
[5.67] WILHELM, A.J., MIJNHOUT, G.S., FRANSSEN, E.J.F., Radiopharmaceuticals in sentinel lymph-node detection – an overview, Eur. J. Nucl. Med. **26** (1999) 36–42.
[5.68] MARIANI, G., et al., Radio-guided sentinel lymph node biopsy in breast cancer surgery, J. Nucl. Med. **42** (2001) 1198–1215.
[5.69] WALLACE, A.M., HOH, C.K., DARRAH, D.D., SCHULTEIS, G., VERA D.R., Sentinel lymph node mapping of breast cancer via intradermal administration of Lymphoseek, Nucl. Med. Biol. **34** (2007) 849–853.
[5.70] McCARTER, M.D., et al., Localization of the sentinel node in breast cancer: Identical results with same-day and day-before isotope injection, Ann. Surg. Oncol. **8** (2001) 682–686.
[5.71] VAN DER ENT, F.W., et al., Sentinel node biopsy in 70 unselected patients with breast cancer: Increased feasibility by using 10 mCi radiocolloid in combination with a blue dye tracer, Eur. J. Surg. Oncol. **25** (1999) 24–29.
[5.72] GREY, R.J., POCKAJ, B.A., ROARKE, M.C., Injection of ^{99m}Tc-labeled sulfur colloid the day before operation for breast cancer sentinel lymph node mapping is as successful as injection the day of operation, Am. J. Surg. **188** (2004) 685–689.
[5.73] POVOSKI, S.P., et al., Prospective randomized clinical trial comparing intradermal, intraparenchymal, and subareolar injection routes for sentinel lymph node mapping and biopsy in breast cancer, Ann. Surg. Oncol. **13** (2006) 1412–1421.
[5.74] NIEWEG, O.E., ESTOURGIE, S.H., VAN RIJK, M.C., KROON, B.B., Rationale for superficial injection techniques in lymphatic mapping in breast cancer patients, J. Surg. Oncol. **87** (2004) 153–156.
[5.75] NOGUCHI, M., INOKUCHI, M., ZEN, Y., Complement of peritumoural and subareolar injection in breast cancer sentinel lymph node biopsy, J. Surg. Oncol. **100** (2009) 100–105.
[5.76] ESTOURGIE, S., et al., Lymphatic drainage patterns from the breast, Ann. Surg. **239** (2004) 232–237.

[5.77] SUAMI, H., PAN, W.R., MANN, G.B., TAYLOR, G.I., The lymphatic anatomy of the breast and its implications for sentinel lymph node biopsy: A human cadaver study, Ann. Surg. Oncol. **15** (2008) 863–871.
[5.78] VERMEEREN, L., et al., SPECT/CT for preoperative sentinel node localization, J. Surg. Oncol. **101** (2010) 184–190.
[5.79] NIEWEG, O.E., ESTOURGIE, S., VALDÉS OLMOS, R.A., "Lymphatic mapping and sentinel node biopsy," Nuclear Medicine in Clinical Diagnosis and Treatment, Vol. 3 (ELL, P.J., GAMBHIR, S.S., Eds) (2004) 229–260.
[5.80] VARGHESE, P., et al., Methylene blue dye—a safe and effective alternative for sentinel lymph node localization, Breast J. **14** (2008) 61–67.
[5.81] RODIER, J.F., et al., Prospective multicentric randomized study comparing periareolar and peritumoural injection of radiotracer and blue dye for the detection of sentinel lymph node in breast sparing procedures: FRANSENODE trial, J. Clin. Oncol. **25** (2007) 3664–3669.
[5.82] SCHERER, K., STUDER, W., FIGUEIREDO, V., BIRCHER A.J., Anaphylaxis to isosulfan blue and cross-reactivity to patent blue V: Case report and review of the nomenclature of vital blue dyes, Ann. Allergy Asthma Immunol. **96** (2006) 497–500.
[5.83] CHENG, G., KURITA, S., TORIGIAN, D.A., ALAVI, A., Current status of sentinel lymph-node biopsy in patients with breast cancer, Eur. J. Nucl. Med. Mol. Imaging **38** (2011) 562–575.
[5.84] BRENOT-ROSSI, I., et al., Nonvisualization of axillary sentinel node during lymphoscintigraphy: Is there a pathologic significance in breast cancer? J. Nucl. Med. **44** (2003) 1232–1237.
[5.85] KRISHNANURTHY, S., et al., A prospective study comparing touch imprint cytology, frozen section analysis, and rapid cytokeratin immunostain for intraoperative evaluation of axillary sentinel lymph nodes in breast cancer, Cancer **115** (2009) 1555–1562.
[5.86] BERNET, L., et al., Diagnosis of the sentinel lymph node in breast cancer: A reproducible molecular method: A multicentric Spanish study, Histopathology **58** (2011) 863–869.
[5.87] SCOPINARO, F., et al., High-resolution hand-held camera for sentinel-node detection, Cancer Biother. Radiopharm. **23** (2008) 43–52.
[5.88] MATHELIN, C., SALVADOR, S., HUSS, D., GUYONNET, L., Precise localization of sentinel lymph nodes and estimation of their depth using a prototype intraoperative mini gamma-camera in patients with breast cancer, J. Nucl. Med. **48** (2007) 623–629.
[5.89] DUCH, J., Portable gamma cameras: The real value of an additional view in the operating theatre, Eur. J. Nucl. Med. Mol. Imaging **38** (2011) 633–635.
[5.90] VIDAL-SICART, S., et al., Added value of intraoperative real-time imaging in searches for difficult-to-locate sentinel nodes, J. Nucl. Med. **51** (2010) 1219–1225.
[5.91] PAREDES, P., et al., Radio-guided occult lesion localisation in breast cancer using an intraoperative portable gamma camera: First results, Eur. J. Nucl. Med. Mol. Imaging **35** (2008) 230–235.
[5.92] WENDLER, T., et al., First demonstration of 3-D lymphatic mapping in breast cancer using freehand SPECT, Eur. J. Nucl. Med. Mol. Imaging **37** (2010) 1452–1461.

[5.93] RAHAUSEN, F.D., et al., Ultrasound-guided lumpectomy of nonpalpable breast cancers: A feasibility study looking at the accuracy of obtained margins, J. Surg. Oncol. **72** (1999) 72–76.
[5.94] SNIDER, H.C., MORRISON, D.G., Intraoperative localization of nonpalpable breast lesions, Ann. Surg. Oncol. **6** (1999) 308–314.
[5.95] KAUFMAN, C.S., et al., Intraoperative ultrasonography guidance is accurate and efficient according to results in 100 breast cancer patients, Am. J. Surg. **186** (2003) 378–382.
[5.96] LUINI, A., ZURRIDA, S., GALIMBERTI, V., PAGANELLI, G., Radio-guided surgery of occult breast lesions, Eur. J. Cancer **34** (1998) 204–205.
[5.97] GENNARI, R., et al., Use of technetium-99m-labeled colloid albumin for preoperative and intraoperative localization of nonpalpable breast lesions, J. Am. Coll. Surg. **190** (2000) 692–698.
[5.98] PAGANELLI, G., LUINI, A., VERONESI, U., Radio-guided occult lesion localization (ROLL) in breast cancer: Maximizing efficacy, minimizing mutilation, Ann. Oncol. **13** (2002) 1839–1840.
[5.99] MARISCAL, A., et al., Radio-guided localization of nonpalpable breast cancer lesions: Randomized comparison with wire localization in patients undergoing conservative surgery and sentinel node biopsy, Am. J. Roentgenol. **193** (2009) 1001–1009.
[5.100] VERNET-TOMAS, M.M., ORTEGA, M., VIDAL, S., COROMINAS, J.M., CARRERAS, R., Factors affecting surgical margins in nonpalpable breast tumours excised with the radio-guided occult lesion localization approach, J. Obstet. Gynaecol. **37** (2011) 422–427.
[5.101] GALLEGOS-HERNANDEZ, J.F., "Lymphatic mapping and biopsy of sentinel lymph node in patients with breast cancer. Results of the first phase of a study", Cir. Cir. **72** 5 (2004) 357-60 (abstract).
[5.102] MacMILLAN, R.D., RAMPAUL R.S., LEWIS, S., EVANS, A.J., Preoperative ultrasound-guided node biopsy and sentinel node augmented node sample is best practice, Eur. J Cancer **40** 2 (2004) 176–8.
[5.103] NADEEM, R., et al., Occult breast lesions: A comparison between radio-guided occult lesion localisation (ROLL) vs. wire-guided lumpectomy (WGL), Breast **14** (2005) 283–289.
[5.104] THIND, C.R., et al. Radio-guided localization of clinically occult breast lesions (ROLL): a DGH experience, Clin Radiol. **60** 6 (2005) 681–6.
[5.105] ZGAJNAR, J., et al., Radioguided occult lesion localization (ROLL) of the nonpalpable breast lesions, Neoplasma. **51** 5 (2004) 385–9.
[5.106] RÖNKÄ, R., VON SMITTEN, K., TASMUTH, T., LEIDENIUS, M., One-year morbidity after sentinel node biopsy and breast surgery, Breast. **14** 1 (2005) 28–36.
[5.107] FRAILE, M., et al., "Radio-guided occult lesion localization combined with sentinel node biopsy in women with breast cancer", Cir. Esp. **77** 1 (2005) 36–39 (abstract).
[5.108] STRNAD, P., et al., Radioguided occult lesion localisation in combination with detection of the sentinel lymph node in non-palpable breast cancer tumours, Eur. J Gynaecol. Oncol. **27** 3 (2006) 236–238.

[5.109] VAN DER PLOEG, I.M.C., et al., Radio-guided occult lesion localisation (ROLL) for non-palpable breast lesions: A review of the relevant literature, Eur. J. Surg. Oncol. **34** (2008) 1–5.
[5.110] LOVRICS, P.J., CORNACCHI, S.D., VORA, R., GOLDSMITH, CH., KAHNAMOUI, K., Systematic review of radio-guided surgery for non-palpable breast cancer, Eur. J. Surg. Oncol. **37** (2011) 388–397.
[5.111] DUARTE, G.M., et al., Radioguided surgery using intravenous 99mTc sestamibi associated with breast magnetic resonance imaging for guidance of breast cancer resection, Breast J. **12** (2006) 202–207.
[5.112] DE CICCO, C., et al., Optimised nuclear medicine method for tumour marking and sentinel node detection in occult primary breast lesions, Eur. J. Nucl. Med. Mol. Imaging **31** (2004) 349–354.
[5.113] MONTI, S., et al., Occult breast lesion localization plus sentinel node biopsy (SNOLL): Experience with 959 patients at the European Institute of Oncology, Ann. Surg. Oncol. **14** (2007) 2928–2931.
[5.114] SARLOS, D., et al., Radio-guided occult lesion localisation (ROLL) for treatment and diagnosis of malignant and premalignant breast lesions combined with sentinel node biopsy: A prospective clinical trial with 100 patients, Eur. J. Surg. Oncol. **35** (2009) 403–408.
[5.115] VAN RIJK, M.C., et al., Sentinel node biopsy and concomitant probe-guided tumour excision of nonpalpable breast cancer, Ann. Surg. Oncol. **14** (2007) 627–632.
[5.116] PATEL, A., et al., Radio-guided occult lesion localization (ROLL) and sentinel node biopsy for impalpable invasive breast cancer, EJSO **30** (2004) 918–923.
[5.117] GREY, R.J., et al., Randomized prospective evaluation of a novel technique for biopsy or lumpectomy of nonpalpable breast lesions: Radioactive seed versus wire localization, Ann. Surg. Oncol. **8** (2001) 711–715.
[5.118] VAN RIET, Y.E.A., et al., Localization of non-palpable breast cancer using a radiolabelled titanium seed, Brit. J. Surg. **97** (2010) 1240–1245.
[5.119] HUGHES, J.H., et al., A multi-site validation trial of radioactive seed localization as an alternative to wire localization, Breast J. **14** (2008) 153–157.
[5.120] JAKUB, J.W., et al., Current status of radioactive seed for localization of non palpable breast lesions, Am. J. Surg. **199** (2010) 522–528.
[5.121] PLEIJHUIS, R.G., et al., Obtaining adequate surgical margins in breast conserving therapy for patients with early stage breast cancer: Current modalities and future directions, Ann. Surg. Oncol. **16** (2009) 2717–2730.
[5.122] KEIDAR, Z., ISRAEL, O., KRAUSZ, Y., SPECT/CT in tumour imaging: Technical aspects and clinical applications, Semin. Nucl. Med. **33** (2003) 205–218.
[5.123] LERMAN, H., et al., Lymphoscintigraphic sentinel node identification in patients with breast cancer: The role of SPECT-CT, Eur. J. Nucl. Med. Mol. Imaging **33** (2006) 6329–6337.
[5.124] MUCIENTES RASILLA, J., et al., SPECT-CT: A new tool for localisation of sentinel lymph nodes in breast cancer patients, Rev. Esp. Med. Nucl. **27** (2008) 183–190.
[5.125] VERMEEREN, L., et al., SPECT/CT for preoperative sentinel node localization, J. Surg. Oncol. **101** (2010) 184–190.

[5.126] VAN DER PLOEG, I.M.C., VALDÉS OLMOS, R.A., KROON, B.B., NIEWEG, O.E., The hybrid SPECT/CT as an additional lymphatic mapping tool in patients with breast cancer, World J. Surg. **32** (2008) 1930–1934.
[5.127] VAN DER PLOEG, I.M., et al., The yield of SPECT/CT for anatomical lymphatic mapping in patients with breast cancer, Eur. J. Nucl. Med. Mol. Imaging **36** (2009) 903–909.

6. GOSTT IN MELANOMA

6.1. INTRODUCTION

6.1.1. Update on melanoma

A CM is potentially the most dangerous form of skin tumour and causes 90% of skin cancer mortality. The incidence of CM is increasing worldwide in white populations (at a rate of 4%–8% per year), especially where fair skinned races receive excessive sun exposure. In central Europe, the annual incidence is 10–14 new cases per 100 000 population, and in southern Europe, it is 6–10 per 100 000 population. The USA has an incidence of 10–25 per 100 000 population, while the highest incidence is recorded in Australia at 50–60 per 100 000 population [6.1, 6.2]. In 2009, an estimated 68 720 new cases of CM were diagnosed in the USA. Of those cases, 8650 patients died of the disease [6.3].

Diagnosis is made clinically, and staging is based upon the American Joint Committee on Cancer (AJCC) system. Historically, the treatment of CM has been primarily surgical, and this is still the case despite advances in adjuvant therapy. CMs are excised with a safety margin of 1–2 cm. The natural evolution of CM most often starts with an orderly progression from the primary site to regional LNs via dermal lymphatics, and then on to distant metastatic sites. If a CM is identified and treated at an early stage, the likelihood of LN metastases is quite low, and patients are usually treated with wide local excision alone. However, the presence or absence of LN metastases remains a key predictor of outcome [6.2].

SLNB in CM was first described in 1992 by Morton et al. [6.3] using a technique of intradermally injected vital blue dye. In 1993, the intraoperative use of the gamma detection probe for radioguided SLNB in CM was first reported by Alex et al. [6.4] at the University of Vermont, using intradermally injected ^{99m}Tc sulphur colloid. Since that time, the use of radioguided SLNB has largely replaced the use of vital blue dye alone for SLNB in CM patients [6.5–6.9].

The technique of SLNB with selective LN dissection (i.e. in the case of metastasis in the SLN) has been widely adopted by surgical oncologists as an alternative to elective LDN or observation for patients with clinically negative regional LNs who are at high risk for nodal metastases [6.8]. The success of this technique has resulted in its use in the treatment of other cutaneous malignancies with regional lymphatic metastatic potential [6.10].

The principal aim of SLNB in patients with CM is to identify the 20%–25% of patients who present with clinically occult regional disease. The procedure can also minimize the morbidity associated with elective LDN, by

identifying those most likely to benefit from LDN after a minor procedure with a greatly diminished risk of lymphoedema or other complications. The technique also increases the identification rate of occult LN metastases by guiding the pathologist to perform extensive analysis of the LN(s) most likely to contain metastatic disease. Furthermore, SLNB identifies patients who may benefit from postoperative adjuvant therapy and provides a means of homogeneous stratification of patients for randomized clinical trials [6.10].

6.1.2. Application of SLNM and SLNB in malignant melanoma

6.1.2.1. Indications for SLNM and SLNB in melanoma

Current indications for SLNM and SLNB using radionuclide methods include the following conditions [6.11–6.19]:

— Intermediate stage primary melanoma (Breslow thickness, 1–4 mm);
— No clinical evidence of LN involvement;
— No clinical evidence of distant tumour spread;
— Patients with high risk lesions of 0.75–0.99 mm in thickness should be considered for SLNB if their melanoma is Clark level IV or V, ulcerated, shows a vertical growth phase, or has lymphatic invasion or a high mitotic rate;
— Patients with tumours thicker than 4 mm may potentially benefit from SLNB.

6.1.2.2. Contraindications for SLNB in melanoma

Based on the same recommendations as mentioned above [6.11–6.19], SLNB is currently contraindicated in the following conditions:

— Extensive previous surgery in the region of the primary tumour site or in the targeted LN basin;
— Patients with known metastases;
— Patients with tumours thinner than 0.75 mm (because less than 2% of these patients have a positive SLN);
— Poor general health status with severe concurrent disease.

Numerous studies have confirmed that SLN status is the single most important independent prognostic factor with respect to disease progression and melanoma specific survival [6.20, 6.21]. When SLNB yields a negative histological result, no further LN surgery is required. On the other hand, when

SLNB shows micrometastases, radical LN dissection is recommended because approximately 5%–12% of these patients will also have metastatic involvement of non-SLNs.

SLNB with selective LN dissection has been accepted in the staging and treatment of CM in the latest AJCC staging guidelines for CM, which incorporate nodal microstaging and which discriminate between microscopic and macroscopic nodal disease [6.22]. Additionally, the NCCN guidelines for the treatment of CM include SLNB with selective LN dissection in their treatment algorithms, as also endorsed by the World Health Organization (WHO). The 7th edition of the AJCC Cancer Staging Manual has already made major revisions to CM staging, and the main features of the TNM melanoma staging system include the following [6.23]:

— Melanoma thickness and tumour ulceration continue to define T category stratification;
— Mitotic rate (defined as mitoses/mm^2) of the primary tumour is an important independent adverse predictor of survival;
— The presence of nodal micrometastases can be defined by either haematoxylin and eosin or immunohistochemical staining;
— M category stratification continues to be primarily defined by the site or sites of distant metastases: non-visceral, i.e. skin/soft tissue/distant nodal (M1a), lung (M1b) and all other visceral metastatic sites (M1c); an increased serum lactic dehydrogenase level also remains a powerful adverse predictor of survival;
— Survival estimates for patients with intralymphatic regional metastases (i.e. satellite and in-transit metastases) are somewhat better than for the remaining cohort of patients with stage IIIB disease;
— Lymphoscintigraphy for SLNM followed by SLNB remain important components of melanoma staging, and should be used (or discussed with the patient) to identify occult stage III regional nodal disease among patients with clinical stage IB or II melanoma.

6.2. LYMPHATIC MAPPING

SLNB with selective LDN is a team effort that requires close collaboration among dermatologists, surgeons, nuclear medicine physicians and pathologists. A multidisciplinary approach is therefore essential for optimal patient care.

The combined use of blue dye plus radiocolloid appears to be superior to using either method alone. Pre-operative lymphoscintigraphy is the first step in the lymphatic mapping procedure and is considered to be a ‘road map’ to guide

the surgeon; this is especially useful for identifying unpredictable lymphatic drainage patterns [6.24].

The value of lymphoscintigraphy relies on several points:

— Identification of all draining hot LNs. Not all hot nodes are SLNs and the SLN is not necessarily the hottest node.
— Identification of all drainage basins. Multiple hot LNs that belong to a single basin should be differentiated from multiple hot nodes that belong to separate basins, and need to be identified at surgery and examined.
— Identification of SLNs and second tier LNs.
— Identification of unpredictable SLNs, including in-transit LNs (i.e. LNs located between the primary tumour site and a drainage basin) and aberrant LNs (i.e. LNs located outside a standard drainage basin). The incidence of metastatic in-transit or aberrant nodes in melanoma has been reported to vary between 14% and 22%. The highest incidence of in-transit SLNs occurs in the posterior trunk followed by the anterior trunk, the head and neck, the upper limbs and the lower limb areas.
— Confirmation of true nodal versus non-nodal sites of uptake, such as skin folds, radiopharmaceutical contamination and lymphangioma, which are common causes of false positive results on conventional planar imaging.

6.2.1.1. Radiotracers

Lymphoscintigraphy is performed by injecting radiocolloid intradermally around the melanoma lesion. While different radiopharmaceuticals are commercially available in different regions of the world, there is no documented difference in the clinical outcome among such different radiocolloids [6.25].

6.2.1.2. Injection procedure

The use of Luer Lock tuberculin syringes is recommended for radiocolloid injection. Approximately 0.4–0.5 mL containing 74 MBq of radiocolloid is administered as 4–8 intradermal 0.1 mL injections (fewer than four may be performed if appropriate) within 1 cm of the melanoma or the excisional biopsy site at which the melanoma was located.

The intradermal injection should be performed using a 25 or 27 G needle. The needle is inserted in a direction as tangential as possible to the skin surface for a few mm inside the skin. This technique entails small volumes of injectate, just enough to produce a visible wheal on the skin. Injections should surround the lesion or biopsy site to best explore lymphatic drainage in all directions. In patients with melanomas located in the head, neck and trunk, radiocolloid

injections must be given roughly equatorially around the lesion (at 3 h, 6 h, 9 h and 12 h) because the drainage may be both cranial and caudal and across the midline of the body. In the extremities, two to three injections will usually be enough, and are given cranial, medial and lateral to the tumour/scar.

Care must be taken to avoid skin contamination with the radiocolloid, an occurrence that can erroneously be confused with LN 'uptake'. For this purpose, the injection site should be covered with a dressing or cotton ball to prevent leakage of the radiocolloid through the needle puncture site.

6.2.1.3. Image acquisition

Following injection, lymphoscintigraphy is performed to assess appropriate radiocolloid migration through the lymphatic vessels and uptake in LNs. A large FOV camera head is preferable, while imaging dual headed cameras will save time. The use of flood sources (^{57}Co or ^{99m}Tc) or alternative techniques (drawing the silhouette with a radioactive pointer) is helpful in providing some anatomical information for the surgeon.

Dynamic scintigraphy is started immediately after injection. High resolution or ultra-high-resolution collimators are important to prevent or reduce septum penetration (which can produce 'star' artefacts) (Fig. 6.1) and to define the lymphatic collectors as they head towards and reach the SLNs (Fig. 6.2). Lead shielding covering the injection site may occasionally be helpful during

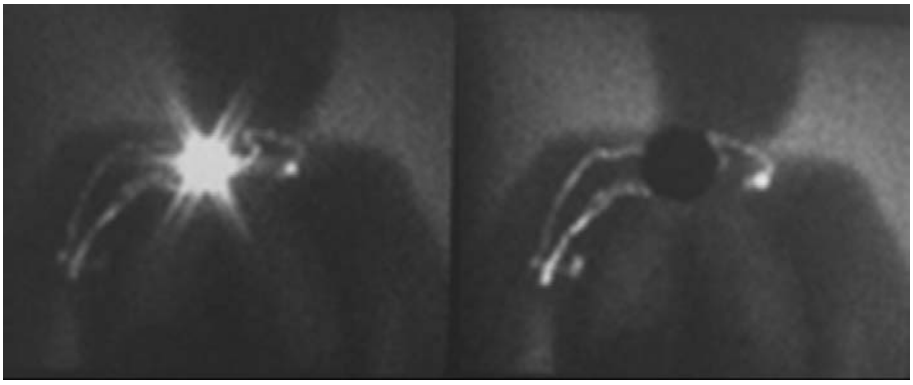

FIG. 6.1. Left: Posterior planar images acquired 20 min after injecting 111 MBq of ^{99m}Tc nanocolloid into a patient with a melanoma on the upper part of the back. Right: Lead shielding covering the injection site may be helpful during image acquisition to better visualize the lymphatic channels and SLNs.

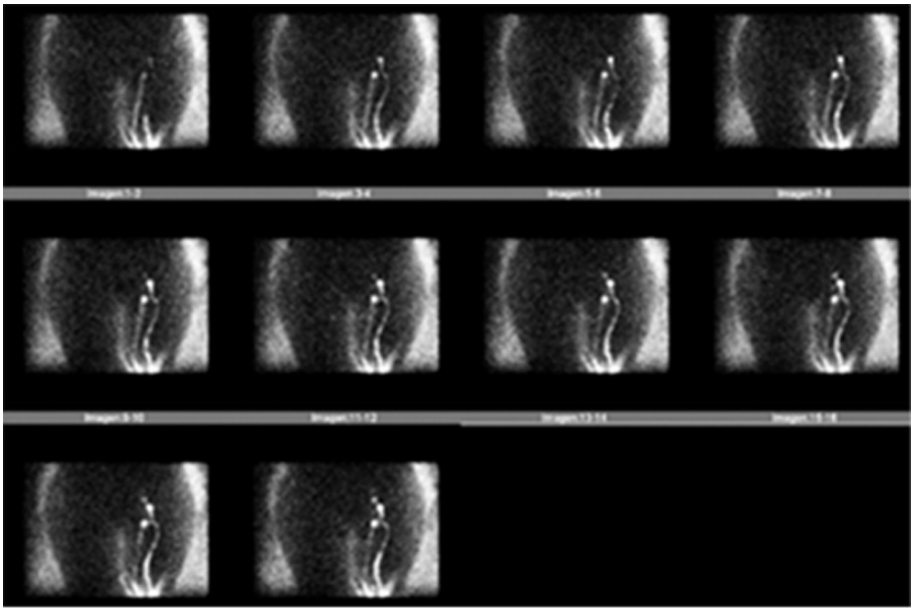

FIG. 6.2. Dynamic anterior planar images (30 s each) acquired over the groin region immediately after injecting 111 MBq of ^{99m}Tc nanocolloid (128 × 128 matrix). Two separate lymphatic channels are clearly depicted. Early dynamic imaging is mandatory to clearly identify the lymphatic channels leading to the first SLN of the respective channel.

static image acquisition to detect SLNs close to the injection site, especially in cases of high activity retention in the injected depots. However, the lead shield itself carries a risk of masking possible SLNs (Fig. 6.3). A 10–20 min dynamic acquisition at 1 frame/min in a 128 × 128 matrix is suggested to determine where the lymphatic collectors are headed.

Static images of 5 min duration and 256 × 256 matrix size should be acquired over the node field to identify the collectors as they reach the actual SLNs. This is important because sometimes, especially in the groin when the melanoma is in the leg, some of the radiocolloid will be seen passing through the SLN on to a second tier node. Delayed 30 min and 2 h images should also be recorded.

Delayed images are helpful in detecting SLNs close to the primary site that may have been obscured in the initial views, and to detect drainage to multiple nodal basins (Fig. 6.4). An anterior view, together with a lateral view, is often helpful in the groin to identify collectors passing to deep iliac or obturator nodes. In the head/neck region, other views such as oblique or vertex views can be combined with or added to the lateral view. Usually, SLN(s) are identified

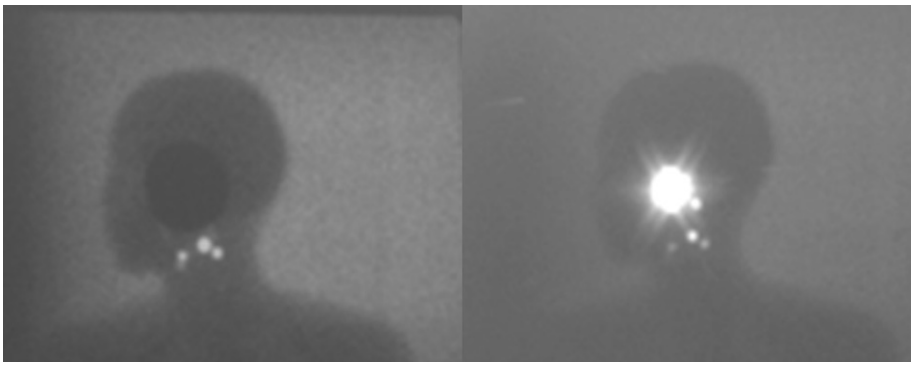

FIG. 6.3. Left lateral images of a patient with a melanoma in her left malar area. Delayed images obtained 2 h after injecting 111 MBq of ^{99m}Tc nanocolloid (256 × 256 matrix). Lead shielding is useful during static image acquisition to detect SLNs close to the injection site. However, the lead shield itself carries the risk of masking draining LNs in the immediate vicinity of the injection site (upper uptake).

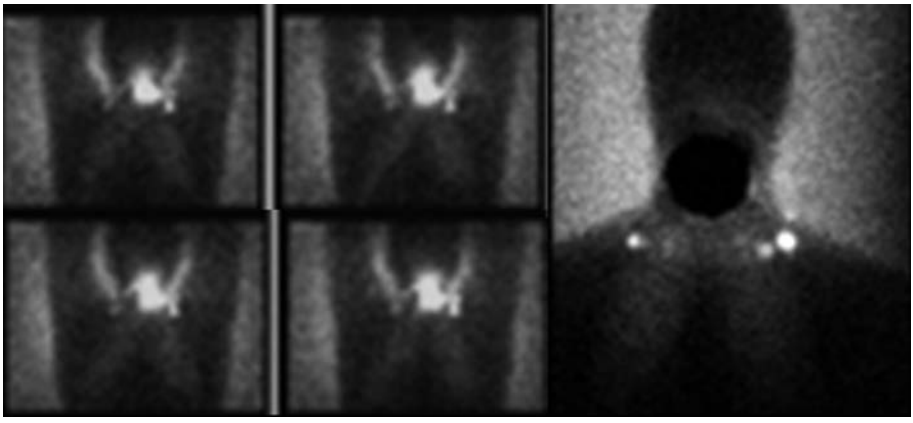

FIG. 6.4. Posterior planar images of a patient with a posterior cervical melanoma. Dynamic acquisition (128 × 128 matrix) is shown in the four small images on the left, and delayed 2 h acquisition (256 × 256 matrix) on the right. Delayed images are helpful in detecting SLNs close to the primary tumour site (which may be obscured in the initial acquisitions) and to detect radiocolloid drainage to multiple nodal basins.

within 30 min of injection, but it is advisable to acquire 2 h images owing to the possibility of delayed or slow drainage to other areas. If no radiocolloid migration from the injection site is observed during dynamic acquisition, gentle massage for 5 min may help. If a collector is seen to taper off or stop along a lymphatic pathway, then massage could be performed along the line of the collector, because

lymph flow is very susceptible to external pressure. If LNs are not seen or weakly depicted, additional delayed images may be considered, up to 24 h after injection. If no visualization persists, reinjection of the radiocolloid is necessary. The site of each hot SLN is marked on the patient's skin for identification in the operating room [6.25, 6.26].

Clinicians should be aware that, while the majority of SLNs are found in the main nodal basins, SLNs may also be found in aberrant areas of drainage, such as the epitrochlear nodal basin in the upper extremities and the popliteal nodal basin in the lower extremities. In the trunk region, lymphatics can drain to multiple nodal basins. Several studies have demonstrated that the lymphatic drainage of melanomas of the head, neck and trunk cannot be predicted reliably using Sappey's classical anatomic guidelines [6.26]. Lymphoscintigraphy can visualize direct drainage to SLNs in aberrant locations. Multiple basin drainage or interval nodes may also be identified by lymphoscintigraphy. This possibility emphasizes the importance of pre-operative lymphoscintigraphy for patients. For CM of the trunk region, pre-operative lymphoscintigraphy demonstrates lymphatic drainage to multiple nodal basins in 17%–32% of patients [6.27–6.29] (Fig. 6.5). Likewise, pre-operative lymphoscintigraphic localization to in-transit (interval, aberrant) SLNs has been demonstrated in 3%–10% of patients. Metastatic disease is found in approximately 18% of these in-transit SLNs, which is similar to the rate found in conventional LN basins, and the status of one basin does not predict the status of the other [6.30–6.32] (Fig. 6.6). On the other hand, the use of pre-operative lymphoscintigraphy can show discordant results with clinical predictions of nodal drainage. In particular, the SLN is not always found in the closest nodal basin. Uren et al. found a 32% discordance rate, and reported a 10% rate of nodal basins draining across the midline [6.33].

6.2.1.4. Surgical procedure

As a complement to lymphoscintigraphic SLNM, blue dye can be injected around the primary tumour or scar (in a similar way to how the radiocolloid was injected) 10–20 min prior to the operation, in a volume of 0.5–1 mL. Because the injection is painful, it should be performed after the patient is anaesthetized. Five minutes of massage at the injection site enhances movement of the dye through the lymphatics to the SLN. Within 5–15 min, the SLN is coloured blue, while washout is evident after approximately 45 min. Use of the blue dye is contraindicated in pregnancy because of the risk of a severe anaphylactic reaction, in patients with earlier allergic reaction to blue dye and in severe renal impairment (methylene blue).

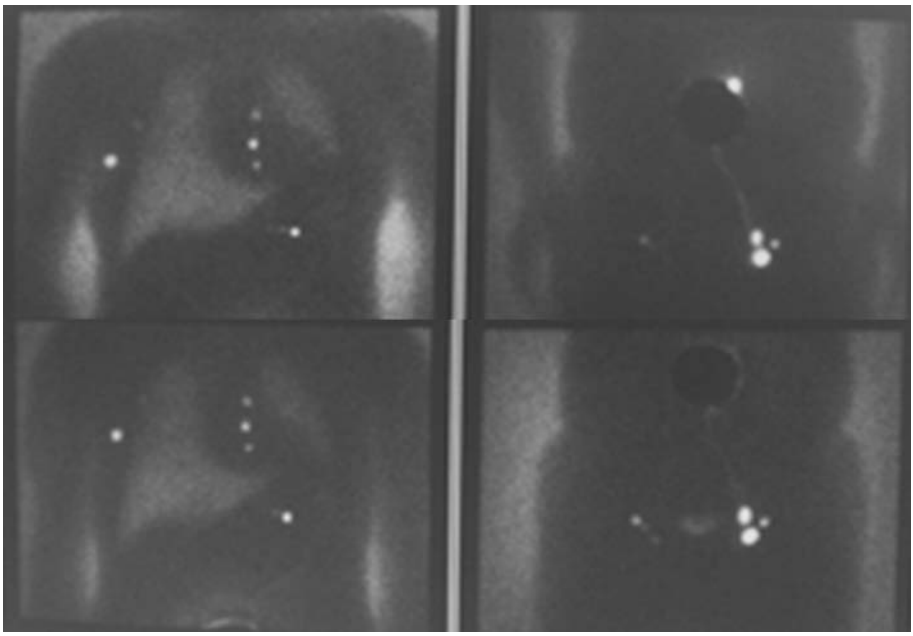

FIG. 6.5. Early (upper row) and delayed (lower row) anterior planar images acquired of a 36 year old man with an umbilical melanoma. Images were acquired after injecting 111 MBq of ^{99m}Tc nanocolloid intradermally at four sites around the biopsy. In truncal and abdominal melanomas, lymphoscintigraphy shows multiple nodal basin drainage in 17%–32% of patients, which is an occurrence that is well demonstrated in this case. Early static images (30 min, 256 × 256 matrix) show lymphatic drainage to both axillae, to the internal mammary chain, bilateral inguinal drainage and left abdominal in-transit node. Delayed (2 h) static images confirm the multiple basin drainage pattern and the existence of numerous SLNs.

Using the lymphoscintigraphy images and skin markings as guides, the probe (placed over the regions of highest counts) can be used to select the optimum location for incision. The surgeon uses the probe to guide dissection to the hot node(s) and explores the surgical bed with the probe after LN excision to confirm removal of the hot node(s). In working with the probe, it is important to direct it away from activity at the injection sites. Counts are recorded per unit time with the probe in the operative field, over the node before excision (in vivo) and after excision (ex vivo). A background tissue count is also recorded with the probe pointing away from the injection site, from nodal activity or from other physiological accumulation sites (i.e. bladder or liver) [6.25, 6.27].

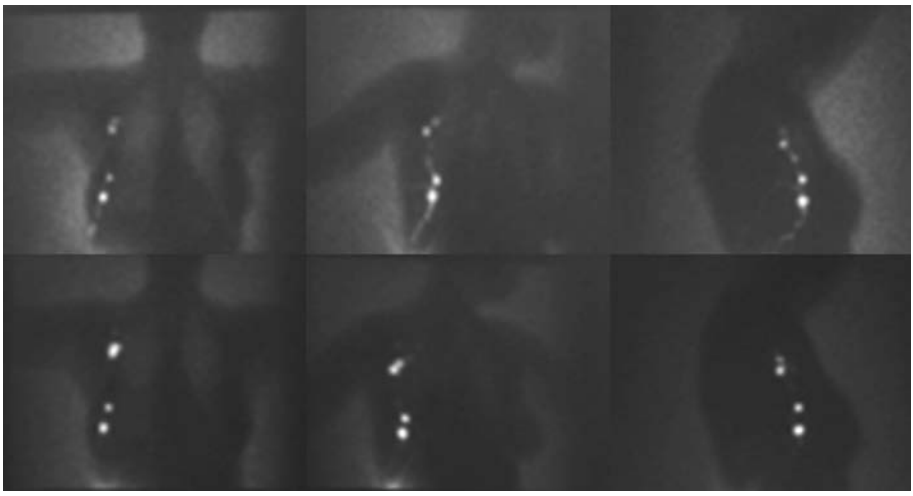

FIG. 6.6. Early (upper row) and delayed (lower row) anterior, anterior right oblique and right lateral planar images (256 × 256 matrix) acquired of a 28 year old woman with a right flank melanoma. Images were acquired after injecting 111 MBq of ^{99m}Tc nanocolloid intradermally around the biopsy scar. In this case, the early images show direct lymphatic drainage to two right paracostal SLNs and to axillary SLNs. Delayed images confirm this drainage pattern. In-transit (or interval/aberrant) SLNs have been demonstrated by lymphoscintigraphy in 3%–10% of patients, and are more frequently observed in the regions of the head, neck, trunk and upper extremities.

6.2.1.5. Interpretation criteria

Early images help in identifying the SLN as the first LN receiving direct drainage from the tumour site. The SLN is not necessarily the hottest node, although that is often the case. LNs with their own lymphatic ducts, or single nodes in a basin, are considered definitive SLNs. LNs with increasing intensity, or nodes appearing between the injection site and the first draining nodes, are considered as high probability SLNs. Nodes classified as definitively or highly probable SLNs on lymphoscintigraphy must be harvested for analysis, regardless of their count intensity.

When a hot node has been removed, the surgical field should be checked for remaining activity. When remaining activity reaches at least ten times the background counts, taken at a location remote from the injection site, the search for additional SLNs should continue.

Even if one hot node was clearly noted on lymphoscintigraphy, in practice, the single scintigraphic spot could actually represent two closely located LNs because of the limited spatial resolution of the gamma camera. LNs closer than

approximately 15–20 mm may well appear as one node, so after removal of one SLN, in a limited number of cases, another hot node may still be present at a nearby location. When other sources of activity are found in the lymphatic basin, the decision of whether to remove them will depend upon the lymphoscintigraphy report, and upon the working definition of 'nodes to remove' (e.g. the '10% rule').

6.3. SPECT/CT CONTRIBUTION TO SLNM AND SLNB

Conventional planar lymphoscintigraphy offers a clear visualization of SLNs, providing practical information on their number and locations for skin marking. However, some important information, such as depth and anatomical relationship of the SLNs with surrounding tissues, cannot be easily obtained using planar lymphoscintigraphy. In this regard, the presence of deep located SLNs in the neck and in other areas is a challenge during surgery, and in some circumstances, such SLNs cannot be resected. There are also conditions where one SLN is obscured by another, or by the injection site, or the SLN contains too little radioactivity, or two adjacent SLNs are thought to be a single node on planar imaging. Lymphoscintigraphy can also be erroneously interpreted when several second tier nodes appear, especially if no dynamic imaging has been performed. Lymphangiomas or lymphatic lakes can also be mistaken for an SLN, which may also happen in the case of cutaneous contamination with radioactivity spilled from the injection site [6.33].

With the new generation of large field gamma cameras, the functional information from SPECT can be combined with the morphological information from CT [6.34–6.37]. Hybrid imaging is acquired with transmission (CT) and emission (SPECT), performed during the same session without changing the patient's position, thus allowing for correct image fusion, provided that there are no motion artefacts. SPECT imaging improves SLN identification and overcomes some of the limitations of planar scintigraphic mapping. However, reconstructed images obtained by acquisition of SPECT images alone are not completely informative, unless combined with anatomical data such as those obtained from the corresponding CT images (Fig. 6.7). The sequential acquisition of SPECT and CT datasets provides inherent coregistration and overcomes many of the problems associated with previous software based fusion methods. The resulting SPECT/CT fused images show SLNs in an anatomical 2-D and 3-D scenario (Fig. 6.8), thus providing an improved road map for surgeons [6.38, 6.39]. In general, SPECT acquisition parameters for SLN include a 128 × 128 matrix size, 180° rotation for each detector and a 3°–6° angle step with a 20–25 s time frame. CT image acquisition can provide sufficient anatomical details also by applying low dose CT with 2–5 mm slices, depending on the part of the body

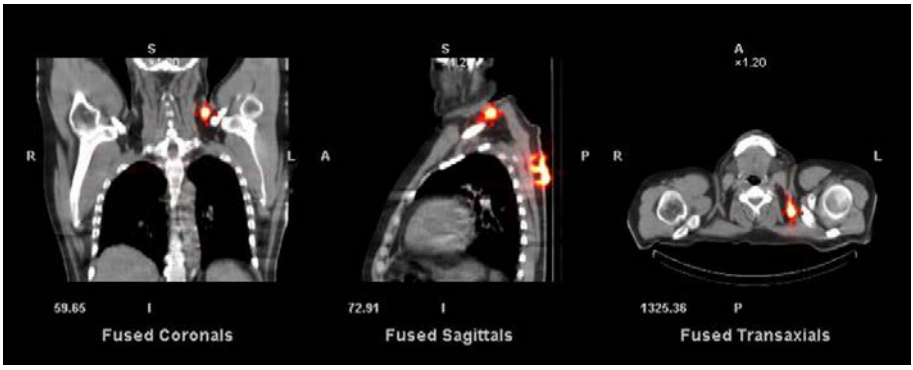

FIG. 6.7. Fused SPECT/CT images obtained 2 h after injecting 111 MBq of ^{99m}Tc nanocolloid in a patient with melanoma of the upper back. Lymphatic drainage to the pretrapezoidal muscle ipsilaterally is clearly identified. Stand alone scintigraphic images of the head and neck area are not informative, unless combined with anatomical data. This example shows the necessity to fuse both modalities to clearly identify unexpected anatomical locations of SLNs.

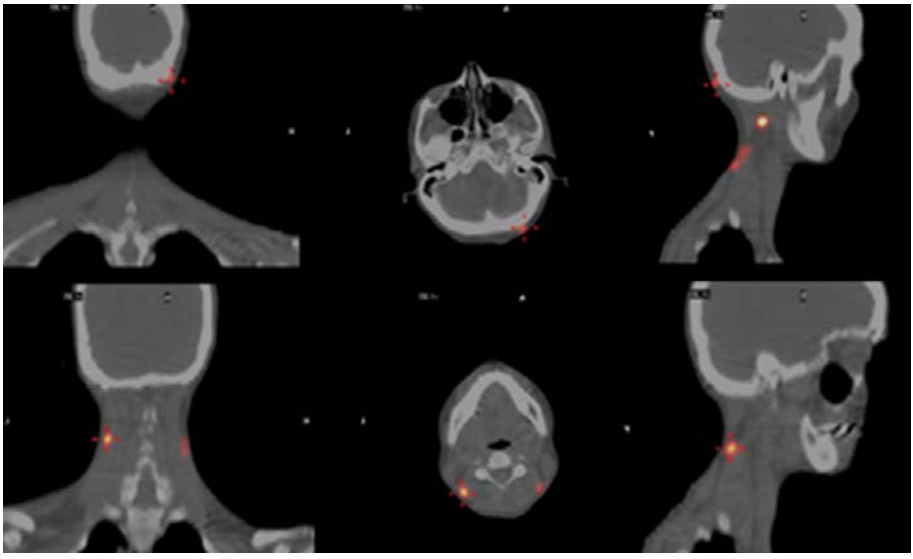

FIG. 6.8. Fused SPECT/CT images obtained 2 h after injecting 111 MBq of ^{99m}Tc nanocolloid in a 21 year old man with a high parietal melanoma. The resulting fused SPECT/CT images show SLNs in a 2-D scenario, providing an improved road map for surgeons. Coronal, sagittal and transaxial slices are depicted, showing several SLNs in the posterior part of the neck.

being imaged. Normally, SPECT/CT images are acquired immediately after the delayed planar images, i.e. 2–4 h after radiocolloid injection [6.25, 6.40]. The added value of SPECT/CT imaging is summarized in the following points:

— Improved localization: The combination of SPECT and CT images solves the limitation of planar scintigraphic imaging by providing an anatomical map. Accurate localization leads to improved patient management, owing to changes in treatment or surgical approaches.
— Higher sensitivity (additional lesions): Better localization of radiocolloid uptake also helps to define the significance of activity accumulation at sites distant from the primary tumour that may otherwise be missed on planar imaging. The detection of additional lesions improves the sensitivity of imaging and the accuracy of disease staging.
— Higher specificity and reduction of false positive findings: The elimination of physiological radiotracer uptake increases specificity by reducing false positive sites of disease. High physiological uptake can be a problem for areas adjacent to some organs such as the liver, spleen and kidneys. The higher specificity of SPECT/CT imaging improves diagnostic confidence and changes patient management by avoiding unnecessary treatment.
— Erroneous lesions: SPECT/CT imaging is a useful tool for assessing the anatomical significance of equivocal areas of tracer uptake on planar lymphoscintigraphic studies, or for defining the functional significance of indeterminate abnormalities detected on cross-sectional imaging. SPECT/CT imaging can help to characterize inconclusive lesions (by planar imaging) in patients with known malignancy.

A recent study from the Netherlands Cancer Institute [6.41] compared SPECT/CT images and conventional pre-operative planar images. The pre-operative detection and anatomic localization of these SLNs was analysed using SPECT/CT imaging. It was also evaluated whether SPECT/CT detected more SLNs than conventional imaging and whether better localization information was provided.

In contrast to conventional imaging, SPECT/CT imaging depicted the SLNs in relation to anatomic structures in all patients. According to the surgeons, SLNs were more accurately localized using SPECT/CT imaging in all cases, and in six patients (30%), they were correctly placed at a different site to that expected on the basis of planar imaging. The surgical approach was planned on the basis of the SPECT/CT images and in 11 out of 20 patients (58%), the surgeons indicated that the approach would have been different if based solely on conventional imaging. In all of those cases, the surgical incision was placed differently, or an intraoperative search was facilitated [6.41].

Although planar lymphoscintigraphy shows the lymphatic pathway and SLN in most cases, subsequent SPECT/CT imaging is more precise in specifying the anatomic location of the nodes. Some SLNs are small and often accumulate very little radioactivity, thus making it difficult to locate such a node with a gamma detection probe through intact skin. In CM patients, SPECT/CT imaging is especially helpful in localizing SLNs draining from primary tumours high on the trunk and in the head and neck area. An intraoperative detection rate as high as 100% has been reported following SPECT/CT imaging. In their study, Van der Ploeg et al. found additional SLNs in 10% of the cases, several of which were metastatic [6.41]. This anatomic functional technique enables more accurate nodal staging and has the potential to reduce morbidity from primary melanomas of the trunk and the head and neck [6.42] (Fig. 6.9). Table 6.1 summarizes the most relevant studies on the use of SPECT/CT imaging in CM patients.

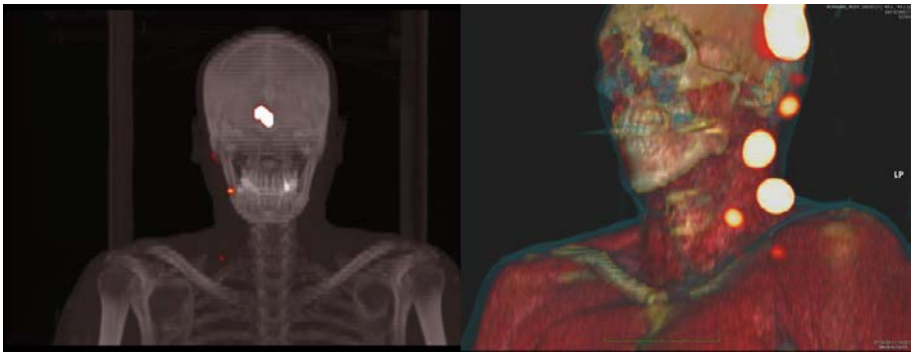

FIG. 6.9. Volume rendering software is a valuable tool that is applied to SPECT/CT data to generate hybrid anatomical and scintigraphic holographic 3-D volumes. This new approach simplifies the process of visual recognition and analysis of large volume of complex information, leading to a better delineation of anatomical structures, in particular, the precise SLN localization, thereby providing a 'road map' to the surgeon for planning the surgical approach. Left: SPECT/CT MIP of a 34 year old woman with a melanoma at the root of the nose. Fused images show an anterior projection of the MIP hologram. Image depicts the injection site (in the midline) and three LNs (orange) localizing to the right preauricular, superficial mandibular and medial aspect of the sternocleidomastoid muscle. Early dynamic studies indicated that the preauricular and mandibular LNs were true SLNs. Courtesy of the Department of Nuclear Medicine, Hospital Clinic, Barcelona. Right: A 48 year old man with a left parietal melanoma. The 3-D image shows two hot SLNs localized postauricular, several cervical SLNs along the sternocleidomastoid muscle (levels 2, 3 and 5) and in the left infraclavicular region. Image courtesy of the Netherlands Cancer Institute.

TABLE 6.1. ADDED VALUE OF SPECT/CT IMAGING FOR SLNM AND SLNB IN PATIENTS WITH CM

Ref.	No. patients	Cohort characteristics	Rate of SLN visualization	SPECT/CT results
Even-Sapir et al. [6.35]	28	22 patients with CM	No data provided	Additional clinical relevant data in head, neck and trunk
Ishiara et al. [6.36]	26	17 patients with CM	SPECT/CT identified 100% versus 85% using blue dye	Better anatomical localization
Vermeeren et al. [6.40]	38	Head and neck only	SPECT/CT identified 100% versus 95% using planar imaging	Additional SLN identified in 16% of cases; change of surgical approach in 55% of cases
Covarelli et al. [6.42]	23	Head and neck only	SPECT/CT identified 100% versus 82% using planar imaging	Shorter surgical time attributed to SPECT/CT
Van der Ploeg et al. [6.41]	85	All CM patients	SPECT/CT identified 100% versus 99% using planar imaging	Change of surgical approach in 35% of cases

CT: computed tomography; CM: cutaneous melanoma; SLN: sentinel lymph node; SLNB: sentinel lymph node biopsy; SLNM: sentinel lymph node mapping; SPECT: single photon emission computed tomography.

Irrespective of the advantages of SPECT/CT imaging, the information obtained using dynamic lymphoscintigraphy remains essential [6.43, 6.44].

6.4. RADIOGUIDED SURGERY BASED ON POSITRON EMISSION FOR MELANOMA

While pre-operative [^{18}F]FDG PET imaging has become a standard of care for melanoma patients with advanced disease [6.45–6.48], the intraoperative use of gamma detection probes following administration of [^{18}F]FDG has also been described in the clinical management of selected cases of metastatic malignant melanoma, and has received increasing interest. Franc et al. reported the results of radioguided surgery in five patients with recurring melanoma who had been injected with 540 ± 118 MBq of [^{18}F]FDG. They found that the intraoperative gamma probe guidance had 89% sensitivity and 100% specificity for the detection of tissues containing recurrent CM [6.49]. Gulec et al. reported on 26 patients with either recurrent or metastatic malignant melanoma who were intravenously injected with 259–370 MBq of [^{18}F]FDG within 1–4 h of the planned time of surgery. It was found that the tumour to background ratio ranged from 1.5:1 to 2.5:1, with a mean of 1.8:1; metastatic lesions as small as 5 mm could be detected [6.50]. It is therefore reasonable that the GOSTT concept is well suited to this new field, i.e. the use of positron detecting probes or probes for detection of the high energy γ annihilation rays for radioguided surgery in patients with recurrent/metastatic melanoma.

6.5. ADDED VALUE OF ADVANCEMENTS IN INTRAOPERATIVE IMAGING/LOCALIZING INSTRUMENTATION

Pre-operative dynamic lymphoscintigraphy visualizes drainage from the tumour site through the afferent lymphatic vessel towards the SLN. Static lymphoscintigraphic images more clearly visualize the SLN. Despite the satisfactory results of this technique, the location of an SLN is sometimes not established clearly enough to enable the surgeon to precisely plan the surgical approach. Although the intraoperative gamma probe is helpful in such situations, an imaging technique that provides a clear perspective of the location of the SLN node in its anatomical surroundings can facilitate surgery. Although hybrid SPECT/CT imaging has the ability to provide such information, as it offers a better road map compared with conventional planar imaging, there is still room for improvement during the intraoperative approach. In fact, even fused and

3-D volume rendering SPECT/CT images are ‘static’, and in some circumstances, SLN retrieval is complicated or even impossible.

Blue dye is less effective in areas of aberrant drainage that may be indicated pre-operatively by lymphoscintigraphy. It also has a limited value in deep nodal basins. However, it is well known in CM that, in particular, the SLN identification rate for melanomas located in the head and neck region is approximately 85%, which is considerably worse than the almost 100% success rate in other regions of the body. In this regard, the head and neck as the site of a primary CM has been found to be a predictive factor for a false negative SLNB, with false negative procedures in this region varying between 12% and 44% [6.51].

The recent introduction of a new generation of portable gamma cameras has stimulated interest for their intraoperative use also for SLNM and SLNB in patients with melanoma. The added value of this approach is expected particularly for melanomas located in the head or neck, and also for melanomas located in other regions of the body and in cases of SLNs located near the injection site, which are difficult to locate using the gamma probe alone. The portable gamma camera is also helpful to exclude a remaining hot spot after the hottest SLN has been harvested (Fig. 6.10). Another challenging condition is the retrieval of in-transit SLNs that, under some circumstances, appear in very rare locations. In a recent study in this setting, the use of a portable gamma camera allowed retrieval of SLNs that, because of their anatomic location, had been missed by conventional gamma probe guidance [6.52]. Thus, the use of tomographic and fused images in the pre-operative setting provides the surgeon with valuable information for planning the most appropriate surgical approach. On the other hand, the use of a portable gamma camera for real time imaging in the operating theatre is expected to improve even further the SLN identification in patients with melanoma, as already demonstrated in other cancers, including head and neck, prostate and breast cancers [6.53–6.56].

The acquisition of additional real time scintigraphic images implies that surgical time may increase by various amounts, depending on the level of team coordination. On the other hand, if the portable gamma camera is not used, the surgeon may need to spend a significant amount of additional time seeking other SLNs or confirming complete SLN removal. Preliminary experience suggests that this extra time is worthwhile in this context for SLNs that are difficult to retrieve, as the use of the gamma camera might reduce the possibility of missing a metastatic SLN [6.52].

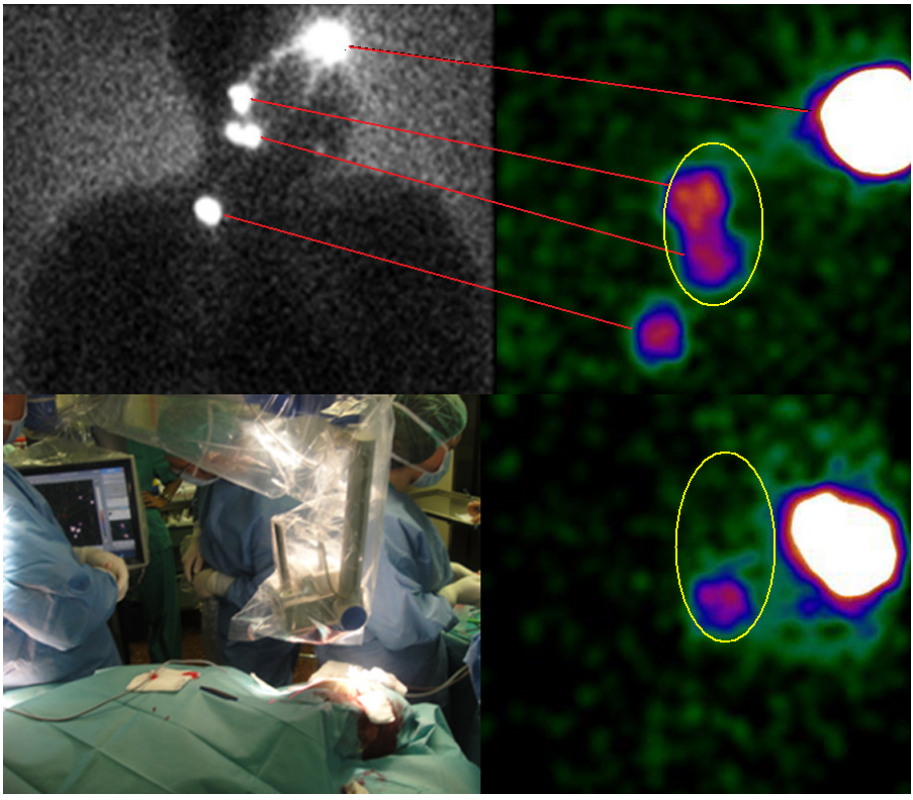

FIG. 6.10. The use of portable gamma cameras is expanding in some radioguided surgery scenarios. Upper left: Delayed right lateral static acquisition in a patient with a frontal melanoma draining to several LNs at different neck levels in the right cervical basin. Upper right: Image acquired using the portable gamma camera showing the same draining pattern. Lower left: Intraoperative monitoring using the portable gamma camera of the lymphatic drainage area. Lower right: Image acquired using the portable gamma camera after resection of two SLNs, depicting one residual SLN to be resected. This example illustrates the added value of close monitoring of the surgical procedure using a portable gamma camera.

The freehand SPECT system mentioned in Chapter 4 of this publication combines acoustic signals with 3-D imaging for the localization of areas with focal radioactivity accumulation in the operating room. The system consists of a spatial localization system and two tracking targets that are fixed on the gamma probe and on the patient, respectively. The localization system consists of an optical camera and an infrared localization device. The 3-D images generated with this freehand SPECT probe are visualized on the screen. The images can be displayed in real time so that information on the depth of a node is available. The

feasibility of 3-D SLN localization using the freehand SPECT system is being tested in patients with melanoma, in addition to patients with breast cancer [6.57].

Additional radioguided surgery techniques have been adapted to this scenario, such as radioguided ultrasound lymph node localization (RULL) for melanoma patients presenting with US suspicious, non-palpable LNs. Investigators from the European Institute of Oncology (Milan, Italy) adapted, for this purpose, the well known breast ROLL approach originally developed for non-palpable breast tumours. In particular, before surgery, approximately 12–15 MBq of ^{99m}Tc MAA in 0.2 mL of saline is injected into the suspicious LN under US guidance using a 25 G needle. A scintigraphic study is then performed to locate tracer activity and to ascertain that the hot spot has been placed in a well defined area. Testori et al. reported preliminary results obtained with this 'new' GOSTT technique in 12 patients with melanoma [6.58]. In all these patients, the hot spots were easily located using the gamma probe, and the radioactive area corresponded to the suspicious LNs. While four resected LNs did not contain metastasis, seven were positive for CM metastasis and one was positive for Hodgkin's disease. These preliminary data suggest that RULL is simple, accurate and allows rapid removal of suspicious, non-palpable LNs compared with conventional techniques.

Another potential tool can ascertain the lymphatic drainage of certain cutaneous zones. Reynolds et al. [6.59] developed software specifically designed to yield a 3-D visualization of skin lymphatic drainage of the body, particularly in the head and neck region. They collected the data obtained from lymphoscintigraphies of 929 patients with head and neck CM performed at the Sydney Melanoma Unit. They then generated a 3-D computer model of the skin and LNs and created heat maps to visualize the relative likelihood that any skin region of the head and neck would drain to a specific LN basin. This model has educational and clinical utility, because when no lymphoscintigraphy is available, it could be used to predict possible SLN basins [6.59].

6.6. MERKEL CELL CARCINOMA

While only approximately 30% of patients with Merkel cell carcinoma present with clinically apparent regional LN metastases, as many as 70% of the remaining patients experience relapses in the regional LNs within 2 years of diagnosis, if the regional LNs are not treated. Half of the patients with regional recurrence proceed to develop systemic disease. Metastasis of Merkel cell carcinoma is believed to follow an orderly progression from the primary tumour to the lymphatic system, before affecting distant sites. LN status in Merkel cell carcinoma has been demonstrated to be a powerful predictor of survival and of

distant metastases. In the meta-analysis by Mehrany et al. with an accrual of 60 patients, 34 out of 35 patients (97%) with tumour negative SLNs had no evidence of recurrence at a median follow-up of 7.3 months [6.60].

The application of the gamma detection probe in radioguided surgery for Merkel cell carcinoma has been limited to SLNB, which is accepted as a standard of care for previously untreated, clinical stage I Merkel cell carcinoma. The technique of radioguided SLNB in these patients is similar to that used for CM. The radiocolloid is injected intradermally in one to four sites around the intact primary lesion, or around the resulting excisional biopsy scar. Maza et al. reported on 23 patients with clinical stage I Merkel cell carcinoma; at least one SLN was detected in all patients, and metastatic involvement was found in 11 out of 23 patients (48%) [6.61]. If SLN metastasis is found, the combination of radiotherapy and selective LDN improves survival when compared with surgery or radiation alone. Chemotherapy may be used as an adjunct to locoregional therapy.

In summary, new devices and approaches have been added to the 'classical' SLNM and SLNB procedures. These new tools allow further refinement of the whole pre-operative and intraoperative procedures, and work is in progress on the search for standardized GOSTT techniques in CM as well as in other types of tumours.

REFERENCES TO CHAPTER 6

[6.1] JEMAL, A., et al., Cancer statistics, 2008, CA Cancer J. Clin. **58** (2008) 71–96.

[6.2] COIT, D.G., et al., Melanoma, J. Natl. Compr. Canc. Netw. **7** (2009) 250–275.

[6.3] MORTON, D.L., et al., Technical details of intraoperative lymphatic mapping for early stage melanoma, Arch. Surg. **127** (1992) 392–399.

[6.4] ALEX, J.C., WEAVER, D.L., FAIRBANK, J.T., RANKIN, B.S., KRAG, D.N., Gamma-probe-guided lymph node localization in malignant melanoma, Surg. Oncol. **2** (1993) 303–308.

[6.5] ALBERTINI, J.J., et al., Intraoperative radio-lympho-scintigraphy improves sentinel lymph node identification for patients with melanoma, Ann. Surg. **223** (1996) 217–224.

[6.6] PIJPERS, R., et al., Sentinel node biopsy in melanoma patients: Dynamic lymphoscintigraphy followed by intraoperative gamma probe and vital dye guidance, World J. Surg. **21** (1997) 788–792.

[6.7] MORTON, D.L., et al., Validation of the accuracy of intraoperative lymphatic mapping and sentinel lymphadenectomy for early-stage melanoma: A multicenter trial, Multicenter Selective Lymphadenectomy Trial Group, Ann. Surg. **230** (1999) 453–463.

[6.8] CHAKERA, A.H., DRZEWIECKI, K.T., EIGTVED, A., JUHL, B.R., Sentinel node biopsy for melanoma: A study of 241 patients, Melanoma Res. **14** (2004) 521–526.

[6.9] COCHRAN, A.J., et al., The Augsburg Consensus, techniques of lymphatic mapping, sentinel lymphadenectomy, and completion lymphadenectomy in cutaneous malignancies, Cancer **89** (2000) 236–241.
[6.10] GERSHENWALD, J.E., SOONG, S.J., BALCH, C.M., AMERICAN JOINT COMMITTEE ON CANCER (AJCC) MELANOMA STAGING COMMITTEE, 2010 TNM staging system for cutaneous melanoma and beyond, Ann. Surg. Oncol. **17** (2010) 1475–1477.
[6.11] TSAO, H., ATKINS, M.B., SOBER, A.J., Management of cutaneous melanoma, N. Engl. J. Med. **351** (2004) 998–1012.
[6.12] WONG, S.L., BRADY, M.S., BUSAM, K.J., COIT, D.G., Results of sentinel lymph node biopsy in patients with thin melanoma, Ann. Surg. Oncol. **13** (2006) 302–309.
[6.13] WRIGHT, B.E., et al., Importance of sentinel lymph node biopsy in patients with thin melanoma, Arch. Surg. **143** (2008) 892–899.
[6.14] SU, L.D., FULLEN, D.R., SONDAK, V.K., JOHNSON, T.M., LOWE, L., Sentinel lymph node biopsy for patients with problematic spitzoid melanocytic lesions: A report on 18 patients, Cancer **97** (2003) 499–507.
[6.15] URSO, C., et al., Sentinel lymph node biopsy in patients with "atypical Spitz tumours." A report on 12 cases, Hum. Pathol. **37** (2006) 816–823.
[6.16] MURALI, R., et al., Sentinel lymph node biopsy in histologically ambiguous melanocytic tumours with spitzoid features (so-called atypical spitzoid tumours), Ann. Surg. Oncol. **15** (2008) 302–309.
[6.17] EVANS, H.L., et al., Lymphoscintigraphy and sentinel node biopsy accurately stage melanoma in patients presenting after wide local excision, Ann. Surg. Oncol. **10** (2003) 416–425.
[6.18] BROWN, R.E., et al., The prognostic significance of non sentinel lymph node metastasis in melanoma, Ann. Surg. Oncol. **17** (2010) 3330–3335.
[6.19] MORTON, D.L., et al., Sentinel-node biopsy or nodal observation in melanoma, N. Engl. J. Med. **355** (2006) 1307–1317.
[6.20] SCOLYER, R.A., MURALI, R., SATZGER, I., THOMPSON, J.F., The detection and significance of melanoma micrometastases in sentinel nodes, Surg. Oncol. **17** (2008) 165–174.
[6.21] BALCH, C.M., et al., An evidence-based staging system for cutaneous melanoma, CA Cancer J. Clin. **54** (2004) 131–149.
[6.22] BALCH, C.M., et al., Final version of 2009 AJCC melanoma staging and classification, J. Clin. Oncol. **36** (2009) 6199–6206.
[6.23] MARIANI, G., et al., Radio-guided sentinel lymph node biopsy in malignant cutaneous melanoma, J. Nucl. Med. **43** (2002) 811–827.
[6.24] CHAKERA, A., et al., EANM-EORTC general recommendations for sentinel node diagnostics in melanoma, Eur. J. Nucl. Med. Mol. Imaging **36** (2009) 1713–1742.
[6.25] ALAZRAKI, N., GLASS, E.C., CASTRONOVO, F., VALDÉS OLMOS, R.A., PODOLOFF, D., Procedure guideline for lymphoscintigraphy and the use of intraoperative gamma probe for sentinel lymph node localization in melanoma of intermediate thickness, J. Nucl. Med. **43** (2002) 1414–1418.

[6.26] SAPPEY, M.P.C., Anatomie, Physiologie, Pathologie, des Vaisseau Lymphatiques Consideres Chez l'Homme et les Vertebres, A. Delahaye & E. Lecrosnier, Paris (1874).
[6.27] LEONG, S.P., et al., Heterogeneous patterns of lymphatic drainage to sentinel lymph nodes by primary melanoma from different anatomic sites, Clin. Nucl. Med. **30** (2005) 150–158.
[6.28] FEDERICO, A.C., et al., Effect of multiple-nodal basin drainage on cutaneous melanoma, Arch. Surg. **143** (2008) 632–637.
[6.29] VIDAL-SICART, S., et al., Is the identification of in-transit sentinel lymph nodes in malignant melanoma patients really necessary? Eur. J. Nucl. Med. Mol. Imaging **31** (2004) 945–949.
[6.30] THOMPSON, J.F., et al., Location of sentinel lymph nodes in patients with cutaneous melanoma: New insights into lymphatic anatomy, J. Am. Coll. Surg. **189** (1999) 195–204.
[6.31] SCARSBROOK, A.F., GANESHAN, A., BRADLEY, K.M., Pearls and pitfalls of radionuclide imaging of the lymphatic system, Part 1: Sentinel node lymphoscintigraphy in malignant melanoma, Br. J. Radiol. **80** (2007) 132–139.
[6.32] UREN, R.F., Lymphatic drainage of the skin, Ann. Surg. Oncol. **11** (2004) 179–185.
[6.33] STATIUS MULLER, M.G., et al., Unpredictability of lymphatic drainage patterns in melanoma patients, Eur. J. Nucl. Med. Mol. Imaging **29** (2002) 255–261.
[6.34] VALDÉS OLMOS, R., VIDAL-SICART, S., NIEWEG, O., SPECT-CT and real-time intraoperative imaging: New tools for sentinel node localization and radio-guided surgery? Eur. J. Nucl. Med. Mol. Imaging **36** (2009) 1–5.
[6.35] EVEN-SAPIR, E., et al., Lymphoscintigraphy for sentinel node mapping using a hybrid SPECT/CT system, J. Nucl. Med. **44** (2003) 1413–1420.
[6.36] ISHIHARA, T., et al., Management of sentinel lymph nodes in malignant skin tumours using dynamic lymphoscintigraphy and the single-photon-emission computed tomography/computed tomography combined system, Int. J. Clin. Oncol. **11** (2006) 214–220.
[6.37] MAR, M.V., MILLER, S.A., KIM, E.E., MACAPINLAC, H.A., Evaluation and localization of lymphatic drainage and sentinel lymph nodes in patients with head and neck melanomas by hybrid SPECT/CT lymphoscintigraphic imaging, J. Nucl. Med. Technol. **35** (2007) 10–16.
[6.38] VERMEEREN, L., et al., SPECT/CT for preoperative sentinel node localization, J. Surg. Oncol. **101** (2010) 184–190.
[6.39] BELHOCINE, T.Z., SCOTT, A.M., EVEN-SAPIR, E., URBAIN, J.L., ESSNER, R., Role of nuclear medicine in the management of cutaneous malignant melanoma, J. Nucl. Med. **47** (2006) 957–967.
[6.40] VERMEEREN, L., et al., SPECT/CT for sentinel lymph node mapping in head and neck melanoma, Head Neck **33** (2011) 1–6.
[6.41] VAN DER PLOEG, I.M., et al., The yield of SPECT/CT for anatomical lymphatic mapping in patients with melanoma, Ann. Surg. Oncol. **16** (2009) 1537–1542.
[6.42] COVARELLI, P., et al., The single-photon emission computed tomography/computed tomography: A new procedure to perform the sentinel node biopsy in patients with head and neck melanoma, Melanoma Res. **17** (2007) 323–328.

[6.43] PATEL, C.N., CHOWDHURY, F.U., SCARSBROOK, A.F., Hybrid SPECT/CT: The end of 'unclear' medicine, Postgrad. Med. J. **85** (2009) 606–613.
[6.44] UREN, R.F., SPECT/CT lymphoscintigraphy to locate sentinel lymph node in patients with melanoma, Ann. Surg. Oncol. **16** (2009) 1459–1460.
[6.45] NATIONAL COMPREHENSIVE CANCER NETWORK, Clinical Guidelines in Oncology for Melanoma (2010), www.nccn.com
[6.46] BRADY, M.S., et al., Utility of preoperative [^{18}]F-fluorodeoxyglucose-positron emission tomography scanning in high-risk melanoma patients, Ann. Surg. Oncol. **13** (2006) 525–532.
[6.47] REINHARDT, M.J., et al., Diagnostic performance of whole body dual modality ^{18}F-FDG PET/CT imaging for N- and M-staging of malignant melanoma: Experience with 250 consecutive patients, J. Clin. Oncol. **24** (2006) 1178–1187.
[6.48] VIDAL-SICART, S., et al., Identification of the sentinel lymph node in patients with malignant melanoma: What are the reasons for mistakes? Eur. J. Nucl. Med. **30** (2003) 362–366.
[6.49] FRANC, B.L., MARI, C., JOHNSON, D., LEONG, S.P., The role of a positron- and high-energy gamma photon probe in intraoperative localization of recurrent melanoma, Clin. Nucl. Med. **30** (2005) 787–791.
[6.50] GULEC, S.A., HOENIE, E., HOSTETTER, R., SCHWARTZENTRUBER, D., PET probe-guided surgery: Applications and clinical protocol, World J. Surg. Oncol. **5** (2007) 65–71.
[6.51] NOWECKI, Z.I., RUTKOWSKI, P., NASIEROWSKA-GUTTMEJER, A., RUKA, W., Survival analysis and clinic-pathological factors associated with false-negative sentinel lymph node biopsy findings in patients with cutaneous melanoma, Ann. Surg. Oncol. **13** (2006) 1655–1663.
[6.52] VIDAL-SICART, S., et al., Added value of intraoperative real-time imaging in searches for difficult-to-locate sentinel nodes, J. Nucl. Med. **51** (2010) 1219–1225.
[6.53] VERMEEREN, L., VALDÉS OLMOS, R.A., KLOP, W.M., BALM, A.J., VAN DEN BREKEL, M.W., A portable gamma camera for intraoperative detection of sentinel nodes in the head and neck region, J. Nucl. Med. **51** (2010) 700–703.
[6.54] VERMEEREN, L., et al., Para-aortic sentinel lymph nodes: Toward optimal detection and intraoperative localization using SPECT/CT and intraoperative real-time imaging, J. Nucl. Med. **51** (2010) 376–382.
[6.55] PAREDES, P., et al., Radio-guided occult lesion localisation in breast cancer using an intraoperative portable gamma camera: First results, Eur. J. Nucl. Med. Mol. Imaging **35** (2008) 230–235.
[6.56] DUCH, J., Portable gamma cameras: The real value of an additional view in the operating theatre, Eur. J. Nucl. Med. Mol. Imaging **38** (2011) 633–635.
[6.57] WENDLER, T., et al., First demonstration of 3-D lymphatic mapping in breast cancer using freehand SPECT, Eur. J. Nucl. Med. Mol. Imaging **37** (2010) 1452–1461.
[6.58] TESTORI, A., et al., Radio-guided ultrasound lymph node localization: Feasibility of a new technique for localizing and excising non-palpable lymph nodes ultrasound suspicious for melanoma metastases, Melanoma Res. **20** (2010) 197–202.

[6.59] REYNOLDS, H.M., SMITH, N.P., UREN, R.F., THOMPSON, J.F., DUNBAR, P.R., Three-dimensional visualization of skin lymphatic drainage patterns of the head and neck, Head Neck **31** (2009) 1316–1325.
[6.60] MEHRANY, K., et al., A meta-analysis of the prognostic significance of sentinel lymph node status in Merkel cell carcinoma, Dermatol. Surg. **28** (2002) 113–117.
[6.61] MAZA, S., et al., Impact of sentinel lymph node biopsy in patients with Merkel cell carcinoma: Results of a prospective study and review of the literature, Eur. J. Nucl. Med. Mol. Imaging **33** (2006) 433–440.

7. GOSTT IN PARATHYROID TUMOURS

7.1. INTRODUCTION

Primary hyperparathyroidism is characterized by the autonomous production of parathyroid hormone (PTH), resulting in hypercalcaemia. This is a relatively common disease, occurring in approximately 1% of the adult population and approximately 2% of the population over 55 years [7.1]. It occurs two to three times more frequently in women than in men. Hyperparathyroidism peaks in incidence in the fourth and fifth decades of life, but can also occur in young children and the elderly [7.2].

Historically, patients have presented with symptoms such as urolithiasis, bone pain and pathological fractures and non-specific symptoms such as depression, lethargy, and vague aches and pains. Since the advent of multichannel biochemical screening, however, patients frequently present without symptoms after being found to have hypercalcaemia during routine laboratory screening [7.3]. The frequency of this previously uncommon clinical scenario, an asymptomatic patient with hyperparathyroidism, has led to controversy and changes in the management of patients with this disease.

The change in clinical presentation of primary hyperparathyroidism has spurred investigation into the natural history of the disease and the indications for treatment. It is generally agreed that surgery is indicated in patients who present with symptomatic disease such as nephrolithiasis, nephrocalcinosis, renal dysfunction, osteopenia with fractures, osteitis fibrosa cystica and altered neurological function with obtundation, delirium or coma. However, the management of patients with asymptomatic hyperparathyroidism remains controversial. To guide clinicians facing such patients, the National Institutes of Health organized a consensus development conference in 1990 to make recommendations on the treatment of primary hyperparathyroidism [7.4]. In 2002, the National Institutes of Health convened another group, a workshop on asymptomatic primary hyperparathyroidism, to revisit these issues and make new recommendations. Revised consensus guidelines outlining the criteria for surgical treatment and management guidelines for observing patients with asymptomatic hyperparathyroidism have been published [7.5, 7.6].

Under these guidelines, the indications for surgery include a serum calcium concentration of 1.0 mg/dL above the upper normal limit, a 24 h urinary calcium excretion of 400 mg or more, a reduction in the creatinine clearance of more than 30%, a bone mineral density with a T score below −2.5 at any site (lumbar spine, femoral neck or total femur) or an age of younger than 50 years.

The use of nuclear imaging, in combination with improved US imaging and the availability of rapid intraoperative PTH assays, has changed the strategy of surgical treatment of primary hyperparathyroidism [7.3, 7.7, 7.8]. Previously, the standard treatment for all patients with primary hyperparathyroidism was a bilateral neck exploration, with the goal of identifying and evaluating all four parathyroid glands. This procedure generally involves making a transverse neck incision of 6–8 cm several cm above the clavicles, which is an incision similar to the one used for thyroid surgery. The two lobes of the thyroid gland are mobilized, both recurrent laryngeal nerves are identified, and the neck is explored to identify the four parathyroid glands. Visual inspection of the glands, sometimes used in conjunction with intraoperative histological assessment of frozen sections, has allowed experienced surgeons to identify the pathological glands and remove them with a success rate in excess of 90% [7.3].

Because 85% or more of patients with primary hyperparathyroidism have a single parathyroid adenoma, only one gland is responsible for their disease.

The goal of surgery for primary hyperparathyroidism is to return the patient's calcium level to normal, although this cannot be the sole index of successful parathyroid surgery; surgery should be accomplished with minimal morbidity, no mortality, low recurrence rates and at a reasonable cost. The success of the surgical treatment depends on the success in the localization and identification of abnormal glands. In this respect, the increased sensitivity of parathyroid imaging allows the surgeon to plan a localized exploration that is designed to remove the common single focus of disease. By adopting this approach, rather than the previous approach of four gland exploration, the surgical incision is much smaller, dissection is minimal, postoperative pain is less and the hospital stay is shorter. This procedure may be carried out as outpatient surgery, even under local anaesthesia.

The ability to pre-operatively localize pathological parathyroid glands has enabled a more focused surgical approach. Most centres nowadays use pre-operative imaging and intraoperative rapid testing of PTH with either a unilateral neck exploration or, increasingly, a minimally invasive single gland exploration for the treatment of patients with primary hyperparathyroidism. Endoscopic parathyroid exploration is performed at a few centres, but has not been widely adopted.

These focused surgical approaches are possible only when pre-operative nuclear imaging suggests the presence of a localized parathyroid adenoma.

A unilateral neck exploration involves making a small incision, generally 3–5 cm long, and exploring one side of the neck to identify both parathyroid glands and the recurrent laryngeal nerve. A focused single gland exploration involves making an incision 2–4 cm long. Some surgeons do not search for the recurrent laryngeal nerve, but rather look immediately for the single abnormal

gland. With both unilateral neck exploration and single gland exploration, rapid intraoperative measurement of PTH levels is used to increase the certainty that the gland or glands responsible for the patient's hyperparathyroidism are addressed at the time of surgery. The half-life of PTH in the circulation is approximately 2 min. Generally, a drop in serum PTH to less than 50% of the measurement taken in the operating room before removal of the suspected gland indicates that the source of the hyperparathyroidism has been removed. The blood sample after removal of the suspected adenoma should be drawn 10 min after the specimen is excised. An analysis of 210 published series using intraoperative PTH concluded that a unilateral neck dissection was completed as intended in 94.5% of the cases. Intraoperative PTH levels resulted in conversion to a bilateral neck exploration in 5.5% of cases, while persistent hypercalcaemia was observed in 1.3% of cases [7.9].

Radioguided minimally invasive surgery for primary hyperparathyroidism is feasible when pre-operative scintigraphy identifies a single focus of radiotracer uptake, indicating a parathyroid adenoma. With the introduction of ^{99m}Tc sestamibi scintigraphy to identify and locate the parathyroid adenoma pre-operatively (see Fig. 7.1), the era of focused exploration or minimally invasive radioguided parathyroidectomy (MIRP) began [7.10–7.13].

MIRP has been used for only approximately 7–8 years; thus, no large scale, long term follow-up data are available yet. However, the more than 95% success rate reported by most studies cited above constitutes a sound basis for favourable MIRP results. This is similar to those experienced using the conventional surgical approach in the long run.

7.2. MIRP AS A FORM OF GOSTT

7.2.1. Parathyroid scintigraphy (pre-operative phase)

The localization of ^{99m}Tc sestamibi in the parathyroid tissue is a function of metabolic activity, with intracellular accumulation of this radiopharmaceutical occurring specifically in the mitochondria. The overall uptake in hyperplastic or adenomatous parathyroid glands is linked to the blood flow, gland size and mitochondrial activity. Similar to other radioactive imaging agents (e.g. ^{201}Tl), ^{99m}Tc sestamibi accumulates both in the thyroid and in the parathyroid tissue within minutes of intravenous administration. However, what makes this tracer especially useful for parathyroid imaging is its different washout rate from the two tissues: ^{99m}Tc sestamibi is released much faster from thyroid than from parathyroid tissue (see Fig. 7.1). This differential retention might be related to some down regulation of the P-glycoprotein system (normally acting as an

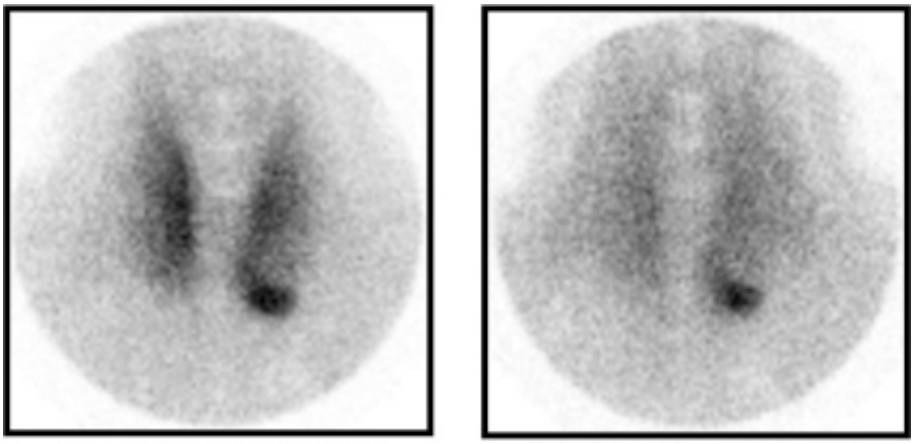

FIG. 7.1. Classical, single tracer, dual phase parathyroid scintigraphy with ^{99m}Tc sestamibi in a patient with primary hyperparathyroidism. Image in the left panel is obtained 15 min post-injection of ^{99m}Tc sestamibi, and shows physiological early uptake in the thyroid gland, with a clear focus of increased accumulation at the lower pole of the left thyroid lobe. Image in the right panel shows the late ^{99m}Tc sestamibi scan (acquired 2.5 h post-injection); while there is still some residual activity in the thyroid gland, the area with focal tracer retention at the lower pole of the left thyroid lobe is much more obvious, thus indicating the presence of a parathyroid adenoma. This pattern of differential washout rates from the thyroid tissue and from the hyperfunctioning/hyperplastic parathyroid glands allows scintigraphic discrimination between the two tissues. In fact, washout is faster from thyroidal parenchyma, while the hyperfunctioning parathyroid tissue (which is especially rich in mitochondria, i.e. the site of intracellular accumulation of ^{99m}Tc sestamibi) retains the tracer longer.

outflux carrier molecule for various substrates, including ^{99m}Tc sestamibi) in the parathyroid tissue. When feasible, concomitant suppression of thyroid uptake (induced by exogenous thyroid hormone administration) obviously improves scintigraphic localization of parathyroid lesions with ^{99m}Tc sestamibi.

High quality scintigraphy using ^{99m}Tc sestamibi can accurately localize parathyroid adenomas in 85%–95% of patients with primary hyperparathyroidism. In addition, SPECT imaging considerably improves the localization of particular ectopic sites that are otherwise difficult to explore, such as the retroesophageal space or mediastinum [7.14, 7.15]. It is crucial to include the entire chest in the imaging field in all ^{99m}Tc sestamibi imaging protocols, for evaluation of potential ectopic sites. Similar to other applications of hybrid fusion imaging represented by SPECT/CT imaging [7.16], implementation of this methodology

in the pre-operative evaluation of patients with hyperparathyroidism considerably improves the performance of parathyroid scintigraphy over SPECT imaging alone, especially for specificity and anatomic accuracy of scintigraphic identification/localization of the hyperfunctioning parathyroid tissue, as demonstrated by a number of clinical investigations [7.17–7.32].

The single tracer, dual phase scintigraphy summarized above is a simple basic procedure originally described by Taillefer et al. [7.33], and is based solely on the differential washout rate of ^{99m}Tc sestamibi from the thyroid and the parathyroid tissue. Planar imaging of the neck and thorax is recorded starting at 15 min, then repeated at 2–3 h after the intravenous injection of ^{99m}Tc sestamibi (approx. 740 MBq). It is advisable to position the patient's neck in hyperextension, to achieve a better image of the gland structures.

The scan is considered positive for parathyroid disease when an area of increased uptake that persists on delayed imaging is found. This dual phase imaging technique is easy to perform and has proven to be highly sensitive and specific, especially in patients with primary hyperparathyroidism [7.34]. Nevertheless, there are two potential caveats in this dual phase scintigraphy procedure. One is represented by solid thyroid nodules that can concentrate ^{99m}Tc sestamibi quite avidly, regardless of whether they are benign or malignant and whether they appear as 'hot' or 'cold' on the ^{99m}Tc pertechnetate scan. The other is the possibility of absent abnormal uptake on delayed imaging, explained by rapid ^{99m}Tc sestamibi washout, similar to that of thyroid tissue, in some parathyroid adenomas, which causes false negative results.

Dual tracer subtraction scintigraphy combines dual phase ^{99m}Tc sestamibi imaging with the administration of a second radiopharmaceutical that accumulates specifically in the thyroid gland and not in the parathyroid tissue; images are then subtracted to allow detection of focal uptakes that are specific for abnormal parathyroid tissue.

The most practical parathyroid imaging technique is the ^{99m}Tc sestamibi/$[^{99m}TcO_4]^-$ dual tracer subtraction technique in which the thyroid imaging agent, ^{99m}Tc pertechnetate, is administered after completion of the late (2–3 h) ^{99m}Tc sestamibi acquisition (see Fig. 7.2). At this late time, most of the ^{99m}Tc sestamibi has already washed out from the thyroid, which, therefore, is easily imaged with the thyroid only imaging radiopharmaceutical. The image acquired 20 min after $[^{99m}TcO_4]^-$ injection therefore combines ^{99m}Tc pertechnetate uptake with some residual activity from the earlier ^{99m}Tc sestamibi administration. The late ^{99m}Tc sestamibi image is subtracted from the combined scan to obtain a 'pure' ^{99m}Tc pertechnetate image, the profile of which will clarify the origin (thyroid versus parathyroid) of abnormal ^{99m}Tc sestamibi uptake. This methodology requires two sets of images, one at 5–15 min (early) and one at 2–3 h (delayed). Investigations have reported good results [7.35–7.37] that are

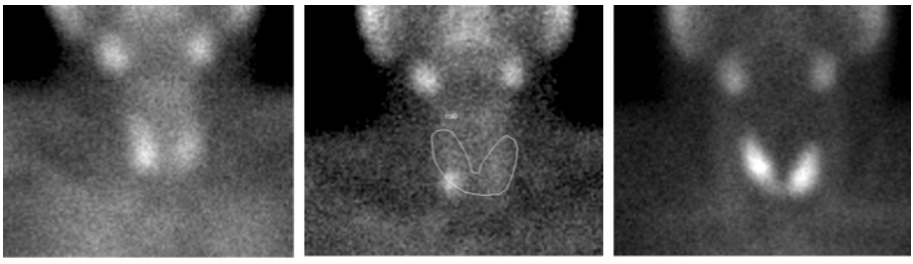

FIG. 7.2. Dual phase parathyroid scintigraphy with ^{99m}Tc sestamibi in a patient with primary hyperparathyroidism (planar acquisitions). Left panel shows physiological early uptake in the thyroid gland with mildly enhanced uptake at the base of the right thyroid lobe (equivocal finding for parathyroid adenoma). Centre panel shows almost complete washout of ^{99m}Tc sestamibi from the thyroid tissue at 2 h post-injection, with clear focal retention of radioactivity below the base of the right thyroid lobe, corresponding to a parathyroid adenoma. The profile superimposed on the late ^{99m}Tc sestamibi scan is transferred from a region of interest manually drawn around the thyroid gland, as subsequently visualized in a pure thyroid gland obtained after injection of ^{99m}Tc pertechnetate (right panel). This procedure helps to topographically localize parathyroid adenomas in cases of equivocal single tracer scans.

similar in accuracy to the subtraction method, although few direct comparison studies have been reported [7.38, 7.39].

7.2.2. Added value of SPECT imaging for pre-operative imaging

Several investigations have reported improved sensitivity in the detection and localization of hyperfunctioning parathyroid glands using SPECT imaging, compared with planar imaging [7.40–7.42]. The addition of anatomic imaging with CT software fusion [7.43] or hybrid SPECT/CT [7.17–7.32] has a proven potential to improve pre-operative localization (see Fig. 7.3). In particular, the most commonly reported added value of SPECT/CT imaging over stand alone SPECT imaging concerns increased specificity in the identification of hyperfunctioning parathyroid tissue (especially if located in ectopic sites), even in patients with concomitant multinodular goitres and/or in the presence of distorted anatomy because of prior surgical procedures in the neck. On the other hand, most studies report moderately increased sensitivity of SPECT/CT imaging versus SPECT imaging alone, although several studies indicate increases in sensitivity up to 30%–40% with SPECT/CT fusion imaging compared to SPECT imaging alone.

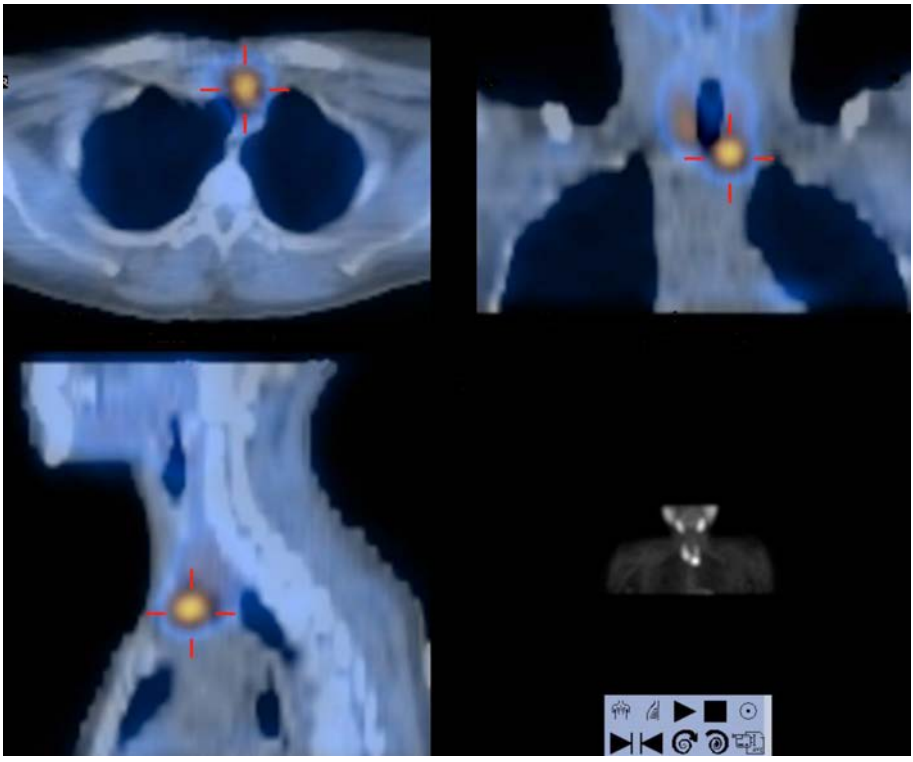

FIG. 7.3. SPECT/CT images obtained of a patient with primary hyperparathyroidism approximately 2 h after intravenous administration of ^{99m}Tc sestamibi. Lower right panel shows the anterior MIP of the head and chest, clearly indicating the parathyroid adenoma as an area of persistent tracer uptake located at the lower pole of the left thyroid lobe. Upper left, upper right and lower left panels show the SPECT/CT fused sections in the transaxial, coronal and sagittal planes, respectively. Both the transaxial and the coronal sections clearly demonstrate the left paraposterior tracheal localization of the parathyroid adenoma, thus providing the surgeon with useful pre-operative information for planning the most adequate approach.

Immediately after planar image acquisition, SPECT images are usually acquired with a step and shoot protocol of 25 s/3° for a total of 60 views per camera head; either a 64 × 64 matrix or a 128 × 128 matrix can be employed. With hybrid SPECT/CT imaging, the CT image acquisitions are performed according to specifications, then the CT sections are reconstructed using the same matrix and slice thickness as for the SPECT sections; the CT image acquisitions are also utilized for correction attenuation using the transmission data of each individual patient. Transverse, coronal and sagittal SPECT images are usually generated using a Hann prefilter and a Butterworth postprocessing filter with two OSEM iterations and a maximum of ten OSEM subsets. Transverse, coronal

and sagittal SPECT/CT images are generated using a Butterworth pre-filter and post-processing filter with four OSEM iterations for a maximum of eight OSEM subsets.

For various radiopharmaceuticals and different types of scintigraphic studies, the superior contrast resolution of SPECT imaging, compared with that of planar imaging, has often translated into increased lesion detection. For parathyroid scintigraphy, several studies have reported higher sensitivity for SPECT imaging than for planar imaging, while the main advantage of SPECT/CT over SPECT imaging is usually represented by a higher specificity.

SPECT imaging is often acquired at a single time interval, either early or late after administration of ^{99m}Tc sestamibi. With early SPECT imaging, one investigational group has reported very high sensitivity (96%) [7.41, 7.44]. Using delayed SPECT imaging, one large study reported slightly lower sensitivity (87%) [7.45]. Only one investigation directly compared early and delayed SPECT images [7.46], where it was confirmed that early SPECT imaging has higher sensitivity (91%) than delayed SPECT imaging (74%).

A particularly important feature of SPECT/CT imaging is that it allows accurate topographic pre-operative localization, not only when hyperfunctioning parathyroid adenomas are found in their expected location (see Fig. 7.4), but especially when the adenomas are located ectopically, for instance, in the mediastinal space (see Fig. 7.5). Because of such an image based guide, the surgeon can plan the most adequate surgical approach for each condition, e.g. a small incision in the neck for an orthotopically located parathyroid adenoma or a thoracotomy for an adenoma located ectopically in the mediastinal space.

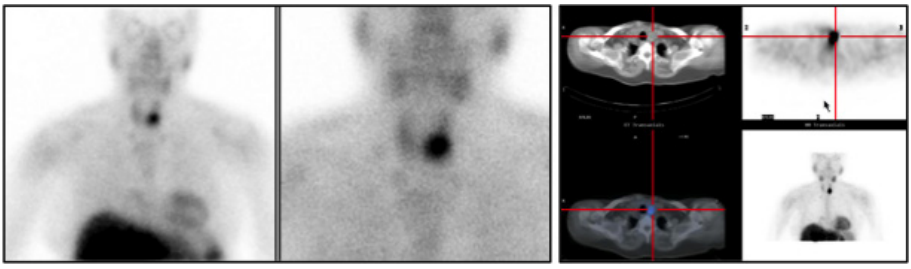

FIG. 7.4. Technetium-99m sestamibi planar images (left panels) and SPECT/CT images (right panels) obtained in a patient with primary hyperparathyroidism. Planar images were recorded approximately 30 min post-injection, with an FOV including the entire chest (but also including a large portion of the head and the upper portion of the abdomen) and as a spot view more closely focused on the upper portion of the chest. The presence of a parathyroid adenoma was judged to be very likely, even on the basis of such early acquisitions. Transaxial SPECT/CT images demonstrate more clearly the relationship of the parathyroid adenoma with the trachea (lower right portion of the right panel shows the anterior MIP of the head and chest).

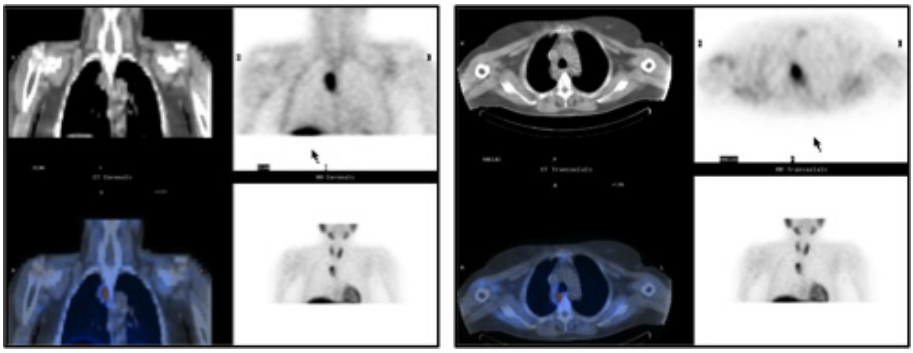

FIG. 7.5. Technetium-99m sestamibi SPECT/CT images obtained of a patient with persistent primary hyperparathyroidism after prior unsuccessful parathyroid surgery. Coronal (left panel) and transaxial (right panel) SPECT/CT images demonstrate the presence of a large parathyroid adenoma located ectopically in the mediastinal space, right of the lower portion of the trachea just above its bifurcation. Lower right portions of both panels show the anterior MIPs of the head and chest.

Software fusion of separately acquired parathyroid SPECT and CT images has been reported to improve the accuracy of localization over that with SPECT alone in a small series of patients [7.47]. Hybrid SPECT/CT imaging has the advantage of sequentially imaging the patient in the same position on the same imaging table and offers the possibility to perform attenuation correction using the transmission data obtained in each individual patient undergoing examination. Other investigators have used a pinhole collimator to increase the spatial resolution and improve the sensitivity of planar parathyroid scintigraphy. The radiation dose to the patient from the CT scans is considerably lower than that caused by any typical single diagnostic CT scan.

7.3. INTRAOPERATIVE PHASE (MIRP USING THE RUBELLO AND MARIANI LOW ^{99M}Tc SESTAMIBI DOSE PROTOCOL)

In the Rubello and Mariani low ^{99m}Tc sestamidi dose protocol, a diagnostic scintigraphic study is performed some days before the operation using the dual tracer [$^{99m}TcO_4$]/^{99m}Tc sestamibi subtraction technique. In patients with distinct ^{99m}Tc sestamibi scintigraphic evidence of a solitary parathyroid adenoma, a low (37 MBq) ^{99m}Tc sestamibi dose is then injected on the day of surgery, in the operating room, approximately 10 min before the operation.

Prior to surgical incision, the patient's neck is scanned with an 11 mm collimated probe to identify the area of maximum count activity in the skin overlying the parathyroid adenoma. A low transverse midline neck incision (approx. 1 cm above the sternal notch) is usually performed to permit easy conversion to bilateral neck exploration, if necessary. High lateral neck access is preferred in some superior adenomas and in ectopic adenomas located at the carotid bifurcation.

The probe is repeatedly inserted through the 15 mm skin incision, guiding the surgeon to the area of maximum count activity corresponding to the parathyroid adenoma; radioactivity is measured with the probe on the parathyroid adenoma, on the thyroid gland and on the background, as well as ex vivo on the parathyroid adenoma to evaluate successful removal of parathyroid tissue; frozen section analysis of the surgical specimen is routinely performed. Radioactivity is then checked on the empty parathyroid bed to evaluate the completeness of the parathyroid tissue resection. Tissue rates are calculated (parathyroid–background, parathyroid–thyroid, thyroid–background); in particular, in the absence of ^{99m}Tc sestamibi avid thyroid nodules, a parathyroid–thyroid ratio higher than 1.5 strongly suggests the presence of a parathyroid adenoma, while typical parathyroid–background ratios range between 2.5 and 4.5. An empty parathyroid bed–thyroid ratio approaching 1 is highly indicative of complete removal of abnormal parathyroid tissue. Finally, the assessment of radioactivity in all four quadrants before the end of the surgical exploration ensures that all hyperfunctioning glands are removed.

Gamma probe guidance enables the surgeon to perform a rather small skin incision with improved cosmesis. The technique can also be performed under local anaesthesia. The operating time is reduced, and the patient can be discharged from hospital earlier [7.48, 7.49].

Recent advances in intraoperative detection of radioactivity distribution within the field of interest are further contributing to improving the ability of surgeons to select the optimal surgical approach and to assess completeness of removal of the target lesion(s). This can be achieved either by using small FOV dedicated imaging probes, and/or by setting up the freehand SPECT probe system originally proposed for facilitating radioguided SLNB [7.50]. The system is composed of a spatial localization system and two tracking targets that are fixed on the intraoperative gamma probe and on the patient, respectively. Before starting surgery and with the patient already positioned on the operating table, the gamma probe is employed to manually scan the target region with different angles of view in a similar manner to that performed when rotating the gamma camera detector head around the patient's body for conventional SPECT imaging. 3-D images (i.e. freehand SPECT) are thus generated and are displayed on a monitor superimposed on the patient's body as recorded using an optical

camera. These combined freehand SPECT and optical images visually guide the surgeon during the procedure, by providing real time information on the depth of the radiolabelled lesion, and help to assess the completeness of surgical removal of all target tissues (see example in Fig. 7.6).

7.4. CONCLUSIONS

MIRP is a very attractive surgical approach to treat patients with primary hyperparathyroidism caused by solitary parathyroid adenoma. This technique has proven to be technically easy, safe and to have a low morbidity rate in the hands of a skilled surgeon [7.51]. There are several advantages of MIRP over bilateral neck exploration in patients with primary hyperparathyroidism caused by a solitary adenoma: smaller surgical incision; less surgical trauma; shorter length of surgery, anaesthesia and hospital stay; less postsurgical pain; better cosmetic results and lower overall cost. In contrast to minimally invasive endoscopic surgery, MIRP can be performed also for reintervention in patients with persistent or recurrent hyperparathyroidism [7.51, 7.52].

FIG. 7.6. Representative images recorded during radioguided removal of two parathyroid adenomas using the freehand SPECT system described in the text. Left: Surface volume rendering of SPECT/CT image demonstrating ^{99m}Tc sestamibi uptake in two parathyroid adenomas located inferiorly to the thyroid gland (indicated by red arrows); the skeletal structure of the patient as visualized by low dose CT is displayed with the window for bone. Centre: Overlay of the surface volume rendering SPECT/CT image (showing both the skeletal structure for topographic reference and the location of the two hyperfunctioning parathyroid adenomas as visualized by ^{99m}Tc sestamibi uptake at the base of the neck) onto the patient's body positioned on the operating table as visualized by the optical camera. Right: Halfway through the surgical procedure, the right parathyroid adenoma has already been removed (and its ex vivo counting rate is being measured with the gamma probe in the lower left part of the panel), while the left parathyroid adenoma can be seen (purple colour) still in place as visualized on the monitor that superimposes the freehand SPECT image onto the patient's body as recorded by the optical camera. Images courtesy of K. Rahbar, Universitätsklinikum Münster, Münster (Germany), as provided by T. Wendler, SurgicEye GmbH, Münich (Germany).

As with other radioguided surgical procedures, the technique requires the whole team to be involved (nuclear medicine specialist, surgeon and pathologist) to combine a satisfactory amount of experience and smooth interaction among team members.

The following recommendations should be taken into account when considering MIRP: (i) the most accurate pre-operative scintigraphic modality available should be used, possibly dual tracer subtraction scintigraphy or dual phase ^{99m}Tc sestamibi SPECT imaging, preferably SPECT/CT imaging; (ii) both in vivo and ex vivo gamma probe counting should be obtained to evaluate the success and completeness of surgery; (iii) radiation exposure to the surgeon and operating room personnel should be minimized by administering the lowest dose of ^{99m}Tc sestamibi proven to be effective for performing MIRP and (iv) intraoperative quick PTH measurement appears to be strictly related to the MIRP protocol employed in each centre.

REFERENCES TO CHAPTER 7

[7.1] MELTON, G.B., et al., Interpretation of ^{99m}Tc sestamibi parathyroid SPECT scan is improved when read by the surgeon and nuclear medicine physician together, Nucl. Med. Commun. **26** (2005) 633–638.

[7.2] BILEZIKIAN, J.P., SILVERBERG, S.J., Asymptomatic primary hyperparathyroidism, N. Engl. J. Med. **350** (2004) 1746–1751.

[7.3] McHENRY, C.R., What's new in general surgery: Endocrine surgery, J. Am. Coll. Surg. **195** (2002) 364–371.

[7.4] AMERICAN ASSOCIATION OF CLINICAL ENDOCRINOLOGIS/AMERICAN ASSOICIATION OF ENDOCRINE SURGEONS TASK FORCE ON PRIMARY HYPERPARATHYROIDISM, The American Association of Clinical Endocrinologists and the American Association of Endocrine Surgeons position statement on the diagnosis and management of primary hyperparathyroidism, Endocr. Pract. **11** (2005) 49–54.

[7.5] BILEZIKIAN, J.P., et al., Summary statement from a workshop on asymptomatic primary hyperparathyroidism: A perspective for the 21st century, J. Clin. Endocrinol. Metab. **87** (2002) 5353–5361.

[7.6] MAHADEVIA, P.J., SOSA, J.A., LEVINE, M.A., ZEIGER, M.A., POWE, N.R., Clinical management of primary hyperparathyroidism and thresholds for surgical referral: A national study examining concordance between practice patterns and consensus panel recommendations, Endocr. Pract. **9** (2003) 494–503.

[7.7] PASIEKA, J.L., What's new in general surgery: Endocrine surgery, J. Am. Coll. Surg. **199** (2004) 437–445.

[7.8] SOSA, J.A., ZEIGER, M.A., Surgery for hyperparathyroidism, Trends Endocrinol. Metab. **10** (1999) 72–75.

[7.9] RUDA, J.M., HOLLENBEAK, C.S., STACK, B.C., A systematic review of the diagnosis and treatment of primary hyperparathyroidism from 1995 to 2003, Otolaryngol. Head Neck Surg. **132** (2005) 359–372.
[7.10] SOFFERMAN, R.A., NATHAN, M.H., FAIRBANK, J.T., FOSTER, R.S., Jr., KRAG, D.N., Preoperative technetium 99m sestamibi imaging: Paving the way to minimal-access parathyroid surgery, Arch. Otolaryngol. Head Neck Surg. **122** (1996) 369–374.
[7.11] NORMAN, J., CHEDA, H., Minimally invasive radio-guided parathyroidectomy facilitated by intraoperative nuclear mapping, Surgery **122** (1997) 998–1004.
[7.12] RUBELLO, D., PELIZZO, M.R., CASARA, D., Nuclear medicine and minimally invasive surgery of parathyroid adenomas: A fair marriage, Eur. J. Nucl. Med. **30** (2003) 189–192.
[7.13] SACKETT, W.R., BARRACLOUGH, B., REEVE, T.S., DELBRIDGE, L.W., Worldwide trends in the surgical treatment of primary hyperparathyroidism in the era of minimally invasive parathyroidectomy, Arch. Surg. **137** (2002) 1055–1059.
[7.14] NEUMANN, D.R., et al., Comparison of double-phase ^{99m}Tc-sestamibi with ^{123}I-^{99m}Tc-sestamibi subtraction SPECT in hyperparathyroidism, Am. J. Roentgenol. **169** (1997) 1671–1674.
[7.15] FRANCIS, I.S., et al., Technetium-99m-sestamibi dual-phase SPECT imaging: Concordance with ultrasound, Nucl. Med. Commun. **20** (1999) 487–488.
[7.16] MARIANI, G., et al., A review on the clinical uses of SPECT/CT, Eur. J. Nucl. Med. Mol. Imaging **37** (2010) 1959–1985.
[7.17] RUBELLO, D., et al., An ectopic mediastinal parathyroid adenoma accurately located by a single-day imaging protocol of Tc-99m pertechnetate-MIBI subtraction scintigraphy and MIBI-SPECT-computed tomographic image fusion, Clin. Nucl. Med. **27** (2002) 186–190.
[7.18] GAYED, I.W., et al., The value of ^{99m}Tc-sestamibi SPECT/CT over conventional SPECT in the evaluation of parathyroid adenomas or hyperplasia, J. Nucl. Med. **46** (2005) 248–252.
[7.19] KRAUSZ, Y., et al., Technetium-99m-MIBI SPECT/CT in primary hyperparathyroidism, World J. Surg. **30** (2006) 76–83.
[7.20] SERRA, A., et al., Role of SPECT/CT in the pre-operative assessment of hyperparathyroid patients, Radiol. Med. **111** (2006) 999–1008.
[7.21] LAVELY, W.C., et al., Comparison of SPECT/CT, SPECT, and planar imaging with single- and dual-phase ^{99m}Tc-sestamibi parathyroid scintigraphy, J. Nucl. Med. **48** (2007) 1084–1089.
[7.22] RUF, J., et al., Impact of image fusion and attenuation correction by SPECT-CT on the scintigraphic detection of parathyroid adenomas, Nuklearmed. **46** (2007) 15–21.
[7.23] ESLAMY, H.K., ZIESSMAN, H.A., Parathyroid scintigraphy in patients with primary hyperparathyroidism: ^{99m}Tc-sestamibi SPECT and SPECT/CT, Radiographics **28** (2008) 1461–1476.
[7.24] FAKHRAN, S., BRANSTETTER, B.F., PRYMA, D.A., Parathyroid imaging, Neuroimag. Clin. N. Am. **18** (2008) 537–549.

[7.25] HARRIS, L., et al., Accuracy of technetium-99m SPECT-CT hybrid images in predicting the precise intraoperative anatomical location of parathyroid adenomas, Head Neck **30** (2008) 509–517.
[7.26] NEUMANN, D.R., OBUCHOWSKI, N.A., DIFILIPPO, F.P., Preoperative ^{123}I/^{99m}Tc-sestamibi subtraction SPECT and SPECT/CT in primary hyperparathyroidism, J. Nucl. Med. **49** (2008) 2012–2017.
[7.27] PAPATHANASSIOU, D., et al., SPECT/CT in localization of parathyroid adenoma or hyperplasia in patients with previous neck surgery, Clin. Nucl. Med. **33** (2008) 394–397.
[7.28] AKRAM, K., PARKER, J.A., DONOHOE, K., KOLODNY, G., Role of single photon emission computed tomography/computed tomography in localization of ectopic parathyroid adenoma: A pictorial case series and review of the current literature, Clin. Nucl. Med. **8** (2009) 500–502.
[7.29] LEVINE, D.S., BELZBERG, A.S., WISEMAN, S.M., Hybrid SPECT/CT imaging for primary hyperparathyroidism: Case reports and pictorial review, Clin. Nucl. Med. **34** (2009) 779–784.
[7.30] YIP, L., PRYMA, D.A., YIM, J., CARTY, S.E., OGILVIE, J.B., Sestamibi SPECT intensity scoring system in sporadic primary hyperparathyroidism, World J. Surg. **33** (2009) 426–433.
[7.31] PATA, G., et al., Clinical appraisal of 99m technetium-sestamibi SPECT/CT compared to conventional SPECT in patients with primary hyperparathyroidism and concomitant nodular goiter, Thyroid **20** (2010) 1121–1127.
[7.32] TAUBMAN, M.L., GOLDFARB, M., LEW, J.I., Role of SPECT and SPECT/CT in the surgical treatment of primary hyperparathyroidism, Intern J. Mol. Imaging **2011** (2011) 141593.
[7.33] TAILLEFER, R., et al., Detection and localization of parathyroid adenomas in patients with hyperparathyroidism using a single radionuclide imaging procedure with technetium-99m-sestamibi (double phase study), J. Nucl. Med. **33** (1992) 1801–1807.
[7.34] TAILLEFER, R., "^{99m}Tc-sestamibi parathyroid scintigraphy", Nuclear Medicine Annual (FREEMAN, L., Ed.) (1995) 51–79.
[7.35] RAUTH, J., SESSIONS, R.B., SHUPE, S.C., ZIESSMAN, H.A., Comparison of Tc-99m MIBI and Tl-201/Tc-99m pertechnetate for diagnosis of primary hyperparathyroidism, Clin. Nucl. Med. **21** (1996) 602–608.
[7.36] BLANCO, I., et al., Double-phase Tc-99m sestamibi scintigraphy in the preoperative location of lesions causing hyperparathyroidism, Clin. Nucl. Med. **23** (1998) 291–297.
[7.37] IRVIN, G.L., III, et al., Ambulatory parathyroidectomy for primary hyperparathyroidism, Arch. Surg. **131** (1996) 1074–1078.
[7.38] LESLIE, W.D., DUPONT, J.O., BYBEL, B., RIESE, K.T., Parathyroid ^{99m}Tc-sestamibi scintigraphy: Dual tracer subtraction is superior to double phase washout, Eur. J. Nucl. Med. Mol. Imaging **29** (2002) 1566–1570.
[7.39] STAUDENHERZ, A., et al., Comparison and histopathological correlation of three parathyroid imaging methods in a population with a high prevalence of concomitant thyroid disease, Eur. J. Nucl. Med. **24** (1997) 143–149.

[7.40] MOKA, D., et al., Technetium 99m MIBI-SPECT: A highly sensitive diagnostic tool for localization of parathyroid adenomas, Surgery **128** (2000) 29–35.
[7.41] SCHACHTER, P.P., ISSA, N., SHIMONOV, M., CZERNIAK, A., LORBERBOYM, M., Early postinjection MIBI-SPECT as the only preoperative localizing study for minimally invasive parathyroidectomy, Arch. Surg. **139** (2004) 433–437.
[7.42] SLATER, A., GLEESON, F.V., Increased sensitivity and confidence of SPECT over planar imaging in dual-phase sestamibi for parathyroid adenoma detection, Clin. Nucl. Med. **30** (2005) 1–3.
[7.43] PROFANTER, C., et al., CT-MIBI image fusion: A new preoperative localization technique for primary, recurrent, and persistent hyperparathyroidism, Surgery **135** (2004) 157–162.
[7.44] LORBERBOYM, M., et al., Incremental diagnostic value of preoperative ^{99m}Tc-MIBI SPECT in patients with a parathyroid adenoma, J. Nucl. Med. **44** (2003) 904–908.
[7.45] CIVELEK, A.C., OZALP, E., DONOVAN, P., UDELSMAN, R., Prospective evaluation of delayed technetium-99m sestamibi SPECT scintigraphy for preoperative localization of primary hyperparathyroidism, Surgery **131** (2002) 149–157.
[7.46] PEREZ-MONTE, J.E., et al., Parathyroid adenomas: Accurate detection and localization with Tc-99m sestamibi SPECT, Radiology **201** (1996) 85–91.
[7.47] PROFANTER, C., et al., CT-MIBI image fusion: A new preoperative localization technique for primary, recurrent, and persistent hyperparathyroidism, Surgery **135** (2004) 157–162.
[7.48] FLYNN, M.B., BUMPOUS, J.M., SCHILL, K., McMASTERS, K.M., Minimally invasive radio-guided parathyroidectomy, J. Am. Coll. Surg. **191** (2000) 24–31.
[7.49] GOLDSTEIN, R.E., BLEVINS, L., DELBEKE, D., MARTIN, W.H., Effect of minimally invasive radio-guided parathyroidectomy on efficacy, length of stay, and costs in the management of primary hyperparathyroidism, Ann. Surg. **231** (2000) 732–742.
[7.50] WENDLER, T., et al., First demonstration of 3-D lymphatic mapping in breast cancer using freehand SPECT, Eur. J. Nucl. Med. Mol. Imaging **37** (2010) 1452–1461.
[7.51] RUBELLO, D., et al., Importance of radio-guided minimally invasive parathyroidectomy using hand-held gamma probe and low ^{99m}Tc-MIBI dose: Technical considerations and long-term clinical results, Q. J. Nucl. Med. **47** (2003) 224–232.
[7.52] NORMAN, J., DENHAM, D., Minimally invasive radio-guided parathyroidectomy in the reoperative neck, Surgery **124** (1998) 1088–1093.

8. GOSTT APPLICATIONS IN THYROID CANCER

8.1. INTRODUCTION

Differentiated thyroid cancer, which includes papillary and follicular histologies, is the most common endocrine malignancy, and its incidence has been increasing over the past three decades. However, this increased incidence is associated with a significant decrease in mortality rates in some countries. Depending on the iodine supply of any given geographic area, the incidence of thyroid cancer ranges between 4 and 12 cases per 100 000 population per year. Thyroid cancer carries a favourable prognosis compared to other cancers. While the best 10 year survival rates are approximately 90%, long term relapse rates remain high, of the order of 20%–40%, depending upon the patient's age and tumour stage at the time of initial treatment. Approximately 80% of patients appear to be rendered disease free by initial treatment [8.1], although optimal outcomes are achieved only via coordinated multimodal therapy.

The standard therapeutic approach to differentiated thyroid carcinoma includes surgery, ablation of thyroid postsurgical remnants with ^{131}I iodide and lifelong TSH suppressive therapy with exogenous thyroid hormone. Surgery is the cornerstone of initial management. Most patients should undergo thyroidectomy with concomitant central neck (level VI) LN dissection. On the other hand, thyroidectomy alone may be appropriate for patients with smaller tumours (T1 or T2) and no suspicious lymphadenopathy [8.2]. Surgery is also indicated in cases of cervical LN metastases and locoregional recurrence.

The main adjuvant therapy is administration of radioactive iodide performed after thyroidectomy, which is indicated for three main reasons: (i) to eradicate microscopic residual tumour foci, (ii) to facilitate follow-up by monitoring the serum levels of thyroglobulin (Tg) and (iii) to perform a highly sensitive ^{131}I whole body scan 3–7 d after administration of the therapeutic activity. After such primary treatment of thyroid cancer, subsequent follow-up is necessary over a period of several years.

The frequency of LN metastases at initial staging is related to the tumour histological type, size of the primary tumour, extent of LN dissection and histological analysis [8.3]. Although the impact of LN metastases on survival of patients with well differentiated thyroid cancer is still controversial, despite complete initial treatment, 5%–20% of patients with well differentiated thyroid carcinoma show residual or recurrent disease, and 10% show distant metastases with relatively high mortality (8%) [8.4]. Recurrences involving cervical LNs are prevalent and are linked to a 12% 30 year cancer mortality rate [8.5].

For the follow-up of low risk patients, assay of the serum Tg levels following administration of recombinant human thyroid stimulating hormone (rTSH) combined with ultrasonography of the neck is sufficient, in most cases. After total thyroidectomy and radioiodine ablation, the level of rTSH stimulated serum Tg should remain below 2 ng/mL.

Recurrent disease is generally associated with increased serum Tg levels, either under TSH suppression and/or following rTSH stimulation. High resolution ultrasonography of the neck is the most accurate diagnostic technique to detect locoregional recurrences of differentiated thyroid cancer [8.6]. Locoregional recurrences are usually suspected on the basis of morphological and signal abnormalities, such as absent hyperechoic hilum, hypoechoic change, round shape, calcification, cystic change, loss of central hilary vessel distribution and peripheral vascularization [8.7]. Ultrasound guided FNAC is highly sensitive for diagnosing LN metastases, although approximately 10% of the samples are non-diagnostic or false negatives [8.8]; sensitivity is increased by assaying Tg in the FNA washing fluid.

Although whole body scintigraphy with ^{131}I iodide has high specificity, it has low sensitivity [8.9], depending on the amount of ^{131}I iodide administered (usually 185 MBq).

Especially in high risk cases (patients under the age of 16 years or over the age of 45 years, certain histological subtypes, tumours greater than 3 cm, tumours extending beyond the thyroid capsule or patients with large, bilateral and multiple LNs metastases at initial diagnosis), the loss of radioiodine concentrating ability by differentiated thyroid cells represents a heavy limitation to the use of radioiodide for either diagnostic localization and/or therapeutic purposes. In patients with low or dedifferentiated thyroid cancer after several courses of radioiodine therapy required by metastatic disease, iodine negative metastases may develop. In these cases, despite clearly elevated serum levels of Tg, radioiodide imaging is negative or demonstrates only a faint uptake.

The method of choice to image these iodine negative metastases is [^{18}F]FDG PET, as the loss of the iodine concentrating ability (loss of differentiation) is generally associated with increased biological aggressiveness, and therefore increased energy/metabolic requirements. In this regard, the introduction of PET imaging has brought a major paradigm shift in the management of recurrent and/or metastatic iodine negative thyroid carcinoma. With [^{18}F]FDG PET/CT, hybrid imaging is especially useful to reduce the rate of false negative cases in subcentimetre tumours [8.10] and false positive findings possibly caused by brown fat, muscle tension and reactive LNs. These factors together considerably improve the overall diagnostic accuracy [8.11, 8.12], thus possibly leading to selection of the optimal therapeutic strategy [8.13]. [Fluorine-18]FDG PET/CT imaging has shown a 92% positive predictive value

in patients with a negative ^{131}I iodide whole body scan and an elevated serum Tg, and a 93% NPV in patients with a negative ^{131}I iodide whole body scan and a low serum Tg [8.14].

8.2. GOSTT IN CERVICAL RECURRENCES FROM DIFFERENTIATED THYROID CANCER

8.2.1. Background

The treatment for locoregional LN recurrences includes therapy with radioiodide, surgery and external radiotherapy, depending on the lesion's morphofunctional features and the clinical features of the disease. The efficacy of the radioiodide therapy is affected essentially by the size of the lesion, the degree of radioiodide uptake and retention, and the dose absorbed by the thyroid cancer cells.

Surgery is the treatment of choice for locoregional recurrences of differentiated thyroid carcinoma, especially for tumours that have lost the ability to accumulate radioiodide, even if it is associated with increased morbidity compared with primary surgery. Surgery is technically more challenging because of the presence of scar tissue and disruption of the normal fascial planes and anatomy, which may result in a greater risk of injury to nerves and other vital structures [8.15].

Planning this type of surgery requires careful pre-operative work for assessing the sites and extent of metastases. US imaging, CT imaging and magnetic resonance imaging (MRI) are sensitive, but are often difficult to interpret because of scar tissue in the thyroid bed and distorted anatomy resulting from prior surgery, which makes the usual landmarks difficult to recognize. Furthermore, despite their relatively high spatial resolution, US imaging, CT imaging and MRI have limited ability in discriminating viable tumour tissue from scar tissue, in determining whether mildly enlarged LNs represent a tumour or a non-malignant process, and in detecting cancer foci that are less than 1 cm in diameter.

Strategies aiding reoperations include marking of the tumour site with a permanent dye or a charcoal suspension, and percutaneous placement of metal wires ending with a block to stay within the LN; intraoperative US guidance may also help in this regard [8.16–8.18].

Radioguided surgery using a hand-held gamma probe represents an alternative, novel approach to facilitate the intraoperative search of locoregional recurrences from differentiated thyroid carcinoma. This approach has initially been proposed following systemic administration of radiopharmaceuticals

that accumulate at the tumour sites with favourable tumour to background ratios [8.19]. The use of radioiodine (^{131}I iodide or ^{123}I iodide, administered at various activities) suffers from serious drawbacks for LN recurrences that have reduced iodine trapping capabilities. In these cases, non-specific tumour seeking radiopharmaceuticals (e.g. ^{99m}Tc sestamibi or ^{99m}Tc tetrofosmin) have been proposed as a guide for radioguided surgery. In particular, ^{99m}Tc sestamibi has demonstrated high sensitivity in identifying iodine negative recurrences, although it has some disadvantages linked to fast physiological washout of the tracer from the tumour lesions and relatively low target to background ratios (TBRs) [8.20, 8.21]. Therefore, neither radioiodide guided nor ^{99m}Tc sestamibi guided surgery has gained vast popularity.

An interesting variant of radioguided surgery is based on local rather than systemic administration of the localizing radiopharmaceutical, to facilitate surgical removal of cervical LN metastases from differentiated thyroid cancer [8.22]. This technique, originally introduced for occult lesions in breast cancer [8.23], is based on intralesional injection of radioactive particles (^{99m}Tc MAAs) that do not migrate from the site of the interstitial injection because of their large size (10–90 μm).

8.2.2. Technique

8.2.2.1. Pre-operative phase

The procedure consists of injecting a suspension of ^{99m}Tc MAA (4–8 MBq) in the tumoural lesion under US guidance 2–3 h before surgery, using a 10 MHz linear probe for small superficial anatomic parts. A 22 G needle is usually employed for intralesional injection of the ^{99m}Tc MAA suspension, under continuous US monitoring of the correct position of the needle tip at the centre of the lesion. The needle is withdrawn under slight aspiration, to minimize the release of residual radioactivity along the needle track. Subsequently, cutaneous projection of the lesion is marked under US guidance (to facilitate minimal access surgery) before gamma camera imaging. Static images with various projections, as appropriate, are generally acquired for approximately 10 min (128 × 128 matrix), employing a large FOV gamma camera equipped with a parallel hole LEHR collimator (±10% window centred on the 140 keV energy peak of ^{99m}Tc). A radioactive point source can help to delineate the cervical contour and to mark the cutaneous projections of the radiolabelled areas. When cutaneous projection of the lesion marked under US guidance and cutaneous projection of the radioactive spot do not match within a 1 cm radius, both positions are marked on the skin.

However, interpretation of planar images alone can be difficult because the information on anatomy is limited to outlining the body contour. In particular, in such patients, hot spots in the neck region can be difficult to localize, as a result of complex anatomy and because the 3-D surface of the structures of the head is not visualized on planar images. It is reasonable to conceive that hybrid SPECT/CT imaging would considerably improve visualization and topographic localization of the recurrences radiolabelled by intralesional injection of ^{99m}Tc MAA, therefore also improving intraoperative detection. Cases of radioactivity leakage during intralesional administration or contamination on the skin can easily be identified using SPECT/CT imaging; distinguishing between leakage and an injection correctly carried out using planar images is often impossible.

8.2.2.2. Intraoperative phase

Surgery is performed under general anaesthesia; the site of the incision is chosen according to both the skin marker(s) and the highest count rate recorded by external counting with the hand-held gamma probe, and also according to cosmetic considerations related to the postsurgical scar.

For intraoperative guidance, the hand-held gamma probe is utilized by the surgeon to locate intrasurgically the spot with the highest count rate, repeating measurements while progressing through the various anatomic structures. Safe resection margins around the 'hot' lesion are identified by a sudden drop in the count rate to the background level, defined as the count rate in the upper region of the chest (corresponding to the apex of the lung). Complete removal of the lesion is ascertained by repeat counting of the surgical bed with the gamma probe, removing any additional radioactive tissue until the residual count rate drops to the background level.

8.2.2.3. Added value of intraoperative imaging and high energy gamma probes

The surgeon can also be helped to find radiolabelled recurrences using another visual element to facilitate the procedure. With radioguided surgery, surgeons localize the target with the aid of an auditive signal (originating from the gamma probe) in addition to the visual one. To further improve the surgical detection of the target(s), portable gamma cameras have been designed to facilitate radioguided surgery. Intraoperative real time imaging using the portable gamma camera provides an overview of all radioactive hotspots in the whole surgical field. The amount of radioactivity within each hot spot can be quantified using the portable gamma camera, and the intraoperative images can be related to the pre-operative scintigraphic images. Continuous monitoring can be used to record the whole procedure, and stepwise monitoring enables localization of

targets and detects remaining activity afterwards. Another clear advantage of the portable gamma camera is the certainty that it can provide on the completeness and accuracy of the radiolabelled lesion ('target') excision because it shows remaining radioactivity.

In patients with low differentiated or dedifferentiated thyroid cancer with iodine negative local recurrences, the new high energy gamma and beta probes can be used to identify and remove [^{18}F]FDG avid lesions. The hand-held high energy gamma probe is an intraoperative device that was first described and developed by Daghighian et al. in 1994 [8.24] as a novel method to direct intraoperative tumour localization. Clinical applications of radioguided surgery based on PET agents are increasing. Most of these procedures involve the use of the PET radiopharmaceutical more widely employed in oncology, [^{18}F]FDG, while other tumour seeking agents, such as ^{68}Ga DOTA TOC for NETs, are becoming increasingly prevalent [8.25]. Probes designed for intraoperative radioguidance after administration of positron emitting radiopharmaceuticals can detect either the high energy annihilation γ rays or the β^+ particles. In the latter case, the probe must be placed in direct contact with the target tissue because such particles have a very short range of penetration in tissues; owing to their design, measurements obtained with these 'beta probes' are not affected by the high background γ radiation generated by the annihilation process.

8.2.3. Conclusions

Accurate localization of recurrent well differentiated thyroid carcinoma is important, especially in patients with non-iodine-trapping tumours because effective therapy depends on surgery. Alternative imaging for non-radioiodine-avid differentiated thyroid cancer includes CT imaging, MRI or the use of non-specific tumour-seeking agents (^{201}Tl chloride, ^{99m}Tc tetrofosmin, ^{99m}Tc sestamibi, ^{111}In pentetreotide, [^{18}F]FDG); all such techniques suffer significant limitations for detecting small recurrences.

Surgery is the treatment of choice for LNs and local recurrences of radioiodine negative differentiated thyroid cancer, as well as for recurrences greater than 1 cm (because their response to radioiodine therapy is suboptimal). Owing to significant increases in morbidity after reoperation, neck dissection should only be performed if there is clinical evidence of LN involvement in this area.

Reoperative central or lateral compartment neck surgery is technically demanding because of scar tissue and distorted anatomy, which increase the risk of failure and morbidity (injury to the recurrent laryngeal nerves and parathyroid glands). Radioguided localization of such occult tumour lesions constitutes a novel approach to the management of non-palpable recurrences of

differentiated thyroid carcinoma. This technique, originally introduced for occult lesions in breast cancer but then also employed for other applications, consists of US guided, intra/perilesional injection of ^{99m}Tc MAAs, which are large particles that do not move from the site of administration.

Technetium-99m MAAs and US guidance are readily available and inexpensive; furthermore, unlike with other modalities, the intralesional injection procedure requires no preparation of the patients. Pre-operative injection is rapid for the operator experienced in US guided FNA, with the only limitations being represented by lesion sites that are inaccessible to FNA (retrovascular and deep mediastinum locations). The US guided technique also allows the detection and labelling of very small lesions, down to 4 mm in diameter, which are especially difficult targets for the other modalities. Local injection of ^{99m}Tc MAA maximizes the target to background radioactivity ratio necessary to identify tumour foci with the gamma probe, and allows immediate or delayed surgery (single day or two day protocol). Furthermore, the minute amount of radioactivity employed entails a negligible radiation exposure to patients and surgical staff. This method, which is used for the localization of cervical recurrences, constitutes a useful adjunct for fast localization of non-palpable lesions in the surgical field, minimizing the morbidity risks of reoperation. A short learning curve is required for the surgeons, who can adopt a minimally invasive approach whenever possible, thus further reducing morbidity risks and operation/hospitalization times. No particular risks are associated with this technique, which is based on optimal collaboration between the departments of nuclear medicine and surgery. This technique represents an optimal therapeutic option in the management of isolated regional recurrences in patients submitted to several neck surgeries, especially when radioiodine cannot be used for therapy and when the lesions are subcentimetres in size. An additional role of this approach is possible also in extended neck dissection, to identify the spatial limits of nodal involvement. Although it does not allow intraoperative gamma probe guided identification of foci that have not been detected pre-operatively, it is nevertheless useful to assess whether surgical resection of all the detected foci is complete.

8.3. SLNM IN WELL DIFFERENTIATED THYROID CANCER

8.3.1. Background

The optimal treatment for differentiated thyroid carcinoma is still under debate; in this regard, sex, size and extracapsular invasion are well defined prognostic factors. Although the presence of LN metastases has traditionally not been considered a crucial prognostic factor, recent studies have led to the

revision of such a perception, especially in high risk patients. Furthermore, LN metastases have been associated with an increased incidence of locoregional recurrences [8.26].

Patients with well differentiated thyroid carcinoma whose bilateral cervical LNs are clinically suspected (enlarged, hard, purplish grapelike LNs at surgical exploration), or are confirmed to be metastatic by FNAC, are candidates for one stage thyroidectomy and bilateral neck LN dissection [8.27]. On the other hand, the management of clinically node negative (cN0) LNs is generally much more conservative and still controversial. For these reasons, different therapeutic strategies have been described in the presence of apparently normal cervical LNs: routine LDN of the central and jugular compartments on the same side as the tumour, LN resection of the central compartment on the same side as the tumour, and ^{131}I iodide ablation of the residual tissue that may include microscopic LN metastases, although efficacy of the latter has been questioned [8.28].

The development of new surgical techniques, of advanced cross-sectional imaging and of refined histopathological and immunohistochemical analysis requires equal development in pre-operative and intraoperative diagnostic procedures that can localize LNs in the thyroid basin for optimal surgical resection. One of the recent developments in this respect is the detection of SLNs [8.29].

8.3.1.1. The concept of SLNM in differentiated thyroid cancer

The concept of SLNM is based on the fact that the first LN in a regional lymphatic basin that receives lymph flow from a primary tumour (the SLN) will be the first affected by metastasis. If such LN(s) can be shown to be free from metastases, it is highly unlikely that other nodes are affected [8.30]. SLNB is nowadays largely employed in patients with breast cancer and melanoma, but its use is increasing also in other solid tumours, such as colorectal cancers [8.31], gynaecological and urological malignancies [8.32–8.34] and differentiated thyroid carcinoma [8.35].

The thyroid gland has an extensive network of draining lymphatics, both intraglandular and extraglandular. The intraglandular lymphatic networks allow for drainage between lobes through the thyroid isthmus. Extraglandular lymphatic drainage of the thyroid isthmus and lower poles of the gland occurs first to the pretracheal (Delphian) and paratracheal (tracheoesophageal groove) nodes and then to the mediastinal nodes. The remainder of the gland drains to the ipsilateral jugular chain of nodes [8.36].

A relatively high proportion of patients with papillary thyroid carcinoma have LN metastases at the time of initial diagnosis and, less frequently, during subsequent follow-up. Incidence of metastases is less frequent in adults than

children (15%–50% versus 80%), but microscopic metastases have been found in up to 80% of the adult patients [8.37]. The central compartment level is involved in approximately 90% of the cases. Involvement of the lateral LNs varies between 51% and 100% in different series, the caudal compartments being involved more frequently than the cranial compartments. Supraclavear LNs are the third site involved in terms of frequency, with a reported rate ranging from 10% to 52%. Contralateral LN involvement is not rare, with an incidence of up to 18% for papillary thyroid cancer [8.38]. It is important to note that distribution of locoregional LN involvement is poorly related to the site of the primary thyroid tumour.

8.3.1.2. Added value of SLNB in differentiated thyroid carcinoma

SLNB was developed as an alternative to elective LN dissection in patients with cN0 disease. Few studies evaluating the utility of SLNB in differentiated thyroid cancer have been published. An initial study by Kelemen et al. [8.39] using blue dye in 17 thyroid cancer patients demonstrated the feasibility of SLNM in thyroid surgery, although the disruption of lymphatic pathways frequently observed during thyroidectomy can make SLN identification difficult. Moreover, parathyroid glands may stain blue, and this may cause their inadvertent removal. Similar results were obtained by Pelizzo et al. in a group of 29 patients with differentiated thyroid cancer [8.40]. Gallowitsch et al. [8.41] and Rettenbacher et al. [8.42] described the use of a radiotracer with intraoperative counting using a hand-held gamma probe.

Since these early reports, a number of other studies have demonstrated that SLNB is indeed an accurate technique for obtaining information about cervical LN involvement in patients undergoing thyroidectomy [8.43].

8.3.2. Technique

Patients with thyroid nodular disease diagnosed for malignancy with FNAC and no evidence of macroscopic LN involvement on the basis of pre-operative US examination generally undergo lymphoscintigraphy 3 h before surgery. One single intratumoural injection of ^{99m}Tc human albumin nanocolloids (approx. 6 MBq in 0.1–0.2 mL saline solution) is administered under US guidance in the nuclear medicine unit.

Immediately after radiocolloid injection, lymphoscintigraphy is performed, starting with a dynamic acquisition, then continuing with 10 min static images with various projections, as appropriate. A large FOV gamma camera equipped with a parallel hole, LEHR collimator is generally employed (128 × 128 matrix, ±10% window centred on the 140 keV energy peak of ^{99m}Tc). A radioactive

point source can help to delineate the cervical contour and to mark the cutaneous projections of the radiolabelled areas.

8.3.2.1. Added value of SPECT/CT imaging in pre-operative imaging

Interpretation of planar images can be difficult because the anatomy information is limited to outlining the body contour. In particular, in these patients, SLNs in the neck region can be difficult to localize as a result of complex anatomy, interlacing lymphatic vessels, unexpected drainage patterns and because the 3-D surface of the structures of the head is not visualized in planar images. Furthermore, SLNs in proximity to the radiocolloid injection area can easily be missed on planar images because some 98% of the injected activity does not migrate from the interstitial injection point, and therefore masks the average 0.16% that ends up in the SLNs.

SPECT/CT imaging can optimize SLN visualization in the head and neck region, thus leading to improved intraoperative detection [8.44–8.48]. In these cases, such an imaging technique is of high value for identifying the topography of the SLNs in relation to several vital vascular and neural structures, to enable their safe removal (see Fig. 8.1).

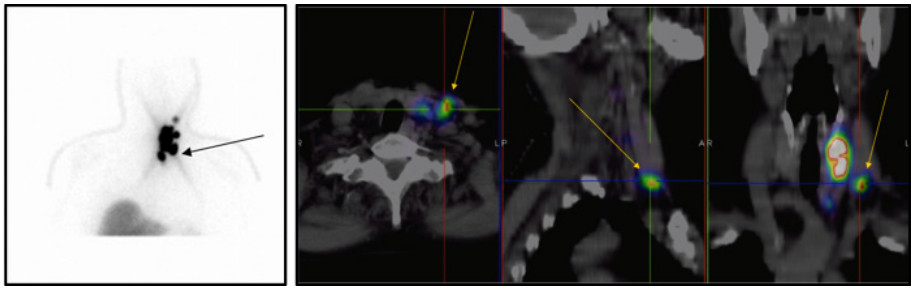

FIG. 8.1. SLNM in a 75 year old woman with papillary microcarcinoma of the left thyroid lobe. Left: Anterior planar view obtained 2 h after US guided intratumoural injection of ^{99m}Tc nanocolloid; radioactivity accumulation in the liver indicates passage of some radiocolloid into the general circulation at this relatively late time point post-injection. The injection site corresponds to the area with greatest radioactivity accumulation just left of the midline; multiple SLNs are visualized in the left cervical region, but the arrow points to the node with the highest radiocolloid uptake, also visualized as the first draining node on prior sequential imaging (the primary SLN). Right: Fused SPECT/CT sections (transaxial, sagittal and coronal) showing more accurately than planar imaging the exact topographic location of the primary SLN (indicated by yellow arrows, in level IV). Images courtesy of L. Feggi and S. Panareo, Nuclear Medicine Service, University Hospital, Ferrara, Italy.

SPECT/CT imaging can also detect SLNs that are missed on planar lymphoscintigraphy in a substantial number of patients. In head and neck cancer, many SLNs are located at a close proximity to the injection area and are therefore easily overlooked in planar imaging (see Fig. 8.2). Cases of non-LN radiocolloid accumulation (e.g. leakage of radioactivity in the oral cavity after injection or contamination on the skin) can be identified using SPECT/CT imaging, while distinguishing between leakage and a true SLN in planar images.

8.3.2.2. Intraoperative phase

At the time of surgery, intraoperative SLN localization is performed using a hand-held gamma probe. After thyroidectomy, the central compartment is bilaterally scanned, searching for other hot spots. Generally, the most radioactive LN and all nodes with a count rate more than 10% of that of the hottest node are removed. Then, the same exploration is carried out for lateral compartments of the neck. The anatomical location of all resected radioactive LNs is recorded and SLNs are sent for intraoperative frozen section histology. When frozen sections of one or more LNs reveal thyroid cancer metastasis, the surgeon performs an enlarged LDN of the involved compartment.

The surgical bed is then checked again to evaluate the completeness of removal of all hot spots. Definitive histology of all resected specimens is performed with haematoxylin and eosin staining, as well as with immunohistochemistry using an antithyroglobulin antibody.

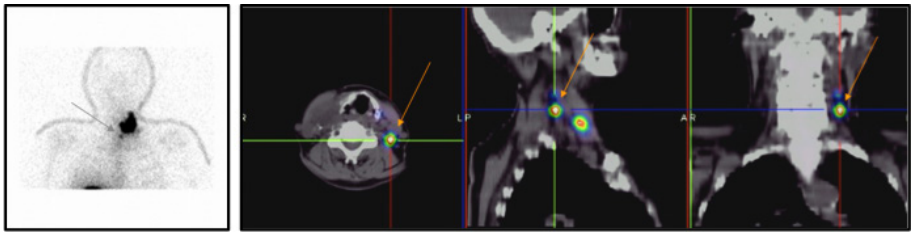

FIG. 8.2. SLNM in a 71 year old woman with papillary carcinoma of the left thyroid lobe. Left: Anterior planar view obtained 2 h after US guided intratumoural injection of ^{99m}Tc nanocolloid. The injection site corresponds to the area with greatest radioactivity accumulation in the left cervical region; only one LN is visualized, just below the thyroid approximately at the midline (grey arrow). Right: Fused SPECT/CT sections (transaxial, sagittal and coronal) selected so that they show part of the radioactivity accumulation at the injection site (visible in the sagittal section, not indicated by a specific mark) and a draining LN in level III (orange arrow); this second SLN had not been identified in the planar image because of the close proximity to the injection site. Images courtesy of L. Feggi and S. Panareo, Nuclear Medicine Service, University Hospital, Ferrara, Italy.

8.3.2.3. Added value of intraoperative imaging

The surgeon can localize SLNs with the aid of another visual element that facilitates the procedure. SLNB is based on a combination of gamma probe counting and blue dye mapping. Surgeons generally localize the SLNs by combining the auditive signal (gamma probe) with the visual one (blue dye). In head and neck cancer patients, the use of blue dye can be problematic, mostly because the blue dye migrates very quickly. For these reasons, use of the blue dye technique in head and neck patients is limited, considering the high density of LNs in the region and the short distances between the injection site and the SLN(s).

Portable, small FOV gamma cameras have been designed to facilitate radioguided surgery. Intraoperative real time imaging using the portable gamma camera provides an overview of all radioactive hot spots in the whole surgical field. The position of the camera can be adjusted to visualize SLNs near the injection area, which are nodes that are easily overlooked using the gamma counting probe alone. Discrimination between SLNs and second tier LNs is facilitated because the amount of radioactivity within each node can be quantified using the portable gamma camera, and the intraoperative images can be related to the pre-operative scintigraphic images. Furthermore, continuous image monitoring can be used to record the whole procedure, such as stepwise monitoring enabling localization of SLNs and detection of remaining activity after LN harvesting.

8.3.3. Conclusions

Surgical treatment is the single most effective therapy for patients with differentiated thyroid cancer, although it is still controversial whether prophylactic cervical LN dissection improves the prognosis of these patients and whether LN status affects patient survival.

The prevalence of LN metastases is relatively high (approx. 40%), even in the presence of small tumours. It could be argued that the rate of local tumour recurrence is reduced by LN dissection. However, systematic dissection of the central compartment area may cause complications, in particular, nerve damage and permanent hypoparathyroidism; this risk might not be justified considering that such LN dissection is not always necessary.

As already demonstrated for other solid tumours, pre-operative SLNM with lymphoscintigraphy and radioguided SLNB may offer significant advantages in comparison with the blue dye technique. For patients with non-palpable nodal metastases, a major advantage of this technique is accurate pre-operative localization of nodal drainage sites, especially if the lymphoscintigraphy is

completed with SPECT/CT imaging. Such an imaging technique provides the surgeon with more precise anatomical information to aid in easier identification of the SLNs during surgery.

It has already been shown that lymphoscintigraphy following intratumoural radiocolloid injection represents a feasible, easy to perform procedure for radioguided SLNM and SLNB in differentiated thyroid carcinoma. This procedure is of value in detecting locoregional metastatic involvement, including in patients with non-palpable LNs or with negative US examinations of the neck [8.49].

Identification and removal of the SLNs have allowed the detection of microscopic metastatic disease. Through selective LN dissection, this procedure can avoid unnecessary nodal dissection, which is an important issue when considering that extensive LDN is associated with non-negligible morbidity.

Boschin et al. have demonstrated that patients defined as N0 at SLNB were all confirmed to be disease free by rTSH stimulated whole body scintigraphy with ^{131}I iodide and serum Tg levels [8.50]. This procedure may also be considered in the selection of patients for postsurgical ablation therapy with ^{131}I iodide. In particular, radioiodide ablation of postsurgical remnants could be avoided in patients defined as N0 on the basis of SLNB, while in patients defined as N1, a therapeutic rather than an ablative activity of ^{131}I iodide could be proposed as the first line treatment.

A major issue that remains to be explored concerns patients with multifocal bilateral tumours, in whom a higher likelihood of metastasis to LNs of both laterocervical compartments is expected. This particular condition could represent a limitation in the staging role of radioguided SLNB in patients with differentiated thyroid cancer.

REFERENCES TO CHAPTER 8

[8.1] MAZZAFERRI, E.L., MASSOLL, N., Management of papillary and follicular (differentiated) thyroid cancer: New paradigms using recombinant human thyrotropin, Endocr. Relat. Cancer **9** (2002) 227–247.

[8.2] BURNS, W.R., ZEIGER, M.A., Differentiated thyroid cancer, Semin. Oncol. **37** (2010) 557–566.

[8.3] SCHLUMBERGER, M., PACINI, F., Thyroid Tumours, Editions Nucleon, Paris (2003).

[8.4] PACE, L., NICOLAI, E., KLAIN, M., SALVATORE, M., Diagnostic value of FDG PET/CT imaging, Q. J. Nucl. Med. Mol. Imaging. **53** (2009) 503–512.

[8.5] MAZZAFERRI, E.L., KLOOS, RT., Current approaches to primary therapy for papillary and follicular thyroid cancer, J. Clin. Endocrinol. Metab. **86** (2001) 1447–1463.
[8.6] AHUJA, A.T., YING, M., YUEN, H.Y., METREWELI, C., Power Doppler sonography of metastatic nodes from papillary carcinoma of the thyroid, Clin. Radiol. **56** (2001) 284–288.
[8.7] LEBOULLEUX, S., et al., Criteria of malignancy for cervical lymph nodes in patients followed up for differentiated thyroid cancer, J. Clin. Endocrinol. Metab. **92** (2007) 3590–3594.
[8.8] TAKASHIMA, S., et al., Nonpalpable lymph nodes of the neck: Assessment with US and US-guided fine-needle aspiration biopsy, J. Clin. Ultrasound **25** (1997) 283–292.
[8.9] CAILLEUX, A.F., BAUDIN, E., TRAVAGLI, J.P., RICARD, M., SCHLUMBERGER, M., Is diagnostic iodine-131 scanning useful after total thyroid ablation for differentiated thyroid cancer? J. Clin. Endocrinol. Metab. **85** (2000) 175–178.
[8.10] YEO, J.S., et al., F-18-fluorodeoxyglucose positron emission tomography as a presurgical evaluation modality for I-131 scan-negative thyroid carcinoma patients with local recurrence in cervical lymph nodes, Head Neck **23** (2001) 94–103.
[8.11] SHREVE, P.D., ANZAI, Y., WAHL, R.L., Pitfalls in oncologic diagnosis with FDG PET imaging: Physiologic and benign variants, Radiographics **19** (1999) 61–77.
[8.12] SHAMMAS, A., et al., ^{18}F-FDG PET/CT in patients with suspected recurrent or metastatic well-differentiated thyroid cancer, J. Nucl. Med. **48** (2007) 221–226.
[8.13] FINKELSTEIN, S.E., et al., Combined [^{18}F]fluorodeoxyglucose positron emission tomography and computed tomography (FDG-PET/CT) for detection of recurrent, ^{131}I-negative thyroid cancer, Ann. Surg. Oncol. **15** (2008) 286–292.
[8.14] HOOFT, L., et al., Diagnostic accuracy of ^{18}F-fluorodeoxyglucose positron emission tomography in the follow-up of papillary or follicular thyroid cancer, J. Clin. Endocrinol. Metab. **86** (2001) 3779–3786.
[8.15] PAI, S.I., TUFANO, R.P., Reoperation for recurrent/persistent well-differentiated thyroid cancer, Otolaryngol. Clin. North. Am. **43** (2010) 353–363.
[8.16] SIPPEL, R.S., et al., Localization of recurrent thyroid cancer using intraoperative ultrasound-guided dye injection, World J. Surg. **33** (2009) 434–439.
[8.17] HARTL, D.M., et al., Charcoal suspension tattoo localization for differentiated thyroid cancer recurrence, Ann. Surg. Oncol. **16** (2009) 2602–2608.
[8.18] BRYANT, J.A., SIDDIQI, N.J., LOVEDAY, E.J., IRVINE, G.H., Presurgical, ultrasound-guided anchor-wire marking of impalpable cervical lymph nodes, J. Laryngol. Otol. **119** (2005) 627–628.
[8.19] NEGELE, T., et al., Radio-guided surgery for persistent differentiated papillary thyroid cancer: Case presentations and review of the literature, Langenbecks Arch. Surg. **391** (2006) 178–186.
[8.20] RUBELLO, D., SALVATORI, M., PELIZZO, M.R., BONI, G., MARIANI, G., "Radio-guided surgery of occult lesions in patients with thyroid cancer", Radio-guided Surgery: A Comprehensive Team Approach (MARIANI, G., GIULIANO, A.E., STRAUSS, H.W., Eds), Springer (2008) 269–277.

[8.21] BOZ, A., et al., Gamma probe-guided resection and scanning with Tc-99m MIBI of a local recurrence of follicular thyroid carcinoma, Clin. Nucl. Med. **26** (2001) 820–822.
[8.22] MARTINO, A., et al., A new radio-guided procedure for localization and surgical treatment of neck node metastasis of papillary thyroid cancer, J. Endocrinol. Invest. **33** (2010) 339–342.
[8.23] PAGANELLI, G., VERONESI, U., Innovation in early breast cancer surgery: Radio-guided occult lesion localization and sentinel node biopsy, Nucl. Med. Commun. **23** (2002) 625–627.
[8.24] DAGHIGHIAN, F., et al., Intraoperative beta probe: A device for detecting tissue labeled with positron or electron emitting isotopes during surgery, Med. Phys. **21** (1994) 153–157.
[8.25] FREESMEYER, M., et al., Intraoperative identification of a neuroendocrine tumour diagnosed by ^{68}Ga-DOTATOC PET but undetectable by surgical palpation or conventional imaging, Nuklearmed. **48** (2009) 50–51.
[8.26] SPRIANO, G., RUSCITO, P., PELLINI, R., APPETECCHIA, M., ROSELLI, R., Pattern of regional metastases and prognostic factors in differentiated thyroid carcinoma, Acta Otorhinolaryngol. Ital. **29** (2009) 312–316.
[8.27] PAN, Y.F., et al., One stage thyroidectomy and bilateral neck dissection for well-differentiated thyroid carcinoma, Zhonghua Zhong Liu Za Zhi **28** (2006) 389–392.
[8.28] HAY, I.D., Selective use of radioactive iodine in the postoperative management of patients with papillary and follicular thyroid carcinoma, J. Surg. Oncol. **8** (2006) 692–700.
[8.29] RUBELLO, D., et al., The role of sentinel lymph node biopsy in patients with differentiated thyroid carcinoma, Eur. J. Surg. Oncol. **32** (2006) 917–921.
[8.30] MARIANI, G., et al., Radio-guided sentinel lymph node biopsy in breast cancer surgery, J. Nucl. Med. **42** (2003) 1198–1215.
[8.31] IDDINGS, D., BILCHIK, A., The biologic significance of micrometastatic disease and sentinel lymph node technology on colorectal cancer, J. Surg. Oncol. **96** (2007) 671–677.
[8.32] ADIB, T., BARTON, D.P., The sentinel lymph node: Relevance in gynaecological cancers, Eur. J. Surg. Oncol. **32** (2006) 866–874.
[8.33] SLIUTZ, G., et al., Lymphatic mapping of sentinel nodes in early vulvar cancer, Gynecol. Oncol. **84** (2002) 449–452.
[8.34] CABANAS, R.M., Application of the sentinel node concept in urogenital cancer, Recent Results Cancer Res. **157** (2000) 141–149.
[8.35] PELIZZO, M.R., et al., Contribution of SLN investigation with ^{99m}Tc-nanocolloid in clinical staging of thyroid cancer: Technical feasibility, Eur. J. Nucl. Med. Mol. Imaging **34** (2007) 934–938.
[8.36] WISEMAN, S.M., HICKS, W.L., Jr., CHU, Q.D., RIGUAL, N.R., Sentinel lymph node biopsy in staging of differentiated thyroid cancer: A critical review, Surg. Oncol. **11** (2002) 137–142.
[8.37] SHAHA, A.R., Management of the neck in thyroid cancer, Otolaryngol. Clin. North Am. **31** (1998) 823–831.

[8.38] MIRALLIÉ, E., et al., Localization of cervical node metastasis of papillary thyroid carcinoma, World J. Surg. **23** (1999) 970–973.
[8.39] KELEMEN, P.R., VAN HERLE, A.J., GIULIANO, A.E., Sentinel lymphadenectomy in thyroid malignant neoplasms, Arch. Surg. **133** (1998) 288–292.
[8.40] PELIZZO, M.R., et al., The sentinel node procedure with patent blue V dye in the surgical treatment of papillary thyroid carcinoma, Acta. Otolaryngol. **121** (2001) 421–424.
[8.41] GALLOWITSCH, H.J., MIKOSCH, P., KRESNIK, E., STARLINGER, M., LIND, P., Lymphoscintigraphy and gamma probe-guided surgery in papillary thyroid carcinoma: The sentinel lymph node concept in thyroid carcinoma, Clin. Nucl. Med. **24** (1999) 744–746.
[8.42] RETTENBACHER, L., SUNGLER, P., GMEINER, D., KÄSSMANN, H., GALVAN, G., Detecting the sentinel lymph node in patients with differentiated thyroid carcinoma, Eur. J. Nucl. Med. **27** (2000) 1399–1401.
[8.43] CARCOFORO, P., et al., Use of preoperative lymphoscintigraphy and intraoperative gamma-probe detection for identification of the sentinel lymph node in patients with papillary thyroid carcinoma, Eur. J. Surg. Oncol. **33** (2007) 1075–1080.
[8.44] EVEN-SAPIR, E., et al., Lymphoscintigraphy for sentinel node mapping using a hybrid SPECT/CT system, J. Nucl. Med. **44** (2003) 1413–1420.
[8.45] WAGNER, A., et al., SPECT-CT for topographic mapping of sentinel lymph nodes prior to gamma probe-guided biopsy in head and neck squamous cell carcinoma, J. Craniomaxillofac. Surg. **32** (2004) 343–349.
[8.46] TERADA, A., et al., Sentinel lymph node radiolocalization in clinically negative neck oral cancer, Head Neck **28** (2006) 114–120.
[8.47] COVARELLI, P., et al., The single-photon emission computed tomography/computed tomography: A new procedure to perform the sentinel node biopsy in patients with head and neck melanoma, Melanoma Res. **17** (2007) 323–328.
[8.48] VAN DER PLOEG, I.M., et al., The yield of SPECT/CT for anatomical lymphatic mapping in patients with melanoma, Ann. Surg. Oncol. **16** (2009) 1537–1542.
[8.49] PELIZZO, M.R., et al., Sentinel lymph node procedure in thyroid carcinoma patients. Our experience, Minerva Chir. **61** (2006) 25–29.
[8.50] BOSCHIN, I.M., et al., ^{99m}Tc nanocolloid sentinel node procedure in thyroid carcinoma, Langenbecks Arch. Surg. **393** (2008) 705–708.

9. GOSTT IN MALIGNANCIES OF THE HEAD AND NECK

9.1. INTRODUCTION

The SLN status provides relevant prognostic information on patients with melanoma [9.1], and in patients with oral cancer, the presence of SLN metastases is a negative prognostic factor [9.2]. Because of the poor sensitivity of US guided FNAC and the considerable morbidity of elective LN dissection, SLNM and SLNB are emerging as the most promising modality to stage the neck. However, SLNB in the head and neck region can be especially challenging, owing to the complex anatomy and the unpredictable lymphatic drainage of this region; high false negative rates have been reported for SLNB in patients with CMs located in the head and neck [9.3–9.6].

9.1.1. Indications for SLNB

The indications for SLNB in patients with melanomas located in the head and neck region are basically the same as those for melanomas located in other areas of the body (see Chapter 6). In summary, patients with a Breslow thickness in the range 1–4 mm who have a clinically and radiologically negative LN status (stage N0) are considered for the procedure. Other prognostic factors, such as ulceration, can also be taken into account when selecting patients for SLNB [9.7]. The low risk of finding LN metastasis in melanoma lesions less than 1 mm in size can be a reason to omit SLNM and SLNB [9.8]. On the other hand, in lesions greater than 4 mm in size, the high risk of synchronous distant metastases may outweigh the possible therapeutic and prognostic benefits of LDN or SLNM [9.9, 9.10].

The role of SLNB in patients with oral cancer is less well defined, and controversies still exist regarding the appropriate indications. Several studies use the procedure to stage patients with T1 or T1–T2 lesions [9.11–9.13], while others find selective LN neck dissection more appropriate in view of the high risk of nodal metastasis [9.14].

In general, patients with transoral resectable T1–T2 tumours and with negative LN assessment on clinical and radiological examination (including FNAC) are considered for SLNB.

9.1.2. Pre-operative mapping of SLNs

Conventional planar lymphoscintigraphy after peritumoural radiocolloid injection is routinely employed for pre-operative SLNM. Four intradermal

injections are used for melanoma, whereas in malignancies of the oral cavity, the radiocolloid is administered intramucosally in three to four sites around the primary lesion. In deeper located malignancies, radiocolloid injection may be guided using US or CT imaging. An activity of 10–60 MBq of radiocolloid has been used when patients have the operation on the same day, while 50–120 MBq is used when the operation takes place the next day [9.15–9.23]. An activity of 70 MBq of ^{99m}Tc nanocolloid leads to optimal visualization of lymphatic drainage in both melanoma and oral cavity malignancies. Lymphoscintigraphy is based on sequential images depicting subsequent phases of radiocolloid migration. Dynamic acquisitions obtained immediately after tracer administration visualize the draining lymph vessels, whereas static planar images after 15 min mostly depict the first draining LNs. Delayed images (2–3 h after injection) enable SLNs to be distinguished from second tier nodes.

Planar images provide a 2-D overview of the lymphatic drainage pattern, from which SLNs can be localized and marked on the patient's skin using an external radioactive marker, such as a ^{57}Co source pen. Anterior views must be complemented with oblique or lateral views to clarify the location of the LNs in relation to the neck levels.

Nevertheless, interpretation of planar images can be difficult because no anatomic information is provided and the 3-D conformation of the structures of the head and neck is not adequately visualized using planar imaging. Furthermore, SLNs located in proximity to or underneath the radiocolloid injection site are frequently masked by the excess activity due to retention of the radiocolloid at the injection site.

9.1.3. Lymphatic drainage and neck nodal groups

According to the AJCC Union for International Cancer Control TNM staging system [9.24], LNs in the neck may be subdivided into specific anatomic subsites and grouped into seven levels on each side of the neck (Fig. 9.1). Level I includes the submental (sublevel IA) and submandibular (sublevel IB) LNs. Level II contains the upper jugular nodes that extend from the inferior border of the hyoid bone to the base of the skull; in relation to the vertical plane defined by the spinal accessory nerve, LNs located anterior (medial) constitute sublevel IIA, and the nodes located posterior (lateral) constitute sublevel IIB. Level III includes the middle jugular LNs, while level IV includes the lower jugular nodes. The posterior border of regions II, III and IV is the posterior border of the sternocleidomastoid muscle, which is the anterior border of level V. This latter group is composed of sublevel VA, which includes the spinal accessory nodes, and sublevel VB, which includes the nodes following the transverse cervical vessels and the supraclavicular nodes, with the exception of

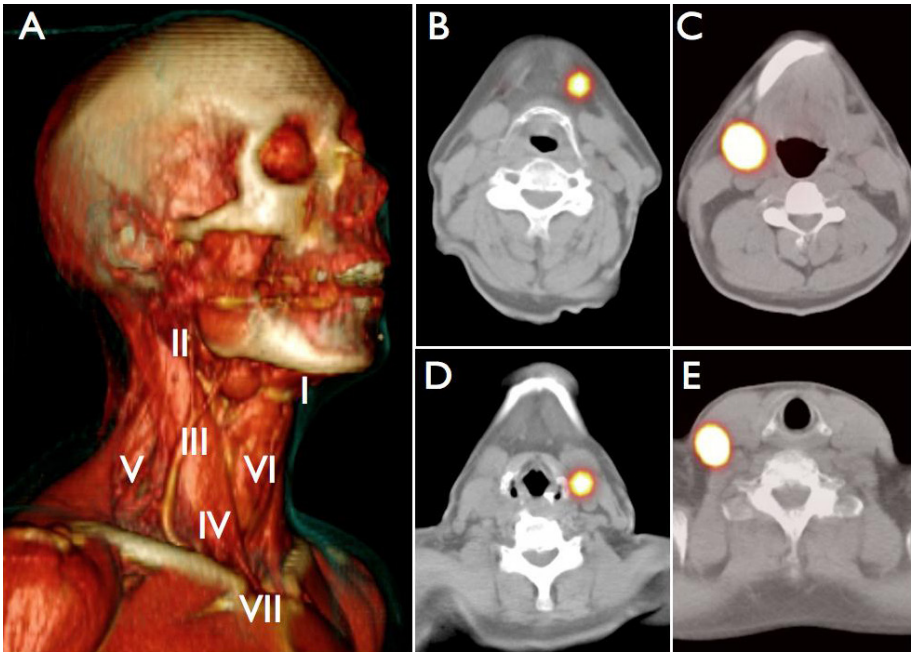

FIG. 9.1. (A) CT based volume rendering of the head and neck region showing the anatomical LN levels of the neck. In the right panels, axial fused SPECT/CT images obtained during an SLNM procedure performed with ^{99m}Tc nanocolloid show examples of SLNs (orange) in left level I (B), right level 2 (C), left level III (D) and right level IV (E).

the Virchow node, which is located in level IV. Level VI contains the pretracheal and paratracheal nodes, the precricoid Delphian node and the perithyroidal nodes, including the LNs along the recurrent laryngeal nerves. Finally, level VII includes the superior mediastinal LNs.

Lymphoscintigraphy shows that lymphatic drainage from head and neck malignancies is mostly multidirectional, with SLNs located in different neck levels in the same patient. Furthermore, in many cases, lymphatic drainage may occur to SLNs located on both sides of the neck (Fig. 9.2). It is therefore very important in the final information to the surgeon to identify the location of the SLNs in relation to the anatomic level in the neck.

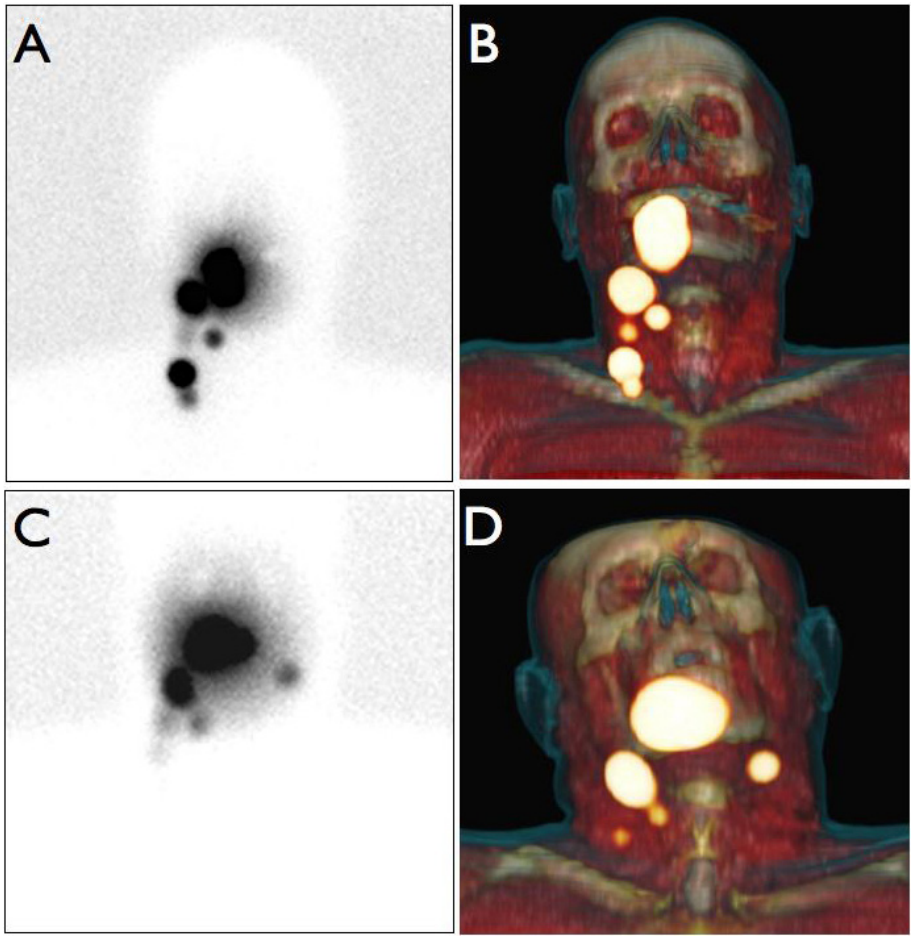

FIG. 9.2. Lymphoscintigraphy with ^{99m}Tc nanocolloid in two different patients with head and neck malignancies. In the upper panels (referring to a patient with a primary tumour in the right border of the tongue), the early planar anterior image shows lymphatic drainage from the injection site to the right side of the neck (A), while SPECT/CT 3-D volume rendering more clearly identifies these SLNs as being located in level II (B). In the lower panels (referring to a patient with a tumour in the floor of the mouth), the early planar anterior image shows lymphatic drainage to both sides of the neck (C), while SPECT/CT 3-D volume rendering more clearly identifies these SLNs as being located in level II on both sides of the neck (D).

9.1.4. Intraoperative SLN detection

A general purpose hand-held gamma probe is routinely used for intraoperative SLN detection in the head and neck region. Although intraoperative injection of patent blue can be performed for additional lymphatic mapping, SLNs in the head and neck region frequently do not stain blue, owing to the fast lymphatic drainage in this area [9.25].

The gamma detection probe detects the signal when pointed straight towards the radioactive SLNs. Deeply located SLNs are difficult to detect, both because of tissue attenuation and because the large amount of radioactivity remaining at the injection site may cause SLNs that are located nearby to be missed.

9.2. SPECT/CT CONTRIBUTION

Hybrid SPECT/CT imaging is frequently used for SLNM in patients with malignancies of the head and neck region, as it can optimize visualization and localization of SLNs in this anatomically complex area [9.15–9.23].

While visualization by planar imaging of lymphatic drainage from head and neck malignancies has been reported to range from 83% to 100% [9.15, 9.16, 9.18, 9.20–9.22], SPECT/CT imaging has been proven to visualize one or more additional SLNs in more than half of the studies [9.15, 9.20, 9.21, 9.26]. These additional SLNs visualized using only SPECT/CT imaging might be tumour positive [9.25]. SLNs better detected using SPECT/CT imaging are especially those adjacent to the radiocolloid injection site, which can be easily missed on planar imaging [9.16, 9.18, 9.26]. Furthermore, areas of focal radioactivity accumulation that can be erroneously interpreted as SLNs on planar imaging alone can correctly be identified as non-nodal radiocolloid uptake (due instead to, for example, tracer leakage or contamination) on SPECT/CT imaging [9.15, 9.21, 9.22, 9.26].

SPECT/CT imaging is therefore very useful for exact anatomic localization of the SLNs [9.15–9.23, 9.26]. This feature is especially important in the head and neck region, where it is crucial from the surgical point of view to identify the topography of SLNs in relation to several vital vascular and neural structures, in order to be able to safely remove these LNs. SPECT/CT imaging can localize the SLNs in relation to the mandible, parotid gland, jugular vein and sternocleidomastoid muscle, and also clarify whether the nodes are superficial underneath the skin or located more deeply underneath other structures. The anatomotopographic information on SLN location provided by SPECT/CT imaging therefore constitutes an important reference for planning the most adequate surgical approach (Fig. 9.3). In this regard, Vermeeren et al. demonstrated that better localization information provided by SPECT/CT imaging frequently

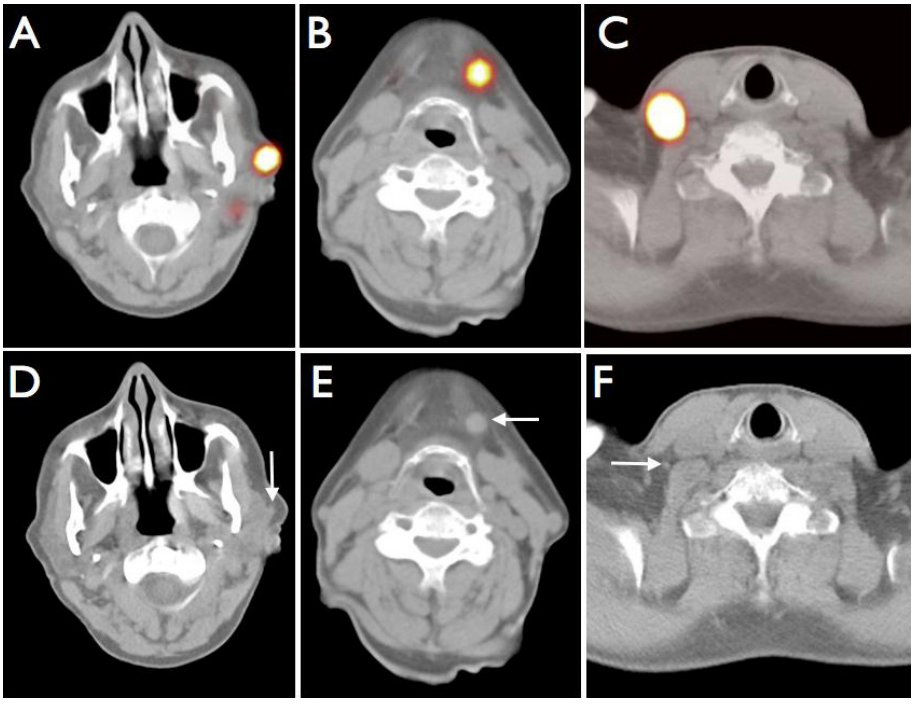

FIG. 9.3. Axial SPECT/CT images showing SLNs located in the left preauricular area (A), left submandibular area (B) and right supraclavear area (C). The same LNs (arrows) are depicted in the corresponding CT sections in relation to anatomical reference points (D–F). The slightly enlarged submandibular SLN was positive for metastasis, while the preauricular and the supraclavear SLNs were tumour free from metastasis.

leads to an adjustment in the surgical approach [9.26]. In addition, Covarelli et al. have proven the clinical relevance of this localization information because the operation time was significantly shorter when SLNB was performed on the basis of SPECT/CT imaging compared to planar imaging [9.23].

In patients with melanomas located in the head or neck, SPECT/CT imaging visualizes more SLNs than conventional planar imaging, and it also depicts their anatomic location. In 28 patients evaluated at the National Cancer Center in Amsterdam [9.26], both planar lymphoscintigraphy and SPECT/CT visualized at least one SLN. Planar imaging visualized a total of 94 SLNs, whereas SPECT/CT imaging showed an additional SLN in six patients. Furthermore, in all patients, SPECT/CT imaging depicted the SLNs in relation to the surrounding anatomic structures. In conclusion, while SLNs can be identified using 2-D imaging, 3-D reconstruction provides an anatomic overview of all LNs in relation to the injection area (Fig. 9.4). According to the surgeons, SLNs were more accurately

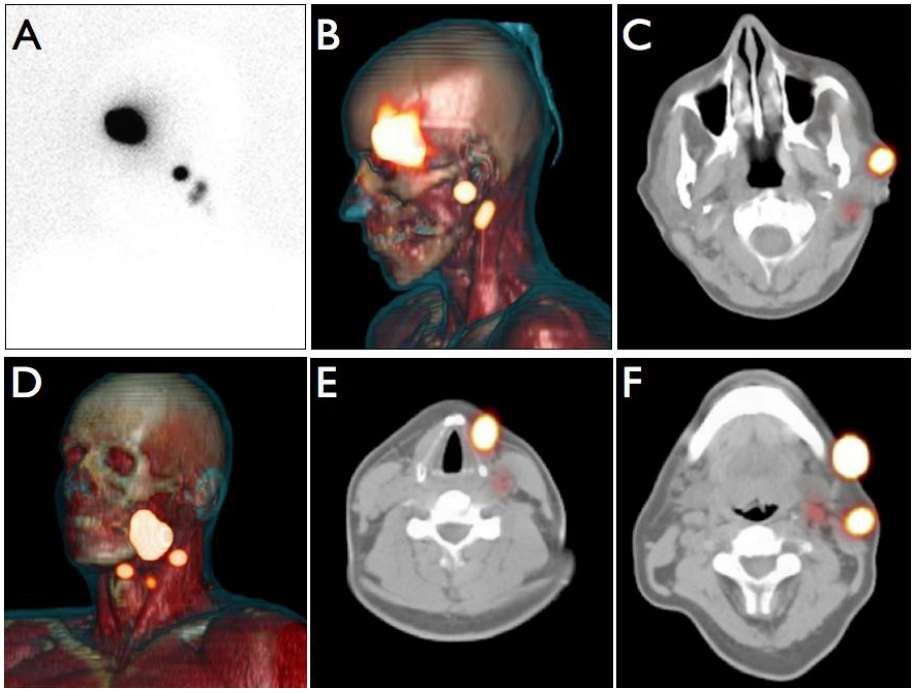

FIG. 9.4. Upper row: A woman with a melanoma in her left frontal area. The early anterior planar image following injecting 74 MBq of ^{99m}Tc nanocolloid shows drainage to the left side of the neck (A). On 3-D SPECT/CT volume rendering (B) and axial fused SPECT/CT images (C), the first draining SLN is visualized in the preauricular LN group, while two second echelon nodes are visualized in the left level II. Lower row: A man with a melanoma in the left mandibular area. The first draining SLNs are in the vicinity of the radiocolloid injection site (D), and are clearly localized by SPECT/CT imaging in levels I (E) and II (F).

localized using SPECT/CT imaging in all cases, and in six patients (30%), SLNs were correctly localized using SPECT/CT imaging in a site different from that suggested by planar imaging. The surgical approach was planned on the basis of SPECT/CT imaging, and in 11 out of 20 patients (58%), the surgeons reported that the approach would have been different if based on planar imaging alone. In these cases, the incision was placed in a different location, or an intraoperative search was facilitated.

Location of a CM in the head and neck has been reported to be a predictive factor for false negative SLNB, with rates ranging between 12% and 44% [9.6, 9.25, 9.27, 9.28]. However, such relatively high false negative rates were observed in studies that did not include SPECT/CT imaging for SLNM.

It is therefore conceivable to assume that performance of SLNB based on SPECT/CT imaging would dramatically improve these findings, by allowing optimal pre-operative SLN localization.

9.3. INTRAOPERATIVE IMAGING

The recently developed portable gamma cameras provide intraoperative visualization of radiotracer distribution within a limited region of the body, focusing on the field of interest for the surgeon [9.29–9.32]. For exploration of the head and neck region, the use of portable gamma cameras has been described in parathyroidectomy guided by imaging with ^{99m}Tc sestamibi [9.29, 9.33]. Another possible application of the portable gamma camera in patients with head and neck malignancies is for localizing SLNs, by providing an overview of all radioactive spots within the surgical field [9.34–9.36]. In fact, the whole procedure of LN excision can be monitored using a portable gamma camera, and SLNs located near the radiocolloid injection site can be detected more easily using gamma camera imaging than by using gamma probe counting. Furthermore, when it is difficult to localize intraoperatively an SLN that had been detected pre-operatively, focused imaging using the portable gamma camera shows the surgeon where the LN is located. Finally, by assessing residual radioactivity after excision of the SLNs, intraoperative imaging using the portable gamma camera can help to assess the completeness of the procedure, possibly leading to detection of additional SLNs not previously identified [9.36]. Regarding the latter, an additional, previously undetected SLN was identified in 24% of the patients with head and neck malignancies (including one SLN as the sole site of metastasis) [9.36]. In fact, in some cases, a focus of intense radiocolloid uptake seen in pre-operative images along the lymphatic drainage pathway corresponds to a cluster of SLNs rather than to a single SLN (Fig. 9.5). Intraoperative imaging using the portable gamma camera after excision of the first, hottest LN can reveal the remaining SLNs.

Acquiring intraoperative images only takes a few minutes, but if more nodes are found and excised because of intraoperative imaging, the procedure is likely to be prolonged.

Although it is not yet routine practice, intraoperative visualization of SLNs using a portable gamma camera is feasible (because acquiring intraoperative images only takes a few minutes) and might actually improve intraoperative detection of SLNs in the head and neck region (Fig. 9.6).

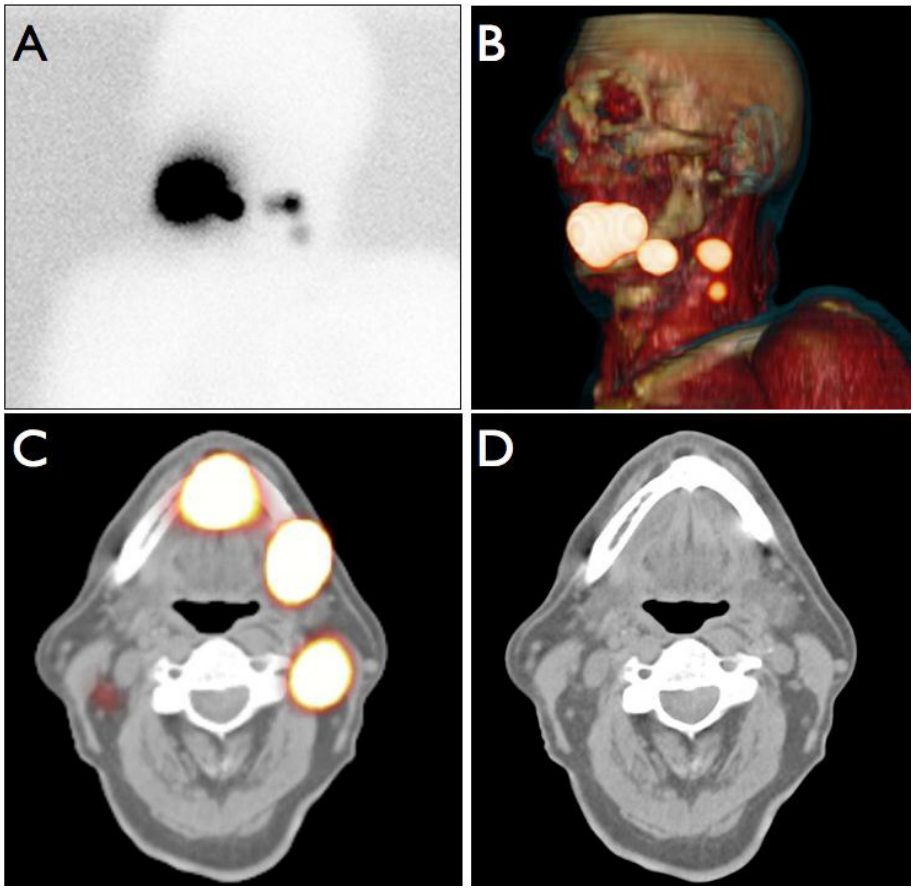

FIG. 9.5. Man with a squamous cell carcinoma of the floor of the mouth. Left anterior oblique delayed image following injecting 74 MBq of ^{99m}Tc nanocolloid shows fast drainage from the injection site in the floor of the mouth to the left side of the neck (A). 3-D SPECT/CT volume rendering (B), as well as an axial fused SPECT/CT image (C) and a CT component (D) demonstrate that the most anterior radioactive spot corresponds to a cluster of SLNs, whereas the posterior hot spot corresponds to a single SLN.

As a concluding remark, the use of PET probes could represent the next step in GOSTT procedures applied to head and neck malignancies. Figure 9.7 shows a PET probe device (control unit and heavy shielded probe for detection of the high energy annihilation γ photons in the upper left corner). The case illustrated in this figure corresponds to a patient with squamous cell malignancy of the tongue, in whom [^{18}F]FDG PET/CT was positive in the left laterocervical area (centre and upper right panels for PET, CT and fused PET/CT images). During radioguided surgery assisted by the PET probe following administration of [^{18}F]FDG, an

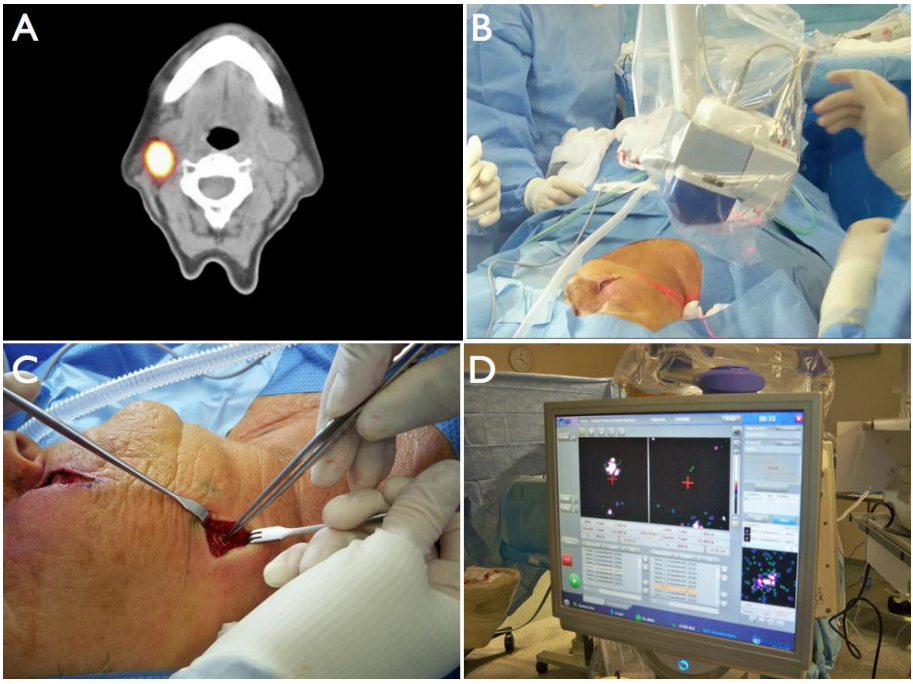

FIG. 9.6. Intraoperative use of the portable gamma camera in a patient with melanoma of the right cheek and a first draining SLN identified pre-operatively by SPECT/CT imaging in level II (A). In the operating room, the portable gamma camera is positioned to acquire a pre-operative scan of the site of the SLN detected on SPECT/CT imaging (B). After SLN resection (C), the excision site is controlled for remaining radioactivity (D). As shown in the display of the portable gamma camera (D), comparison of the scan acquired before (left) and after (right) resection confirms completeness of SLN harvesting.

enlarged LN was retrieved under radioguidance and excised (lower left panel), revealing macroscopic metastatic involvement (lower right panel).

On the other hand, the anecdotal case mentioned above is consistent with a prior report describing a similar approach in a group of 21 patients with head and neck cancer in whom LN metastasis was suspected (mostly on the basis of US findings) [9.37]. Intraoperative use of a PEP (with surgery being performed at variable times after administering 250–320 MBq [^{18}F]FDG) enabled identification of LN metastasis in 20 out of 21 patients with a positive [^{18}F]FDG PET/CT scan. Tumour to background ratios measured using the PEP during surgery were comparable with those derived from semiquantitative analysis of the PET scan. It was concluded therefore that radioguided surgery under guidance of a PEP after administration of [^{18}F]FDG is highly promising as a surgical approach to LN neck dissection [9.37].

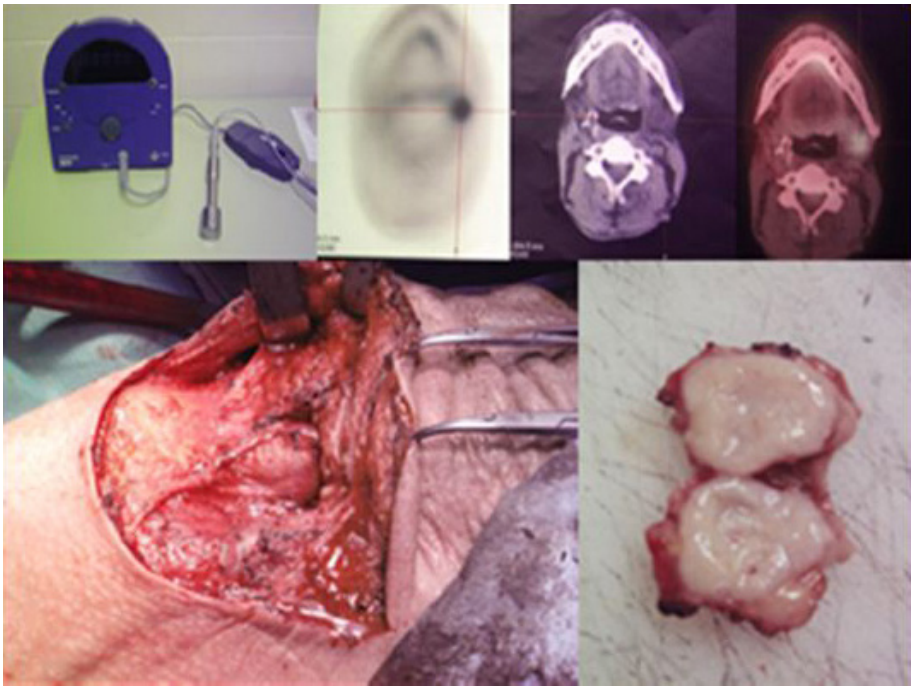

FIG. 9.7. A PET probe device (control unit and heavy shielded probe for detection of the high energy annihilation γ photons in the upper left corner). The case illustrated corresponds to a patient with squamous cell malignancy of the tongue, in whom [^{18}F]FDG PET/CT was positive in the left laterocervical area (centre and upper right panels for PET, CT and fused PET/CT images). During radioguided surgery assisted by the PET probe following administration of [^{18}F]FDG, an enlarged LN was retrieved under radioguidance and excised (lower left panel), revealing macroscopic metastatic involvement (lower right panel).

REFERENCES TO CHAPTER 9

[9.1] GERSHENWALD, J.E., et al., Multi-institutional melanoma lymphatic mapping experience: The prognostic value of sentinel lymph node status in 612 stage I or II melanoma patients, J. Clin. Oncol. **17** (1999) 976–983.

[9.2] KOVÁCS, A.F., et al., Positive sentinel lymph nodes are a negative prognostic factor for survival in T1-2 oral/oropharyngeal cancer-a long-term study on 103 patients, Ann. Surg. Oncol. **16** (2009) 233–239.

[9.3] TANIS, P.J., NIEWEG, O.E., VAN DEN BREKEL, M.W., BALM, A.J., Dilemma of clinically node-negative head and neck melanoma: Outcome of "watch and wait" policy, elective lymph node dissection, and sentinel node biopsy—a systematic review, Head Neck **30** (2008) 380–389.

[9.4] JANSEN, L., et al., Sentinel node biopsy for melanoma in the head and neck region, Head Neck **22** (2000) 27–33.
[9.5] NOWECKI, Z.I., RUTKOWSKI, P., NASIEROWSKA-GUTTMEJER, A., RUKA, W., Survival analysis and clinicopathological factors associated with false-negative sentinel lymph node biopsy findings in patients with cutaneous melanoma, Ann. Surg. Oncol. **13** (2006) 1655–1663.
[9.6] CARLSON, G.W., et al., Regional recurrence after negative sentinel lymph node biopsy for melanoma, Ann. Surg. **248** (2008) 378–386.
[9.7] VAQUERANO, J., et al., American Joint Committee on Cancer clinical stage as a selection criterion for sentinel lymph node biopsy in thin melanoma, Ann. Surg. Oncol. **13** (2006) 198–204.
[9.8] THOMPSON, J.F., SHAW, H.M., Is sentinel lymph node biopsy appropriate in patients with thin melanomas: Too early to tell? Ann. Surg. Oncol. **13** (2006) 279–281.
[9.9] CROWLEY, N.J., SEIGLER, H.F., The role of elective lymph node dissection in the management of patients with thick cutaneous melanoma, Cancer **66** (1990) 2522–2527.
[9.10] ESSNER, R., CHUNG, M.H., BLEICHER, R., Prognostic implications of thick (>or=4-mm) melanoma in the era of intra-operative lymphatic mapping and sentinel lymphadenectomy, Ann. Surg. Oncol. **9** (2002) 754–761.
[9.11] CIVANTOS, F., et al., Sentinel node biopsy for squamous cell carcinoma of the head and neck, J. Surg. Oncol. **97** (2008) 683–690.
[9.12] PALERI, V., et al., Sentinel node biopsy in squamous cell cancer of the oral cavity and oral pharynx: A diagnostic meta-analysis, Head Neck **27** (2005) 739–747.
[9.13] STOECKLI, S.J., Sentinel node biopsy for oral and oropharyngeal squamous cell carcinoma of the head and neck, Laryngoscope **117** (2007) 1539–1551.
[9.14] FERLITO, A., SILVER, C.E., RINALDO, A., Elective management of the neck in oral cavity squamous carcinoma: Current concepts supported by prospective studies, Br. J. Oral. Maxillofac. Surg. **47** (2009) 5–9.
[9.15] EVEN-SAPIR, E., et al., Lymphoscintigraphy for sentinel node mapping using a hybrid SPECT/CT system, J. Nucl. Med. **44** (2003) 1413–1420.
[9.16] WAGNER, A., et al., SPECT-CT for topographic mapping of sentinel lymph nodes prior to gamma probe-guided biopsy in head and neck squamous cell carcinoma, J. Craniomaxillofac. Surg. **32** (2004) 343–349.
[9.17] LOPEZ, R., et al., Multimodal image registration for localization of sentinel nodes in head and neck squamous cell carcinoma, J. Oral. Maxillofac. Surg. **62** (2004) 1497–1504.
[9.18] THOMSEN, J.B., et al., Sentinel lymph node biopsy in oral cancer: Validation of technique and clinical implications of added oblique planar lymphoscintigraphy and/or tomography, Acta. Radiol. **46** (2005) 569–575.
[9.19] TERADA, A., et al., Sentinel lymph node radiolocalization in clinically negative neck oral cancer, Head Neck **28** (2006) 114–120.
[9.20] BILDE, A., et al., The role of SPECT-CT in the lymphoscintigraphic identification of sentinel nodes in patients with oral cancer, Acta. Otolaryngol. **126** (2006) 1096–1103.

[9.21] KHAFIF, A., et al., Lymphoscintigraphy for sentinel node mapping using a hybrid single photon emission CT (SPECT)/CT system in oral cavity squamous cell carcinoma, Head Neck **28** (2006) 874–879.
[9.22] KESKI-SÄNTTI, H., et al., Sentinel lymph node mapping using SPECT-CT fusion imaging in patients with oral cavity squamous cell carcinoma, Eur. Arch. Otorhinolaryngol. **263** (2006) 1008–1012.
[9.23] COVARELLI, P., et al., The single-photon emission computed tomography/computed tomography: A new procedure to perform the sentinel node biopsy in patients with head and neck melanoma, Melanoma Res. **17** (2007) 323–328.
[9.24] EDGE, S.B., et al. (Eds), AJCC Cancer Staging Manual, 7th edn, Springer (2010).
[9.25] CHAO, C., et al., Sentinel lymph node biopsy for head and neck melanomas, Ann. Surg. Oncol. **10** (2003) 21–26.
[9.26] VERMEEREN, L., VALDÉS OLMOS, R.A., KLOP, W.M., VAN DER PLOEG, I.M., NIEWEG, O.E., SPECT/CT for sentinel lymph node mapping in head and neck melanoma, Head Neck **33** (2011) 1–6.
[9.27] VAN DER PLOEG, I.M.C., VALDÉS OLMOS, R.A., NIEWEG, O.E., RUTGERS, E.J., KROON, B.B., The additional value of SPECT/CT in lymphatic mapping in breast cancer and melanoma, J. Nucl. Med. **48** (2007) 1756–1760.
[9.28] DE WILT, J.H., et al., Correlation between preoperative lymphoscintigraphy and metastatic nodal disease sites in 362 patients with cutaneous melanomas of the head and neck, Ann. Surg. **239** (2004) 544–552.
[9.29] SANCHEZ, F., et al., Performance tests of two portable mini gamma cameras for medical applications, Med. Phys. **33** (2006) 4210–4220.
[9.30] SCHILLACI, O., et al., Sentinel node detection with imaging probe, Tumouri **88** (2002) 32–35.
[9.31] MATHELIN, C., et al., A new intra-operative gamma camera for the sentinel lymph node procedure in breast cancer, Anticancer Res. **28** (2008) 2859–2864.
[9.32] KITAGAWA, W., SHIMIZU, K., AKASU, H., Radio-guided parathyroidectomy for primary hyperparathyroidism using the solid-state, multi-crystal gamma camera, Med. Sci. Monit. **9** (2003) 53–56.
[9.33] ORTEGA, J., et al., Potential role of a new hand-held miniature gamma camera in performing minimally invasive parathyroidectomy, Eur. J. Nucl. Med. Mol. Imag. **43** (2007) 165–169.
[9.34] FERNÁNDEZ, M.M., et al., A flat-panel-based mini gamma camera for lymph nodes studies, Nucl. Instrum. Methods Phys. Res. **527** (2004) 92–96.
[9.35] TSUCHIMOCHI, M., et al., A prototype small CdTe gamma camera for radio-guided surgery and other imaging applications, Eur. J. Nucl. Med. Mol. Imag. **30** (2003) 1605–1614.
[9.36] VERMEEREN, L., VALDÉS OLMOS, R.A., KLOP, W.M., BALM, A.J., VAN DEN BREKEL, M.W., A portable gamma-camera for intraoperative detection of sentinel nodes in the head and neck region, J. Nucl. Med. **51** (2010) 700–753.
[9.37] MELLER, B., et al., High energy probe for detecting lymph node metastases with ^{18}F-FDG in patients with head and neck cancer, Nuklearmed. **45** (2006) 153–159.

10. GOSTT APPLICATIONS IN NON-SMALL-CELL LUNG CANCER

10.1. INTRODUCTION

This chapter covers the potential uses of intraoperative radioguided localization and resection of solitary pulmonary nodules to assist minimally invasive surgical resection, as well as the potential uses of SLNM in patients with non-small-cell lung cancer.

10.2. SOLITARY PULMONARY NODULES

10.2.1. Background

One of the most common manifestations of lung cancer is a solitary pulmonary nodule, which is a condition that is defined as a spherical radiographic opacity that measures up to 3 cm in diameter and is completely surrounded by lung tissue. Because of the widespread use of CT imaging in the investigation of patients with respiratory symptoms, the solitary pulmonary nodule is a frequent incidental finding [10.1]. A solitary pulmonary nodule may represent early stage lung cancer, which is a devastating disease with an overall 5 year mortality rate of approximately 84%, which can be as low as 47% with early detection and surgery [10.2].

While diagnostic evaluation of focal pulmonary lesions should be accurate and efficient to facilitate prompt resection of malignant tumours, whenever possible, surgery should be avoided in cases of benign disease [10.3]. Up to 55% of solitary pulmonary nodules are reported to be malignant. Poor prognosis of lung cancer is directly associated with its delayed presentation; in fact, signs and symptoms are rarely present until the malignancy has become advanced—a stage where it is usually unresectable.

The differential diagnosis of a solitary pulmonary nodule includes neoplastic, infectious, inflammatory, vascular, traumatic and congenital lesions. Other benign aetiologies for solitary pulmonary nodules are rheumatoid nodules, intrapulmonary LNs, plasma cell granulomas and sarcoidosis. Some clinical features, such as older age, history of cigarette smoking and previous history of cancer, all increase the probability that a solitary pulmonary nodule is malignant [10.4]. Because the solitary pulmonary nodule is, by definition, a radiographic finding, diagnostic workup is usually based on radiological findings and criteria. However, diagnosing lung cancer based on chest X rays alone can

be quite difficult, and spiral CT with intravenous contrast enhancement is the imaging modality of choice. This evaluation should therefore be performed on any newly diagnosed solitary pulmonary nodule because it provides exact anatomic location as well as some important contrastographic features that characterize the nodule.

The introduction of [^{18}F]FDG PET imaging into clinical routines has taken the evaluation of solitary pulmonary nodules beyond morphological analysis, to yield functional and metabolic analysis of disease [10.5–10.10]. However, in addition to a somewhat low sensitivity of [^{18}F]FDG PET imaging for nodules smaller than 1 cm in size, this imaging technique can also yield false negative results in cases of carcinoid tumours or bronchoalveolar carcinomas, as these tumours may not have a high [^{18}F]FDG uptake [10.11]. On the other hand, false positive results can be seen in lung lesions with an infectious or inflammatory aetiology, such as tuberculosis or histoplasmosis, or in rheumatoid nodules [10.12].

It has also been shown that scintigraphy with ^{99m}Tc depreotide (an SST analogue, based on the principle that malignant nodules express a higher level of SSTRs than benign nodules) has sensitivity and specificity similar to those of [^{18}F]FDG PET imaging [10.13].

Percutaneous FNA biopsy has been used for characterizing pulmonary nodules for more than 25 years. CT guided, FNA biopsy has become an important diagnostic tool, particularly for nodules 5–15 mm in diameter (97.7% sensitivity and 100% specificity) [10.14].

Based on the above considerations, any patient with a newly detected solitary pulmonary nodule not showing benign looking calcifications should be considered to have a malignancy, until proven otherwise. Surgical resection is the ideal approach, as it is both diagnostic and therapeutic.

10.2.2. Technique

In the 1990s, the development of a procedure for ROLL by interstitial injection of ^{99m}Tc MAAs in patients with non-palpable breast tumours spurred interest in this approach for lesions outside the breast as well [10.15], and clinical experience with this approach is increasing in several tumoural domains. Therefore, even if few reports have been published so far concerning applications of ROLL techniques in patients with peripheral solitary pulmonary nodules [10.16–18], it is now possible to set some guidelines for performing this procedure. The information provided here is based mostly on the experience acquired at the University of Pisa Medical School, Italy, where the procedure is generally performed for thoracoscopic resection of the nodule(s).

10.2.2.1. Pre-operative phase

Small pulmonary nodules (generally less than 2 cm in maximum diameter and with their margin reaching at most 5 mm from the visceral pleura) are localized using CT imaging. Injection of the ^{99m}Tc MAA particles into the solitary pulmonary nodule can be performed either on the same day of surgery or 24–36 h before surgery.

Local anaesthesia of the thoracic wall is performed and then, under CT guidance, a 22 G needle is introduced into the lesion or just in contact with it; a volume of a suspension, composed of 0.2 mL of ^{99m}Tc MAA (5 MBq for a single day procedure or 10–15 MBq for a next day procedure) and 0.1–0.2 mL of non-ionic contrast, is then injected. Acquisition of a CT scan is repeated after injection to confirm exact placement of the injectate, based on visualization of the contrast medium in the solitary pulmonary nodule or close to it, as well as to exclude possible complications of the procedure (bleeding and/or a pneumothorax).

10.2.2.2. Operative phase

Either immediately after intranodular injection (single day procedure) or the next day, the patient is transferred to the operating room. Under general anaesthesia, with orotracheal selective intubation and with the patient in the lateral position, a pneumothorax is induced and a 7 mm trocar for the videothoracoscope is introduced, usually through the sixth or seventh intercostal space along the midaxillary line. After a first exploration of the pleural space, a second 11.5 mm trocar is positioned, with this approach being planned according to the radiological site of the nodule and the position of the lobes on thoracoscopic vision. An intraoperative gamma probe is introduced through this trocar. An area of the lung far from the suspected one is scanned first to reset the system and evaluate background activity, and then the pleural surface of the target area is scanned to localize the radioactive source. Once the area with the higher value of radioactivity is identified, a third trocar is introduced, choosing the site that allows maximum manoeuvrability of endostapler devices for the wedge resection. Before firing the endostapler, a careful instrumental palpation of the identified area is always performed. Moreover, any residual radioactivity is searched for with the probe below the stapler to assess the safe depth of the resection. Once wedge resection is performed, the nodule is extracted from the pleural cavity into an endoscopic bag through the largest porthole, to avoid possible tumour seeding to the chest wall. Frozen section examination is immediately performed and, in case of a primary lung cancer and provided that the patient has adequate pulmonary reserve, the procedure is completed with lobectomy.

10.2.3. Conclusions

Video assisted thoracic surgery is an interesting and emerging procedure for the diagnosis and treatment of peripheral pulmonary nodules. However, when the nodule is either too small or too deep beneath the pleural surface, failure in localization and, as a consequence, conversion to open surgery may be necessary. When relying only on thoracoscopic exploration and endoscopic palpation, this event is more likely if the distance between the nodule and the nearest pleural surface is more than 5 mm and/or if the nodule is less than 10 mm in size [10.19].

To overcome such limitations, several techniques have been developed for pre-operative localization of deeper nodules. Percutaneous hookwire placement and methylene blue injection under CT guidance have been widely used, either alone or together. However, these techniques do have some failures (because of displacement of the wire or intraparenchymal diffusion of the dye) and/or complications (pneumothorax and/or haemothorax). Moreover, when employing such localization techniques, the time elapsed between pre-operative positioning of the hookwire (or blue dye injection) and surgery itself must be kept to a minimum, while intralesional injection of ^{99m}Tc MAAs for radioguided surgery can be performed even 24–36 h before surgery.

The radioguided approach described here for solitary pulmonary nodules can yield the exact location of the nodule and its depth from the pleural surface, to ensure safe surgical margins of the excision and avoid thoracotomy for palpation to search for the lesion. On the other hand, the possibility remains to perform radioguided surgery after systemic administration of a tumour seeking radiopharmaceutical, with optimal tumour localizing properties yielding sufficiently high TBRs.

[Fluorine-18]FDG constitutes one such potential radiopharmaceutical, as it has already been explored for other regions of the body [10.20–10.23]. Intratumoural accumulation of the PET agent [^{18}F]FDG can be used as a guide to identify lesion margins of solitary pulmonary nodules by means of probes capable of detecting the high energy γ rays. Technetium-99m depreotide could constitute an alternative single photon emitting radiopharmaceutical, based on high expression of subtype 2 SSTRs in malignancies of the lung, including small cell cancer. Depreotide is a synthetic peptide that carries an SSTR binding domain. In a pilot study involving 17 patients at the University of Pisa Medical School, intraoperative radioguidance proved to be successful for localizing the solitary pulmonary nodule in all cases with a positive SPECT/CT study except one, with intraoperative TBRs of 2.3 ± 0.8, therefore closely mirroring the corresponding values observed on the SPECT images [10.24, 10.25].

10.3. SLNM AND SLNB IN NON-SMALL-CELL LUNG CANCER

10.3.1. Background

Once the diagnosis of non-small-cell lung cancer is confirmed, patients should be staged as accurately as possible on the basis of clinical, radiological and histopathological information. Staging based on the TNM classification, as recommended by the AJCC, is the primary prognostic factor for survival in these patients [10.26]. The main goals of staging are to assist in determining appropriate treatment options (surgery versus non-surgical therapies) and in predicting prognosis.

Traditional staging modalities include history and physical examinations, laboratory tests and non-invasive staging techniques such as conventional chest X rays, CT imaging, bone scans, MRI and PET imaging using [^{18}F]FDG. If these tests do not demonstrate the presence of metastatic disease or of locally unresectable disease, then further invasive staging techniques may be necessary, including bronchoscopy, mediastinoscopy and thoracoscopic surgery.

Additional invasive procedures for defining the N stage, such as complete thoracic LDN or nodal sampling, may help to further stratify patients into appropriate therapeutic and prognostic categories. In this regards, mediastinal LN dissection can result in the implementation of effective therapeutic strategies when it helps to discover nodal metastatic non-small-cell lung cancer [10.26, 10.27]. However, this procedure is not therapeutic per se. Moreover, it potentially involves severe complications, which is particularly worrying considering that in a certain fraction of patients, LN metastasis is not found at histology; these patients have therefore undergone a potentially harmful, yet unnecessary surgical procedure.

Although several studies on SLNM and SLNB in patients with non-small-cell lung cancer have been published, this procedure cannot yet be considered to be a part of clinical practice for this disease.

Lung resection for non-small-cell lung cancer combined with mediastinal LN dissection leads to greater production of postoperative exudates than with resection alone, although such morbidity is not particularly relevant [10.28]. In this regard, the main advantage of SLNM and SLNB lies in directing extensive histopathological examination selectively to the first node(s) receiving lymph draining from the tumour. Exquisitely sensitive analysis techniques (serial sectioning of virtually the entire SLN for conventional haematoxylin and eosin staining or for immunohistochemistry, and reverse transcription polymerase chain reaction analysis) can be applied, thus increasing the chance of detecting occult micrometastases [10.29]. In fact, more careful pathological examination of LNs that had previously been reported as negative for metastatic involvement

in resected lung cancer patients has revealed micrometastatic disease in over 20% of such patients classified as N0, thus determining upstage in a considerable fraction [10.30].

For SLNM and SLNB, two agents (blue dye and radiopharmaceuticals) have been employed; the agents are generally injected around the tumour and then monitored using direct visualization (blue dye) or using gamma counting of individual LN stations to determine the first site of efferent lymphatic drainage from the tumour. In 1999, Little et al. described SLNM in non-small-cell lung cancer using isosulfan blue [10.31]. Unfortunately, because it was difficult to detect the blue dye in the LNs in the thoracic cavity, the rate of SLN detection was too low to be clinically useful.

10.3.2. Technique

In 2002, Liptay et al. described radioguided SLNM in patients with non-small-cell lung cancer. They intraoperatively injected ^{99m}Tc sulphur colloid directly into lung tumours, achieving an 82% rate of SLN detection using an intraoperative gamma probe [10.29]. They were, however, unable to obtain useful counts from the upper mediastinal LN during surgery, owing to an interference signal from radioactivity that had migrated from the lung into the trachea [10.31]. To overcome this problem, Nomori et al. pre-operatively injected ^{99m}Tc tin colloid peritumourally under CT guidance, and then detected SLNs using an intraoperative gamma probe [10.32]. Subsequently, other groups also employed the CT guided technique, achieving 64%–87% rates of SLN detection and confirming the technique's feasibility for clinical use [10.33, 10.34].

The main advantage of pre-operative radiocolloid injection is that it also enables intraoperative gamma counting for the upper mediastinal LNs because any radioactivity that may have migrated from the injection site into the trachea is cleared during the elapsed period between injection and surgery. Pre-operative transbronchoscopical injection of the radiocolloid may be an additional useful alternative to CT guided injection [10.35].

Based on these reports indicating the feasibility of both preoperative and intraoperative modalities of radiocolloid injection for identifying the first sites of potential nodal metastases of non-small-cell lung cancer, Melfi et al. [10.34] explored both mapping procedures: for 19 patients, using CT guided pre-operative injection of 37 MBq of ^{99m}Tc nanocolloid, and for 10 patients using intraoperative injection. As a slight modification to the approach of Nomori et al. [10.32], the CT guided radiocolloid injection was performed 1–2 h rather than 24 h before surgery. The cumulative success rate in SLN identification was 96%, and no false negative results were observed. The only failure in SLN identification was observed in one patient with a large tumour. Similar to other reports,

two different SLNs were found in 28% of patients, and approximately 20% of the SLNs were located in the mediastinum. Furthermore, in two patients, immunohistochemistry revealed micrometastasis that had gone undetected with conventional haematoxylin and eosin staining. No complications were observed during the mapping procedure; no pneumothorax nor bleeding were observed during the intratumoural injection under CT guidance [10.34].

As already demonstrated for other applications of SLNM, particularly in challenging anatomic regions such as the head and neck [10.36–10.40], hybrid imaging with SPECT/CT is expected to optimize mapping/localization of SLNs in patients with non-small-cell lung cancer.

10.3.3. Conclusions

Although several studies and ongoing trials have demonstrated the feasibility and safety of radioguided SLNB in patients with non-small-cell lung cancer, a standard technique has not yet been established [10.41].

While radioguided SLNM and SLNB may allow, in some cases, a more accurate characterization of unique patterns of lymphatic drainage from the tumour, the potential role of SLN evaluation for limiting mediastinal node dissection remains to be evaluated. Possible patterns of skip lymphatic drainage are a cause of special concern. However, SLN identification may direct accurate histopathological analysis, especially with extensive serial sectioning and immunohistochemistry, thus helping the surgeon to adopt the adequate level of nodal dissection tailored to individual patients.

Further experience and large scale multicentre trials are necessary before this surgical procedure could be widely accepted for treating this type of cancer and for avoiding complete mediastinal LDN in cases of early stage tumours.

REFERENCES TO CHAPTER 10

[10.1] WAHIDI, M.M., et al., Evidence for the treatment of patients with pulmonary nodules: When is it lung cancer?: ACCP evidence-based clinical practice guidelines (2nd edition), Chest **132** (2007) 94–107.

[10.2] HARDERS, S.W., MADSEN, H.H., RASMUSSEN, T.R., HAGER, H., RASMUSSEN, F., High resolution spiral CT for determining the malignant potential of solitary pulmonary nodules: Refining and testing the test, Acta. Radiol. **52** (2011) 401–409.

[10.3] WINER-MURAM, H., The solitary pulmonary nodule, Radiology **239** (2006) 34–49.

[10.4] SWENSON, S.I., et al., The probability of malignancy in solitary pulmonary nodules: Application to small radiologically indeterminate nodules, Arch. Intern Med. **57** (1997) 849–855.
[10.5] DEWAN, N.A., et al., Likelihood of malignancy in a solitary pulmonary nodule, Chest **112** (1997) 416–422.
[10.6] DUHAYLONGSOD, F.G., et al., Detection of primary and recurrent lung cancer by means of F-18 fluorodeoxyglucose positron emission tomography (FDG PET), J. Thorac. Cardiovasc. Surg. **110** (1995) 130–139.
[10.7] HERDER, G.J., et al., The performance of 18-F-fluorodeoxyglucose positron emission tomography in small solitary pulmonary nodules, Eur. J. Nucl. Med. Mol. Imaging **31** (2004) 1231–1236.
[10.8] LOWE, V.J., et al., Prospective investigation of positron emission tomography in lung nodules, J. Clin. Oncol. **16** (1998) 1075–1084.
[10.9] LOWE, V.J., HOFFMAN, J.M., DELONG, D.M., PATZ, E.F., COLEMAN, R.E., Semiquantitative and visual analysis of FDG-PET images in pulmonary abnormalities, J. Nucl. Med. **35** (1994) 1771–1776.
[10.10] NOMORI, H., et al., Visual and semiquantitative analyses for F-18 fluorodeoxyglucose PET scanning in pulmonary nodules 1 cm to 3 cm in size, Ann. Thorac. Surg. **79** (2005) 984–988.
[10.11] GOLDSMITH, S.I., KOSTAKOGLU, L., Nuclear medicine imaging of lung cancer, Radiol. Clin. North. Am. **38** (2000) 511–524.
[10.12] KIM, S.C., et al., Fluoro-deoxy-glucose positron emission tomography for evaluation of indeterminate lung nodules: Assigning a probability of malignancy may be preferable to binary readings, Ann. Nucl. Med. **22** (2008) 165–170.
[10.13] BLUEM, J.E., HANDMAKER, H., RINNE, N.A., The utility of a SST-type receptor binding peptide radiopharmaceutical (P829) in the evaluation of solitary pulmonary nodules, Chest **115** (1999) 224–232.
[10.14] MUKHERJEE, S., et al., Computed tomography-guided fine needle aspiration cytology of solitary pulmonary nodules suspected to be bronchogenic carcinoma: Experience of a general hospital, J. Cytol. **27** (2010) 8–11.
[10.15] LUINI, A., et al., Comparison of radio-guided excision with wire localization of occult breast lesions, Br. J. Surg. **86** (1999) 522–525.
[10.16] BONI, G., et al., Gamma probe-guided thoracoscopic surgery of small pulmonary nodules, Tumouri **86** (2000) 364–366.
[10.17] CHELLA, A., et al., A pilot study of the role of Tc-99m radionuclide in localization of pulmonary nodular lesions for thoracoscopic resection, Eur. J. Cardiothorac. Surg. **18** (2000) 17–21.
[10.18] AMBROGI, M.C., et al., A strategy for thoracoscopic resection of small pulmonary nodules, Surg. Endosc. **19** (2005) 1644–1647.
[10.19] CIRIACO, P., et al., Video-assisted thoracoscopic surgery for pulmonary nodules: Rationale for preoperative computed tomography-guided hookwire localization, Eur. J. Cardiothorac. Surg. **25** (2004) 429–433.
[10.20] ESSNER, R., et al., Application of an [^{18}F]fluorodeoxyglucose-sensitive probe for the intraoperative detection of malignancy, J. Surg. Res. **96** (2001) 120–126.

[10.21] ZERVOS, E.E., DESAI, D.C., DEPALATIS, L.R., SOBLE, D., MARTIN, E.W., ^{18}F-labeled fluorodeoxyglucose positron emission tomography-guided surgery for recurrent colorectal cancer: A feasibility study, J. Surg. Res. **97** (2001) 9–13.

[10.22] MELLER, B., et al., Conventional gamma and high energy probe for radio-guided dissection of metastases in a patient with recurrent thyroid carcinoma with ^{99m}Tc-MIBI and ^{18}F-FDG, Nuklearmed. **44** (2005) 23–25.

[10.23] MANCA, G., et al., Simultaneous detection of breast tumour resection margins and radio-guided sentinel node biopsy using an intraoperative electronically-collimated probe with variable energy window: A case report, Clin. Nucl. Med. **36** (2011) 196–198.

[10.24] BONI, G., et al., ^{99m}Tc-depreotide in the surgical patients with pulmonary malignancy: Correlation between scintigraphic data and intrasurgical findings [Abstract], Q. J. Nucl. Med. **48** (2004) 43.

[10.25] BONI, G., et al., Clinical utility ^{99m}Tc-depreotide as diagnostic procedure and intraoperative marker for radio-guided surgery in patients with pulmonary malignancy, Eur. J. Nucl. Med. Mol. Imaging **32** (2005) 49–50.

[10.26] TSIM, S., O'DOWD, C.A., MILROY, R., DAVIDSON, S., Staging of non-small cell lung cancer (NSCLC): A review, Respir. Med. **104** (2010) 1767–1774.

[10.27] KELLER, S.M., ADAK, S., WAGNER, H., JOHNSON, D.H., Mediastinal lymph node dissection improves survival in patients with stages II and IIIa non-small cell lung cancer, Eastern Cooperative Oncology Group, Ann. Thorac. Surg. **70** (2000) 358–366.

[10.28] ALLEN, M.S., et al., Morbidity and mortality of major pulmonary resections in patients with early-stage lung cancer: Initial results of the randomized, prospective ACOSOG Z0030 trial, Ann. Thorac. Surg. **81** (2006) 1013–1020.

[10.29] LIPTAY, M.J., et al., Intraoperative sentinel lymph node mapping in non-small-cell lung cancer improves detection of micrometastases, J. Clin. Oncol. **20** (2002) 1984–1988.

[10.30] RIQUET, M., MANAC'H, D., LE PIMPEC-BARTHES, F., DUJON, A., CHEHAB, A., Prognostic significance of surgical-pathologic N1 disease in non-small cell carcinoma of the lung, Ann. Thorac. Surg. **67** (1999) 1572–1576.

[10.31] LITTLE, A.G., DEHOYOS, A., KIRGAN, D.M., ARCOMANO, T.R., MURRAY, K.D., Intraoperative lymphatic mapping for non-small cell lung cancer: The sentinel node technique, J. Thorac. Cardiovasc. Surg. **117** (1999) 220–224.

[10.32] NOMORI, H., et al., Use of technetium-99m tin colloid for sentinel lymph node identification in non-small cell lung cancer, J. Thorac. Cardiovasc. Surg. **124** (2002) 486–492.

[10.33] SUGI, K., FUKUDA, M., NAKAMURA, H., KANEDA, Y., Comparison of three tracers for detecting sentinel lymph nodes in patients with clinical N0 lung cancer, Lung Cancer **39** (2003) 37–40.

[10.34] MELFI, F.M., et al., Intraoperative radio-guided sentinel lymph node biopsy in non-small cell lung cancer, Eur. J. Cardiothorac. Surg. **23** (2003) 214–220.

[10.35] LARDINOIS, D., et al., Bronchoscopic radioisotope injection for sentinel lymph-node mapping in potentially resectable non-small-cell lung cancer, Eur. J. Cardiothorac. Surg. **23** (2003) 824–827.
[10.36] EVEN-SAPIR, E., et al., Lymphoscintigraphy for sentinel node mapping using a hybrid SPECT/CT system, J. Nucl. Med. **44** (2003) 1413–1420.
[10.37] WAGNER, A., et al., SPECT-CT for topographic mapping of sentinel lymph nodes prior to gamma probe-guided biopsy in head and neck squamous cell carcinoma, J. Craniomaxillofac. Surg. **32** (2004) 343–349.
[10.38] TERADA, A., et al., Sentinel lymph node radiolocalization in clinically negative neck oral cancer, Head Neck **28** (2006) 114–120.
[10.39] COVARELLI, P., et al., The single-photon emission computed tomography/computed tomography: A new procedure to perform the sentinel node biopsy in patients with head and neck melanoma, Melanoma Res. **17** (2007) 323–328.
[10.40] VAN DER PLOEG, I.M., et al., The yield of SPECT/CT for anatomical lymphatic mapping inpatients with melanoma, Ann. Surg. Oncol. **16** (2009) 1537–1542.
[10.41] MINAMIYA, Y., OGAWA, J., The current status of sentinel lymph node mapping in non-small cell lung cancer, Ann. Thorac. Cardiovasc. Surg. **11** (2005) 67–72.

11. GOSTT APPLICATIONS IN MALIGNANCIES OF THE GASTROINTESTINAL TRACT

11.1. INTRODUCTION

The concept of radioguided surgery, or better, of the complex of procedures encompassed by the term GOSTT, has tremendously expanded over the last few years, and has evolved into what is now considered an established discipline within the practice of surgery, where it has revolutionized the surgical management of many malignancies, including gastrointestinal cancer.

The basic and advanced nuclear medicine procedures required for providing a road map in gastrointestinal surgery, with the help of an intraoperative gamma detection probe aided, or not, with the use of a dedicated small FOV gamma camera, include the use of radiolabelled MAbs (for radioimmunoguided surgery (RIGS)), of receptor based radiopharmaceuticals (e.g. OctreoScan), of metabolic agents labelled with positron emitting radionuclides (e.g. [^{18}F]FDG), of ^{99m}Tc MAAs to be injected intralesionally (for intraoperative localization of occult lesions) and of radiocolloids (for lymphoscintigraphy and SLNB).

11.2. RIGS

In the mid-1970s, crucial advances in immunology led to widespread interest in the development of MAbs that could be radiolabelled for performing immunoscintigraphy of primary or secondary tumours. The availability of these radiolabelled tumour seeking agents constituted the first step towards RIGS, as pioneered by Martin and Carey [11.1] in patients with colorectal cancer. It was actually their experience that guided the development of dedicated hand-held gamma probes for intraoperative guidance based on count rates, resulting in considerably improved intraoperative sensitivity over external radioimmunodetection.

In the early 1990s, the development of second generation MAbs specifically for colon cancer led to further improvements in RIGS for patients with this malignancy. Subsequent pilot clinical studies revealed efficient tumour localization in 86% of patients with primary colorectal cancer and in 97% of patients with recurrent disease [11.2].

These encouraging results indicated that the application of RIGS in patients with primary or recurrent colorectal cancer might yield clinically relevant information regarding the pattern of disease, especially if performing

immunohistochemical staining of RIGS positive LNs with anticytokeratin MAbs to increase the likelihood of identifying occult tumour cells in these nodes [11.2].

Most of the clinical trials for RIGS in colorectal cancer have utilized an antiTAG-72 MAb labelled with ^{125}I. AntiTAG-72 MAbs have evolved from first generation ^{125}I labelled murine B72.3 MAbs to second generation ^{125}I labelled murine CC49 MAbs, and finally to third generation ^{125}I labelled humanized CC49 MAbs [11.3].

11.3. RIGS WITH THE B72.3 MURINE MAb

In 1991, Martin and Carey [11.1] reported the impact of the RIGS approach in a group of 86 patients with recurrent colorectal cancer undergoing a second look procedure. In particular, while 53 patients (62%) were deemed resectable by traditional evaluation, only 40 patients (47%) turned out to be actually resectable using RIGS. Retroperitoneal disease was a common finding for RIGS non-resectability. Two, three, four and five year survival data were reported for three stratifications of patients: RIGS resectable (n = 40), traditional non-resectable (n = 33) and RIGS non-resectable (n = 13). Overall survival rate for the RIGS resectable group was 83%, versus 21% and 31% for the traditional non-resectable and RIGS non-resectable groups, respectively. Significant differences in survival were observed in the RIGS resectable versus traditional non-resectable ($P < 0.0001$), as well as in RIGS resectable versus RIGS non-resectable ($P < 0.0008$); difference in survival was not significant between the traditional non-resectable versus RIGS non-resectable patients ($P = 0.24$).

Several subsequent clinical trials [11.4–11.10] have confirmed and somewhat extended the original observations reported by Martin and Carey [11.1], employing either the same B72.3 MAb, the second generation antiTAG-72 CC49 MAb (including a humanized version) or the antiCEA F023C5 MAb, with all such agents being radiolabelled with ^{125}I (see Table 11.1). In the different trials, clinical outcome of RIGS has been assessed either based on changes in surgical strategy based on RIGS findings, on differences in classification of patients as to resectability or non-resectability of tumour lesions (by conventional criteria and by RIGS findings, respectively), or on differences in overall survival according to classification of patients (by conventional criteria and by RIGS findings, respectively). Overall, changes in surgical strategy and in classification as to disease free status have had a relevant clinical impact on a proportion of patients ranging between approximately 10% and 30%, while differences in survival have reached very high levels of statistical significance (with P values between 0.0001 and 0.0008) (see Table 11.1).

TABLE 11.1. SUMMARY OF THE MAIN RESULTS OF CLINICAL TRIALS WITH RIGS IN PATIENTS WITH PRIMARY AND/OR RECURRENT COLORECTAL CANCER

Reference	Recurrent tumour (*n*)	Primary tumour (*n*)	B72.3	MAb CC49	(*n*) F023C5	Clinical impact [a]
Martin and Carey [11.1]	86	—	86	—	—	13/53 (24.5%) $P < 0.0001/0.0008$ for survival
Cohen et al. [11.4]	72	32	104	—	—	3/30 (10%)
Arnold et al. [11.7]	—	31	—	31	—	10/37 (27%) $P < 0.0001$ for survival
Bertsch et al. [11.9]	131	—	86	45	—	$P < 0.0001$ for survival
Bertoglio et al. [11.5]	16	—	16	—	—	5/16 (31.3%)
Percivale et al. [11.6]	64	—	30	—	34	7/30 (23.3%) 3/34 (8.8%)
Arnold et al. [11.10]	—	97	—	97(HU)	—	$P < 0.0002$ for survival

[a] Clinical impact is represented either by change in surgical strategy based on RIGS findings, by difference in classification as to resectability by conventional criteria and by RIGS, or by difference in survival between patients classified as disease free based on conventional criteria or on RIGS findings.

A modified RIGS approach has been reported, based on administration of the antiCEA MAb ^{99m}Tc arcitumomab [11.11], performing surgery within 24 h after intravenous administration rather than 20–24 d post-administration when employing the ^{125}I labelled MAbs described above. This approach has been employed in a total of 25 patients, and the clinical benefit of RIGS in this setting has been described, although the study was more exploratory in nature rather than a carefully designed prospective study.

Unlike investigations of colorectal cancer, only a single report has been published, in 1997, on RIGS in patients with pancreatic cancer. LaValle et al. [11.12], from Ohio State University, assessed the extent of disease in ten patients with pancreatic adenocarcinoma that were deemed resectable by pre-operative CT scan. Each patient received 74 MBq (2 mCi) of ^{125}I CC49 MAb and then underwent surgery after precordial counting with the gamma probe revealed adequate clearance of the blood pool background (mean 26.1 d, range 7–35 d). Traditional assessment of the abdomen was compared to RIGS assessment. Three patients underwent pancreatic resection for locoregional disease. The other seven patients had visceral metastases, carcinomatosis or both, detected at the time of laparotomy. All sites suspicious for tumours using traditional assessment of the abdomen were found to be RIGS positive. Previously unknown pancreatic adenocarcinoma identified only by RIGS assessment was found to be disseminated to both the abdominal viscera and lymphatics. RIGS detected significantly more total sites (viscera and lymphatics) of metastatic disease than traditional assessment (73 sites versus 31 sites for RIGS versus traditional assessment, $P < 0.05$), with the greatest difference being observed for dissemination to the lymphatics (44 sites versus 6 sites for RIGS versus traditional assessment, $P < 0.001$). Despite these very encouraging early results, no further work has been done on RIGS for pancreatic cancer.

Although the conceptually simple technique of RIGS has been investigated and refined for almost 30 years, it still has inherent limitations. Scarce availability of specific MAbs has been overcome only in selected cases, such as colorectal cancer; in the majority of all remaining tumours, the efficacy of RIGS remains uncertain. Other critical issues, such as choice of the radionuclide to label the MAb, are still controversial. Thus, the initial enthusiasm generated by early results with RIGS has been dampened over the past decade. Growing knowledge of antigen–antibody relationships and the development of new and superior tumour targeting agents might constitute the basis for future further advances with RIGS as a predictor of long term survival in colorectal cancer patients.

11.4. [FLUORINE-18]FDG DIRECTED SURGERY

The most recent application of intraoperative gamma counting probe for radioguided surgery in colorectal cancer is represented by identification of [^{18}F]FDG avid tumours. This technique was first described by Desai et al. [11.13, 11.14] at Ohio State University. Fourteen colorectal cancer patients received [^{18}F]FDG intravenously (148–211 MBq (4.0–5.7 mCi)) 58–110 min prior to intraoperative evaluation with a high energy collimated gamma detection probe. Single or multiple tumour foci were correctly identified in 13 out of 14 patients, using the gamma detection probe, as [^{18}F]FDG avid tissue, and this was correlated with hypermetabolic activity on prior pre-operative diagnostic [^{18}F]FDG PET imaging. Those observations have been further confirmed by several other clinical reports [11.15–11.19]. Most recently, a combined approach of pre-operative diagnostic [^{18}F]FDG PET imaging and intraoperative gamma probe detection has been advocated to potentially provide the surgeon with a real time, intraoperative road map for accurately locating and determining the extent of tumour recurrence in patients with colorectal cancer [11.18]. In this series, patients received an average of 370–555 MBq (10–15 mCi) of [^{18}F]FDG 30–60 min prior to intraoperative evaluation using the gamma detection probe. It was found that intraoperative evaluation using the gamma detection probe was more sensitive in detecting the extent of abdominal and pelvic recurrence, while pre-operative [^{18}F]FDG PET imaging was more sensitive in detecting liver metastases and other distant metastases [11.18].

The use of [^{18}F]FDG directed surgery for the surgical management of gastric cancer has been described in a few reports. Gulec et al. [11.19] reported on a single case of gastric cancer in which [^{18}F]FDG directed surgery helped to identify and resect a hypermetabolic metastatic LN during gastrectomy and extended node dissection. Piert et al. [11.20] reported on the use of [^{18}F]FDG directed surgery in three patients with gastric adenocarcinomas and two with adenocarcinoma of the gastroesophageal junction.

11.5. RADIOGUIDED LOCALIZATION OF OCCULT COLONIC LESIONS

During both open surgery and laparoscopic surgery, difficulties can be encountered when resecting small polyps, residual tumour tissue after incomplete endoscopic excisional biopsies, small lesions located in the right or left colonic flexure, in the presence of perivisceritis, etc. Traditionally, these difficulties are approached by marking the site(s) to be resected (or their margins) either with tattoos or with metallic clips placed during endoscopy. In addition to possible

complications (especially when employing metallic clips), these markings are not always easily identified during surgery.

Experience is now starting to accumulate on the use of intraoperative guidance with a gamma probe (usually designed specifically for laparoscopic use) following endoscopic intralesional ^{99m}Tc MAA injection performed a few hours before surgery. Although the reports published so far are only preliminary (42 patients in two separate studies) [11.21, 11.22], the results obtained with this procedure of radioguided surgery for the intraoperative localization of occult colonic lesions consistently show extremely high rates of surgical success (100%) and contribute to reducing as much as possible the invasiveness of surgical procedures as well as the overall duration of surgery. Extremely similar results have been independently obtained by the University of Pisa, Italy (nuclear medicine and general surgery teams) in 12 patients with colonic lesions (unpublished data).

11.6. SLNB FOR TUMOURS OF THE GASTROINTESTINAL TRACT

Both blue dye and radiocolloids are used for SLNM and SLNB in patients with cancer of the gastrointestinal tract. Interstitial injection is performed either submucosally around the tumour (during endoscopy prior to surgery) or subserosally (during open or laparoscopic surgery) [11.23].

In oesophageal cancer, a close correlation has been found between the number of SLNs (identified using ^{99m}Tc labelled rhenium sulphide), LN status, pathological stage and number of metastatic nodes. SLNB is especially useful in minimally invasive surgery. LN status is the most powerful prognostic factor in oesophageal cancer, and accurate staging is necessary to distinguish potentially curable patients from those with locally advanced disease. In particular, although oesophagectomy remains the standard of care in early stage tumours (stages I and IIA), its role is being questioned in patients with locally advanced disease (stages IIB and III) because of the generally poor outcomes following surgical resection alone. The overall 5 year survival rate for patients with oesophageal cancer is 20%–25% (60%–70% for patients with stage I disease, 5%–10% for patients with stage III disease). SPEC/CT imaging optimizes pre-operative lymphatic mapping as it can visualize multiple routes of lymphatic drainage, especially if the tumour is located at a junction.

In Japan, the high incidence of gastric cancer has led to special emphasis on the exploration of the value of SLNB for patients with this type of tumour. The standard treatment for early cases is gastrectomy with en bloc LN dissection. Lymphatic mapping has disclosed unexpected and/or aberrant sites of drainage, thus guiding surgeons to perform a regional dissection approach tailored to the

individual patient. Both conventional histochemistry and molecular biology techniques have been applied in the search for micrometastatic involvement of the SLN(s) [11.23].

Multiple reports exist on the feasibility of radioguided SLNB for gastric cancer [11.24]. Many of these reports from eastern Asia specifically describe a purely laparoscopic approach to radioguided SLNB in the treatment of cases with early stage gastric cancer [11.23]. Most frequently, ^{99m}Tc tin colloid has been used for lymphoscintigraphy, especially in eastern Asia. However, ^{99m}Tc colloidal rhenium sulphide, ^{99m}Tc sulphur colloid and ^{99m}Tc nanocolloidal albumin have also been employed. These radiocolloids are generally injected endoscopically in up to four submucosal sites around the tumour between 2 h and 24 h before surgery. The two largest series reported so far are by Kitagawa et al. [11.25] and Uenosono et al. [11.26]. In 2002, Kitagawa et al. [11.25] identified at least one SLN in 138 out of 145 patients (95.2%) with presumed cT1N0 or cT2N0 gastric cancer. The SLN was positive in 22 out of 24 patients who had LN metastases, thus demonstrating a 98.6% accuracy in the assessment of the regional LN status on the basis of the SLN status. In 2005, Uenosono et al. [11.26] identified SLN(s) in 99 out of 104 patients (95.2%) with presumed cT1 or cT2 gastric cancer. Excluding three technical failures in radiocolloid injection, the identification rates were 99% (78/79) and 95% (21/22) for cT1 and cT2 lesions, respectively. LN metastases and/or micrometastases were found in 28 patients (15 cT1 and 13 cT2), and the resultant false negative rate, sensitivity and accuracy were significantly better for cT1 tumours than for cT2 tumours ($P < 0.001$, $P = 0.004$ and $P < 0.001$, respectively). While the possibility exists for radioguided SLNB to help to individualize the surgical approach for patients with early stage gastric cancer, additional studies are required to evaluate its actual clinical impact.

Aberrant lymph drainage, leading to modification of the intended surgical approach, can be identified in as many as 5%–8% of the patients with colorectal cancer. SLNM and SLN analysis performed using molecular biology techniques can detect micrometastases in up to 14% of the cases, thus identifying a subgroup of patients who can benefit from adjuvant chemotherapy. In a study of 492 consecutive patients (401 with colon cancer and 91 with rectal cancer), the overall success rate for radioguided SLN identification was 97.8%, with most of the failures occurring in rectal cancers (8.8% of the cases versus 0.7% for colon cancer), most likely because of local submucosal lymphatic fibrosis induced by neoadjuvant radiation therapy administered prior to surgery [11.27]. The overall accuracy rate for predicting LN metastases was 95.4% (with 89.3% sensitivity), while the overall incidence of skip metastasis was 10.9%. A minimum number of LNs must be assessed for accurate staging of patients with colorectal cancer, as nodal status (the number of nodes resected and the presence of micrometastases) is crucial for planning treatment after primary surgery. Inadequate retrieval and

assessment of SLNs is associated with a worse outcome (e.g. in stage II patients) [11.28]. Although SLNM per se (either with blue dye or radiocolloids) does not generally modify the surgical procedure (which usually follows standardized protocols), it does identify the crucial node(s) to be submitted for extensive analysis with sophisticated laboratory techniques searching for micrometastases. Adjuvant chemotherapy is performed in the positive cases. The lymphotropic agents are most frequently injected subserosally during open surgery, with a specificity approaching 100% when using the blue dye, and during laparoscopic procedures [11.28]. Submucosal injection is generally performed during endoscopy prior to surgery, and the use of radiocolloids is increasing versus the use of blue dye. Also in this case, SPECT/CT imaging improves pre-operative localization of SLNs.

The potential advantages of SLNM for patients with colorectal cancers and malignant polyps are less obvious than for those with breast cancer or melanoma, and the procedure is generally performed in strictly controlled clinical trials.

The application of the gamma detection probe in radioguided surgery for anal cancer has been limited to radioguided SLNB [11.29–11.36]. In general, ^{99m}Tc sulphur colloid, ^{99m}Tc nanocolloidal human albumin, ^{99m}Tc colloidal rhenium sulphide and ^{99m}Tc antimony trisulphide colloid have been utilized; four subdermal or submucosal injections are performed around the primary tumour, with a total administered activity ranging from 5 MBq to 37 MBq (0.135–1 mCi). SLN visualization was generally demonstrated in 75%–100% of the patients with anal cancer. There were three common pathways of lymphatic drainage (including drainage to inguinal, iliac and mesorectal lymphatic basins) and the very frequent finding of bilateral lymphatic drainage emphasizes the importance of pre-operative lymphoscintigraphy for most effectively performing radioguided SLNB in anal cancer. The inguinal region was the predominant lymphatic drainage pathway, representing the most accessible site of localization to perform a minimally invasive radioguided SLNB procedure. Radioguided SLNB in the inguinal region was useful in identifying inguinal LN metastases in approximately 10%–40% of such patients. However, there is yet to be a large scale prospective clinical trial to assess the clinical efficacy of radioguided SLNB in anal cancer.

REFERENCES TO CHAPTER 11

[11.1] MARTIN, E.W., CAREY, L.C., Jr., Second-look surgery for colorectal cancer, Ann. Surg. **214** (1991) 321–327.

[11.2] POVOSKI, S., et al., A comprehensive overview of radio-guided surgery using gamma detection probe technology, World J. Surg. Oncol. **7** (2009) 1–67.

[11.3] SUN, D., et al., Radioimmunoguided surgery (RIGS), PET/CT image-guided surgery, and fluorescence image-guided surgery: Past, present, and future, J. Surg. Oncol. **96** (2007) 297–308.
[11.4] COHEN, A.M., et al., Radioimmunoguided surgery using iodine125 B72.3 in patients with colorectal cancer, Arch. Surg. **126** (1991) 349–352.
[11.5] BERTOGLIO, S., et al., Radioimmunoguided surgery benefits in carcinoembryonic antigen-directed second-look surgery in the asymptomatic patient after curative resection of colorectal cancer, Semin. Surg. Oncol. **15** (1998) 263–267.
[11.6] PERCIVALE, P., et al., Radioimmunoguided surgery with different iodine-125 radiolabeled monoclonal antibodies in recurrent colorectal cancer, Semin. Surg. Oncol. **15** (1998) 231–234.
[11.7] ARNOLD, M.W., YOUNG, D.C., HITCHCOCK, C.L., SCHNEEBAUM, S., MARTIN, E.W., Jr., Radioimmunoguided surgery in primary colorectal carcinoma: An intraoperative prognostic tool and adjuvant to traditional staging, Am. J. Surg. **170** (1995) 315–318.
[11.8] MURARO, R., et al., Generation and characterization of B72.3 second generation monoclonal antibodies reactive with the tumour-associated glycoprotein 72 antigen, Cancer Res. **48** (1988) 4588–4596.
[11.9] BERTSCH, D.J., BURAK, W.E., YOUNG, D.C., ARNOLD, M.W., MARTIN, E.W., Jr., Radioimmunoguided surgery improves survival for patients recurrent colorectal cancer, Surg. **118** (1995) 634–638.
[11.10] ARNOLD, M.W., et al., Staging of colorectal cancer: Biology vs. morphology, Dis. Colon Rectum **41** (1998) 1–6.
[11.11] GIOFFRÈ FLORIO, M.A., et al., Personal experience using radioimmunoguided surgery (RIGS), Ann. Ital. Chir. **78** (2007) 433–437.
[11.12] LaVALLE, G.J., MARTÍNEZ, D.A., SOBEL, D., DEYOUNG, B., MARTIN, E.W., Jr., Assessment of disseminated pancreatic cancer: A comparison of traditional exploratory laparotomy and radioimmunoguided surgery, Surgery **122** (1997) 867–873.
[11.13] DESAI, D.C., et al., Intraoperative gamma detection of FDG distribution in colorectal cancer, Clin. Positron Imaging **2** (1999) 325.
[11.14] DESAI, D.C., et al., Correlative whole-body FDG-PET and intraoperative gamma detection of FDG distribution in colorectal cancer, Clin. Positron Imaging **3** (2000) 189–196.
[11.15] ZERVOS, E.E., DESAI, D.C., DEPALATIS, L.R., SOBLE, D., MARTIN, E.W., ^{18}F-labeled fluorodeoxyglucose positron emission tomography-guided surgery for recurrent colorectal cancer: A feasibility study, J. Surg. Res. **97** (2001) 9–13.
[11.16] ESSNER, R., et al., Application of an [^{18}F]fluorodeoxyglucose-sensitive probe for the intraoperative detection of malignancy, J. Surg. Res. **96** (2001) 120–126.
[11.17] ESSNER, R., DAGHIGHIAN, F., GIULIANO, A.E., Advances in FDG PET probes in surgical oncology, Cancer **8** (2002) 100–108.
[11.18] SARIKAYA, I., et al., Combined use of preoperative ^{18}F FDG-PET imaging and intraoperative gamma probe detection for accurate assessment of tumour recurrence in patients with colorectal cancer, World J. Surg. Oncol. **5** (2007) 80.

[11.19] GULEC, S.A., PET probe-guided surgery, J. Surg. Oncol. **96** (2007) 353–357.
[11.20] PIERT, M., et al., Positron detection for the intraoperative localisation of cancer deposits, Eur. J. Nucl. Med. Mol. Imaging **34** (2007) 1534–1544.
[11.21] REZZO, R., SCOPINARO, G., GAMBARO, M., MICHETTI, P., ANFOSSI, G., Radio-guided occult colonic lesion identification (ROCLI) during open and laparoscopic surgery, Tumouri **88** (2002) 19–22.
[11.22] D'ANNIBALE, A., SERVENTI, A., ORSINI, C., MORPURGO, E., Locating polyps by endoscopy with or without videolaparoscopy, radio-guided occult colonic lesion identification or magnetic endoscopic imaging: The way forward to complete polyp removal, Tech. Coloproctol. **8** (2004) 295–299.
[11.23] KITAGAWA, Y., FUJII, H., MUKAI, M., KUBO, A., KITAJIMA, M., "Sentinel lymph node mapping in esophageal and gastric cancer", Selective Sentinel Lymphadenectomy for Human Solid Cancer, Vol. 127 (LEONG, S., KITAJIMA, M., KITAGAWA, Y., Eds), Springer (2005) 123–139.
[11.24] GRETSCHEL, S., et al., Efficacy of different technical procedures for sentinel lymph node biopsy in gastric cancer staging, Ann. Surg. Oncol. **14** (2007) 2028–2035.
[11.25] KITAGAWA, Y., et al., Radio-guided sentinel node detection for gastric cancer, Br. J. Surg. **89** (2002) 604–608.
[11.26] UENOSONO, Y., et al., Detection of sentinel nodes and micrometastases using radioisotope navigation and immunohistochemistry in patients with gastric cancer, Br. J. Surg. **92** (2005) 886–889.
[11.27] BILCHIK, A., et al., Aberrant drainage of missed micrometastases: The value of lymphatic mapping and focused analysis of sentinel lymph nodes in gastrointestinal neoplasms, Ann. Surg. Oncol. **8** (2001) 82–85.
[11.28] SAHA, S., DAN, A.G., VIEHL, C.T., ZUBER, M., "Sentinel lymph node mapping in colon and rectal cancer: its impact on staging, limitations, and pitfalls", Selective Sentinel Lymphadenectomy for Human Solid Cancer, Vol. 127 (LEONG, S., KITAJIMA, M., KITAGAWA, Y., Eds), Springer (2005) 105–122.
[11.29] KESHTGAR, M.R., AMIN, A., TAYLOR, I., ELL, P.J., The sentinel node in anal carcinoma, Eur. J. Surg. Oncol. **27** (2001) 113–114.
[11.30] RABBITT, P., PATHMA-NATHAN, N., COLLINSON, T., HEWETT, P., RIEGER, N., Sentinel lymph node biopsy for squamous cell carcinoma of the anal canal, ANZ J. Surg. **72** (2002) 651–654.
[11.31] PÉLEY, G., et al., Inguinal sentinel lymph node biopsy for staging anal cancer, Scand. J. Surg. **91** (2002) 336–338.
[11.32] PERERA, D., PATHMA-NATHAN, N., RABBITT, P., HEWETT, P., RIEGER, N., Sentinel node biopsy for squamous-cell carcinoma of the anus and anal margin, Dis. Colon Rectum **46** (2003) 1027–1031.
[11.33] ULMER, C., et al., Sentinel node biopsy in anal cancer — a promising strategy to individualize therapy, Onkologie **26** (2003) 456–460.
[11.34] DAMIN, D.C., ROSITO, M.A., SCHWARTSMANN, G., Sentinel lymph node in carcinoma of the anal canal: A review, Eur. J. Surg. Oncol. **32** (2006) 247–252.

[11.35] GRETSCHEL, S., et al., Lymphatic mapping and sentinel lymph node biopsy in epidermoid carcinoma of the anal canal, Eur. J. Surg. Oncol. **34** (2008) 890–894.
[11.36] MISTRANGELO, M., et al., Feasibility of the sentinel node biopsy in anal cancer, Q. J. Nucl. Med. Mol. Imaging **53** (2009) 3–8.

12. GOSTT IN MALIGNANCIES OF THE FEMALE REPRODUCTIVE SYSTEM

12.1. CERVICAL CANCER

12.1.1. Introduction

Cervical cancer is the third most frequent gynaecological cancer and the primary cause of death in women of child bearing age [12.1]. It mainly spreads locally to adjacent pelvic organs, but can also spread lymphatically, and some rare cases of haematogenous spread to the lungs, liver, bones or brain have been reported. The most important prognostic factor is locoregional LN invasion, including the pelvic and para-aortic nodes [12.2, 12.3].

LN invasion is related to tumoural invasion of the lymphatic vascular space [12.4]. In stage Ia1 (microinvasive carcinoma), nodal invasion is approximately 1% [12.5]; therefore, hysterectomy without LDN is appropriate. In locally advanced cervical cancer, there is an incidence of nodal pelvic invasion of between 11.5% and 21% [12.6, 12.7], which decreases to 0.5%–7.3% when only stage Ia2 is considered [12.8]. In these early stages (Ia2–Ib1), treatment is radical hysterectomy and pelvic LDN, to confirm the nodal status and possible risk of para-aortic invasion. If there is a risk of developing nodal metastasis (i.e. depth of invasion or parametrial infiltration) or LN enlargement is seen on imaging, the treatment is primary chemoradiation.

Several studies confirm the orderly progression of metastatic disease. The most frequent location of pelvic nodal metastases is the obturator group, followed by the external iliac group [12.9]. Drainage will go to the pelvic nodes, the common iliac and finally the para-aortic nodes [12.6]. Para-aortic metastasis without pelvic invasion is rare [12.10–12.12].

Given the low rate of nodal invasion in locally advanced cervical cancer (Ia2–Ib1) and the orderly progression of the spread of the disease, there is a well established indication for SLNM in these cases. In addition to SLNM, SLNB plays an important role in this condition; in fact, if an SLN is positive at intraoperative histopathology, there is no need to complete surgery with hysterectomy because the appropriate treatment would be chemoradiation. Therefore, SLNB provides prognostic information on nodal status and can also help to avoid morbidity from unnecessary overtreatment.

SLNM starts with the peritumoural/periorificial injection of radiocolloid in the four quadrants of the cervix, using a 20 or 22 G spinal needle. The best detection rate is achieved using blue dye and radiocolloid, with a success rate of over 90% [12.13, 12.14]. This combination technique can detect SLNs more

frequently in the para-aortic region than a single marker [12.15]. The need for lymphoscintigraphy has, at times, been called into question [12.16], and the introduction of hybrid equipment (SPECT/CT) has clearly demonstrated an improvement in SLN detection (see Section 12.1.2). Moreover, lymphoscintigraphy provides a lymphatic mapping of the tumour and can detect unusual drainage patterns, such as drainage directed to the para-aortic or presacral LNs. Lymphoscintigraphy requires the acquisition of planar images in anterior and lateral views. Most medical centres obtain images at 30 min and 60–120 min after injection. The injection and images can be carried out the day before surgery or on the same day as surgery. The option of acquiring late planar images or a SPECT/CT study makes acquisition on the previous day more desirable.

It is important to consider SLN detection of each side independently, rather than carrying out an analysis per patient. There is a reduced number of false negative SLNs if LDN is performed on a side with no drainage [12.17], even in more advanced stages (Ib2–IIa) [12.18].

The usefulness of SLNM in cervical cancer has been evaluated in a large series of 507 women [12.14] and in reviews that comprise 831 patients [12.19]. A detection rate consistently greater than 90% (93.5%–96%) was found using the combined technique, with a high NPV (94%–97%) and a false negative rate of 8%. The most interesting result is the higher detection rate and NPV in tumours smaller than 2 cm (94% versus 84% for the detection rate and 99% versus 89% for NPV).

In summary, the benefits of SLNM and SLNB are a better knowledge of nodal status — owing to the detection of unusual drainage (to para-aortic or presacral nodes) patterns [12.20] and the possibility of ultrastaging, with the detection of micrometastases [12.21, 12.22] — and a reduction in morbidity. This morbidity would have been caused by unnecessary LDNs or overtreatment in patients who can be treated optimally with only chemoradiation after surgery, especially when SLNB is performed during laparoscopy. Patients who benefit most from this procedure are women with a cervical tumour smaller than 4 cm (with best results found in tumours of < 2 cm [12.4, 12.14]) and in early stage Ia2–Ib1. Exclusion criteria are: pregnancy, previous chemotherapy, previous pelvic LDN, and nodal or parametrial invasion detected by other imaging techniques. A prior cone biopsy is not a contraindication [12.14] because similar results to those in patients with no previous histories of intervention have been observed [12.23–12.25].

Some aspects that have yet to be clarified are the minimum number of patients required to validate this technique, the minimum number of patients needed for a learning curve and what would be the acceptable margin of false negative cases.

12.1.2. SPECT/CT imaging contribution to SLNM

Hybrid equipment combining functional imaging (SPECT) with anatomical information (CT) has come into use in the last decade. Application of these systems for SLNM has been widely developed in breast cancer, melanoma and head and neck tumours. SPECT/CT imaging provides a 3-D image with better spatial resolution and a more precise localization of the SLNs than planar imaging.

The information provided by planar images, with only anterior and lateral views of the pelvis, is limited. Instead, after reconstruction, cross-sectional slices of SPECT/CT imaging provide better spatial resolution and orientation and can be analysed for optimizing surgical planning.

There are very few studies involving the use of SPECT/CT imaging for SLNM in cervical cancer [12.20, 12.26–12.28], and they include small series of patients. The largest study was carried out by Martínez et al. [12.26] and comprised 41 patients. Results are, in general, heterogeneous. One study found a higher SLN detection rate compared with blue dye and hand-held probe detection [12.28], with an improvement in detection rates from 70% to 100%. On the other hand, Martínez et al. found greater sensitivity using the combined technique than by using SPECT or CT imaging alone (100% versus 95% detection rate) and suggested improved detection using contrast enhanced CT. SPECT/CT images are clearly useful in the detection of parametrial SLNs [12.26–12.28] and SLNs that are in unusual locations.

There is still some room for improvement in the technical details. First, a higher activity of radiocolloid is recommended when the acquisition is performed the day before surgery. Second, an adequate learning curve for SPECT/CT image interpretation should be considered by the surgical and nuclear team (Martínez et al. [12.26] found an increase in the detection of bilateral drainage from 39% to 55% after completion of the learning curve). Finally, it is important to consider each side as a separate LN area.

12.1.3. Added value of advancements in intraoperative imaging/localizing instrumentation

Recently, a new agent for SLNM has been tested in gynaecological malignancies, especially in cervical cancer; the new equipment employed to visualize this agent consists of a multispectral fluorescence camera that provides intraoperative visualization of the tracer. A fluorescent tracer (indocyanine green) is injected at the beginning of surgery and visualized during surgical examination of the pelvic region [12.29].

The use of PET imaging in the management of patients with cervical cancer is restricted to the initial staging of the disease and the diagnosis of recurrence. Few studies use this technique as an intraoperative tool, although there are two possible fields for development of this technology: PET/CT imaging as a guide for biopsy and the use of PET probes. PET guided surgery has been developed in ovarian cancer. The use of these devices is covered in more detail in Section 12.4.

Finding an active hypermetabolic mass of non-pathological size on PET/CT imaging is not uncommon, and the use of non-diagnostic non-contrast-enhanced CT imaging as a guide for needle biopsy is not possible. Tatli et al. [12.30] obtained successful results in 14 patients with the fusion of PET/CT and CT images obtained during the biopsy procedure.

12.2. ENDOMETRIAL CANCER

12.2.1. Introduction

Endometrial cancer is the most common malignancy of the female genital tract [12.31]. Pelvic or para-aortic node involvement denotes a worse prognosis, with a 5 year survival rate of between 44% and 52% [12.32]. In high grade endometrial cancer or in patients with a high risk tumour histology (clear cell or papillary serous), the standard of care is a surgical staging, including pelvic and para-aortic LDN. However, in low risk endometrial cancer, the incidence of nodal invasion is very low, and there is still no clear consensus for management. In some patients, a histological low grade classification is modified and increased after pathological examination of the whole tumour sample. In these cases, a prior surgical staging would have been of benefit. The diagnosis of nodal invasion can modify management, by indicating the need for adjuvant therapy.

The use of SLNM and SLNB can provide not only a surgical staging without increasing the number of complications frequently associated with complete LDN, but also ultrastaging owing to immunochemistry examination of the resected SLNs. Although several studies of SLN detection in endometrial cancer have been carried out, there is still not enough scientific evidence for validation of this procedure for routine clinical use (see Table 12.1). One of the most controversial aspects is the modality of radiocolloid injection.

Three different modalities of injection have been described in the literature: cervical injection, endometrial peritumoural injection assisted by hysteroscopy and myometrial/subserosal injection.

TABLE 12.1. SLN DETECTION IN ENDOMETRIAL CANCER

Reference	*n*	Injection site	Tracer	Surgery	Detection rate (%)	Lymphatic examination	FN (%)
Mais et al. [12.33]	34	Cervical	Blue	LSC versus LT	82 versus 41	—	—
Abu-Rustum et al. [12.34]	42	Cervical versus cervical + subserosal	RT / RT + blue	LSC or LT	86	Pelvic + PaAo	0
Robova et al. [12.35]	91	Subserosal versus HSC	RT + blue / RT	LT	73 versus 50	Pelvic + PaAo	—
Barranger et al. [12.36]	33	Cervical	RT + blue	LSC	81.8	—	0
Perrone et al. [12.37]	54	Cervical versus myometrial (HSC)	RT/RT	LSC	70 versus 65	Pelvic versus Pelvic + PaAo	—
Clement et al. [12.38]	5	HSC	RT + blue	LSC	40	Pelvic + PaAo	—
Ballester et al. [12.39]	46	Cervical	RT + blue	LSC	87	Pelvic + PaAo	0
Bats et al. [12.40]	43	Cervical	RT + blue	—	69.8	Pelvic	0
Delpech et al. [12.41]	23	—	RT + blue	LSC	82.6	—	0
Delaloye et al. [12.42]	60	HSC	RT + blue	LT	82	Pelvic + PaAo	0
Lopes et al. [12.43]	40	Myometrial	Blue	LT	77.5	—	4

TABLE 12.1. SLN DETECTION IN ENDOMETRIAL CANCER (cont.)

Reference	*n*	Injection site	Tracer	Surgery	Detection rate (%)	Lymphatic examination	FN (%)
Altgassen et al. [12.44]	25	Subserosal	Blue	—	92	—	NPV 92.5
Li et al. [12.45]	20	Subserosal	Blue	LT	75	Pelvic	0
Frumovitz et al. [12.46]	18	Subserosal (fundus)	RT + blue	LT	45	—	—
Dzvincuk et al. [12.47]	33	Cervical	RT	—	—	Pelvic + PaAo	0
Gien et al. [12.48]	16	Myometrial and/or Subserosal	Blue	LT	44	—	NPV 86

FN: false negative; HSC: hysteroscopy; LSC: laparoscopy; LT: laparotomy; NPV: negative predictive value; PaAo: para-aortic nodes; RT: radiotracer; SLN: sentinel lymph node; —: no data.

Cervical injection is the easiest type. It can be performed the day before surgery, thus allowing the acquisition of lymphoscintigraphic images following radiocolloid injection. In this regard, the use of radiocolloid mapping increases the possibility of detection using SPECT/CT imaging. Cervical injection is performed periorificially, as per cervical cancer, in four quadrants. The detection rate obtained is the highest out of the three injection modalities, and ranges from 70% to 87% [12.33, 12.36, 12.37, 12.39, 12.40]. One study has compared it to hysteroscopic injection [12.37] and has obtained better results than with cervical administration. Other studies have proposed adding a subserosal injection [12.49] or fundal injection [12.34], without, however, achieving higher SLN detection rates.

Endometrial injection during hysteroscopy allows direct infiltration of the radiocolloid around the tumour. The procedure can be performed at the beginning of surgery, although with this approach, it is not possible to perform lymphoscintigraphy with a large FOV gamma camera. The detection rate achieved using this modality of injection ranges between 40% and 65% [12.38, 12.42, 12.48].

Finally, injection in the corpus uteri in a myometrial or subserosal location results in detection rates between 45% and 92% [12.35, 12.44–12.46]. It can be performed during surgery and usually only the blue dye agent is injected. The number of injections seems to play an important role, with a minimum of three locations being required [12.46].

Until now, the largest series reported is that of Robova et al. [12.35], which includes 91 patients. They compared subserosal injection (both radiocolloid and blue dye) with hysteroscopic injection (radiocolloid only). The SLN detection rate was better with subserosal injection (73% versus 50%), but it was concluded that both modalities of injection provided results that were too poor to consider SLNM and SLNB performed using this approach to detection as an alternative to surgical staging in endometrial cancer.

In summary, SLNM and SLNB in endometrial cancer are not a standard of care. Although the results are promising, the lack of consensus over the best modality of injection does not permit standardization of the technique, which is therefore still in a validation phase.

12.2.2. SPECT/CT imaging contribution to SLNM

The deep location of the corpus uteri and its unique and complex lymphatic drainage pattern is probably responsible for a correlation of SLNM with surgical findings poorer than those observed for most other tumours [12.50].

Data on the use of SPECT/CT imaging for SLNM in endometrial cancer are still scarce (see Fig. 12.1). So far, Pandit-Taskar et al. [12.28] have reported

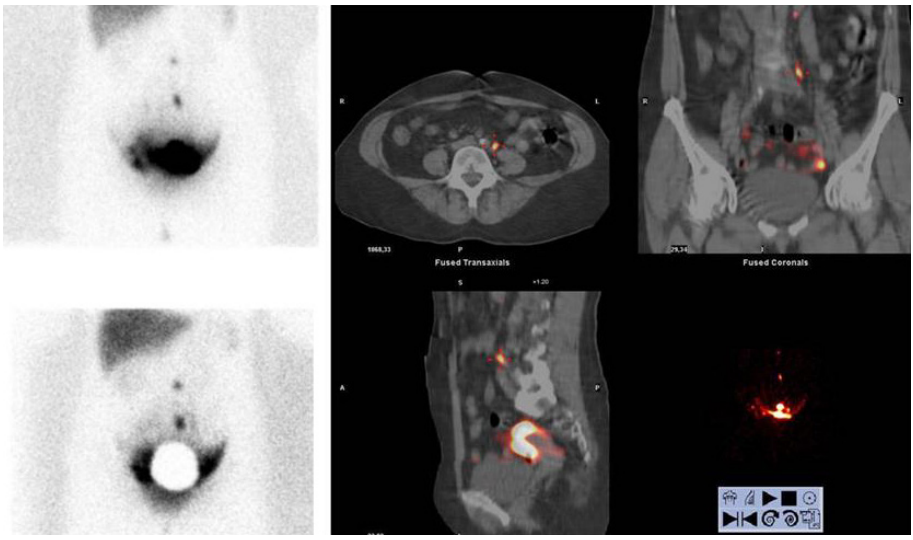

FIG. 12.1. SLNM in a patient with endometrial cancer. Planar images (early acquisition in upper left panel, late acquisition in lower left panel) show radiocolloid drainage to the left pelvis and para-aortic region. SPECT/CT images (right panels) more clearly depict lymphatic drainage to specific LN groups on both sides of the pelvis.

the largest series, which includes 40 patients. In 32 cases, the procedure was performed the day prior to surgery, and with this protocol, it was recommended to increase the activity of the radiocolloid injected to 148 MBq (4 mCi), to ensure a higher change of SLN detection. A higher detection rate was found using SPECT/CT imaging (100%) than when using planar lymphoscintigraphy (75%), the hand-held probe (93%) or blue dye alone (83%), and this emphasized the advantages of acquiring morphofunctional topographic information (as provided by hybrid SPECT/CT imaging) for detecting the para-aortic SLNs.

12.2.3. Added value of advancements in intraoperative imaging/localizing instrumentation

Recently introduced intraoperative instruments such as the portable gamma camera have been used in endometrial cancer, although with limited published results so far. Vidal-Sicart et al. [12.51] reported their findings in two cases of high risk endometrial cancer, three cases of cervical cancer (Fig. 12.2) and one patient with vulvar melanoma. The procedure of SLNM was performed as usual, but imaging was added by using a portable gamma camera during surgery as a complementary tool to aid SLN localization before resection. The use of a ^{153}Gd pointer in vulvar cancer or ^{125}I seeds in the other gynaecological

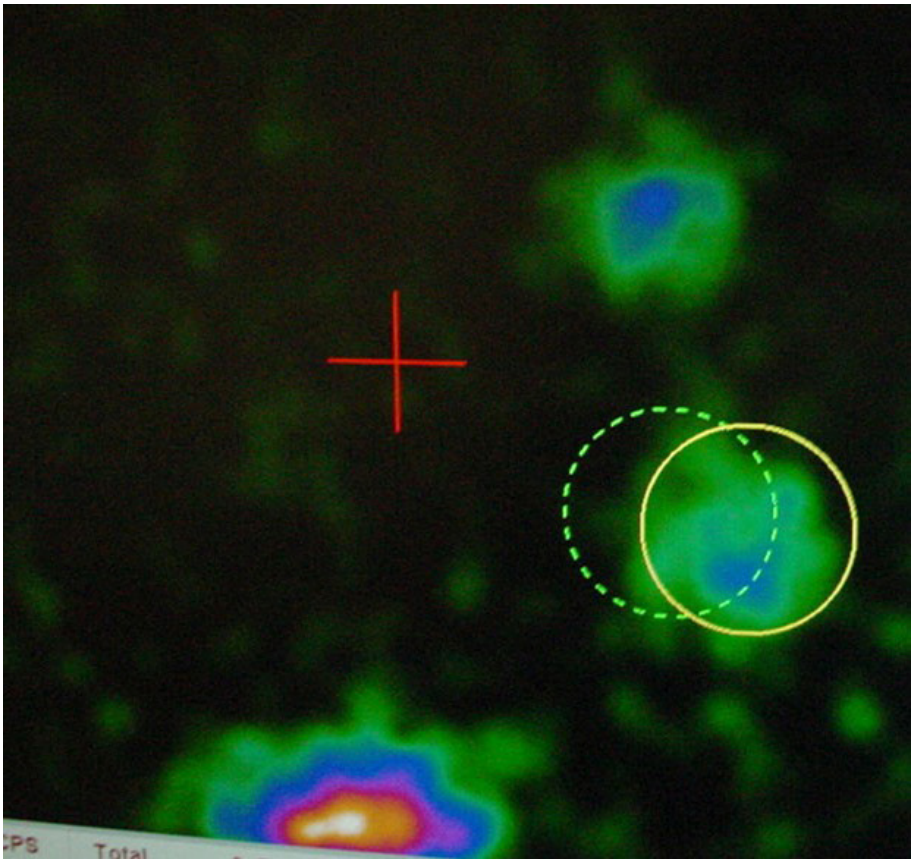

FIG. 12.2. Intraoperative image acquired using the portable gamma camera. The continuous circle indicates the SLN and the dotted circle denotes the ^{125}I seed.

malignancies confirmed correct SLN identification. After SLN removal, an additional image of the surgical field was acquired, to confirm successful resection (absence of any residual activity). The imaging procedure takes between 5 min (in vulvar and cervical cancer) and 15 min (in endometrial cancer); this represents a relatively minor portion of the overall surgical time. It was concluded that the use of the portable gamma camera was more helpful in parametrial nodes (because, in this location, the gamma probe suffers from interference of activity from the injection site) and in precaval nodes (where gamma probe counting suffers from liver interference). A detection rate of 92% (12 out of 13 SLNs) was reported when using the portable gamma camera versus 77% when using the hand-held gamma probe alone.

12.3. VULVAR CANCER

12.3.1. Introduction

Vulvar cancer is the least frequent malignancy of the female genital tract, and is responsible for only 0.3% of all cancer deaths in women [12.52]. Regional nodal status has an important prognostic value, as the 5 year survival rate decreases from 94.7% when the LNs are negative to 62% when they are positive [12.53]. When first diagnosed, 30% of cases show nodal invasion, with 10%–20% of these nodes being located in the pelvic area. When a tumour is confined to one side of the vulva, more than 80% of nodal metastases are ipsilateral. Treatment includes radical vulvectomy and inguinofemoral LDN, which are both associated with a high morbidity.

The superficial location of vulvar tumours makes the tracer injection for SLNM easier than in other gynaecological tumours, which is a factor that explains the large experience reported in this field. Table 12.2 [12.54–12.64] shows the most relevant studies published during the last decade. The largest series has been reported by Van der Zee et al. [12.54], with 403 patients. Inguinofemoral LDN was performed only when SLN invasion was confirmed by histopathology. The results obtained show reduced morbidity both in the short term (wound breakdown, cellulitis) and in the long term (lymphoedema) in patients who underwent SLNB alone (without completion of LDN because of a negative SLN status) versus patients in whom LDN was performed because the SLN was found to be metastatic.

Early studies in vulvar cancer were performed using blue dye as the sole agent, with a detection rate approaching 90% (86%–88%) [12.64]. However, the introduction of a radiocolloid improved the detection rate to 95%–100% [12.57, 12.58, 12.60, 12.61, 12.63]. The currently accepted methodology includes injection of both agents (radiocolloid and blue dye) after the application of an anaesthetic cream or spray such as lidocaine or ethyl chloride. Lymphoscintigraphy starts with a dynamic acquisition and planar images. SPECT/CT imaging is not widely used in these patients because drainage to deep lymphatic basins is less frequent than in other tumours. Although the vulva is a midline organ, the rate of unilateral drainage is quite high [12.61, 12.62]. While several groups avoid bilateral LDN when the tumour and its drainage are unilateral [12.61], other groups prefer to also perform complete contralateral LDN, to ensure that failure of detecting lymphatic drainage on one side was not because of lymph blockade caused by massive metastatic involvement of LNs. The advantages of performing SLNB over de novo LDN are reduced morbidity [12.54], possible upstaging and, according to one study, shortened surgical time [12.65].

TABLE 12.2. RESULTS OF SLNM AND SLNB IN VULVAR CANCER

Reference	*n*	Tracer	Stage	Unilateral (%)	LDN	Detection (%)	FN/NPV (%)
Lindell et al. [12.55]	77	RT + Bl	—	—	SLN + LDN	98	FN 2.7
Radziszewski et al. [12.56]	62	RT + Bl	I–II	NR	SLN + LDN	99	FN 6
Hampl et al. [12.57]	127	RT + Bl	T1–T3	16	SLN + LDN	98	FN 7.7
Johann et al. [12.58]	45	NR	T1,T2	NR	LDN when SLN +	95	FN 2.2
Van der Zee et al. [12.54]	403	RT + Bl	T1,T2 <4 cm	45	LDN when SLN +	—	—
Moore et al. [12.59]	36	RT + Bl	I–IV	—	LDN when SLN +	—	—
Hauspy et al. [12.60]	41	RT + Bl	I–II	54	SLN + LDN	95	FN 0
Vidal-Sicart et al. [12.61]	70	RT + Bl	Ib1–III	60	SLN + LDN (50), when SLN + (20)	97	VPN 100
Sliutz et al. [12.62]	26	RT + Bl	Early stage	77	SLN + LDN	100	FN 0
Sideri et al. [12.63]	44	RT	T1–T2	25	SLN + LDN	100	NPV 100
Levenback et al. [12.64]	52	Bl	T1–T2 (87%)	—	SLN + LDN	88	NPV 100

Bl: blue; FN: false negative; LDN: lymphadenectomy; NPV: negative predictive value; NR: not reported; RT: radiotracer; SLN: sentinel lymph node; SLNB: sentinel lymph node biopsy; SLNM: sentinel lymph node mapping; —: no data.

Well established indications for SLNM and SLNB as the standard of care in vulvar cancer include squamous cell carcinoma Ib–II less than 4 cm in size, without clinically obvious nodal metastases. Although the published experience is rather scarce, the indications for SLNB in vulvar melanoma are basically the same as for any other CM [12.66].

12.3.2. SLN detection in vaginal cancer

Although there are very few studies regarding SLNM in patients with vaginal cancer, they consistently report successful SLN detection [12.67–12.69]. Frumovitz et al. [12.70] performed lymphatic mapping with lymphoscintigraphy for radiotherapy planning in 14 patients. The pattern of lymphatic drainage in 79% of the patients was detected, with bilateral LNs in 55% of cases. The most frequent location was the inguinal basin (45%).

12.3.3. SPECT/CT imaging contribution to SLNM accuracy

The superficial location of vulvar cancer facilitates both radiocolloid injection and the surgical approach, as well as a fast and successful drainage to inguinofemoral nodes. In these cases, SPECT/CT imaging helps to identify the SLN location in a 3-D space, but does not help in surgical management or to increase the final number of detected SLNs. There are only three reported cases, all in vulvovaginal melanoma, where SLN detection with SPECT/CT imaging was higher than with gamma probe counting alone [12.71, 12.72].

12.3.4. Added value of advancements in intraoperative imaging/localizing instrumentation

Experience using the portable gamma camera was described in Section 12.2 on endometrial cancer.

The use of a multispectral fluorescence camera combined with injection of indocyanine as the lymphatic drainage agent has been reported in ten patients with vulvar cancer [12.29]. During surgery, a fluorescence camera allows visualization of the fluorescent tracer, thus precisely locating the SLN; the success rate of this approach was greater than with the blue dye (89% versus 72%).

12.4. OVARIAN CANCER

12.4.1. Introduction

The incidence of positive LNs in early stage ovarian cancer is low, ranging from 5.1% to 15% [12.73]. Pelvic and para-aortic LDN involves a rather long surgical time and possible morbidity. Therefore, SLNM should be considered in patients with ovarian cancer.

It is well known that capsular rupture of an ovarian cancer during surgery can lead to tumour spread in the abdominal cavity, and this can make injection of a lymphatic drainage agent around the tumour more difficult. Lymphatic mapping of epithelial ovarian tumours has been described by Negishi et al. [12.74]. They injected carbon particles in 11 patients diagnosed with endometrial or fallopian tubal cancer who were undergoing pelvic and para-aortic LDN to avoid tumoural spread, and showed bilateral lymphatic drainage in 64% patients. In all the cases, drainage occurred to para-aortic SLNs, while SLN location in the common iliac and the external iliac chains was observed in 26% and 9% of the cases, respectively.

12.4.2. Added value of advancements in intraoperative imaging/localizing instrumentation

The most relevant advancement in intraoperative instrumentation for ovarian cancer is the introduction of PET probes. In fact, the hypermetabolic pattern of ovarian cancer makes diagnosis and PET guided localization of recurrent masses feasible. Recurrent disease, which is easily diagnosed using PET/CT imaging, can present as a massive spread along the abdominal cavity, and must be treated with chemotherapy; recurrence may also appear at a small isolated tumoural focus. In these particular cases, the use of a hand-held PET probe can guide surgery by identifying the hypermetabolic tumour lesion and distinguishing it from normal or scar tissue. PET guided surgery is especially useful in the detection of non-palpable lesions or lesions covered by fibrotic tissue. The main technical difficulty is the high physiological uptake of [^{18}F]FDG in surrounding tissue: liver, spleen, kidneys, bladder, etc. This high activity, together with the low spatial resolution of some devices, makes it unsuitable as a guide for margin resection. One of the benefits of this kind of surgery is the decrease in surgical morbidity, owing to the direct lesion localization with the probe and a reduction in the incision size. Before surgery, a PET image is recommended to localize the tumoural foci and to plan resection.

Despite the potential benefits of this procedure, PET guided surgery is still not widely used. The main problems are: (i) non-specific localization, because the probe can detect either tumoural and inflammatory tissue, (ii) technical difficulties, as described above, owing to the high activity in the abdominal cavity (a minimum tumour to background ratio of 1.5:1 is recommended) [12.75], (iii) the relatively large sizes of the probes, which do not allow their use during laparoscopic surgery, (iv) radiation of the staff, although some studies define an annual maximum of 260 h of this type of surgery [12.76] and (v) cost related considerations.

Many studies have been published on the use of PET probes for radioguided surgery in ovarian cancer. However, such a long list dramatically decreases when only in vivo or clinical application studies are included. In fact, there are only three groups that have actually performed PET probe radioguided surgery in ovarian cancer patients, with a total of five patients [12.77–12.79]. The smallest lesion detected was 2 cm wide [12.77, 12.79].

The next step in gynaecological surgery would be the development of endoscopic devices to minimize surgical morbidity and increase the detection rate due to better visualization during these procedures.

REFERENCES TO CHAPTER 12

[12.1] JEMAL, A., et al., Cancer statistics, 2006, CA Cancer, J. Clin. **56** (2006) 106–130.

[12.2] STEHMAN, F.B., et al., Carcinoma of the cervix treated with radiation therapy. I. A multi-variate analysis of prognostic variables in the Gynecologic Oncology Group, Cancer **67** (1991) 2776–2785.

[12.3] MacDONALD, O.K., CHEN, J., DODSON, M., LEE, C.M., GAFFNEY, D.K., Prognostic significance of histology and positive lymph node involvement following radical hysterectomy in carcinoma of the cervix, Am. J. Clin. Oncol. **32** (2009) 411–416.

[12.4] ZARGANIS, P., et al., The sentinel node in cervical cancer patients: Role of tumour size and invasion of lymphatic vascular space, In Vivo **23** (2009) 469–473.

[12.5] ELLIOTT, P., et al., Early invasive (FIGO stage IA) carcinoma of the cervix: A clinico-pathologic study of 476 cases, Int. J. Gynecol. Cancer **10** (2000) 42–52.

[12.6] SAKURAGI, N., et al., Incidence and distribution pattern of pelvic and paraaortic lymph node metastasis in patients with stages Ib, IIa and IIb cervical carcinoma treated with radical hysterectomy, Cancer **85** (1999) 1547–1554.

[12.7] LAI, C.H., CHANG, H.C., CHANG, T.C., HSUEH, S., TANG, S.G., Prognostic factors and impacts of adjuvant therapy in early-stage cervical carcinoma with pelvic node metastases, Gynecol. Oncol. **51** (1993) 390–396.

[12.8] ROGERS, L.J., LUESLEY, D.M., Stage IA2 cervical carcinoma: How much treatment is enough? Int. J. Cancer **19** (2009) 1620–1624.

[12.9] BENEDETTI-PANICI, P., et al., Lymphatic spread of cervical cancer: An anatomical and pathological study based on 225 radical hysterectomies with systematic pelvic and aortic lymphadenectomy, Gynecol. Oncol. **62** (1996) 19–24.
[12.10] LEA, J.S., SHEETS, E.E., DUSKA, L.R., MILLER, D.S., SCHORGE, J.O., Early-stage cervical adenocarcinoma treated by surgical intent: The role of para-aortic lymph node dissection, Gynecol. Oncol. **84** (2002) 285–288.
[12.11] HACKETT, T.E., et al., Surgical predictors of para-aortic metastases in early-stage cervical carcinoma, Gynecol. Oncol. **59** (1995) 15–19.
[12.12] BADER, A.A., WINTER, R., HAAS, J., TAMUSSINO, K.F., Where to look for the sentinel lymph node in cervical cancer, Am. J. Obstet. Gynecol. **197** (2007) 678.
[12.13] VAN DE LANDE, J., et al., Sentinel lymph node detection in early stage uterine cervix carcinoma: A systematic review, Gynecol. Oncol. **106** (2007) 604–613.
[12.14] ALTGASSEN, C., et al., Multicenter validation study of the sentinel lymph node concept in cervical cancer: AGO Study Group, J. Clin. Oncol. **26** (2008) 2943–2951.
[12.15] MARNITZ, S., et al., Topographic distribution of sentinel lymph nodes in patients with cervical cancer, Gynecol. Oncol. **103** (2006) 35–44.
[12.16] LAVOUÉ, V., et al., Sentinel lymph node procedure followed by laparoscopic pelvic and paraaortic lymphadenectomy in women with IB2-II cervical cancer, Ann. Surg. Oncol. **14** (2007) 2654–2661.
[12.17] HAUSPY, J., et al., Sentinel lymph nodes in early stage cervical cancer, Gynecol. Oncol. **105** (2007) 285–290.
[12.18] CIBULA, D., et al., Sentinel node (SLN) biopsy in the management of locally advanced cervical cancer, Gynecol. Oncol. **115** (2009) 46–50.
[12.19] FRUMOVITZ, M., RAMIREZ, P.T., LEVENBACK, C.F., Lymphatic mapping and sentinel lymph node detection in women with cervical cancer, Gynecol. Oncol. **110** (2008) 17–20.
[12.20] KUSHNER, D.M., et al., Laparoscopic sentinel lymph node mapping for cervix cancer—a detailed evaluation and time analysis, Gynecol. Oncol. **106** (2007) 507–512.
[12.21] FADER, A.N., et al., Sentinel lymph node biopsy in early-stage cervical cancer: Utility of intraoperative versus postoperative assessment, Gynecol. Oncol. **111** (2008) 13–17.
[12.22] EUSCHER, E.D., et al., Ultrastaging improves detection of metastases in sentinel lymph nodes of uterine cervix squamous cell carcinoma, Am. J. Surg. Pathol. **32** (2008) 1336–1343.
[12.23] BUIST, M.R., et al., Laparoscopic detection of sentinel lymph nodes followed by lymph node dissection in patients with early stage cervical cancer, Gynecol. Oncol. **90** (2003) 290–296.
[12.24] SEONG, S.J., et al., Detection of sentinel lymph nodes in patients with early stage cervical cancer, J. Korean. Med. Sci. **22** (2007) 105–109.
[12.25] VAN DAM, P.A., et al., Intraoperative sentinel node identification with technetium-99m-labeled nanocolloid in patients with cancer of the uterine cervix: A feasibility study, Int. J. Gynecol. Cancer **13** (2003) 182–186.

[12.26] MARTÍNEZ, A., et al., Hybrid imaging by SPECT/CT for sentinel lymph node detection in patients with cancer of the uterine cervix, Gynecol. Oncol. **119** (2010) 431–435.
[12.27] ZHANG, W.J., ZHENG, R., WU, L.Y., LI, X.G., CHEN, S.Z., Clinical application of sentinel lymph node detection to early stage cervical cancer, Ai Zheng **25** (2006) 224–228.
[12.28] PANDIT-TASKAR, N., et al., Single photon emission computed tomography SPECT-CT improves sentinel node detection and localization in cervical and uterine malignancy, Gynecol. Oncol. **117** (2010) 59–64.
[12.29] CRANE, L.M., et al., Multispectral real-time fluorescence imaging for intraoperative detection of the sentinel lymph node in gynecologic oncology, J. Vis. Exp. **44** (2010) 2225.
[12.30] TATLI, S., et al., Abdominal masses sampled at PET/CT-guided percutaneous biopsy: Initial experience with registration of prior PET/CT images, Radiology **256** (2010) 305–311.
[12.31] AMANT, F., et al., Endometrial cancer, Lancet **366** (2005) 491–505.
[12.32] PARTRIDGE, E.E., SHINGLETON, H.M., MENCK, H.R., The National Cancer Data Base report on endometrial cancer, J. Surg. Oncol. **61** (1996) 111–123.
[12.33] MAIS, V., et al., Intraoperative sentinel lymph node detection by vital dye through laparoscopy or laparotomy in early endometrial cancer, J. Surg. Oncol. **101** (2010) 408–412.
[12.34] ABU-RUSTUM, N.R., et al., Sentinel lymph node mapping for grade 1 endometrial cancer: Is it the answer to the surgical staging dilemma? Gynecol. Oncol. **113** (2009) 163–169.
[12.35] ROBOVA, H., et al., Lymphatic mapping in endometrial cancer: Comparison of hysteroscopic and subserosal injection and the distribution of sentinel lymph nodes, Int. J. Gynecol. Cancer **19** (2009) 391–394.
[12.36] BARRANGER, E., et al., Laparoscopic sentinel node mapping using combined detection for endometrial cancer: A study of 33 cases—is it a promising technique? Am. J. Surg. **197** (2009) 1–7.
[12.37] PERRONE, A.M., et al., Cervical and hysteroscopic injection for identification of sentinel lymph node in endometrial cancer, Gynecol. Oncol. **111** (2008) 62–67.
[12.38] CLEMENT, D., et al., Sentinel lymph nodes in endometrial cancer: Is hysteroscopic injection valid? Eur. J. Gynaecol. Oncol. **29** (2008) 239–241.
[12.39] BALLESTER, M., DUBERNARD, G., ROUZIER, R., BARRANGER, E., DARAI, E., Use of the sentinel node procedure to stage endometrial cancer, Ann. Surg. Oncol. **15** (2008) 1523–1529.
[12.40] BATS, A.S., et al., Does sentinel node biopsy improve the management of endometrial cancer? Data from 43 patients, J. Surg. Oncol. **97** (2008) 141–145.
[12.41] DELPECH, Y., et al., The sentinel node concept in endometrial cancer: Histopathologic validation by serial section and immunohistochemistry, Ann. Oncol. **18** (2007) 1799–1803.

[12.42] DELALOYE, J.F., et al., Intraoperative lymphatic mapping and sentinel node biopsy using hysteroscopy in patients with endometrial cancer, Gynecol. Oncol. **106** (2007) 89–93.
[12.43] LOPES, L.A., et al., Sentinel lymph node in endometrial cancer, Int. J. Gynecol. Cancer **17** (2007) 1113–1117.
[12.44] ALTGASSEN, C., PAGENSTECHER, J., JORNUNG, D., DIEDRICH, K., HORNEMANN, A., A new approach to label sentinel nodes in endometrial cancer, Gynecol. Oncol. **105** (2007) 457–461.
[12.45] LI, B., et al., A pilot study of sentinel lymph nodes identification in patients with endometrial cancer, Bull. Cancer **94** (2007) 1–4.
[12.46] FRUMOVITZ, M., et al., Lymphatic mapping and sentinel node biopsy in women with high-risk endometrial cancer, Gynecol. Oncol. **104** (2007) 100–103.
[12.47] DZVINCUK, P., PILKA, R., KUDELA, M., KORANDA, P., Sentinel lymph node detection using 99mTc-nanocolloid in endometrial cancer, Ceska Gynekol. **71** (2006) 231–236.
[12.48] GIEN, L.T., KWON, J.S., CAREY, M.S., Sentinel node mapping with isosulfan blue dye in endometrial cancer, J. Obstet. Gynaecol. Can. **27** (2005) 1107–1112.
[12.49] HOLUB, Z., JABOR, A., KLIMENT, L., Comparison of two procedures for sentinel lymph node detection in patients with endometrial cancer: A pilot study, Eur. J. Gynaecol. Oncol. **23** (2002) 53–57.
[12.50] BALLESTER, M., ROUZIER, R., COUTANT, C., KERROU, K., DARAI, E., Limits of lymphoscintigraphy for sentinel node biopsy in women with endometrial cancer, Gynecol. Oncol. **112** (2009) 348–352.
[12.51] VIDAL-SICART, S., et al., Added value of intraoperative real-time imaging in searches for difficult-to-locate sentinel nodes, J. Nucl. Med. **51** (2010) 1219–1225.
[12.52] HACKER, N.F., BEREK, J.S., LAGASSE, L.D., LEUCHTER, R.S., MOORE, J.G., Management of regional lymph nodes and their prognostic influence in vulvar cancer, Obstet. Gynecol. **61** (1983) 408–412.
[12.53] BURGER, M.P., et al., The importance of the groin node status for the survival of T1 and T2 vulval carcinoma patients, Gynecol. Oncol. **57** (1995) 327–334.
[12.54] VAN DER ZEE, A.G., et al., Sentinel node dissection is safe in the treatment of early-stage vulvar cancer, J. Clin. Oncol. **26** (2008) 884–889.
[12.55] LINDELL, G., et al., Evaluation of preoperative lymphoscintigraphy and sentinel node procedure in vulvar cancer, Eur. J. Obstet. Gynecol. Reprod. Biol. **152** (2010) 91–95.
[12.56] RADZISZEWSKI, J., et al., The accuracy of the sentinel lymph node concept in early stage squamous cell vulvar carcinoma, Gynecol. Oncol. **116** (2010) 473–477.
[12.57] HAMPL, M., HANTSCHMANN, P., MICHELS, W., HILLEMANNS, P., GERMAN MULTICENTER STUDY GROUP, Validation of the accuracy of the sentinel lymph node procedure in patients with vulvar cancer: Results of a multicenter study in Germany, Gynecol. Oncol. **111** (2008) 282–288.
[12.58] JOHANN, S., KLAESER, B., KRAUSE, T., MUELLER, M.D., Comparison of outcome and recurrence-free survival after sentinel lymph node biopsy and lymphadenectomy in vulvar cancer, Gynecol. Oncol. **110** (2008) 324–328.

[12.59] MOORE, R.G., et al., Isolated sentinel lymph node dissection with conservative management in patients with squamous cell carcinoma of the vulva: A prospective trial, Gynecol. Oncol. **109** (2008) 65–70.
[12.60] HAUSPY, J., et al., Sentinel lymph node in vulvar cancer, Cancer **110** (2007) 1015–1023.
[12.61] VIDAL-SICART, S., et al., Validation and application of the sentinel lymph node concept in malignant vulvar tumours, Eur. J. Nucl. Med. Mol. Imaging **34** (2007) 384–391.
[12.62] SLIUTZ, G., et al., Lymphatic mapping of sentinel nodes in early vulvar cancer, Gynecol. Oncol. **84** (2002) 449–452.
[12.63] SIDERI, M., et al., Detection of sentinel nodes by lymphoscintigraphy and gamma probe guided surgery in vulvar neoplasia, Tumouri **86** (2000) 359–363.
[12.64] LEVENBACK, C., et al., Intraoperative lymphatic mapping and sentinel node identification with blue dye in patients with vulvar cancer, Gynecol. Oncol. **83** (2001) 276–281.
[12.65] HEFLER, L.A., et al., Inguinal sentinel lymph node dissection vs. complete inguinal lymph node dissection in patients with vulvar cancer, Anticancer Res. **28** (2008) 515–517.
[12.66] TRIFIRÒ, G., et al., Sentinel node detection by lymphoscintigraphy and sentinel lymph node biopsy in vulvar melanoma, Eur. J. Nucl. Med. Mol. Imaging **37** (2010) 736–741.
[12.67] DHAR, K.K., DAS, N., BRINKMAN, D.A., BEYNON, J.L., WOLLAS, R.P., Utility of sentinel node biopsy in vulvar and vaginal melanoma: Report of two cases and review of the literature, Int. J. Gynecol. Cancer **17** (2007) 720–723.
[12.68] DESCHEEMAEKER, V., et al., Radioisotopic location of the sentinel node in vaginal mucous melanoma before laparoscopic sampling, Surg. Laparosc. Endosc. Percutan. Tech. **18** (2008) 195–196.
[12.69] VAN DAM, P., SONNEMANS, H., VAN DAM, P.J., VERKINDEREN, L., DIRIX, L.Y., Sentinel node detection in patients with vaginal carcinoma, Gynecol. Oncol. **92** (2004) 89–92.
[12.70] FRUMOVITZ, M., et al., Lymphatic mapping and sentinel lymph node detection in women with vaginal cancer, Gynecol. Oncol. **108** (2008) 478–481.
[12.71] KIM, W., MENDA, Y., WILLIS, J., BARTEL, T.B., GRAHAM, M.M., Use of lymphoscintigraphy with SPECT/CT for sentinel node localization in a case of vaginal melanoma, Clin. Nucl. Med. **31** (2006) 201–202.
[12.72] KOBAYASHI, K., et al., Sentinel node mapping in vulvovaginal melanoma using SPECT/CT lymphoscintigraphy, Clin. Nucl. Med. **34** (2009) 859–861.
[12.73] CASS, I., et al., Pattern of lymph node metastases in clinically unilateral stage I invasive epithelial ovarian carcinomas, Gynecol. Oncol. **80** (2001) 56–61.
[12.74] NEGISHI, H., et al., Lymphatic mapping and sentinel node identification as related to the primary sites of lymph node metastasis in early stage ovarian cancer, Gynecol. Oncol. **94** (2004) 161–166.

[12.75] GULEC, S.A., DAGHIGHIAN, F., ESSNER, R., PET-probe: Evaluation of technical performance and clinical utility of a handheld high-energy gamma probe in oncologic surgery, Ann. Surg. Oncol. (2006) DOI: 10.1245/ASO.2006.05.047.
[12.76] ANDERSEN, P.A., et al., Radiation exposure to surgical staff during F-18-FDG-guided cancer surgery, Eur. J. Nucl. Med. Mol. Imaging **35** (2008) 624–629.
[12.77] COHN, D.E., et al., Novel perioperative imaging with 18F-FDG PET/CT and intraoperative 18F-FDG detection using a handheld gamma probe in recurrent ovarian cancer, Gynecol. Oncol. **110** (2008) 152–157.
[12.78] GULEC, S.A., HOENIE, E., HOSTETTER, R., SCHWARTZENTRUBER, D., PET probe-guided surgery: Applications and clinical protocol, World J. Surg. Oncol. **5** (2007) 65–72.
[12.79] BARRANGER, E., et al., Laparoscopic resection of occult metastasis using the combination of FDG-positron emission tomography/computed tomography image fusion with intraoperative probe guidance in a woman with recurrent ovarian cancer, Gynecol. Oncol. **96** (2005) 241–244.

13. GOSTT IN MALIGNANCIES OF THE MALE REPRODUCTIVE SYSTEM

13.1. PROSTATE CANCER

13.1.1. Introduction

Prostate cancer predominantly occurs in elderly men: the median age at diagnosis is 72 years. In the USA, more than 200 000 new patients are diagnosed every year. LN staging is important for both prognosis and therapeutic management. In the presence of regional LN metastasis, local therapy, such as radiotherapy or radical prostatectomy, and androgen deprivation therapy cannot be performed with curative intentions. Limited nodal involvement may instead be treated with a combination of long term androgen deprivation therapy and extended LN dissection, or with external beam radiation therapy. None of the available diagnostic imaging modalities provides a reliable assessment of LN metastasis because their sensitivity is particularly limited in metastases smaller than 5 mm. Extended pelvic lymphadenectomy (EPL) is therefore the gold standard for identification of LN metastases in prostate cancer patients [13.1]. However, EPL is associated with various complications (venous thrombosis, lymphocele, lower extremity oedema and ureteral injury), the incidence of which increases with the number of dissected LNs, varying from 10.5% for one to five LNs removed to 24.3% when dissection includes more than 20 LNs [13.2]. The area of EPL has a certain topographic extension; in general, the common iliac artery is cleared only up to the crossing of the ureter, the external iliac vessels are the lateral border of the LN dissection area, and the internal iliac is usually cleared from the bifurcation to just beyond the superior vesical artery. The EPL area includes the obturator fossa, which consists of the tissue between the external iliac vein and the obturator nerve.

Radioguided SLNB during open surgery has been proposed as an alternative to EPL, to reduce the complications associated with extensive LDN [13.3]. Subsequently, the procedure has also been validated for laparoscopy [13.4]. The advantages of SLNB are a lower incidence of complications and, at least in principle, the possibility to explore a larger area than commonly performed during EPL.

For both EPL and SLNB, the use of predictive nomograms is very important to define the probability of nodal involvement for each patient on an individual basis. In particular, the probability of LN metastases in the pelvis increases with the level of prostate specific antigen (PSA), the biopsy grade (Gleason score) and the clinical T stage. Taking these factors into consideration results in patients with

relatively favourable pre-operative risk factors being excluded from LDN; in fact, the procedure is currently reserved principally for patients with intermediate or poor prognosis (clinical stage > T2b/T3, PSA > 10 ng/mL or Gleason > 6). However, SLNB has been able to identify metastases also in 6.8%–10.7% of the patients with favourable risk factors [13.5].

13.1.2. Radiocolloid administration and lymphoscintigraphy

Lymphoscintigraphy for SLNM is an essential component of the SLNB procedure [13.3–13.12]. Because most of the experience published so far is limited to European countries, the most commonly used radiopharmaceutical has been ^{99m}Tc nanocolloid. Under continuous transrectal US monitoring, the radiocolloid is injected into the prostate transrectally using a needle of size 0.5 mm × 150 mm. As prostate cancer may be multifocal, radiocolloid injections are performed in both lobes of the organ. An activity of approximately 240 MBq in 0.4 mL is recommended because the SLN visualization rate tends to decrease when smaller activities are injected [13.9]. The particle concentration also appears to be important, and the use of a reduced labelling dilution volume (0.4 mL ^{99m}Tc pertechnetate per 0.2 mg nanocolloid) leads to visualization of more SLNs, as well as greater radiocolloid uptake in the SLNs visualized [13.10]. The radiocolloid is usually divided into two to four aliquots for injection, depending on the prostate volume. A three way system is recommended, and after each depot of the radiocolloid, saline is used for flushing radioactivity remaining in the needle. Early planar images, to assess first draining LNs, and delayed planar images, to differentiate first echelon nodes from second echelon nodes, are required for adequate scintigraphic mapping of lymphatic drainage (Fig. 13.1).

13.1.3. Lymphatic drainage of the prostate and nodal groups in the pelvis

Early planar images of lymphoscintigraphy are acquired 15 min after radiocolloid administration, and may visualize the first draining LNs in almost 88% of the cases [13.11]. Delayed images may be acquired 2–4 h after injection. On delayed imaging, the SLN visualization rate increases to more than 95%. Early and delayed images must be carefully compared for correct interpretation, so that secondary tier LNs can be distinguished from the first draining SLNs. Such a discrimination must take into account the anatomical LN basins of the pelvis. As a rule, late appearing LNs located higher in the same basin are considered to be second echelon LNs, while late appearing LNs in distal or more ventral and dorsal basins suggest direct draining from the prostate. The latter LNs should therefore be considered to be SLNs. Lateral views acquired in addition to the anterior view can help to distinguish dorsal from more ventrally located SLNs.

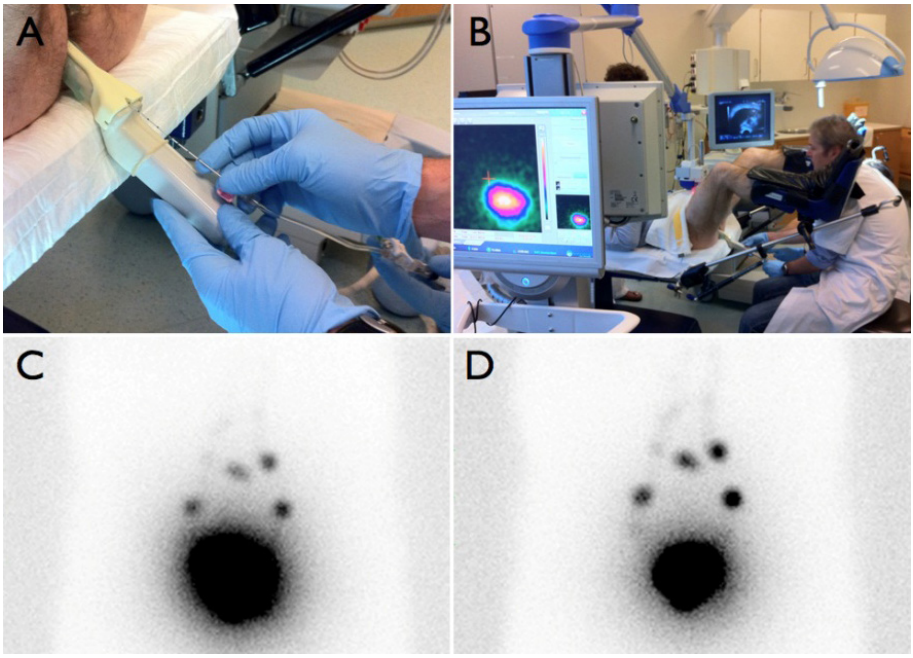

FIG. 13.1. Radiocolloid administration under transrectal US guidance using a long needle and a three way system (A). The radiocolloid is divided into two to four aliquots for injection. The procedure can also be monitored using a portable gamma camera to verify adequate radiocolloid retention in the prostate (B). In the case illustrated here, early (C) and delayed (D) planar images show at least four SLNs with direct drainage from the prostate.

The major groups of LNs that receive drainage from the prostate follow the iliac vessels [13.13]. The common iliac LNs are located caudal of the aortic bifurcation and are subdivided into three groups: the lateral, the medial and the middle. This latter basin is located in the lumbosacral fossa and is delimitated by the promontorium, the psoas muscle and the common iliac vessels.

The external iliac LNs are located caudal to the bifurcation of the common iliac vessels and cranial to the inguinal ligament; they are similarly subdivided into three groups: lateral, middle and medial. The lateral (lateral of the artery) and middle (between the artery and the vein) LNs are located more in the proximity of the anterior abdominal wall, and the medial LNs are located along the cranial segment of the external iliac artery. Although they are still the subject of some debate, the obturator LNs are generally considered to be a part of the medial subgroup.

The internal iliac LNs are located more posteriorly in the pelvis, and include the lateral sacral nodes (adjacent to the paired lateral sacral arteries), the presacral nodes (anterior to the sacrum and posterior to the mesorectal fascia) and

the anterior nodes (at the origin of the proximal branches of the anterior division of the internal iliac artery; this subgroup includes the hypogastric nodes).

Lymphatic drainage from the prostate is also possible to the para-aortic basins (adjacent to the most distal part of the aorta and just before the bifurcation) and to perivisceral basins (including LNs in the mesorectal fat, along the inferior mesenteric vessels or perivesical). Some examples are shown in Fig. 13.2.

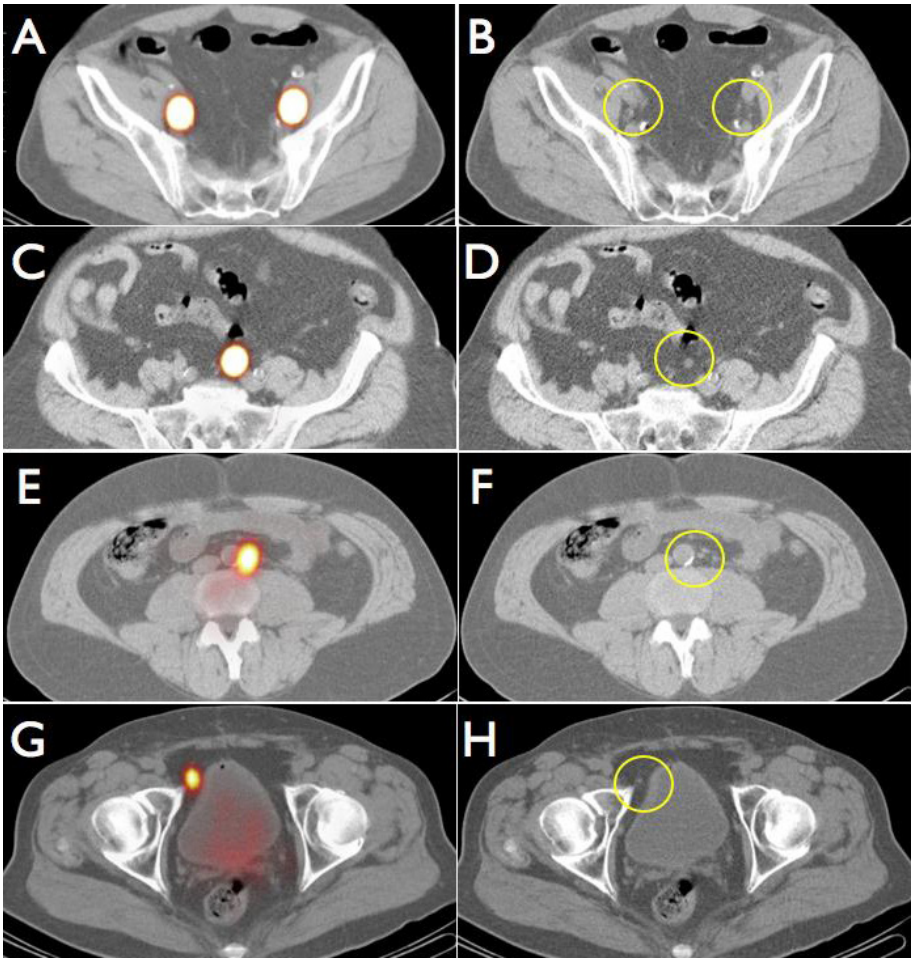

FIG. 13.2. Axial SPECT/CT fusion images (left panels) showing radioactive SLNs. In the corresponding CT images (right panels), the yellow circles indicate such LNs in the obturator (A, B), mesenteric (C, D), para-aortic (E, F) and perivesical (G, H) locations.

13.1.4. Added value of SPECT/CT imaging for SLNM

Hybrid imaging using SPECT/CT enables accurate anatomical localization of SLNs. After acquisition of CT images (40 mA·s, 2 mm slices) and SPECT images in the same session, the SPECT signal is corrected for tissue attenuation and scatter. Fused SPECT/CT, CT and SPECT images may be displayed simultaneously using similar 2-D display planes as for conventional CT images (axial, sagittal and coronal). Visualization of SLNs can be emphasized using multireconstruction plane (MRP) and MIP display techniques, while surface volume rendering display may depict the SLNs in a 3-D configuration (Fig. 13.3). A 98% SLN visualization rate has been found when employing SPECT/CT imaging (versus 91% for planar images). In 96% of the cases, SLNs are localized inside the conventional area of the EPL, but there is a considerable number of SLNs in regions not routinely explored by EPL [13.14]. In this regard, SPECT/CT

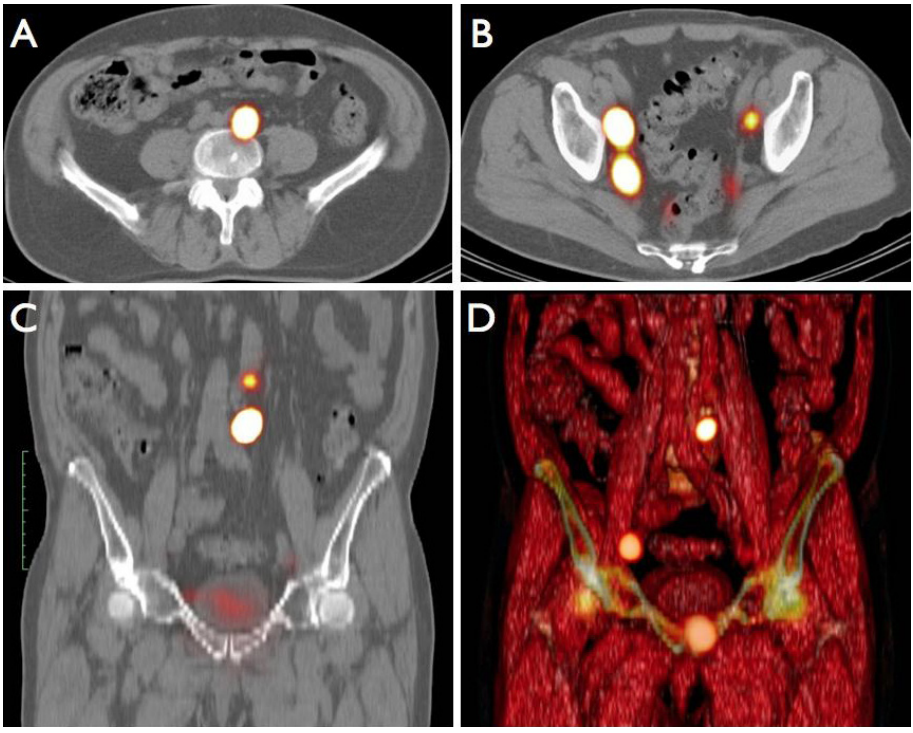

FIG. 13.3. Axial SPECT/CT images showing SLNs at the level of the aorta bifurcation (A) and along the iliac vessels (B). Coronal SPECT/CT image showing a para-aortic SLN and a second echelon LN (C). 3-D volume rendering (D) showing the same para-aortic node and an iliac node on the right.

imaging has led to localizing SLNs in aberrant areas of drainage [13.15] such as proximal to the most distal part of the aorta, in the vicinity of the common iliac artery above the crossing of the ureter, around the inferior mesenteric vessels, in the perivesical area, and near the umbilical ligament.

SPECT/CT imaging is mostly performed after acquisition of the delayed planar images and must be interpreted in combination with conventional lymphoscintigraphy. In fact, sequential planar images are important to identify the LNs draining directly from the tumour site, although they provide only limited information about their anatomical localization. On the other hand, using SPECT/CT imaging, it is possible to further localize SLNs both inside and outside the pelvis. In many cases, early appearing LNs seen as single foci of radiocolloid uptake on planar images are displayed as separate LNs in different basins by SPECT/CT imaging, and are considered to be SLNs. In other cases, intense LN uptake seen on the fused images may correspond to a cluster of SLNs as depicted on the CT component of the hybrid acquisition (Fig. 13.4).

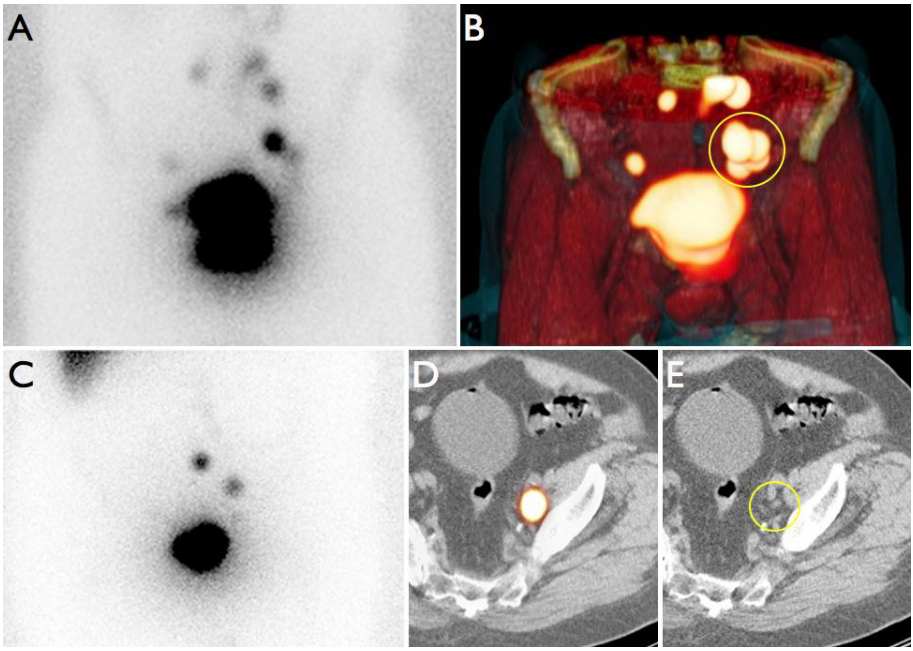

FIG. 13.4. Planar anterior image (A) showing drainage to both iliac areas. On 3-D volume rendering (B), a cluster of radioactive SLNs is seen in the left iliac region (circle). In another patient, iliac LNs are seen (C). Note that the most lateral SLN (seen on fused image D) corresponds to a cluster of LNs on the CT image (circled in E).

SPECT/CT images therefore provide useful information to the urologist, which may lead to a significant shortening of the surgical time required for the SLNB procedure [13.8]. SPECT/CT images may also provide important information for planning radiotherapy, with particular reference to treatment volume and optimization of irradiation fields in the pelvis [13.16].

13.1.5. Intraoperative SLN identification

The original validation of the SLNB procedure in patients with prostate cancer was based on gamma probe guidance during open surgery to detect the radioactive SLNs [13.3]; surgery is commonly performed the day after radiocolloid tracer administration and lymposcintigraphy, and an SLN identification rate greater than 95% has been reported [13.5, 13.9].

In more than 2000 patients submitted to SLNB according to this approach, only 11 false negative cases (5.5%) have been reported [13.12]; this acceptable rate confirms the reliability of the method to stage the pelvis. SLN metastases have been found in 13%–35% of the cases in patients of the intermediate prognostic group.

The SLNB procedure has been validated during laparoscopic surgery, with the use of a laparoscopic gamma probe [13.4]. In three series including a total of 188 patients, no false negative cases have been found [13.4, 13.7, 13.11]. Pre-operative anatomical information on the site of the SLNs is especially important during laparoscopic surgery, both for planning the optimal surgical approach and for directing gamma probe detection. For this purpose, the SPECT/CT images should be available for display to the surgeon in the operating room. Similar considerations justify the use of portable gamma cameras for intraoperative imaging, as a tool to facilitate localization and resection of SLNs. By using a ^{125}I seed placed on the collimator of the laparoscopic probe, it is possible to use the device as a pointer to localize the SLN on the screen, based on the different displays of the signals from ^{125}I (circle) and ^{99m}Tc (radioactive SLN). After matching the two signals on the screen and achieving confirmation using the gamma probe acoustic signals, SLN dissection can follow (Fig. 13.5). This approach was recently evaluated in 55 patients [13.17]. Out of 178 SLNs visualized on SPECT/CT imaging, 16 (9%) could not be visualized using the portable gamma camera because of a weak signal, and 13 (7%) could not be visualized because of their location in close proximity to the site of intraprostatic radiocolloid injection. Nevertheless, in 15 patients, the ^{125}I seed pointer was important to directly localize LNs (principally those along the aorta and the common iliac artery cranial of the ureter crossing), while in the remaining patients, imaging using the portable gamma camera was used to verify adequate

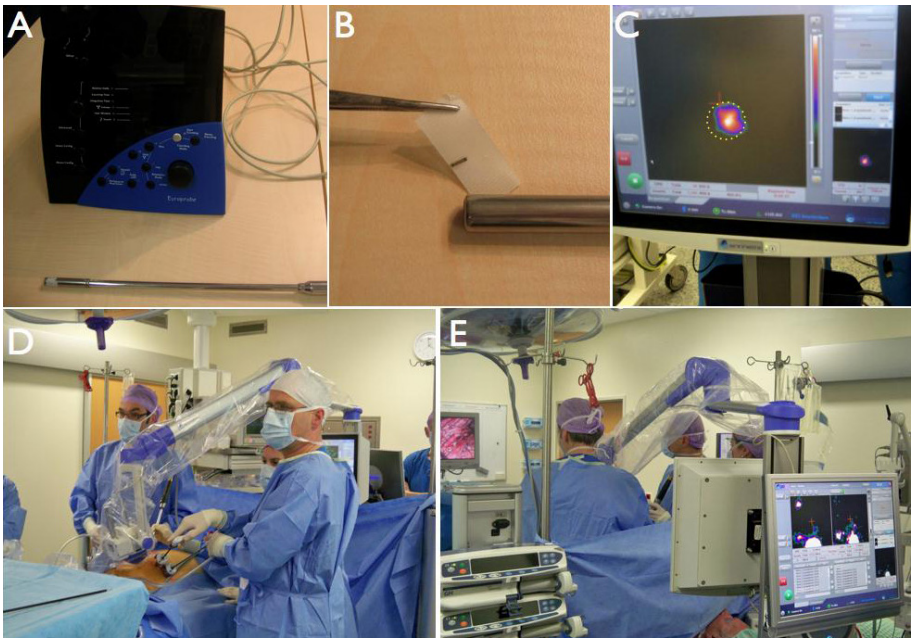

FIG. 13.5. Intraoperative SLN detection using a laparoscopic gamma probe (A) with a ^{125}I seed placed on the collimator (B) to enable its use as a pointer. This pointer is used for localization of the SLN on the screen (dotted circle in C) in the operating room (D, E).

SLN excision, leading to the identification of 17 additional SLNs not previously detected. In two of these cases, the SLNs so identified were tumour positive.

13.2. PENILE CANCER

13.2.1. Introduction

Penile cancer is a rare disease in industrialized countries, with an age adjusted standardized incidence of approximately 1 per 100 000 population per year [13.18]. More than 95% of these tumours are squamous cell carcinomas. As is common in squamous cell carcinoma, the pattern of dissemination is predominantly lymphogenic. The primary draining LNs of penile carcinoma are invariably located in the inguinal lymphatic region [13.19, 13.20]. Thereafter, metastatic dissemination continues to the pelvic LNs and/or to distant sites [13.19, 13.20].

While most patients (up to 80%) diagnosed with penile squamous cell carcinoma in industrialized countries present without any palpable

abnormalities in the groin [13.21], approximately 20% of them present with palpable LNs [13.21]. The presence of metastatic LN involvement is the single most important prognostic factor for cancer specific death in patients with penile carcinoma [13.22–13.28]. Treatment of patients with clinically obvious LN metastases is straightforward, and consists of regional LDN.

Instead, optimal management of cN0 patients has been the subject of a long debate [13.29]. Approximately 20%–25% of these patients harbour occult nodal metastasis. These occult metastases are, by definition, not detected by physical examination. Although prophylactic inguinal LDN offers the best chance of cure, it turns out to be unnecessary in approximately 75%–80% of patients [13.30]. Furthermore, this procedure is associated with substantial morbidity. Both these factors have prompted many investigators to advise a surveillance policy in cN0 patients. However, in non-randomized, retrospective series, patients undergoing inguinal LDN when disease became clinically apparent had a worse outcome than those undergoing early inguinal node dissection for occult metastases (a 35% 5 year disease specific outcome versus 80%) [13.31–13.33]. Accurate patient selection of those patients with occult metastases is the basis for curative management. Because currently available non-invasive staging techniques are hampered by lack of accuracy [13.34], (minimally) invasive staging therefore remains necessary for the time being.

In 1994, dynamic SLN biopsy (DSNB) was introduced at the Netherlands Cancer Institute for staging cN0 patients. After pre-operative lymphoscintigraphy and using an intraoperative gamma detection probe and blue dye, only the LNs on a direct lymphatic drainage pathway are removed via a small inguinal incision [13.35–13.37]. If the SLN is tumour positive, complete ipsilateral LDN is performed. Groins with tumour free LNs are instead managed using close surveillance, thereby avoiding the morbidity associated with LDN. Lymphoscintigraphy visualizes, in a dynamic fashion, the individual drainage patterns of each patient.

The most significant drawback of DSNB was found to be a false negative rate as high as 22% in the initial series [13.38]. After analysis of the false negative cases, several modifications were made to the DSNB procedure, with the aim of decreasing the false negative rate and thus of increasing sensitivity [13.39, 13.40]. Histopathological analysis was expanded with serial sectioning of the harvested SLNs. Furthermore, pre-operative ultrasonography of cN0 groins with FNAC of suspicious nodes was added, as well as exploration of groins in cases of non-visualization during scintigraphy and intraoperative palpation of the wound to identify suspicious nodes that failed to pick up any radiocolloid. With these modifications, the procedure has evolved into a reliable, minimally invasive staging technique with an overall 93%–95% sensitivity and very low morbidity [13.35, 13.41].

While the results of DSNB have become more satisfactory in terms of sensitivity, general acceptance of this staging technique is still low, most likely because of issues related to reproducibility of the procedure in less experienced centres [13.42]. One of the main differences probably justifying lower sensitivity of alternative protocols may be the lack of screening with US imaging and FNAC to detect metastasis in LNs that fail to pick up the radiocolloid.

Concerns have arisen as to whether enough experience could be obtained to guarantee reliable SLNB procedures in different centres, considering the relative rarity of penile carcinoma and the associated learning curve. In a large combined prospective series of 323 patients at two tertiary referral hospitals (the Netherlands Cancer Institute in Amsterdam and St George's Hospital in London), which use essentially the same modern DSNB protocol, the procedure has shown to be reliable and to involve a low complication rate [13.37]. The combined sensitivity of DSNB was 93%, with 100% specificity [13.37]. Complications occurred in less than 5% of the explored groins. Moreover, no learning curve could be demonstrated in the initial 30 procedures in the series at St George's Hospital. Similar results were reported in a recent study from Denmark [13.43].

DSNB is also feasible in cN0 patients who have had previous primary tumour resection [13.44]. While, formerly, such patients were managed with close surveillance or prophylactic inguinal LDN (both with associated disadvantages), 'post-resection DSNB' seems to represent a reliable staging method to detect occult metastases [13.44].

13.2.2. SPECT/CT imaging contribution and interpretation for SLNM

For penile carcinoma, the radiocolloid is injected intradermally. Subcutaneous administration is easier to accomplish, but may not delineate the route of drainage from an overlying cutaneous site. Furthermore, radiocolloid drainage from the dermis is much faster than drainage from subcutaneous tissue. Application of a spray containing 10% xylocaine 30 min before radiocolloid injection is recommended. Alternatively, a lidocaine/prilocaine based cream may be used. This local anaesthesia ensures that subsequent radiocolloid injections are well tolerated and relatively easy to perform. A volume of 0.3 mL, containing 74 MBq of the radiocolloid, is administered intradermally around the tumour. Injection is divided into three depots of 0.1 mL each. Each depot is injected, raising a wheal. The radiocolloid is injected proximally to the tumour. For large tumours not restricted to the glans, the radiocolloid can be administered in the prepuce. Injection margins within 1 cm from the primary tumour are recommended. In patients with an excision biopsy scar, injections may also be administered using similar margins. When keeping an injection distance of 5 mm, 100% reproducibility for penile lymphoscintigraphy has been reported [13.45].

Lymphoscintigraphy must match the SLN concept, and therefore must be able to visualize the lymphatic channels and to identify the LNs receiving direct drainage from the tumour. To detect these SLNs, gamma camera acquisition is subdivided into two parts:

— Dynamic scintigraphy, performed during the first 10 min after radiocolloid injection, preferably in both the anterior and the lateral projection. The dynamic study is helpful to identify lymphatic collectors and the first directly draining LNs.
— Static planar images at 20–30 min and 2 h post-injection. Additional images at 4 h, or radiocolloid reinjection are recommended when no SLNs are visualized at 2 h. To improve image interpretation and SLN identification, the use of simultaneous transmission scanning by means of a flood source of ^{57}Co or ^{99m}Tc provides information about the body contour.

In penile lymphoscintigraphy, the dorsal lymphatic channels of the penis are observed first, immediately after peritumoural radiocolloid injection. The most frequent pattern of visualization (80%) is bilateral drainage to both groins. This pattern is, however, asynchronous in two thirds of the cases and frequently late LN uptake of the contralateral side is only visualized on delayed imaging [13.46]. Drainage from the injection site mostly occurs through one or two afferent lymphatic vessels, leading to visualization of one or two SLNs in each groin. In some cases, a cluster of inguinal LNs may be visualized (Fig. 13.6).

At the Netherlands Cancer Institute, SPECT/CT images are recorded immediately after the 2 h planar images. The SPECT/CT system (Symbia T, Siemens, Erlangen, Germany) consists of a dual head, variable angle gamma camera equipped with LEHR collimators and a spiral CT system optimized for rapid rotation. SPECT image acquisition is performed using 4°–6° angle steps. For CT acquisition (130 kV, 40 mA·s, B30s kernel), 5 mm slices are obtained. After reconstruction, SPECT images are corrected for attenuation and scatter. Both SPECT and CT axial 5 mm slices are generated and subsequently fused for evaluation. Fused SPECT/CT imaging has contributed to better understanding of the location of SLNs in penile carcinoma, as it enables anatomical localization of the SLNs previously identified during planar lymphoscintigraphy. The main advantage of SPECT/CT imaging is its possibility to distinguish inguinal from iliac LNs.

One study has shown that in patients with penile carcinoma, the SLNs are generally located in Daseler's superior and central inguinal zones, which are superior to and directly overlying the saphenofemoral junction, respectively [13.19]. Higher tier LNs were also located in these inguinal zones and in the pelvic region. These findings suggest that the extent of inguinal LN

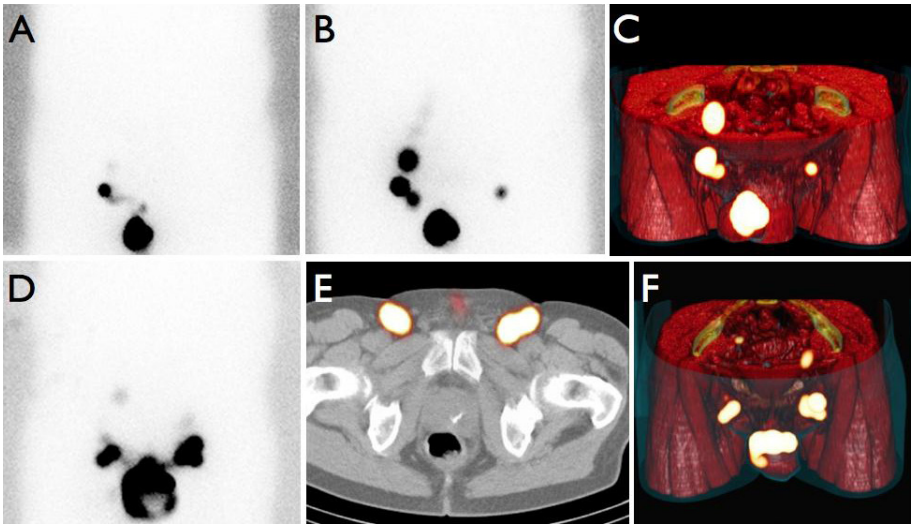

FIG. 13.6. Lymphoscintigraphy showing early drainage to the right groin (A) and delayed SLN visualization in the left groin (B). SPECT/CT image displayed using volume rendering (C) shows more accurately the anatomical localization, thus differentiating inguinal from iliac nodes. In another patient, bilateral drainage is seen in the planar image (D), while the SPECT/CT image shows a cluster of SLNs in the left groin and two SLNs in the right groin (E, F).

dissection could be reduced to removal of the superior and central inguinal zones. This surgical approach may decrease the postoperative morbidity associated with the procedure (Fig. 13.7).

13.2.3. PET/CT imaging in penile carcinoma

In one study, the role of [^{18}F]FDG PET/CT imaging in penile carcinoma has been explored [13.47]. Similar to that observed when staging patients with squamous cell carcinomas of the head and neck region and melanoma [13.48, 13.49], PET/CT imaging seems to have low sensitivity (20%–50%) in staging cN0 patients because small metastases are frequently missed [13.50]. On the other hand, PET/CT imaging is more accurate for staging clinically node positive patients, by determining the extent of metastatic disease beyond the groins [13.51] (Fig. 13.8). Despite surgery and postoperative radiotherapy, patients with penile carcinoma and extensive metastatic disease have a dismal outcome and are therefore candidates for systemic treatment rather than surgery. Therefore, PET/CT imaging can be of value for pre-operative patient selection.

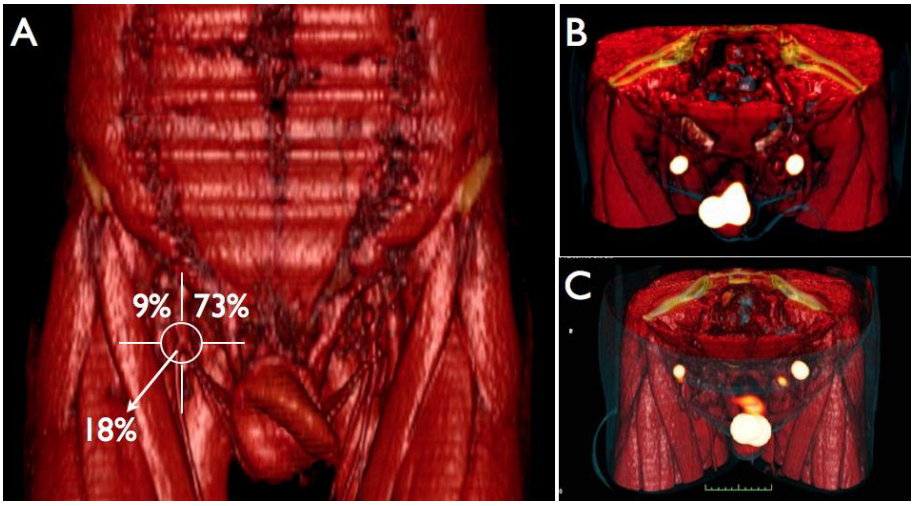

FIG. 13.7. Lymphatic drainage in penile carcinoma and the five inguinal zones of Daseler (A). In the majority of patients, SLNs are seen in the superior medial quadrant (73%), superior lateral (9%) and central (18%) quadrants. Drainage to the inferior quadrants is rare. On SPECT/CT images with volume rendering, SLNs are found in both inguinal superior medial quadrants (B); in another patient, lateral superior SLNs are seen on both sides of the groin.

13.3. TESTICULAR CANCER

13.3.1. Introduction

Testicular cancer is the most frequent malignancy in young men, with an almost 100% rise in incidence in the last 20 years. Overall, approximately two thirds of patients have clinical stage I disease at the time of diagnosis [13.52]. Clinical stage I seminoma and non-seminoma are defined by a negative CT scan of the chest, abdomen and pelvis, plus normal or normalized serum values of alpha fetoprotein, human chorionic gonadotropin and lactate dehydrogenase. In cases of mixed seminomatous/non-seminomatous tumours, treatment options are directed by the factor with the highest malignant potential, which is the non-seminoma component. Generally, the absence of LNs larger than 1.0 cm results in the classification as clinical stage I.

The management of regional LNs in stage I testicular cancer is still surrounded by controversy. The established treatment options for non-seminoma consist of surveillance, retroperitoneal LDN or chemotherapy. Treatment options for seminoma at this stage are surveillance, radiotherapy or chemotherapy. Because of the low incidence of occult LN metastases, primary treatment for

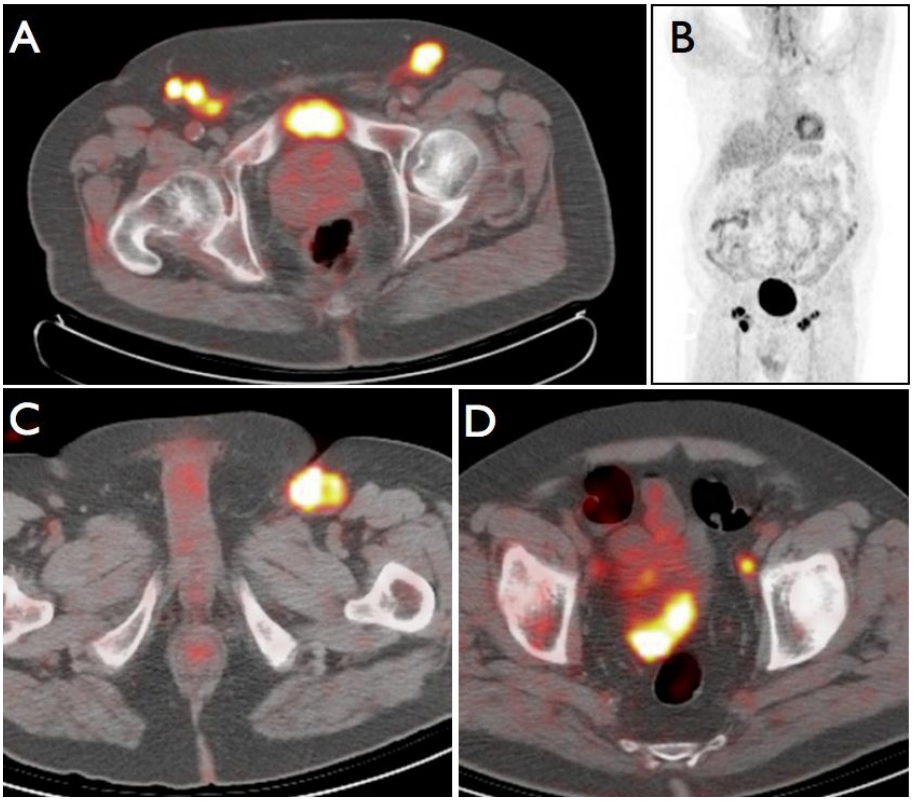

FIG. 13.8. PET/CT images showing [^{18}F]FDG avid LN metastases in both groins (A), but not in other regions (B). In another patient with [^{18}F]FDG avid LN metastases in the left groin (C), a left iliac LN metastasis is also seen (D).

non-seminoma in the form of retroperitoneal LDN or chemotherapy results in overtreatment in 65%–75% of patients. Overtreatment in seminoma with routine adjuvant radiotherapy is even higher because occult metastases are present in less than 20% of the patients. On the other hand, a surveillance policy requires an intensive, frequent follow-up with costly examinations, and may result in detection of LN metastases at a later stage. Until now, methods for selection of patients who need adjuvant therapy have been unsatisfactory. Therefore, diagnostic techniques that enable patients with LN metastasis to be treated at an early stage while preventing unnecessary treatment of those without dissemination are highly necessary. In this regard, the SLN procedure has good potential.

13.3.2. Radiocolloid administration and lymphatic mapping procedures

The SLNB procedure was introduced for patients with stage I disease [13.53–13.55]. The radiocolloid was administered by injection around the tumour, while laparoscopic gamma probe guided laparoscopic SLN removal was usually performed the next day. The SLNs were pre-operatively visualized in 95% of patients. The route of ^{99m}Tc nanocolloid administration was evaluated in a feasibility study in patients with stage I testicular cancer [13.55]. Funicular administration showed only LN uptake in the inguinal region, which does not reflect testicular tumour drainage. Intratesticular administration resulted in retroperitoneal SLN visualization, in accordance with the known drainage patterns. This latter method proved to be easy to perform and was well tolerated under local anaesthesia. No side effects were observed.

13.3.2.1. Recommendations for pre-operative imaging

In Europe, ^{99m}Tc nanocolloid is the most frequently used radiopharmaceutical for SLNM and SLNB. Before radiocolloid injection, local anaesthesia is obtained with a funicular block using 2% lidocaine, performed by the urologist in the outpatient clinic. In the nuclear medicine department, a single aliquot of the radiocolloid (mean 99 MBq, range 52–135 MBq) in a volume of 0.2 mL is injected with a fine needle into the testicular parenchyma.

Similar to penile cancer, the rapid lymphatic drainage from the testicle necessitates dynamic gamma camera acquisition, to enable discrimination between first and second echelon LNs in the retroperitoneum. Immediately following radiocolloid injection, anterior and lateral dynamic images are obtained with a dual head gamma camera over 10 min to visualize the lymphatic flow and to identify such early draining LNs. Static images are obtained 5 min after the dynamic study. Late static images are obtained 2–4 h after injection and are required to distinguish first echelon nodes from higher echelon nodes (if there is no SLN visualization in the early dynamic and static images), and to identify unexpected drainage patterns.

13.3.3. Lymphatic drainage of the testis

Lymphatics from the right testis drain primarily to regions that are lateral, anterior and medial to the vena cava and anterior to the aorta. Lymphatic drainage from the left testis is primarily to areas that are lateral, anterior and medial to the aorta [13.56]. SLNs may therefore be pre-operatively detected at interaortocaval, para-aortic or preaortic locations. However, in some patients, SLNs may be seen also along the testicular vessels.

13.3.4. Contribution of SPECT/CT imaging

Accurate staging with SLNB can be achieved only if all LNs on a direct drainage pathway from the tumour are detected. Because lymphatic drainage of tumours draining to areas deeply within the abdomen is often complex, pre-operative localization is mandatory. In the above mentioned studies [13.53–13.55], pre-operative lymphatic mapping was performed using planar lymphoscintigraphy only. However, this technique can only provide 2-D information, and exact pre-operative anatomical SLN localization is not possible. Integrated SPECT/CT imaging allows 3-D visualization. With the combination of SPECT and CT imaging in a single device, the nodal radiocolloid uptake detected by SPECT can be fused with CT, thus providing the surgeon with better information on the anatomic location of the SLNs. Previous reports on the use of SPECT/CT imaging for SLNM have shown favourable results using this modality in other malignancies [13.57]. In these studies, SPECT/CT imaging not only provided useful anatomic information about SLN localization, but also detected additional SLNs. To date, no studies evaluating the value of SPECT/CT imaging for pre-operative SLNM in patients with testicular cancer have been published. So far, SPECT/CT imaging has been performed for SLNM at the Netherlands Cancer Institute in ten stage I testicular cancer patients over the 2006–2011 period. SPECT/CT imaging enabled accurate SLN localization and provided anatomical reference points to plan SLN laparoscopic retrieval in all patients (Fig. 13.9). In one patient, SLN metastases were found. No recurrences developed in the nine patients with a tumour free SLN after a median follow-up of 20 months.

13.3.5. Additional value of recent advances in intraoperative imaging

The urologist localizes an SLN guided by the audio pitch based on the number of γ ray counts measured using a laparoscopic gamma probe. Intraoperative spatial orientation using this device can sometimes be difficult, as a laparoscopic probe does not provide visual information. The use of a portable gamma camera to intraoperatively guide the laparoscopic localization in testicular cancer has been reported by Brouwer et al. [13.58]. Current portable gamma cameras are capable of detecting two different signals: the signal of the ^{99m}Tc radiocolloid for SLN detection and the signal of a ^{125}I seed pointer placed on the tip of the laparoscopic gamma probe. The hot tip of the probe can be moved to the hot node guided by the image of the portable camera. This approach not only provides exact localization information, but also helps to quantify the number of radioactive nodes and the amount of radioactivity within the nodes, facilitating discrimination between an SLN and a node further downstream. After

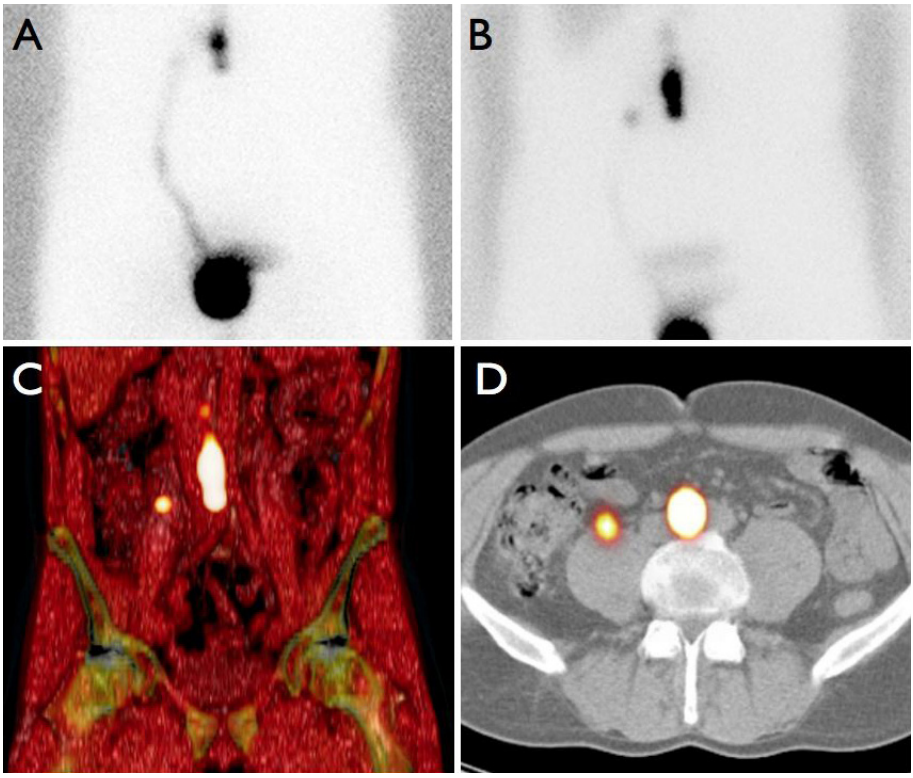

FIG. 13.9. Lymphoscintigraphy showing retroperitoneal drainage after radiocolloid injection in the right testicle (A). Delayed images (B) show also a radioactive lateral LN. With SPECT/CT imaging, this node is anatomically localized along the testicular vessels (C, D).

removal of all presumed SLNs, the portable gamma camera can show whether there is any remaining SLN that has to be removed, or a second echelon node that can be confidently left in place. This approach provides certainty about completeness of the surgical procedure and thus complements the laparoscopic probe (Fig. 13.10).

13.3.6. Conclusions

Current data indicate the feasibility of SLNM and SLNB in patients with stage I testicular tumours. Use of this technique in combination with laparoscopic SLNB may be of value in identifying occult LN metastases, thereby preventing undertreatment or overtreatment. Both SPECT/CT imaging, using modern gamma cameras, and intraoperative imaging, using portable gamma cameras,

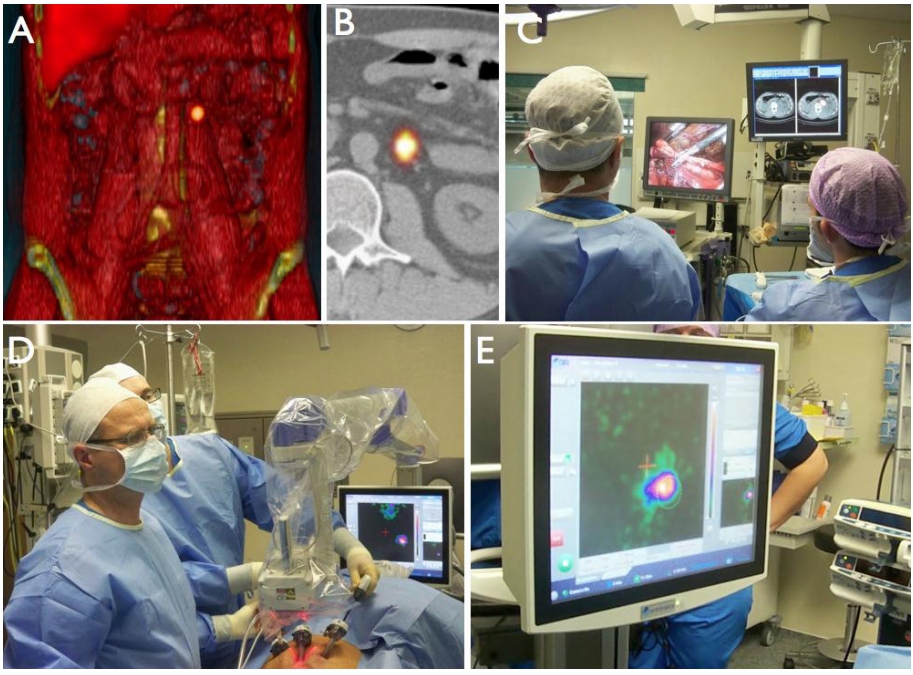

FIG. 13.10. SPECT/CT image showing an SLN in the proximity of the left testicular vessels on volume rendering (A) and axial (B) images. This SLN is localized in the operating room guided by SPECT/CT information (C) and using a portable gamma camera (D, E) for real time display.

facilitate the laparoscopic procedure. Further investigations are still required to establish the clinical value of SLNB in this disease.

REFERENCES TO CHAPTER 13

[13.1] AUS, G., et al., EAU guidelines on prostate cancer, Eur. Urol. **48** (2005) 546–551.

[13.2] WINTER, A., WAWROSCHEK, F., "Lymphadenectomy in prostate cancer", Controversies in the Treatment of Prostate Cancer (MOSER, L., SCHOSTAK, M., MILLER, K., HINKELBEIN, W., Eds), Frontiers of Radiation Therapy and Oncology, Vol. 41, Karger (2008) 58–67.

[13.3] WAWROSCHEK, F., VOGT, H., WECKERMANN, D., WAGNER, T., HARZMANN, R., The sentinel lymph node concept in prostate cancer—first results of gamma probe-guided sentinel lymph node identification, Eur. Urol. **36** (1999) 595–600.

[13.4] JESCHKE, S., et al., Detection of early lymph node metastases in prostate cancer by laporoscopic radioisotope guided sentinel lymph node dissection, J. Urol. **173** (2005) 1943–1946.
[13.5] WECKERMANN, D., WAWROSCHEK, F., HARZMANN, R., Is there a need for pelvic lymph node dissection in low risk prostate cancer patients prior to definitive local therapy? Eur. Urol. **47** (2005) 45–51.
[13.6] SILVA, B., et al., Use of the gamma probe in sentinel lymph node biopsy in patients with prostate cancer, Nucl. Med. Commun. **26** (2005) 1081–1086.
[13.7] CORVIN, S., et al., Laparoscopic sentinel lymph node dissection—a novel technique for the staging of prostate cancer, Eur. Urol. **49** (2006) 280–285.
[13.8] WARNCKE, S.H., et al., Detection rate and operating time required for gamma probe-guided sentinel lymph node resection after injection of technetium-99m nanocolloid into the prostate with and without preoperative imaging, Eur. J. Urol. **52** (2007) 126–133.
[13.9] BRENOT-ROSSI, I., et al., Radioguided sentinel lymph node dissection in patients with localised prostate carcinoma: Influence of the dose of radiolabelled colloid to avoid failure of the procedure, Eur. J. Nucl. Med. Mol. Imaging **35** (2008) 32–38.
[13.10] VERMEEREN, L., MEINHARDT, W., VAN DER POEL, H.G., VALDÉS OLMOS, R.A., Optimizing the colloid particle concentration for improved preoperative and intraoperative image-guided detection of sentinel nodes in prostate cancer, Eur. J. Nucl. Med. Mol. Imaging **37** (2010) 1328–1334.
[13.11] MEINHARDT, W., VALDÉS OLMOS, R.A., VAN DER POEL, H.G., BEX, A., HORENBLAS, S., Laparoscopic sentinel node dissection for prostate carcinoma: Technical and anatomical observations, Br. J. Urol. **102** (2008) 714–747.
[13.12] HOLL, G., DORN, R., WENGENMAIR, H., WECKERMANN, D., SCIUK, J., Validation of sentinel lymph node dissection in prostate cancer: Experience in more than 2,000 patients, Eur. J. Nucl. Med. Molec. Imaging **36** (2009) 1377–1382.
[13.13] McMAHON, C.J., ROFSKY, N.M., PEDROSA, I., Lymphatic metastases from pelvic tumors: Anatomic classification, characterization and staging, Radiology **254** (2010) 31–46.
[13.14] VERMEEREN, L., et al., Value of SPECT/CT for detection and anatomic localization of sentinel lymph nodes before laparoscopic sentinel node lymphadenectomy in prostate carcinoma, J. Nucl. Med. **50** (2009) 865–870.
[13.15] VERMEEREN, L., MEINHARDT, W., VALDÉS OLMOS, R.A., Prostatic lymphatic drainage with sentinel nodes at the ventral abdominal wall visualized with SPECT/CT: A case series, Clin. Nucl. Med. **35** (2010) 71–73.
[13.16] GANSWINDT, U., et al., Distribution of prostate sentinel nodes: A SPECT-derived anatomic atlas, Int. J. Radiat. Oncol. Biol. Phys. **79** (2011) 1364–1372.
[13.17] VERMEEREN, L., VALDÉS OLMOS, R.A., MEINHARDT, W., HORENBLAS, S., Intraoperative imaging for sentinel node identification in prostate carcinoma: Its use in combination with other modalities, J. Nucl. Med. **52** (2011) 741–744.
[13.18] HERNANDEZ, B.Y., et al., Burden of invasive squamous cell carcinoma of the penis in the United States, 1998-2003, Cancer **113** (2008) 2883–2891.

[13.19] LEIJTE, J.A., VALDÉS OLMOS, R.A., NIEWEG, O.E., HORENBLAS, S., Anatomical mapping of lymphatic drainage in penile carcinoma with SPECT-CT: Implications for the extent of inguinal lymph node dissection, Eur. Urol. **54** (2008) 885–890.
[13.20] ZHU, Y., et al., Prospectively packaged ilioinguinal lymphadenectomy for penile cancer: The disseminative pattern of lymph node metastasis, J. Urol. **181** (2009) 2103–2108.
[13.21] PERSSON, B., SJODIN, J.G., HOLMBERG, L., WINDAHL, T., The National Penile Cancer Register in Sweden 2000-2003, Scand. J. Urol. Nephrol. **41** (2007) 278–282.
[13.22] SRINIVAS, V., MORSE, M.J., HERR, H.W., SOGANI, P.C., WHITMORE W.F., Penile cancer: Relation of extent of nodal metastasis to survival, J. Urol. **137** (1987) 880–882.
[13.23] RAVI, R., Correlation between the extent of nodal involvement and survival following groin dissection for carcinoma of the penis, Br. J. Urol. **72** (1993) 817–819.
[13.24] HORENBLAS, S., VAN TINTEREN, H., Squamous cell carcinoma of the penis, IV. Prognostic factors of survival: Analysis of tumor, nodes and metastasis classification system, J. Urol. **151** (1994) 1239–1243.
[13.25] LONT, A.P., et al., Pelvic lymph node dissection for penile carcinoma: Extent of inguinal lymph node involvement as an indicator for pelvic lymph node involvement and survival, J. Urol. **177** (2007) 947–952.
[13.26] SANCHEZ-ORTIZ, R.F., PETTAWAY, C.A., The role of lymphadenectomy in penile cancer, Urol. Oncol. **22** (2004) 236–244.
[13.27] PANDEY, D., MAHAJAN, V., KANNAN, R.R., Prognostic factors in node-positive carcinoma of the penis, J. Surg. Oncol. **93** (2006) 133–138.
[13.28] ORNELLAS, A.A., et al., Surgical treatment of invasive squamous cell carcinoma of the penis: Brazilian National Cancer Institute long-term experience, J. Surg. Oncol. **97** (2008) 487–495.
[13.29] WESPES, E., The management of regional lymph nodes in patients with penile carcinoma and reliability of sentinel node biopsy, Eur. Urol. **52** (2007) 15–16.
[13.30] HEGARTY, P.K., et al., Prospective study of 100 cases of penile cancer managed according to European Association of Urology guidelines, BJU Int. **98** (2006) 526–531.
[13.31] McDOUGAL, W.S., Carcinoma of the penis: Improved survival by early regional lymphadenectomy based on the histological grade and depth of invasion of the primary lesion, J. Urol. **154** (1995) 1364–1366.
[13.32] LONT, A.P., et al., Management of clinically node negative penile carcinoma: Improved survival after the introduction of dynamic sentinel node biopsy, J. Urol. **170** (2003) 783–786.
[13.33] KROON, B.K., et al., Patients with penile carcinoma benefit from immediate resection of clinically occult lymph node metastases, J. Urol. **173** (2005) 816–819.
[13.34] HUGHES, B., LEIJTE, J., SHABBIR, M., WATKIN, N., HORENBLAS, S., Non-invasive and minimally invasive staging of regional lymph nodes in penile cancer, World J. Urol. **27** (2009) 197–203.

[13.35] LEIJTE, J.A., KROON, B.K., VALDÉS OLMOS, R.A., NIEWEG, O.E., HORENBLAS, S., Reliability and safety of current dynamic sentinel node biopsy for penile carcinoma, Eur. Urol. **52** (2007) 170–177.
[13.36] HADWAY, P., SMITH, Y., CORBISHLEY, C., HEENAN, S., WATKIN, N.A., Evaluation of dynamic lymphoscintigraphy and sentinel lymph-node biopsy for detecting occult metastases in patients with penile squamous cell carcinoma, BJU Int. **100** (2007) 561–565.
[13.37] LEIJTE, J.A., et al., Two-center evaluation of dynamic sentinel node biopsy for squamous cell carcinoma of the penis, J. Clin. Oncol. **27** (2009) 3325–3329.
[13.38] TANIS, P.J., et al., Dynamic sentinel node biopsy for penile cancer: Reliability of a staging technique, J. Urol. **168** (2002) 76–80.
[13.39] KROON, B.K., et al., How to avoid false-negative dynamic sentinel node procedures in penile carcinoma, J. Urol. **171** (2004) 2191–2194.
[13.40] KROON, B.K., VALDÉS OLMOS, R., NIEWEG, O.E., HORENBLAS, S., Non-visualization of sentinel lymph nodes in penile carcinoma, Eur. J. Nucl. Med. Mol. Imaging **32** (2005) 1096–1099.
[13.41] KROON, B.K., LONT, A.P., VALDÉS OLMOS, R.A., NIEWEG, O.E., HORENBLAS, S., Morbidity of dynamic sentinel node biopsy in penile carcinoma, J. Urol. **173** (2005) 813–815.
[13.42] SPIESS, P.E., et al., Preoperative lymphoscintigraphy and dynamic sentinel node biopsy for staging penile cancer: Results with pathological correlation, J. Urol. **177** (2007) 2157–2161.
[13.43] JENSEN, J.B., JENSEN, K.M., ULHOI, B.P., NIELSEN, S.S., LUNDBECK, F., Sentinel lymph-node biopsy in patients with squamous cell carcinoma of the penis, BJU Int. **103** (2009) 1199–1203.
[13.44] GRAAFLAND, N.M., et al., Nodal staging in penile carcinoma by dynamic SLN biopsy after previous therapeutic primary tumour resection, Eur. Urol. **58** (2010) 748–751.
[13.45] KROON, B.K., VALDÉS OLMOS, R.A., NIEWEG, O.E., HORENBLAS, S., Reproducibility of lymphoscintigraphy for lymphatic mapping in patients with penile carcinoma, J. Urol. **174** (2005) 2214–2217.
[13.46] VALDÉS OLMOS, R.A., et al., Penile lymphoscintigraphy for sentinel node identification, Eur. J. Nucl. Med. **28** (2001) 581–585.
[13.47] SCHER, B., et al., ^{18}F-FDG PET/CT for staging of penile cancer, J. Nucl. Med. **46** (2005) 1460–1465.
[13.48] NG, S.H., et al., Prospective study of [^{18}F]fluorodeoxyglucose positron emission tomography and computed tomography and magnetic resonance imaging in oral cavity squamous cell carcinoma with palpably negative neck, J. Clin. Oncol. **24** (2006) 4371–4376.
[13.49] EL-MARAGHI, R.H., KIELAR, A.Z., PET vs sentinel lymph node biopsy for staging melanoma: A patient intervention, comparison, outcome analysis, J. Am. Coll. Radiol. **5** (2008) 924–931.

[13.50] LEIJTE, J.A., et al., Prospective evaluation of hybrid ^{18}F-fluorodeoxyglucose positron emission tomography/computed tomography in staging clinically node-negative patients with penile carcinoma, BJU Int. **104** (2009) 640–644.
[13.51] GRAAFLAND, N.M., et al., Scanning with ^{18}F-FDG-PET/CT for detection of pelvic nodal involvement in inguinal node-positive penile carcinoma, Eur. Urol. **56** (2009) 339–345.
[13.52] BRAY, F., et al., Trends in testicular cancer incidence and mortality in 22 European countries: Continuing increases in incidence and declines in mortality, Int. J. Cancer **118** (2006) 3099–3111.
[13.53] OHYAMA, C., et al., Lymphatic mapping and gamma probe guided laparoscopic biopsy of sentinel lymph node in patients with clinical stage I testicular tumor, J. Urol. **168** (2002) 1390–1395.
[13.54] TANIS, P.J., HORENBLAS, S., VALDÉS OLMOS, R.A., HOEFNAGEL, C.A., NIEWEG, O.E., Feasibility of sentinel node lymphoscintigraphy in stage I testicular cancer, Eur. J. Nucl. Med. Mol. Imaging **29** (2002) 670–673.
[13.55] SATOOH, M., et al., Intraoperative, radio-guided sentinel lymph node mapping in laparoscopic lymph node dissection for stage I testicular carcinoma, Cancer **103** (2005) 2067–2072.
[13.56] MEACHAM, R.B., HUCKINS, C., LIPSHULTZ, L., "Anatomy and embryology of the testicle", Principles and Management of Testicular Cancer (JAVADPOUR, N., Ed.), Thieme (1986) 13–32.
[13.57] VERMEEREN, L., et al., SPECT/CT for preoperative sentinel node localization, J. Surg. Oncol. **101** (2010) 184–190.
[13.58] BROUWER, O.R., et al., SPECT/CT and a portable gamma-camera for image-guided laparoscopic sentinel node biopsy in testicular cancer, J. Nucl. Med. **52** (2011) 551–554.

14. GOSTT IN MALIGNANCIES OF THE KIDNEY AND BLADDER

14.1. CANCERS OF THE KIDNEY

14.1.1. Introduction

Renal cell carcinoma (RCC) is the most common type of renal cancer, accounting for approximately 3% of all adult malignancies and 90%–95% of all kidney neoplasms [14.1, 14.2]. In the European Union, there were over 60 000 new cases of kidney cancer and 26 000 deaths in 2006 alone [14.3]. Worldwide, mortality as a result of RCC exceeds 100 000 patients each year [14.4], with incidence and mortality rate increasing by 2%–3% per decade [14.1].

Metastatic disease is present in more than 25% of patients at diagnosis of RCC (mRCC), and almost 95% of these have multiple sites affected [14.1]. The disease remains one of the most treatment resistant malignancies, and is associated with a poor prognosis. Reports maintain that only approximately 23% of patients presenting with mRCC will be alive 5 years later [14.5].

Surgical intervention is the primary treatment for early stage RCC; however, surgery alone has limited benefit in patients with metastatic disease, except for palliative reasons [14.6]. For advanced disease, nephrectomy may only be curative if all metastatic deposits are excised [14.7].

LN metastasis is one of the major factors affecting the prognosis and survival of RCC patients. Different studies suggest that the true incidence of isolated LN metastases in clinically localized disease is small, with an incidence of 4%–22.5% in patients without evidence of other metastatic disease [14.8–14.11]. Once LN metastases are present, survival rates drop considerably and range from 0% to 20% within 5 years after surgery. Although the presence of LN metastases has a major influence on a patient's prognosis [14.12, 14.13], the effect of LDN on survival benefit is controversial. Some retrospective studies found a therapeutic benefit of this procedure [14.14, 14.15], while others found no survival improvement of a routine LDN compared to nephrectomy only [14.8, 14.16]. Retrospective studies suggest that survival benefit may occur when clinically suspected nodes are removed, but may be absent in clinically unsuspected nodes [14.17, 14.18]. The results of the only randomized trial failed to demonstrate a survival benefit in patients undergoing LDN for clinically unsuspected nodes [14.8, 14.19]. Further uncertainty exists with regard to the extent of LDN. In a series of 1558 patients who had at least one LN examined after LDN for RCC, Joslyn et al. reported an inverse correlation between number

of pN+ and cancer specific survival, but no association of survival with the number of LNs examined [14.20].

14.1.2. Lymphatic drainage of the kidney and metastatic spread in RCC

In RCC, it is often believed that the draining LNs are in the hilar region branching off into the paracaval, interaortal or para-aortal retroperitoneal LNs, depending on the side of the renal tumour. However, the exact patterns of direct lymphatic drainage are unknown. Lymphatic drainage patterns were previously assessed by analysing lymphatic metastasis within LDN specimens or lymphatic dissemination patterns on autopsy.

In nephrectomy series, metastases are generally detected in 'regional' LDNs, and the extent of the LDN is not clear. As in the case of other tumours, the accuracy of detecting LN metastases increases with the amount of sampled nodes. Terrone et al. [14.21] found a 13.6% rate of LN metastases in 608 patients. The median (range) number of nodes removed was 9 (1–43); there was a statistically significant correlation between the number of nodes removed and the percentage of nodal involvement ($r = 0.6$; $P < 0.01$). The rate of pN+ was significantly higher in the patients with more than 13 nodes than in those with less than 13 nodes examined (20.8% versus 10.2%; $P < 0.001$). For organ confined and locally advanced tumours, there was a statistically significant difference in the pN+ rate between patients (3.4% versus 10.5%) with less than 13 nodes or 13 nodes or more that were examined (19.7% versus 32.2%). It was concluded that the proportion of tumours classified as pN+ increases with the number of LNs examined and that more than 12 LNs need to be assessed for optimal staging. This was independent from the extent of the LN dissection [14.21].

Analysing 1828 autopsy records, Saitoh and co-workers described a broad variation in the anatomical localization of LN metastases [14.22]. Because most patients had multiple lymphatic metastases, it cannot be concluded which node was the first involved node. Interestingly though, ipsilateral renal hilar LN metastases were only found in 7% of the patients, while pulmonary hilar LN metastases were found in 66.2%, retroperitoneal in 36%, para-aortal in 26.8% and supraclavear metastases in 20.7% of the patients [14.22]. Hulten and co-workers described single metastases in a peripheral supraclavear LN in one patient and in an iliac LN in two patients without any further metastasis [14.23]. Johnsen and Hellsten found single mediastinal LN metastases in eight patients, supraclavear metastases in one patient and axillary metastases in one patient [14.24]. Because all those patients had massive systemic metastases, those rare single LN metastases were regarded as an expression of haematogenous tumour spread subsequently involving the LNs. On the other hand, those single positive

nodes may chronologically represent the first metastatic site with subsequent haematogenous spread.

In one of the first studies performed to elucidate the drainage pattern, Parker found extreme variations of lymphatic drainage between individual cases by injecting blue dye at high pressure into normal cadaveric kidneys [14.25]. More recently, Assouad and co-workers injected normal kidneys of 16 cadavers with a blue modified Gerota mass and dissected lymph vessels until their termination [14.26]. Renal lymphatics have been found to reach very distant nodes (e.g. aortic bifurcation, celiac or mesenteric LNs and contralateral LNs). Furthermore, it was found that the lymphatic vessels were always connected to the origin of the thoracic duct, some directly without traversing any retroperitoneal LNs. It was argued that this feature may play an important role in the frequently observed pulmonary and mediastinal metastatic spread in RCC [14.27]. Isolated mediastinal LN metastases are more frequently observed in RCC compared to tumours in other organs [14.28–14.30].

14.1.3. LN dissection

Despite decades of research, the role of LDN in RCC remains controversial. The results of the single prospective randomized European Organization for Research and Treatment of Cancer (EORTC) 30881 study concerning LDNs do not demonstrate a survival benefit [14.19]. The incidence of unsuspected LN metastases was the lowest in the literature, at only 4%. It has been argued that this may be because of the relatively small size of the renal tumour lesion in this trial, with a median diameter of 5.5 cm. However, other factors responsible for a lack of survival benefit from LDN may be the unpredictability of lymphatic drainage of RCC and the assumption that the main route of metastatic spread is haematogenous. In former series, between 58% and 95% of patients with LN involvement have associated haematogenous metastases [14.12, 14.13], which is why LN metastases are regarded as a significant indicator of systemic disease and adverse prognosis. Patients with pN0 have a 75% 5 year survival, whereas patients with pN+ have a 20% 5 year survival rate [14.9, 14.18]. Therefore, extensive LDN may only prolong time to progression, but not survival. The high percentage of concurrent systemic disease with LN involvement has resulted in the view that the likelihood of identifying a patient with LN only involvement is low. As a consequence, routine LDN for all patients, to identify those few with LN only metastases who would potentially benefit from LDN, does not seem to be justified. However, the final results of the 30881 trial coordinated by the EORTC have often been falsely interpreted and quoted as a support that LDN is not necessary. This is not in line with the original conclusion of the study [14.19]. In fact, it was cautiously concluded that LDN combined with radical

nephrectomy does not increase morbidity or mortality, but its efficacy in terms of prolonged survival could not be demonstrated. In the EORTC view, this was largely dependent on the small number of LN metastases detected by LDN, and they went on to stress that the results did not mean that LDN should be completely abandoned. In individual cases, a patient may benefit from LDN, though it was argued that it is difficult to identify the individual patients. The current consensus is that suspicious LNs, either at imaging or palpation, should be removed during nephrectomy.

In addition, there is evidence that lymphatic drainage in RCC is less predictable than currently thought. The reported drainage through the thoracic duct mentioned in Section 14.1.2 is intriguing, and raises the hypothesis that landing sites of RCC may, in fact, not be within the boundaries of the proposed retroperitoneal templates. Clinically, drainage through the thoracic duct may explain the isolated mediastinal LN metastases that are more frequently observed in RCC compared to tumours in other organs [14.28–14.30]. Therefore, a potential reason for the lack of evidence supporting locoregional retroperitoneal LDN and the low detection of LN metastases in CT negative locoregional nodes may simply be the fact that landing sites of RCC are located outside the region of dissection in a significant percentage of cases. To improve the accuracy of LDN in RCC, it is of paramount importance to first understand the location and drainage to the SLN.

This consideration may be of particular significance because there is published evidence that patients with very early LN metastases and no systemic metastatic disease can potentially be cured by LDN [14.9]. In addition, Canfield et al. observed that patients with only one pN+ but without systemic disease survived significantly longer after LDN than patients with more than one pN+ (37.5 months versus 14.5 months) [14.31]. The true incidence of early LN metastasis without distant metastatic disease is unknown, but seems to be significantly correlated to tumour size. In nephrectomy and autopsy studies, microscopic LN metastases were frequently observed in smaller tumours [14.9, 14.32].

Because of the widespread use of US imaging, a stage shift has taken place in RCC, in that an increasing number of patients is diagnosed at an earlier stage, with consequently smaller renal tumours. At the same time, retrospective studies reveal that even small tumours have potential for early lymphatic or distant metastatic spread. In an autopsy study, 254 patients had renal tumours smaller than 3 cm, and 3.5% revealed early LN metastases, which increased to 21% in tumours that were 4–5 cm in size [14.24]. In the nephrectomy series of Hashimoto et al. [14.33] and Matsuyama et al. [14.34], these values were 4% and 2.5%, respectively, for tumours of 4 cm and less. Thus, a considerable number of patients with pT1 tumours may have early lymphatic metastases. Contrary to the

historical data where patients with LN metastases often have additional systemic disease, stage shift may result in an increasing number of patients with early LN metastases only who may benefit from removal of these lesions. In addition, the introduction of more effective therapy with tyrosine kinase inhibitors has revived interest in adjuvant treatment concepts.

More accurate LN staging is warranted to determine the risk of recurrence or progression. Sequential lymphoscintigraphy for SLNM and SLNB in RCC may enhance early detection of LN metastases without the associated morbidity of extensive LDN.

14.1.4. Contribution of SPECT/CT and intraoperative imaging

The only report available analysing SLNM in the kidneys concerns administration of ^{99m}Tc radiocolloid intraoperatively in a porcine model [14.35]. In this study, the tracer and blue dye were injected into the renal parenchyma after exposure with a flank incision. In four pigs, SLNs were successfully removed within 10 min after injection following detection with a gamma probe [14.35].

The feasibility of the procedure and the location of the SLN including sampling at nephrectomy in clinically non-metastatic RCC patients has been investigated and reported [14.36]. Inclusion criteria were localized parenchymal kidney tumours not exceeding 10 cm (cT1–cT2), no metastatic disease on imaging and clinical examination (cN0, cM0), age greater than 18 years, life expectancy more than 3 months, WHO performance status 0 or 1 and fit for surgery, and no prior systemic treatment with biological response modifiers, tyrosine kinase inhibitors, MAbs or chemotherapy. Patients underwent pre-operative lymphoscintigraphy on the day before nephrectomy. Technetium-99m nanocolloid was injected percutaneously in a volume of 0.4 mL and an activity of 225 MBq into the primary lesion under US guidance. CT guidance was only indicated in cases of inappropriate imaging using US (Fig. 14.1).

Primary tumours up to 4 cm in size were injected centrally in a volume of 0.4 mL. In cases of tumours between 4 cm and 7 cm in size, two to three depots of 0.4 mL in total were injected around the centre. There were no patients with tumours larger than 7 cm. Following injection, anterior and lateral lymphoscintigraphy of the affected site was obtained after 20 min, 2 h and 4 h. After delayed planar imaging, SPECT and low dose CT images were acquired using a hybrid camera (SymbiaT, Siemens, Erlangen, Germany). After correction for attenuation and scatter, corresponding SPECT and CT axial 5 mm slices were generated. Images were subsequently fused and analysed using 2-D orthogonal reslicing in the axial, sagittal and coronal directions. In addition, a 3-D presentation, using volume rendering, was generated to localize SLNs in relation

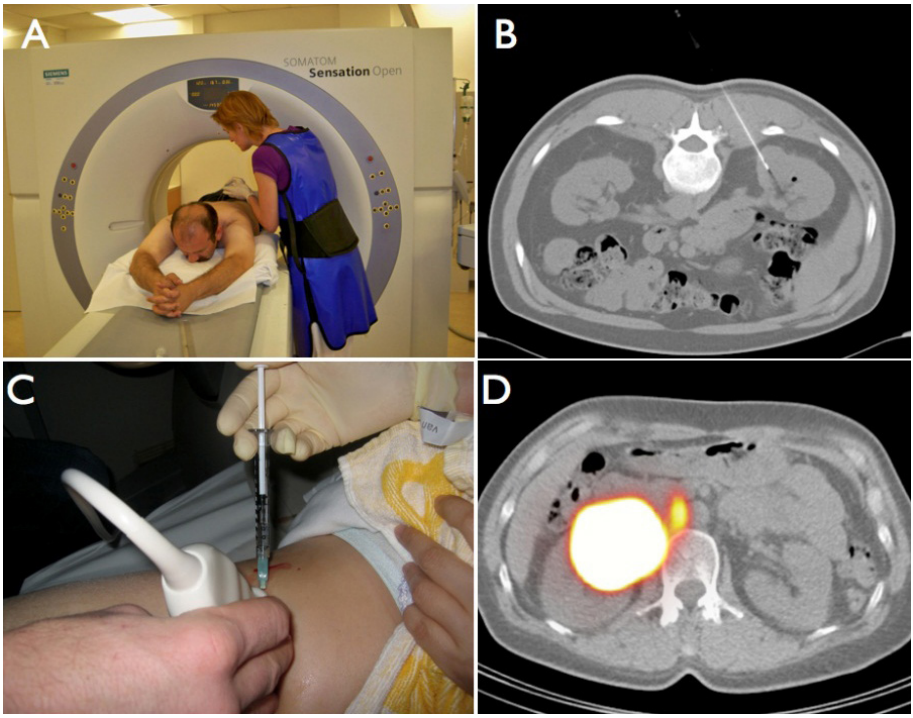

FIG. 14.1. CT guided radiocolloid administration in a patient with a tumour in the right kidney (A, B). In another patient, injection is guided using US imaging (C) and a para-aortic SLN is subsequently visualized on the SPECT/CT image (D) medial from the injection site.

to anatomic structures. All images were available on a separate SPECT/CT imaging screen in the operating theatre (Fig. 14.2).

The LNs in each station appearing on early planar lymphoscintigraphy were considered to be SLNs. LNs appearing on delayed images in the same stations were considered to be second echelon nodes. If SPECT/CT imaging showed hot spots in other areas or on a side with no previous drainage, those were also considered to be SLNs. To provide an orientation point for incision, levels of the SLNs were marked on the skin. Those marks also functioned as a centring point for intraoperative radioguidance using the portable gamma camera. Patients underwent an open or laparoscopic transperitoneal nephrectomy. In cases of tumours up to 4 cm in size, a nephron sparing tumour resection was performed. Intraoperative SLN detection and localization was assisted by gamma probe counting in combination with imaging using a portable gamma camera (Fig. 14.2). The use of this portable gamma camera has been described previously [14.37]. Patent blue was not used for intraoperative SLN localization. Eight patients, seven with right sided RCC, were included with a mean age of 55 years (range 45–77 years), and the mean tumour

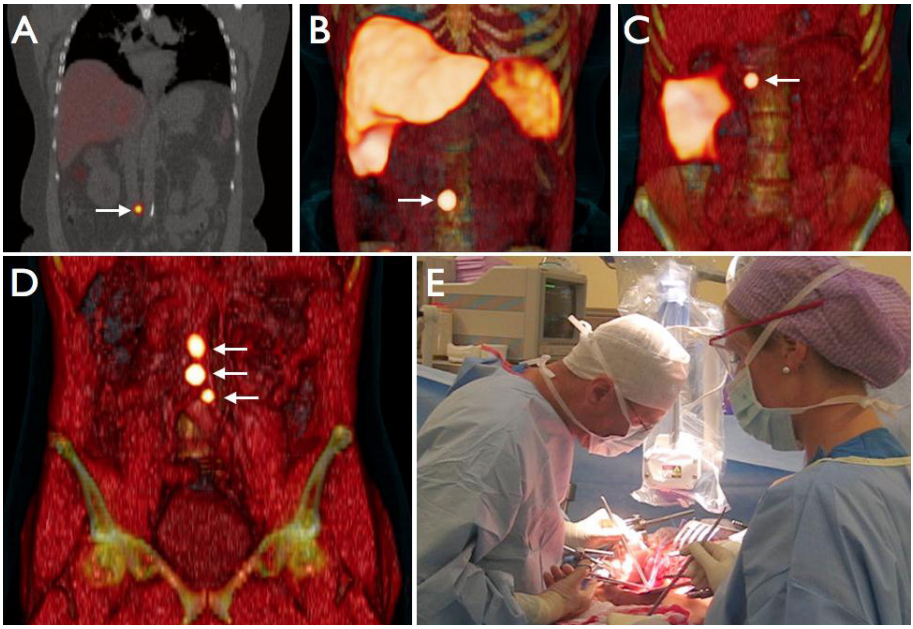

FIG. 14.2. Coronal SPECT/CT images showing SLNs (arrows) at various levels along the aorta in different patients (A–D). SLN localization in the operating room using a portable gamma camera (E).

size was 4 cm (range 3.5–6 cm). In two patients, no drainage was visualized; RCCs were of clear cell subtype with no LN metastases.

The initial experience has been extended to 20 patients [14.38] in the context of a prospective trial. An overview of the currently included patients and SLN locations is given in Fig. 14.3. SPECT/CT imaging detected the SLN in 14 out of 20 patients (70%), including 4 patients with non-visualization on planar lymphoscintigraphy. A total of 26 SLNs were seen; 17 para-aortic (including interaortocaval), 4 retrocaval, 1 hilar, 1 celiac trunk, 1 internal mammary, and 2 mediastinal and pleural. The latter four nodes were not harvested, according to protocol. All other SLNs, except for two weakly radioactive interaortocaval nodes, were identified and excised with a mean additional time of 20 min. None of the removed SLNs and locoregional LNs were tumour bearing.

14.1.5. SLNB and other imaging modalities

The diagnostic and therapeutic value of this technique remains to be investigated. Direct lymphatic drainage from renal cancer has never been studied in vivo and may help to shed light on the unpredictable location of LN metastasis. The absence of lymphatic drainage on imaging in 30% of patients

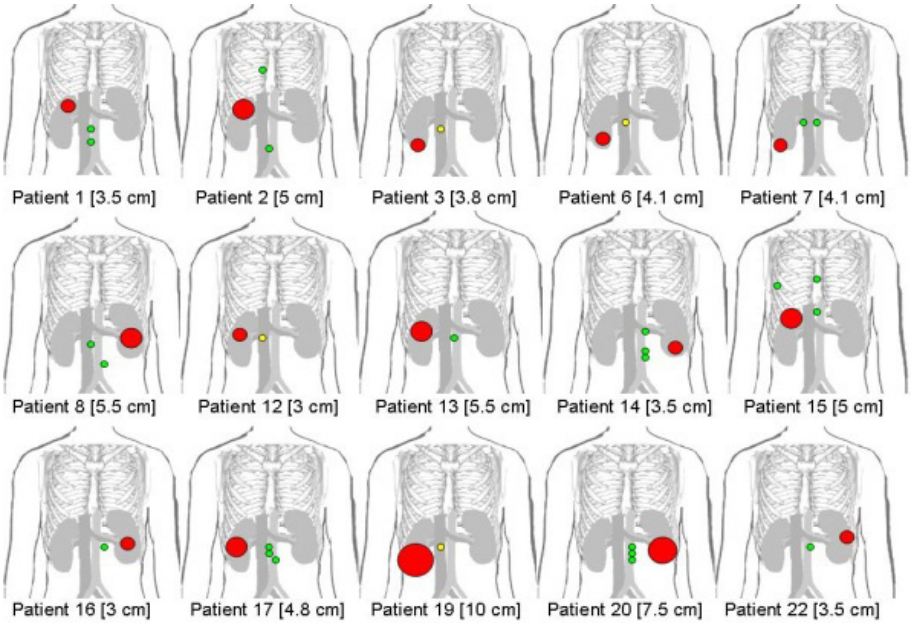

FIG. 14.3. SLN location in correlation to tumour size and location in 15 patients with lymphatic drainage on imaging. Primary tumours are red. The SLNs are green, except those SLNs in retrocaval locations (yellow). Patients 2 and 15 had SLNs outside the retroperitoneal template in addition to a retroperitoneal site.

is of concern, regarding a potential clinical application of this technique as no SLN could be identified, although SPECT/CT imaging demonstrated technically correct deposition of the radiocolloid in the tumour. This may be caused by lack of drainage of the intratumoural radiocolloids through lymphatic vessels. Alternatively, the radiocolloid in the tumour may have drained directly into the thoracic duct without any interposition of LNs.

Further studies are required to demonstrate if accurate mapping of lymphatic drainage and sampling of SLNs may lead to early detection of LN metastasis in cN0 and non-metastatic RCC. In addition, it will be of interest to assess whether LDN can be abandoned in patients with pathologically negative SLNs.

CT imaging seems to be sensitive enough to exclude the probability of regional LN metastases. In CT negative LNs, metastases were found in only 3%–4% of cases [14.16, 14.19]. Conversely, CT suspicious LNs were false positive in 58% of the cases in one series [14.19].

In the currently largest series of Kang and co-workers, [^{18}F]FDG PET imaging had a low sensitivity (75%) for detecting LN metastases, although with 100% specificity [14.39]. In a small series of nine patients, lymphotropic

nanoparticle enhanced MRI for assessing LNs in RCC revealed 100% sensitivity and 95.7% specificity [14.40]. In comparison to these techniques, however, the SLN strategy has the advantage of image guided tissue sampling. Ultimately, trials will have to demonstrate reliable detection of occult LN metastases at low false negative rates and, in particular, that LDN is no longer warranted in pathologically negative SLNs.

In conclusion, intraoperative SLN identification and SLNB after pre-operative detection using SPECT/CT imaging is surgically feasible and safe in patients with RCC. Preliminary data suggest that SLNs from the kidney are mainly located in the para-aortic, paracaval and interaortocaval regions, but aberrant LNs might receive direct drainage through the thoracic duct.

14.2. BLADDER CANCER

14.2.1. Introduction

Transitional cell carcinoma of the urinary bladder is one of the ten most frequently diagnosed cancers worldwide, with an incidence of 10.1 per 100 000 in males and 2.5 per 100 000 in females [14.41]. Approximately 25% of urinary bladder cancers present muscular invasion at diagnosis and account for approximately 80% of disease related deaths [14.42]. Approximately 33% of patients with muscle invasive urinary bladder cancer (iUBC) present with undetected dissemination at the time of primary treatment.

Generally, surgical treatment for iUBC consists of cystectomy and the removal of regional LNs. The extent of LDN performed in conjunction with cystectomy and the questions as to whether this technique is merely a staging procedure or a therapeutic intervention are still matters of discussion [14.43, 14.44]. The standard approach is to perform extended LN dissection (i.e. anatomical borders: the genitofemoral nerve lateral, the bladder wall medial and the aortic bifurcation proximal). Nevertheless, the extent of LN dissection varies considerably because of differences in surgical techniques. In particular, controversy exists as to whether higher, third echelon LNs, around the inferior mesenteric artery and down to the aortic bifurcation, should routinely be dissected. Therefore, limited LN dissection, consisting of removing the lymphatic tissue in the obturator fossa distal to the bifurcation of the common iliac vessels, is currently recommended as a staging procedure in most European countries [14.45, 14.46].

The overall 50% 5 year survival rate in patients undergoing radical cystectomy is assumed to be related to undetected metastatic dissemination to unidentified LNs [14.47]. Indeed, in cases of LN involvement at time of surgery,

typically found in 20%–25% of patients, the 5 year survival rates is lower (23%–35%) [14.48, 14.49].

CT imaging of the abdomen and thorax is often used to evaluate extravesical growth and distant metastasis in iUBC, but the sensitivity for detecting nodal metastasis is low [14.50]. Even if MRI and [^{18}F]FDG PET imaging showed better results, presently, there is no available imaging technique that is reliable for accurate LN staging in iUBC [14.51, 14.52].

14.2.2. SLN procedure

A new and still experimental approach for bladder cancer is to intraoperatively identify SLNs, and to use the presence of cancer cells or molecular markers in the SLN to guide the extent of LN dissection [14.45, 14.46]. Because regional LN metastasis, if present, is located in the SLN, extensive LN dissection may not be beneficial to patients whose SLNs are free of metastatic cells [14.45].

Because of the wide interpatient variation in LN drainage from the bladder, anatomical location alone cannot be used to identify SLNs in iUBC [14.49]. Pre-operative intravesical injection of blue dye and radiocolloid have thus been explored for identifying LNs that drain iUBC [14.45]. Detection and visualization of the SLN included pre-operative lymphoscintigraphy, intraoperative gamma probe detection and visual inspection of blue dye uptake in the LN (Fig. 14.4).

Pre-operative lymphoscintigraphy is very sensitive, but is difficult to use in patients with bladder cancer. The lymphatic pattern in the pelvis is complex. Lymphoscintigraphy is a planar imaging modality, with a lack of anatomical spatial resolution. Thus, radioactivity from the primary injection sites may interfere with SLN visualization, especially when the SLN is located close to the primary tumour. Furthermore, even if in most cases, LNs can be identified using a small hand-held intraoperative probe, it is difficult to transfer pre-operatively identified nodes to corresponding anatomical locations [14.46, 14.53].

False negative findings could either be related to technical problems (radiocolloid injection or image quality) or to the possibility of a massively metastatic SLN losing its ability to accumulate and retain the radiocolloid [14.54].

Hybrid gamma cameras can associate lymphoscintigraphy, performed as SPECT, and CT. This combination of lymphoscintigraphy with CT imaging provides more information on pre-operative anatomic localization of SLNs in iUBC and facilitates SLN detection during surgery [14.14, 14.15]. The yield of detected SLNs is increased using SPECT/CT imaging. Explanations for this finding might be found both in the timing of detection (some identified nodes may therefore be second and third echelon nodes) or in the possibility of simultaneous SLNs originating from different parts of large tumours, with different sections of the bladder having individual and separate drainage routes

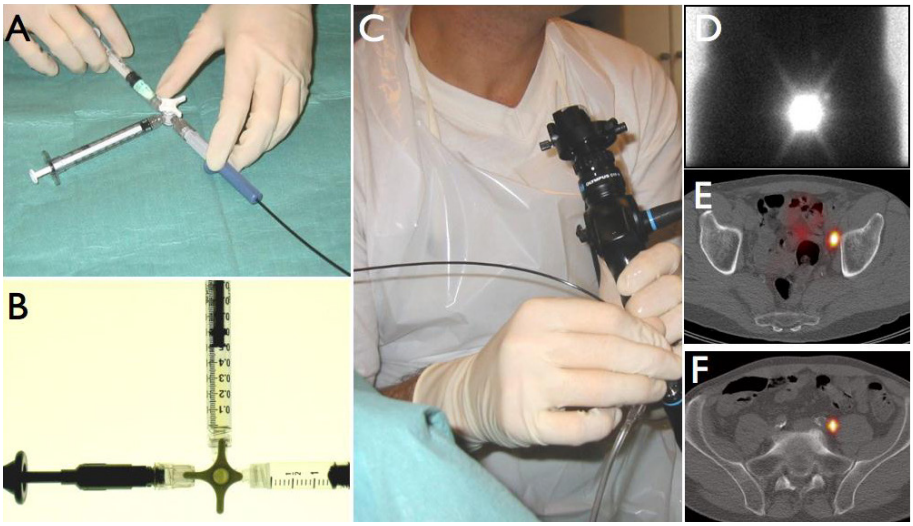

FIG. 14.4. Radiocolloid injection in bladder cancer using a needle fitted over a three way stopcock with one Luer Lock system (A, B), under endoscopic guidance (C). Early anterior planar scintigraphic image (D). SPECT/CT imaging reveals left iliac lymphatic drainage with SLNs along the iliac vessels (E, F).

(this factor could also explain crossover phenomena and bilateral distribution of nodal metastases) [14.54].

14.2.3. Methodology

14.2.3.1. Radiopharmaceutical used

Technetium-99m nanocolloid, divided into four equal parts, is used; the total radioactivity injected varies in the range 20–30 MBq if surgery is to follow on the same day or 50–150 MBq if surgery takes place on the next day. The total activity is divided equally into four injection sites, each receiving approximately 1 mL [14.46, 14.54].

14.2.3.2. Injection technique

Radiocolloid injection is performed via a transurethral approach, while the patient is in the lithotomy position. A long Williams cystoscopic injection needle directed by a ureteral catheter deflecting bridge (Albarran bridge) is used to inject the radiocolloid into the detrusor muscle, in four different sites adjacent to the visible bladder tumour or tumour base [14.46, 14.54]. Caution should be used

not to inject directly beneath the mucous membrane or to penetrate the muscular wall, nor to infiltrate the radiocolloids around the bladder (Fig. 14.4).

14.2.3.3. Imaging techniques

Before lymphoscintigraphy, an indwelling catheter is used to empty the bladder and wash out excess radiocolloid from the bladder cavity. Planar scans of the pelvis are recorded 1–3 h after injection in the anterior, posterior and lateral views. The injections sites can be masked with a lead shield to improve visualization of the small amount of activity retained in the SLNs.

14.2.3.4. SPECT/CT imaging

SPECT and subsequent CT scans are acquired in a single imaging session using a hybrid SPECT/CT gamma camera. For SPECT, sixty 3° angle views (30 s each) are acquired with a low energy, general purpose collimator and a 128 × 128 matrix. Low dose CT is used for anatomic data, and the two acquisitions are fused to produce a combined picture for interpretation

14.2.3.5. Analysis

Radiocolloid migration indicates lymphatic drainage from the primary tumour, and suspected SLNs are visualized as well delineated hot spots with increasing radioactivity clearly separated from the sites of injection. LN dissection is thus pre-operatively planned.

14.2.3.6. Surgical detection

SLNB is performed under guidance using a hand-held gamma detection probe in the operating room. The associated blue dye injection, performed under the same conditions, often improves SLN identification. After completion of LDN and cystectomy, the pelvic cavity and nodal basins should be explored using the gamma probe for residual radioactivity. Remaining radioactive tissue should be identified and removed.

14.2.4. Conclusions

In addition to the pathological stage, the histological status of regional LNs represents one of the most important predictors of survival in patients with iUBC. Pre-operative LN staging in iUBC is still problematic. However, the

rationale of staging has not yet been clearly addressed, and MRI, CT imaging and [^{18}F]FDG PET imaging have not shown any major advantages.

Identification, location and subsequent pathological examination of the SLN, the first node of the regional LN basin, reflects the nodal status of the remaining regional nodes. The SLN is specific in each individual. Its detection, which is still experimental in urological malignancies, allows the identification of a small volume of representative nodal tissue for thorough pathological evaluation.

Disadvantages of lymphoscintigraphy include the time and cost of examination, and sometimes the difficulties in interpreting the images. However, hybrid SPECT/CT imaging improves pre-operative anatomic localization of SLNs in iUBC.

Thus, SLNM and SLNB may provide correct estimation of metastatic LN involvement in iUBC, and thus lead to more specific and individually tailored surgical approaches.

REFERENCES TO CHAPTER 14

[14.1] GUPTA, K., MILLER, J.D., LI, J.Z., RUSSELL, M.W., CHARBONNEAU, C., Epidemiologic and socioeconomic burden of metastatic renal cell carcinoma (mRCC): A literature review, Cancer, Treat. Rev. **34** (2001) 193–205.

[14.2] JEMAL, A., et al., Cancer statistics, 2009, CA Cancer J. Clin. **59** (2009) 225–249.

[14.3] FERLAY, J., et al., Estimates of the cancer incidence and mortality in Europe in 2006, Ann. Oncol. **18** (2007) 581–592.

[14.4] BASSO, M., CASSANO, A., BARONE, C., A survey of therapy for advanced renal cell carcinoma, Urol. Oncol. **28** (2001) 121–133.

[14.5] MOTZER, R.J., et al., Prognostic factors for survival in previously treated patients with metastatic renal cell carcinoma, J. Clin. Oncol. **22** (2001) 454–463.

[14.6] FLANIGAN, R.C., YONOVER, P.M., The role of resection for patients with renal carcinoma, Curr. Oncol. Rep. **3** (2001) 424–432.

[14.7] LJUNGBERG, B., et al., Renal cell carcinoma guideline, Eur. Urol. **51** (2001) 1502–1510.

[14.8] BLOM, J.H., VAN POPPEL, H., MARECHAL, J.M., Radical nephrectomy with and without lymph node dissection: Preliminary results of the EORTC randomized phase III protocol 30881, Eur. Urol. **36** (1999) 570–575.

[14.9] PANTUCK, A.J., et al., Renal cell carcinoma with retroperitoneal lymph nodes. Impact on survival and benefits of immunotherapy, Cancer **97** (2003) 2995–3002.

[14.10] ROBSON, C.J., CHURCHILL, B.M., ANDERSON, W., The results of radical nephrectomy for renal cell carcinoma, Trans. Am. Assoc. Genitourin. Surg. **60** (1968) 122–129.

[14.11] WATERS, W.B., RICHIE, J.P., Aggressive surgical approach to renal cell carcinoma: Review of 130 cases, J. Urol. **122** (1979) 306–309.
[14.12] FREEDLAND, S.J., DEKERNION, J.B., Role of lymphadenectomy for patients undergoing radical nephrectomy for renal cell carcinoma, Rev. Urol. **5** (2003) 191–195.
[14.13] PHILLIPS, C.K., TANEJA, S.S., The role of lymphadenectomy in the surgical management of renal cell carcinoma, Urol. Oncol. **22** (2004) 214–223.
[14.14] GIULIANI, L., GIBERTI, C., MARTORANA, G., ROVIDA, S., Radical extensive surgery for renal cell carcinoma: Long-term results and prognostic factors, J. Urol. **143** (1990) 468–473.
[14.15] PIZZOCARO, G., PIVA, L., Pros and cons of retroperitoneal lymphadenectomy in operable renal cell carcinoma, Eur. Urol. **18** (1990) 22–23.
[14.16] MINERVINI, A., LILAS, L., MORELLI, G., Regional lymph node dissection in the treatment of renal cell carcinoma: Is it useful in patients with no suspected adenopathy before or during surgery? BJU Int. **88** (2001) 169–172.
[14.17] GIBERTI, C., ONETO, F., MARTORANA, G., ROVIDA, S., CARMIGNANI, G., Radical nephrectomy or renal cell carcinoma: Long-term results and prognostic factors on a series of 328 cases, Eur. Urol. **31** (1997) 40–48.
[14.18] PANTUCK, A.J., et al., Renal cell carcinoma with retroperitoneal lymph nodes: Role of lymph node dissection, J. Urol. **169** (2003) 2076–2083.
[14.19] BLOM, J.H., et al., Radical nephrectomy with and without lymph-node dissection: Final results of European Organization for Research and Treatment of Cancer (EORTC) randomized phase 3 trial 30881, Eur. Urol. **55** (2009) 28–34.
[14.20] JOSLYN, S.A., SIRINTRAPUN, S.N., KONETY, B.R., Impact of lymphadenectomy and nodal burden in renal cell carcinoma: Retrospective analysis of the National Surveillance, Epidemiology, and End Results database, Urology **65** (2005) 675–680.
[14.21] TERRONE, C., et al., The number of lymph nodes examined and staging accuracy in renal cell carcinoma, BJU Int. **91** (2003) 37–40.
[14.22] SAITOH, H., NAKAYAMA, M., NAKAMURA, K., SATOH, T., Distant metastasis of renal adenocarcinoma in nephrectomized cases, J. Urol. **127** (1982) 1092–1095.
[14.23] HULTEN, L., ROSENCRANTZ, M., SEEMAN, T., WAHLQVIST, L., AHREN, C., Occurrence and localization of lymph node metastases in renal carcinoma, Scand. J. Urol. Nephrol. **3** (1969) 129–133.
[14.24] JOHNSEN, J.A., HELLSTEN, S., Lymphatogenous spread of renal cell carcinoma: An autopsy study, J. Urol. **157** (1997) 450–453.
[14.25] PARKER, A.E., Studies on the main posterior lymph channels of the abdomen and their connections with the lymphatics of the genito-urinary system, Am. J. Anat. **56** (1935) 409–443.
[14.26] ASSOUAD, J., RIQUET, M., FOUCAULT, C., HIDDEN, G., DELMAS, V., Renal lymphatic drainage and thoracic duct connections: Implications for cancer spread, Lymphology **39** (2006) 26–32.
[14.27] ASSOUAD, J., RIQUET, M., BERNA, P., DANEL, C., Intrapulmonary lymph node metastasis and renal cell carcinoma, Eur. J. Cardio-Thorac. **31** (2007) 132–134.

[14.28] MAHON, T.G., LIBSHITZ, H.I., Mediastinal metastases of infradiaphragmatic malignancies, Eur. J. Radiol. **15** (1992) 130–134.
[14.29] RIQUET, M., LE PIMPEC BARTHES, F., SOUILAMAS, R., HIDDEN, G., Thoracic duct tributaries from intrathoracic organs, Ann. Thorac. Surg. **73** (2002) 892–898.
[14.30] WRIGHT, F.W., Enlarged hilar and mediastinal nodes (and especially lower right hilar node enlargement) as a sign of metastasis of a renal tumor, Clin. Radiol. **28** (1977) 431–436.
[14.31] CANFIELD, S.E., et al., Renal cell carcinoma with nodal metastases in the absence of distant metastatic disease (clinical stage TxN1-2M0): The impact of aggressive surgical resection on patient outcome, J. Urol. **175** (2006) 864–869.
[14.32] HELLSTEN, S., BERGE, T., LINELL, F., Clinically unrecognised renal carcinoma: Aspects of tumour morphology, lymphatic and haematogenous metastatic spread, Br. J. Urol. **55** (1983) 166–170.
[14.33] HASHIMOTO, K., et al., Tumour size and regional lymph node metastasis in patients with M0 renal cell carcinoma: Analysis in those having regional lymph node dissection, Hinyokika Kiyo **51** (2005) 621–625.
[14.34] MATSUYAMA, H., et al., Clinical significance of lymph node dissection in renal cell carcinoma, Scand. J. Urol. Nephrol. **39** (2005) 30–35.
[14.35] BERNIE, J.E., ZUPKAS, P., MONGA, M., Intraoperative mapping of renal lymphatic drainage: Technique and application in a porcine model, J. Endourol. **17** (2003) 235–237.
[14.36] BEX, A., et al., Feasibility of sentinel node detection in renal cell carcinoma: A pilot study, Eur. J. Nucl. Med. Mol. Imaging **37** (2010) 1117–1123.
[14.37] VERMEEREN, L., et al., Intraoperative radioguidance with a portable gamma camera: A novel technique for laparoscopic sentinel node localisation in urological malignancies, Eur. J. Nucl. Med. Mol. Imaging **36** (2009) 1029–1036.
[14.38] STUDER, U.E., SCHERZ, S., SCHEIDEGGER, J., Enlargement of regional lymph nodes in renal cell carcinoma is often not due to metastases, J. Urol. **144** (1990) 243–245.
[14.39] KANG, D.E., WHITE, R.L., Jr., ZUGER, J.H., SASSER, H.C., TEIGLAND, C.M., Clinical use of fluorodeoxyglucose F 18 positron emission tomography for detection of renal cell carcinoma, J. Urol. **171** (2004) 1806–1809.
[14.40] GUIMARAES, A.R., et al., Pilot study evaluating use of lymphotrophic nanoparticle-enhanced magnetic resonance imaging for assessing lymph nodes in renal cell cancer, Urology **71** (2008) 708–712.
[14.41] PLOEG, M., ABEN, K.K., KIEMENEY, L.A., The present and future burden of urinary bladder cancer in the world, World J. Urol. **27** (2009) 289–293.
[14.42] PROUT, G.R., Jr., GRIFFIN, P.P., SHIPLEY, W.U., Bladder carcinoma as a systemic disease, Cancer **43** (1979) 2532–2539.
[14.43] BELLMUNT, J., et al., Bladder cancer: ESMO Practice Guidelines for diagnosis, treatment and follow-up, ESMO Guidelines Working Group, Ann. Oncol. **21** (2010) S134–S136.
[14.44] STEIN, J.P., SKINNER, D.G., The role of lymphadenectomy in high-grade invasive bladder cancer, Urol. Clin. North Am. **32** (2005) 187–197.

[14.45] SHERIF, A., DE LA TORRE, M., MALMSTRÖM, P.U., THÖRN, M., Lymphatic mapping and detection of sentinel nodes in patients with bladder cancer, J. Urol. **166** (2001) 812–815.
[14.46] LIEDBERG, F., CHEBIL, G., DAVIDSSON, T., GUDJONSSON, S., MANSSON, W., Intraoperative sentinel node detection improves nodal staging in invasive bladder cancer, J. Urol. **175** (2006) 84–88.
[14.47] LEISSNER, J., et al., Extended radical lymphadenectomy in patients with urothelial bladder cancer: Results of a prospective multicenter study, J. Urol. **171** (2004) 139–144.
[14.48] LERNER, S.P., et al., The rationale for en bloc pelvic lymph node dissection for bladder cancer patients with nodal metastases: Long-term results, J. Urol. **149** (1993) 758–764.
[14.49] STEIN, J.P., SKINNER, D.G., Radical cystectomy for invasive bladder cancer: Long-term results of a standard procedure, World J. Urol. **24** (2006) 296–304.
[14.50] PAIK, M.L., SCOLIERI, M.J., BROWN, S.L., SPIRNAK, J.P., RESNICK, M.I., Limitations of computerized tomography in staging invasive bladder cancer before radical cystectomy, J. Urol. **163** (2000) 1693–1696.
[14.51] HAIDER, E.A., et al., Magnetic resonance imaging of the urinary bladder: Cancer staging and beyond, Can. Assoc. Radiol. J. **59** (2008) 241–258.
[14.52] APOLO, A.B., et al., Clinical value of fluorine-18 2-fluoro-2-deoxy-D-glucose positron emission tomography/computed tomography in bladder cancer, J. Clin. Oncol. **28** (2010) 3973–3978.
[14.53] MALMSTRÖM, P.U., et al., Early metastatic progression of bladder carcinoma: Molecular profile of primary tumour and sentinel lymph node, J. Urol. **168** (2002) 2240–2244.
[14.54] SHERIF, A., GARSKE, U., DE LA TORRE, M., THÖRN, M., Hybrid SPECT-CT: An additional technique for sentinel node detection of patients with invasive bladder cancer, Eur. Urol. **50** (2006) 83–91.

15. GOSTT IN NEUROENDOCRINE TUMOURS

15.1. INTRODUCTION AND CLINICAL BACKGROUND

Neuroendocrine tumours (NETs) are considered relatively rare tumours that have the characteristic property of secreting bioactive substances, such as amines and hormones. They constitute a heterogeneous group characterized by generally good prognosis, although important disparities exist in their evolution/progression potential. The degree of tumour differentiation is evaluated by histological criteria and proliferative markers (Ki67). In the forms characterized by a more aggressive pattern of growth, the clinical benefit of therapeutic strategies is limited [15.1–15.3].

Early diagnosis and precise localization of these tumours are crucial for optimal management and are particularly helpful for planning potentially curative resection. While morphological imaging procedures (US imaging, CT imaging and MRI) are often inadequate to evaluate NET differentiation and stage, nuclear medicine imaging has gained a crucial role for optimal planning of patient management. In fact, the presence of neuroamine uptake mechanisms and/or peptide receptors on the cell membrane of these tumours constitutes the basis for the clinical use of specific radiolabelled ligands, both for imaging and for therapy of NETs [15.4, 15.5].

Radioiodinated MIBG, a norepinephrine analogue, was the first radiopharmaceutical used to specifically depict and localize catecholamine secreting tumours (pheochromocytomas, paragangliomas and neuroblastomas) and is still regarded as a first choice imaging technique for diagnosis and follow-up of these tumours [15.6].

An SST analogue labelled with ^{111}In (^{111}In DTPA D-Phe^{1}-octreotide or OctreoScan), is used as a diagnostic agent to image endodermic derived NETs, particularly those expressing a high density of SSTRs on their cell membranes, such as, typically, gastroenteropancreatic (GEP) tumours [15.7]. Five different SSTR subtypes have been identified so far. Nevertheless, the potential of somatostatin receptor scintigraphy (SRS) (which is routinely employed for localizing the primary NETs, evaluating disease extension and monitoring the effect of treatment) is somewhat limited by a certain variability in receptor expression within this heterogeneous group of tumours. Moreover, this radiopharmaceutical binds with high affinity only to SSTR type 2 [15.8].

On the other hand, other functional imaging procedures using PET also appear to be a promising and useful supplement for characterization of NETs [15.9]. In particular, numerous studies have reported the clinical value of [^{18}F]FDG for localizing both the primary tumour and distant metastatic lesions.

Furthermore, [^{18}F]FDG uptake is higher in poorly differentiated NETs, which are, in general, characterized by reduced SSTR expression and high metabolic and proliferative activity (and therefore by high glucose consumption) [15.10, 15.11]. Conversely, the uptake of radiolabelled SST analogues is higher for typical, well differentiated carcinoid tumours. Moreover, the ability of NETs to store biogenic amines constitutes the pathophysiological basis for imaging these tumours with an additional PET tracer, 6-^{18}F fluoro-L-dopamine, to improve the detection of well or moderately differentiated NETs [15.12]. Finally, new SST analogues with different receptor affinities, as well as other peptides, are currently under investigation and will, in the future, further improve our diagnostic and therapeutic capabilities. There is also growing interest in the use of ^{68}Ga DOTA TOC for PET imaging of NETs, particularly for detecting small tumours or tumours expressing only a low density of SSTRs [15.13–15.19].

Because surgery is the only curative therapeutic option for NETs, the efficacy of surgical treatment depends on complete excision of all the tumour tissue; therefore, pre-operative localization of primary and metastatic tumours is crucial.

Intraoperative gamma probe guided detection made possible by the administration of a specific radiolabelled compound with adequate uptake in NETs may allow precise localization and identification of even small tumours, thus helping to reduce the high rate of unsuccessful surgical explorations in patients with NETs. In fact, the detection of microscopic and clinically occult lesions enables more complete tumour resection. This real time intraoperative detection procedure overcomes many of the limitations encountered with conventional external scintigraphy [15.10].

In principle, the possibility of efficient intraoperative detection of tumours using this technique is based on numerous factors including: (i) biodistribution of the radiopharmaceutical (e.g. tumour specific uptake, physiological uptake in normal organ/tissues or clearance kinetics), (ii) physical properties of the labelling radionuclide (e.g. emitted radiation, energy, half-life) and (iii) probe engineering. All these factors ultimately determine the TBR and the detection threshold.

For successful tumour detection, a minimum TBR of 1.5–2.0:1 is required in the operative field. Nevertheless, a ratio above 2.4 makes differences between tumour tissue and normal adjacent tissue more reliable. In clinical practice, a several fold higher ratio can be observed [15.20, 15.21].

15.2. PROBES

15.2.1. Gamma detection

By providing real time response and positioning flexibility, the hand-held intraoperative gamma probe has become the new supplemental tool for inspection and palpation procedures traditionally performed by the surgeon.

The use of high energy radionuclides such as ^{131}I requires heavy mechanical shielding around the detector, thus making the gamma probe heavy and bulky, thereby reducing its acceptance by the surgeon. Isotopes such as ^{99m}Tc or ^{111}In have excellent physical properties for external and intraoperative imaging. Therefore, a single dose of the radiopharmaceutical can be used for pre-operative scintigraphy, intraoperative localization and postoperative evaluation of the results of surgical treatment [15.22].

Specific tracer accumulation relates to the size and morphology of the tumour and to high density expression of specific receptor subtypes. Even if undesirable background activity produced by sites of physiological uptake/excretion close to the tumour lesions can be blocked or shielded, the major limitation of intraoperative detection is still high background activity. It is thus extremely important to avoid directing the probe towards sites of physiological tracer accumulation. Intraoperative gamma probe scanning requires careful, slow, searching of suspected areas, a procedure that can be time consuming owing to subtle differences in activity concentrations because of variable backgrounds according to the specific anatomic location.

15.2.2. Detection of positron emission

It is expected that an intraoperative probe that directly explores intraoperatively lesions emitting positrons would be more sensitive and accurate than conventional PET imaging, which is still limited by suboptimal spatial resolution. These hand-held PET intraoperative probes are capable of detecting either positrons or the high energy γ photons produced by the annihilation event [15.23]. Sites of accumulation for radiopharmaceuticals labelled with positron emitters can be detected by two methods: direct detection of the β^+ particles or detection of the 511 keV annihilation photons. In the latter instance, it is possible to adapt a conventional gamma probe to detect the high energy photons [15.24]. Nevertheless, phantom experiments indicate that overall counts detected are greater for the beta probe than for the gamma probe [15.25]. The main drawback of the beta probe is because of the short range of positrons in tissue, which might prevent the detection of tumour sites hidden behind even a thin layer of benign tissue. Moreover, the additional time required

during the surgical procedure should be considered and adequately taken into account [15.26–28].

An ideal intraoperative device should combine beta detection and coincidence detection of the paired annihilation photons with high sensitivity [15.29]. Currently, the clinical use of PET probes has been limited to clinical trials; thus, no standard protocols have been developed so far [15.24, 15.26–15.28].

15.3. HISTOPATHOLOGICAL SUBTYPES AND INTRAOPERATIVE DETECTION

15.3.1. Neuroectodermal tumours

The use of an intraoperative gamma probe after injection of radioiodinated MIBG may be helpful for detecting and removing small recurrent tumours in the adrenal region. In cases of pheochromocytoma [15.30–15.33] or neuroblastoma [15.34, 15.35], complete resection guided by the intraoperative gamma probe has resulted in postoperative normalization of urinary normetanephrine excretion.

Historically, early intraoperative detection procedures were performed using ^{125}I MIBG. In this case, pre-operative scintigraphy with ^{123}I MIBG was performed to localize tumour sites [15.36]. To increase the signal to noise ratio between the tumour and blood or adjacent normal tissues (e.g. a healthy liver), ^{125}I MIBG was injected at least 2 d before surgery. Thyroid uptake of free radioiodide released in the course of MIBG degradation in vivo should be prevented by the administration of Lugol's solution. Internal contamination is the main risk for surgical staff because external exposure is minimal [15.31].

For intraoperative detection of recurrent pheochromocytoma, Ricard et al. proposed to administer 740 kBq to 37 MBq of ^{125}I MIBG 48 h before surgery. This technique permitted the discovery of small (<1 cm) and non-palpable tumour lesions. The probe was particularly useful in cases of ectopic localization posterior to the vena cava, behind the liver, but also when the tumour foci were surrounded by intense fibrosis [15.31].

Another option is to use ^{123}I MIBG both for pre-operative scintigraphy and for intraoperative detection [15.37]. Adams et al. injected 180 MBq of ^{123}I MIBG 4–5 h before surgery. This procedure enabled the localization of all paravertebral subdiaphragmatic lesions (size >2 cm) of recurrent pheochromocytoma seen in the pre-operative MIBG scan. High liver uptake overshadowed intraoperatively potential sites of tumoural MIBG uptake, especially in the subdiaphragmatic/paravertebral region, leading to low TBRs [15.38].

Tumours of the carotid body are uncommon non-chromaffin paragangliomas that generally express high density SSTRs, which is a feature

that enables their localization by SRS. Martinelli et al. injected 180 MBq of ^{111}In DTPA D-Phe^{1}-octreotide 24 h before surgery, and the intraoperative gamma probe successfully identified all neck lesions, resulting in a mean TBR of 3 [15.39].

15.3.2. Neuroendodermal tumours

Imaging of NETs with radiolabelled SST analogues has high sensitivity and specificity, especially if performed using SPECT rather than planar acquisitions. However, the images acquired using SPECT alone generally lack anatomic details for precise intraoperative localization, while SPECT/CT imaging has obvious advantages over SPECT imaging alone for the purpose of anatotopographic localization of tumour lesions; nevertheless, the density of SSTRs in a lesion still remains a more important factor for tumour detection than size of the lesion. Therefore, scintigraphy (especially SPECT/CT) followed by intraoperative detection can localize these tumours with greater precision and sensitivity. The main advantage of intraoperative detection versus external SRS is high sensitivity, especially for detecting metastatic LNs. Removal of a primary NET together with all LN metastases, even in the presence of multiple liver metastases, has significantly delayed progression of the disease when appropriately treated [15.20, 15.21, 15.30].

Several factors may affect scintigraphic visualization of SSTRs and the sensitivity of intraoperative detection, including the expression of different subtypes of receptors (because of the varying binding affinities for the different radiolabelled SST analogues), and the time interval between radiopharmaceutical administration and surgery. In this regard, images acquired 24 h post-injection of the ^{111}In labelled analogue provide a better image quality with a high TBR; this is therefore the optimal time for intraoperative detection. Nevertheless, the procedure is somewhat limited by a certain incidence of false positive results, owing to tracer accumulation in the activated lymphocytes (which express SSTRs) within inflammatory infiltrates.

Initial intraoperative detection studies have been performed using ^{125}I labelled octreotide [15.40] or lanreotide [15.41], which were the first available radioiodinated SST analogues. Benevento et al. [15.42] proposed to inject 20 MBq of [^{125}I-Tyr^{3}] octreotide and 20 MBq of ^{125}I lanreotide. With the low energy emission of ^{125}I, tissue background is rather low and, when employed in patients with gastrointestinal NETs, the procedure was able to detect gamma emissions in a 4 mm submucosal duodenal lesion, in a retroduodenal LN and in a 7 mm submucosal mass of the second portion of the duodenum. The technique, however, required temporary bile duct occlusion to prevent the arrival of radioactivity excreted with the bile into the gut lumen [15.42].

The introduction of ^{111}In DTPA D-Phe^{1}-octreotide, which has consistently lower hepatobiliary excretion than the above radiopharmaceuticals, has improved the sensitivity of pre-operative imaging in patients with GEP NETs. Initial studies were based on the pre-operative injection of 140–300 MBq of ^{111}In octreotide [15.43, 15.44]. However, such early experience was somewhat disappointing, both because of the high energy photons emitted by ^{111}In and because of the high background activity from the liver, spleen and kidneys not allowing a reliable intraoperative detection of small abdominal lesions [15.44].

To avoid artefacts caused by the intestinal accumulation of radioactivity, Ohrvall et al. proposed to routinely administer laxatives on the day prior to surgery and throughout the procedure [15.45, 15.46]. By adopting this precaution, all lesions larger than 5 mm could be identified intraoperatively using the gamma probe. The TBR was slightly more favourable for small intestinal/mesenteric carcinoid lesions compared with pancreatic lesions, although the proportion of lesions detected was the same. The gamma probe thus appears to have appropriate shielding against non-specific radiation, making it suitable for ^{111}In based detection within the abdominal cavity. The mean radioactivity uptake in the identified lesions was approximately sevenfold that of the background activity. However, special attention was required not to expose the detector surface to the high activity emitted from normal organs, e.g. the liver, spleen or kidneys. For this reason, the procedure is not appropriate for the detection of liver metastases [15.45, 15.46].

Sufficient collimation and shielding has improved intraoperative lesion detection by gamma probe counting after administration of ^{111}In labelled octreotide, mainly because of improved TBRs (4:1 or higher) [15.44, 15.47–15.57].

Another interesting option for intraoperative detection of NETs of the gastrointestinal tract is to use ^{99m}Tc EDDA/HYNIC (ethylene diamine diacetic acid / hydrazinonicotinamide) octreotate [15.58]. This novel SST analogue has a higher affinity to SSTR subtype 2, a higher internalization rate and a lower liver uptake. Furthermore, the lower photon energy of ^{99m}Tc allows more effective shielding of background activity during intraoperative detection. The more intense tumour uptake is particularly important in the case of small pancreatic NETs, which are usually difficult to localize preoperatively. For patients with GEP NETs, Hubalewska-Dydejczyk et al. proposed to inject 740 MBq of ^{99m}Tc octreotate 24 h before surgery [15.21]. In carcinoid tumours, the TBRs for LN metastases were 1.9–3.9, which are substantially lower than those for primary tumours (16.9–50.5), owing to their location close to the mesenteric root and retroperitoneal space. The smallest LN detected intraoperatively using this method was 6 mm. In cases of pancreatic NETs, the smallest lesion identified using the hand-held probe (not palpated by the surgeon) was an 8 mm

tumour. The TBRs were 1.8 for insulinomas and 2.5 for glucagonoma, which were much lower than the TBRs measured from SPECT images (within the 3.5–10.5 range). This is because of the retroperitoneal location of the pancreas and the corresponding high background activity [15.21].

In summary, based on the published data, the optimal strategy to perform gamma probe guided surgery in NETs would be: (i) to assess the uptake features of the lesion with pre-operative scintigraphy, (ii) to inject 100–150 MBq of ^{111}In octreotide on the day before surgery, (iii) to administer laxatives starting on the day before surgery and (iv) to use appropriate probes for ^{111}In detection.

15.3.3. Intraoperative detection of NETs with positron emitting radiopharmaceuticals

Studies have been conducted using [^{18}F]FDG, which is the most common tracer used in oncology. Its uptake reflects the glycolytic activity of tissues, which is non-specifically enhanced in most cancer cells and in inflammatory cells. [Fluorine-18]FDG PET imaging is able to detect most high grade cancers, but has poor sensitivity in well differentiated cancers. Although relatively low diagnostic performances have been reported in small series of patients with NETs, the scan nevertheless provides important prognostic information because [^{18}F]FDG avidity increases with the level of dedifferentiation, aggressiveness and volume of tumour [15.9, 15.11, 15.25].

Physiological high uptake of [^{18}F]FDG in the brain reduces the TBRs for lesions located in the head and neck region. Similar considerations apply for cardiac uptake in the chest, for kidney uptake and for bladder accumulation in the abdomen and pelvis. In the latter instance, intraoperative bladder catheterization minimizes interference from bladder accumulation when exploring the pelvis using the gamma probe [15.24]. Gulec et al. injected 200–600 MBq of [^{18}F]FDG 2–6 h before surgery [15.24]. All the NET lesions identified on PET/CT imaging were detected by the PET probe, with their sizes ranging from 0.8 cm to 4 cm. The PET probe, however, was clearly most useful for detecting lesions that had not been found on initial visual and manual exploration. Some occult lesions included tumour masses measuring 2 cm or greater, located in regions with difficult surgical access (postsurgical adhesions or scar tissue) [15.24].

Radioguided surgery of NETs employing [^{18}F]FDG as the tumour seeking agent has some definite limitations. First, this technique may not be cost effective. Second, false positive results can occur, owing to sites with physiologically high [^{18}F]FDG uptake. Moreover, the PET probe detects all [^{18}F]FDG avid lesions and cannot differentiate malignancies from inflammation.

15.4. CONCLUSION

In the near future, the development of more specific ligands and alternative radionuclides for labelling should further improve the intraoperative identification of tumour lesions in patients suffering from NETs. Further improvements in the procedure are expected owing to ongoing improvements in the design of gamma probes and beta probes, such as novel materials for detection, novel collimation systems, peroperative statistical analysis of probe measurements and ergonomic probe design for exploration in restricted anatomical spaces.

REFERENCES TO CHAPTER 15

[15.1] REICHLIN, S., Somatostatin, N. Engl. J. Med. **309** (1983) 1495–1501.

[15.2] CAPLIN, M.E., et al., Carcinoid tumour, Lancet **352** (1998) 799–805.

[15.3] YAO, J.C., et al., One hundred years after 'carcinoid': Epidemiology of and prognostic factors for neuroendocrine tumors in 35,825 cases in the United States, J. Clin. Oncol. **26** (2008) 3063–3072.

[15.4] HOEFNAGEL, C.A., Metaiodobenzylguanidine and somatostatin in oncology: Role in the management of neural crest tumours, Eur. J. Nucl. Med. **21** (1994) 561–581.

[15.5] BOMBARDIERI, E., MacCAURO, M., DE DECKERE, E., SAVELLI, G., CHITI, A., Nuclear medicine imaging of neuroendocrine tumours, Ann. Oncol. **12** (2001) 51–61.

[15.6] HATTNER, R.S., HUBERTY, J.P., ENGELSTAD, B.L., GOODING, C.A., ABLIN, A.R., Localization of m-iodo (I-131) benzylguanidine in neuroblastoma, Am. J. Radiol. **143** (1984) 373–374.

[15.7] KRENNING, E.P., et al., Somatostatin receptor scintigraphy with [^{111}In-DTPA-D-Phe^{1}]- and [^{123}I-Tyr^{3}]-octreotide: The Rotterdam experience with more than 1000 patients, Eur. J. Nucl. Med. **20** (1993) 716–731.

[15.8] KRENNING, E.P., et al., Localisation of endocrine-related tumours with radioiodinated analogue of somatostatin, Lancet **1** (1989) 242–244.

[15.9] PACAK, K., EISENHOFER, G., GOLDSTEIN, D.S., Functional imaging of endocrine tumors: Role of positron emission tomography, Endocr. Rev. **25** (2004) 568–580.

[15.10] PASQUALI, C., et al., Neuroendocrine tumor imaging: Can ^{18}F-fluorodeoxyglucose positron emission tomography detect tumors with poor prognosis and aggressive behavior? World. J. Surg. **22** (1998) 588–592.

[15.11] ADAMS, S., et al., Limited value of fluorine-18 fluorodeoxyglucose positron emission tomography for the imaging of neuroendocrine tumours, Eur. J. Nucl. Med. **25** (1998) 79–83.

[15.12] HOEGERLE, S., et al., Whole-body ^{18}F DOPA PET for detection of gastrointestinal carcinoid tumors, Radiology **220** (2001) 373–380.

[15.13] MINN, H., KAUHANEN, S., SEPPÄNEN, M., NUUTILA, P., ^{18}F-DOPA: A multiple-target molecule, J. Nucl. Med. **50** (2009) 1915–1918.

[15.14] HAUG, A., et al., Intraindividual comparison of ^{68}Ga-DOTA-TATE and ^{18}F-DOPA PET in patients with well-differentiated metastatic neuroendocrine tumours, Eur. J. Nucl. Med. Mol. Imaging **36** (2009) 765–770.
[15.15] CARRASQUILLO, J.A., CHEN, C.C., Molecular imaging of neuroendocrine tumors, Semin. Oncol. **37** (2010) 662–679.
[15.16] SCHIESSER, M., et al., Value of combined 6-[^{18}F]fluorodihydroxyphenylalanine PET/CT for imaging of neuroendocrine tumours, Br. J. Surg. **97** (2010) 691–697.
[15.17] PUTZER, D., et al., Comparison of ^{68}Ga-DOTA-Tyr^{3}-octreotide and ^{18}F-fluoro-L-dihydroxyphenylalanine positron emission tomography in neuroendocrine tumor patients, Q. J. Nucl. Med. Mol. Imaging **54** (2010) 68–75.
[15.18] FANI, M., et al., Radiolabeled bicyclic somatostatin-based analogs: A novel class of potential radiotracers for SPECT/PET of neuroendocrine tumors, J. Nucl. Med. **51** (2010) 1771–1779.
[15.19] AMBROSINI, V., et al., ^{68}Ga-DOTA-NOC PET/CT clinical impact in patients with neuroendocrine tumors, J. Nucl. Med. **51** (2010) 669–673.
[15.20] SCHNEEBAUM, S., et al., Clinical applications of gamma-detection probes — radioguided surgery, Eur. J. Nucl. Med. **26** (1999) 26–35.
[15.21] HUBALEWSKA-DYDEJCZYK, A., et al., Radio-guided surgery with the use of [^{99m}Tc-EDDA/HYNIC]octreotate in intra-operative detection of neuroendocrine tumours of the gastrointestinal tract, Eur. J. Nucl. Med. Mol. Imaging **34** (2007) 1545–1555.
[15.22] ADAMS, S., BAUM, R.P., Intraoperative use of gamma-detecting probes to localize neuroendocrine tumors, Q. J. Nucl. Med. **44** (2000) 59–67.
[15.23] DAGHIGHIAN, F., et al., Intraoperative beta probe: A device for detecting tissue labeled with positron or electron emitting isotopes during surgery, Med. Phys. **21** (1994) 153–157.
[15.24] GULEC, S.A., HOENIE, E., HOSTETTER, R., SCHWARTZENTRUBER, D., PET probe-guided surgery: Applications and clinical protocol, World J. Surg. Oncol. **5** (2007) 65.
[15.25] TAÏEB, D., et al., ^{18}F-FDG avidity of pheochromocytomas and paragangliomas: A new molecular imaging signature? J. Nucl. Med. **50** (2009) 711–717.
[15.26] ESSNER, R., et al., Application of an [^{18}F]fluorodeoxyglucose-sensitive probe for the intraoperative detection of malignancy, J. Surg. Res. **96** (2001) 120–126.
[15.27] ESSNER, R., DAGHIGHIAN, F., GIULIANO, A.E., Advances in FDG PET probes in surgical oncology, Cancer J. **8** (2002) 100–108.
[15.28] GONZÁLEZ, S.J., et al., An analysis of the utility of handheld PET probes for the intraoperative localization of malignant tissue, J. Gastrointest. Surg. **15** (2011) 358–366.
[15.29] SCHILLACI, O., PET probes and oncological surgery: A productive new marriage for nuclear medicine? Eur. J. Nucl. Med. Mol. Imaging **34** (2007) 1530–1533.
[15.30] TENENBAUM, F., RICARD, M., Peroperative detection probes. Evaluation and perspectives in endocrinology, Ann. Endocrinol. **58** (1997) 39–46.

[15.31] RICARD, M., et al., Intraoperative detection of pheochromocytoma with iodine-125 labelled meta-iodobenzylguanidine: A feasibility study, Eur. J. Nucl. Med. **20** (1993) 426–430.
[15.32] BUHL, T., MORTENSEN, J., KJAER, A., I-123 MIBG imaging and intraoperative localization of metastatic pheochromocytoma: A case report, Clin. Nucl. Med., **27** (2002) 183–185.
[15.33] FUERTES MANUEL, J., et al., ^{123}I-MIBG SPECT-CT combined with gamma probe for radioguided localization of pheochromocytoma, Rev. Esp. Med. Nucl. **24** (2005) 418–421.
[15.34] AGARU, A., et al., ^{123}I MIBG mapping with intraoperative gamma probe for recurrent neuroblastoma, Mol. Imaging Biol. **10** (2008) 19–23.
[15.35] WACHOWIAK, R., et al., Residual lymph node metastasis in stage 4 neuroblastoma-advantage of radio-guided surgery? Pediatr. Hematol. Oncol. **27** (2010) 471–475.
[15.36] PROYE, C.A., et al., Intraoperative radionuclear ^{125}I-labeled metaiodobenzylguanidine scanning of pheochromocytomas and metastases, Surgery **111** (1992) 634–639.
[15.37] SPAPEN, H., et al., Pre- and peroperative diagnosis of metastatic pheochromocytoma in multiple endocrine neoplasia type 2a, J. Endocrinol. Invest. **12** (1989) 729–731.
[15.38] ADAMS, S., ACKER, P., LORENZ, M., STAIB-SEBLER, E., HÖR, G., Radioisotope-guided surgery in patients with pheochromocytoma and recurrent medullary thyroid carcinoma: A comparison of preoperative and intraoperative tumor localization with histopathologic findings, Cancer **92** (2001) 263–270.
[15.39] MARTINELLI, O., et al., Carotid body tumors: Radioguided surgical approach, J. Exp. Clin. Cancer Res. **28** (2009) 148.
[15.40] SCHIRMER, W.J., et al., Intraoperative localization of neuroendocrine tumors with ^{125}I-TYR^{3}-octreotide and a hand-held gamma-detecting probe, Surgery **114** (1993) 745–751.
[15.41] WOLTERING, E.A., et al., Detection of occult gastrinomas with iodine 125-labeled lanreotide and intraoperative gamma detection, Surgery **116** (1994) 1139–1147.
[15.42] BENEVENTO, A., DOMINIONI, L., CARCANO, G., DIONIGI, R., Intraoperative localization of gut endocrine tumors with radiolabeled somatostatin analogs and a gamma-detecting probe, Semin. Surg. Oncol. **15** (1998) 239–244.
[15.43] AHLMAN, H., et al., Clinical efficacy of octreotide scintigraphy in patients with midgut carcinoid tumors and evaluation of intraoperative scintillation detection, Br. J. Surg. **81** (1994) 1144–1149.
[15.44] WANGBERG, B., et al., Intraoperative detection of somatostatin-receptor-positive neuroendocrine tumours using indium-111-labelled DTPA-D-Phe^{1}-octreotide, Br. J. Cancer **73** (1996) 770–775.
[15.45] OHRVALL, U., et al., Intraoperative gamma detection reveals abdominal endocrine tumors more efficiently than somatostatin receptor scintigraphy, Cancer **80** (1997) 2490–2494.
[15.46] OHRVALL, U., et al., A gamma detector probe with ex vivo detection of carcinoid tumors superior to intraoperative palpation, Cancer **80** (1997) 2495–2500.
[15.47] ADAMS, S., et al., Intraoperative gamma probe detection of neuroendocrine tumors, J. Nucl. Med. **39** (1998) 1155–1160.

[15.48] CIRILLO, F., BOTTINI, A., LIMA, G., ALQUATI, P., Radioguided surgery in the treatment of gastro-entero-pancreatic neuroendocrine tumors, Minerva Chir. **55** (2000) 517–521.
[15.49] BENJEGÅRD, S.A., et al., Intraoperative tumour detection using ^{111}In-DTPA-D-Phe^{1}-octreotide and a scintillation detector, Eur. J. Nucl. Med. **28** (2001) 1456–1462.
[15.50] ALBERTARIO, S., et al., Radioguided surgery for gastrinoma: A case report, Tumori **88** (2002) 41–43.
[15.51] BANZO, J., et al., In-111 DTPA octreotide scintigraphy and intraoperative gamma probe detection in the diagnosis and treatment of residual lymph node metastases of a rectal carcinoid tumor, Clin. Nucl. Med. **30** (2005) 308–311.
[15.52] FILIPPI, L., et al., Intraoperative gamma probe detection of head and neck paragangliomas with ^{111}In-pentetreotide: A pilot study, Tumori **91** (2005) 173–176.
[15.53] GROSSRUBATSCHER, E., et al., Use of radioguided surgery with [^{111}In]-pentetreotide in the management of an ACTH-secreting bronchial carcinoid causing ectopic Cushing's syndrome, J. Endocrinol. Invest. **28** (2005) 72–78.
[15.54] YÜKSEL, M., EZIDDIN, S., LADWEIN, E., HAAS, S., BIERSACK, H.J., ^{111}In-pentetreotide and ^{123}I-MIBG for detection and resection of lymph node metastases of a carcinoid not visualized by CT, MRI or FDG-PET, Ann. Nucl. Med. **19** (2005) 611–615.
[15.55] HOSOYA, Y., et al., Multiple gastric carcinoids associated with parietal cell hyperplasia: Intraoperative detection with a radiolabeled somatostatin analog, Gastric Cancer **11** (2008) 123–126.
[15.56] HODOLIC, M., et al., Radioguided surgery and systemic radionuclide therapy of neuroendocrine tumours, In Vivo **24** (2010) 97–100.
[15.57] SERRANO VICENTE, J., et al., Radioguided surgery of intestinal carcinoid tumor relapse. Role of SPECT-CT, Rev. Esp. Med. Nucl. **29** (2010) 177–180.
[15.58] HODOLIC, M., FETTICH, J., RUBELLO, D., Influence of tumour size and uptake of ^{99m}Tc-octreotide on radio-guided surgery for neuroendocrine tumors, Minerva Endocrinol. **34** (2009) 89–96.

16. RADIATION PROTECTION ISSUES IN GOSTT PROCEDURES

16.1. SLNB AND ROLL

In radioguided SLNB procedures, a ^{99m}Tc colloidal agent is injected interstitially adjacent to the primary tumour. The radiolabelled particles must have a suitable size range, so that they may be transported via the lymphatic system. The protocols used in different centres differ for radiopharmaceutical characteristics and for injected activities. Most European investigators administer up to 15 MBq of ^{99m}Tc albumin nanocolloids 16–24 h before surgery, while in the USA, up to 74 MBq of ^{99m}Tc sulphur colloid is commonly injected 1–3 h before surgery. Similar protocols are adopted for radioguided SLNB in patients with CM; also in this case, in radioguided SLNB for malignant CM, 1 d or 2 d protocols are shown to be equally efficient for SLN detection, and the total injected activity varies from approximately 5 MBq to 120 MBq (multiple perilesional aliquots are usually injected). For the 2 d procedure, injected activity should be calculated (adjusted for physical decay) so that on day 2, at least 10 MBq is still present in the patient (when surgery with intraoperative SLN detection is performed under gamma probe guidance).

In ROLL, ^{99m}Tc MAAs (relatively large particles that do not migrate from the site of interstitial injection) are injected directly into the tumour under mammographic or ultrasonographic guidance. In this case, up to 15 MBq of ^{99m}Tc MAA is normally used 16–24 h before surgery.

16.1.1. Biodistribution

Technetium-99m nanocolloids: Between 95% and 99% of the administered radioactivity is retained as a localized source at the injection site, while up to 5% of the injected activity (relative to the time of injection) is retained in the SLNs at the time of surgical excision [16.1, 16.2].

Because total radioactivity circulating in the blood pool only reaches approximately 1% of the total injected activity [16.3–16.5,], radiocolloid uptake via the reticuloendothelial system into the liver, spleen and bone marrow is virtually negligible. Total urinary excretion within the first 16 h is less than 2% of the administered activity (range 0.1%–1.9%) [16.5].

Technetium-99m sulphur colloid: This radiocolloid is cleared from the injection site with a mean half-time of 31.1 ± 24.2 h (median 20.6 h, range 4–77 h, all values being corrected for physical decay of ^{99m}Tc) [16.6].

Technetium-99m MAAs: Given the large size of these particles, it can be assumed that all injected radioactivity is retained at the injection site virtually indefinitely; the time course of activity at this time therefore corresponds simply to the physical decay of ^{99m}Tc.

16.1.2. Surgical staff exposure

Exposure data around patients have been measured and reported by many investigators [16.4, 16.7–16.11]. Mariani et al. [16.12] analysed data reported in several publications and concluded that the air kerma rate K around patients can be calculated by applying a simple inverse square law around the injection site and considering the air kerma rate reported for a ^{99m}Tc point source (0.0235 μGy·h^{-1}·MBq^{-1} at 1 m) in the Radionuclide and Radiation Protection Data Handbook 2002 [16.13]:

$$K\ (\mu\text{Gy/h}) = 0.0235 A f_{\text{att}} f_{\text{r}} d^{-2} \text{e}^{-\left(\frac{0.693t}{6}\right)} \tag{16.1}$$

where

A is the injected activity (MBq);
f_{att} is the attenuation factor;
f_{r} is the retained fraction;
d is the distance from the injection site (m);
t is the time of surgery (h);

and f_{att} and f_{r} can conservatively be set to 1.

Reported radiation doses to surgeons, operating theatre nurses and pathologists directly measured by some investigators are shown in Table 16.1 [16.3, 16.5, 16.11, 16.14–16.18]. Radiation doses per procedure to the surgeon's torso and hands (skin) vary in the ranges 0.2–0.8 μSv and 1.7–3.2 μSv, respectively, per MBq of activity present at time of surgery; it should be mentioned that a single much higher value (60 μSv/MBq) was reported by Waddington et al. for the surgeon's hands [16.3]. Radiation doses per procedure to the theatre nurse vary between 0.1 μSv/MBq and 0.255 μSv/MBq. Radiation doses to the pathologist's hands vary between 0.16 μSv/MBq and 1.8 μSv/MBq of activity present at the time of handling the tissue sample, while a single value of 0.02 μSv/MBq is available for the pathologist's torso.

TABLE 16.1. RADIATION DOSES TO STAFF DURING RADIOGUIDED SLNB PROCEDURES (MEASURED VALUES)

Reference	Dose (μSv) to:				
	Surgeon's hands (skin)	Surgeon's torso	Theatre nurse	Pathologist's hands (skin)	Pathologist's torso
Breast carcinoma	—	—	—	—	—
Miner et al. [16.14] (37 MBq injected 3.5 h before surgery)	102 ± 58	—	—	—	—
Law et al. [16.15] (10 MBq at time of surgery)	17.77	4.55	2.55	0.12 (3 d after surgery)	<0.01 (3 d after surgery)
Waddington et al. [16.3] (10–15 MBq injected 18–24 h before surgery) (38 procedures) 4 h before surgery (1 procedure)	120 ± 23 (tumour excision) 60 ± 40 (SLNB) 70	<1 (20 out of 38 procedures) <2 (18 out of 38 procedures) 4	—	—	—
Morton et al. [16.11] (40 MBq injected day before surgery)	13	—	—	9	—
Klausen et al. [16.5] (16 ± 9 MBq injected at time of surgery)	40 ± 40	10 ± 20 (abdomen)	—	<1 (2.4 MBq ± 3.7)	—

TABLE 16.1. RADIATION DOSES TO STAFF DURING RADIOGUIDED SLNB PROCEDURES (MEASURED VALUES) (cont.)

Reference	Dose (μSv) to:				
	Surgeon's hands (skin)	Surgeon's torso	Theatre nurse	Pathologist's hands (skin)	Pathologist's torso
de Kanter et al. [16.16] (30 MBq injected 4 h before surgery)	61	3.7 (torso) 8.2 (abdomen)	1.9	3	0.4 (torso) 1 (abdomen)
Malignant cutaneous melanoma		—	—	—	—
Miner et al. [16.14] (18.5 MBq injected 3.5 h before surgery)	17.5 ± 17.5 40 ± 40 (assistant)	—	—	—	—
Sera et al. [16.17] (100 MBq day before surgery)	159 ± 23	<1 (96%) <2 (4%)	<1 (88%) <2 (2%) <4.5 (10%)	—	—
Nejc et al. [16.18] (74 MBq injected 24 h before surgery)	5.84 ± 6.91	—	4.44 ± 5.54	—	—

SLNB: sentinel lymph node biopsy; —: no data.

The wide variations in the reported values can be explained by some differences in the types of surgery and surgical technique, as well as by the low number of procedures evaluated in some of the studies. Perhaps most importantly, the doses rates measured are close to the detection limit of the thermoluminescent dosimeters used, thus they can be affected by variations in background exposure; all the above factors combine to contribute to reducing the accuracy of the measurements, and therefore to the variability observed.

Table 16.2 [16.3, 16.5, 16.9, 16.11, 16.19] reports estimated radiation doses to surgeons, operating theatre nurses and pathologists. The high value of equivalent dose to the pathologist's hands indicated by Waddington et al. (42.45 μSv/MBq) [16.3] has been calculated under very conservative assumptions considering exposure of the fingers at a distance of 1 cm from the specimen for 15 min.

16.1.3. Radioactivity in tissue specimens and radioactive clinical waste

Table 16.3 [16.3, 16.5, 16.7, 16.8, 16.11] summarizes the activity in tissue specimen and in clinical waste reported by some investigators.

16.1.4. Patient exposure

16.1.4.1. SLNB in breast cancer

For radioguided SLNB in breast cancer, estimations of patient exposures have been reported based on two different assumptions. The first approach assumes that the radiocolloid is distributed homogeneously throughout the entire breast tissue [16.3], while the second approach considers specifically the irradiation from the small breast tissue volumes where radioactivity is injected/present [16.20]. In the latter case, the dose to the breast tissue where radioactivity is present is excluded from the calculations because this tissue is excised during surgery.

Pandit-Taskar et al. [16.21] consider also the contribution to the effective dose from the radioactivity circulating in blood, while other studies also take into account that irradiation ceases at time of surgery when most of the injected radioactivity is removed from the breast. Moreover, Law et al. [16.20] evaluate effective doses specifically following injection in either the left or the right breast. Therefore, it is not surprising that values reported by different groups differ so greatly, depending on the different assumptions made (see Table 16.4) [16.19–16.21].

TABLE 16.2. RADIATION DOSES TO STAFF DURING RADIOGUIDED SLNB PROCEDURES (ESTIMATED VALUES)

Reference	Dose (μSv) to:				
	Surgeon's hands (skin)	Surgeon's torso	Theatre nurse	Pathologist's hands (skin)	Pathologist's torso
Breast carcinoma					
Cremonesi et al. [16.7] (11 MBq injected 16 h before surgery)	4.5 ± 0.2	0.9 ± 0.3	0.7 ± 0.2	0.8 ± 0.1	0.15 ± 0.04
Waddington et al. [16.3] (15 MBq injected 24 h before surgery, 60 min surgery)	—	—	—	39.8 [a] 0.664 [b]	0.169 [a] 0.009 [b]
Morton et al. [16.11] (40 MBq injected day before surgery)	—	0.5	0.05	—	0.6
Morton et al. [16.11] (20 MBq injected same day of surgery)	—	1.9	0.2	—	2.5
Klausen et al. [16.5] (21 ± 13 MBq at time of pathological analysis)	—	—	—	7	1.3
Brenner et al. [16.9] (30 MBq injected 3–5 h before surgery)	42	1.8	0.44	22.2	0.84

TABLE 16.2. RADIATION DOSES TO STAFF DURING RADIOGUIDED SLNB PROCEDURES (ESTIMATED VALUES) (cont.)

Reference	Dose (μSv) to:				
	Surgeon's hands (skin)	Surgeon's torso	Theatre nurse	Pathologist's hands (skin)	Pathologist's torso
Malignant cutaneous melanoma					
Alazraki et al. [16.19] (<18.5 MBq injected 0.5–3 h before surgery)	5–94	—	—	—	—

SLNB: sentinel lymph node biopsy; —: no data.

[a] Primary tumour.

[b] Sentinel lymph node.

TABLE 16.3. RADIOACTIVITY IN TISSUE SPECIMENS AND IN CLINICAL WASTE FROM RADIOGUIDED SLNB PROCEDURES

Reference	Radioactivity (MBq) in:		
	Tumour specimen	Lymph nodes	Swabs and gauzes
Morton et al. [16.11] (40 MBq injected day before surgery)	0.6–1.2	<0.002	0.001–0.1
Morton et al. [16.11] (20 MBq injected same day of surgery)	3.7–10.2	<0.2	0.2–1.9
Klausen et al. [16.5] (16 ± 9 MBq injected at time of surgery)	2.4 ± 3.70	0.085 ± 0.194	—
Cremonesi et al. [16.7] (11 MBq injected 16 h before surgery)	0.9 (0.4–1.1)	0.009 (0.0007–0.015)	0.013 (0–0.1)
Motta et al. [16.8] (11.6 ± 0.6 MBq injected 24 h before surgery)	1.689 (injection site)	0.048	0.005–0.012
Motta et al. [16.8] (3.11 ± 0.85 MBq injected 24 h before surgery)	0.594 (injection site)	0.015	0.003–0.012

TABLE 16.3. RADIOACTIVITY IN TISSUE SPECIMENS AND IN CLINICAL WASTE FROM RADIOGUIDED SLNB PROCEDURES (cont.)

Reference	Radioactivity (MBq) in:		
	Tumour specimen	Lymph nodes	Swabs and gauzes
Waddington et al. [16.3] (15 MBq injected 24 h before surgery)	<0.94	<0.047	0.205
Waddington et al. [16.3] (15 MBq injected 4 h before surgery)	<9.4	<0.47	—

SLNB: sentinel lymph node biopsy; —: no data.

TABLE 16.4. RADIATION EXPOSURE OF PATIENTS UNDERGOING RADIOGUIDED SLNB PROCEDURES (ESTIMATES)

Reference	Effective dose (μSv/MBq)	Dose to uterus/fetus (μGy/MBq):			
		Adult woman	3 months' pregnant woman	6 months' pregnant woman	9 months' pregnant woman
Breast carcinoma					
Law et al. [16.20] [a] (injection in left breast)	2.71	0.18 (ovary)	—	—	—
Law et al. [16.20] (injection in right breast)	2.52	0.14 (ovary)	—	—	—
Pandit-Taskar et al. [16.21]	24.7	0.17	0.192	0.644	0.694
Malignant cutaneous melanoma					
Alazraki et al. [16.19] (15–35 MBq injected 0.5–3 h before surgery)	2.71	—	—	—	—

SLNB: sentinel lymph node biopsy; —: no data.

[a] Law et al. [16.20] consider also the contribution due to a transmission scan performed to facilitate anatomic identification of the body contour (effective dose: 3 μSv; dose to ovary: 1.7 μGy).

A realistic but still conservative hypothesis may consider that a fraction of approximately 25% of the injected activity is homogeneously distributed in the breast tissue, 1% is present in the circulating blood and the remaining 74% is concentrated in a small volume inside the breast. According to these assumptions, the effective dose can be obtained by summing up all three contributions. Excision of radioactive tissue is not taken into account. For the first two contributions, the medical internal radiation dose method can be applied, while for the third contribution, the data reported by Law et al. [16.20] may be used. Thus, an effective dose lower than 7 μSv/MBq injected can reasonably be considered.

As shown in Table 16.4, the dose to the uterus/fetus calculated by Pandit-Taskar et al. [16.21] varies between 0.17 μGy/MBq for a non-pregnant woman and 0.694 μGy/MBq for a 9 months' pregnant woman. Doses to the ovary independently estimated by Law et al. [16.20] confirm these data.

16.1.4.2. SLNB in CM

In the case of radioguided SLNB for malignant CM, the effective patient dose was calculated by Alazraki et al. [16.19] as 1.9 μSv/MBq injected activity, assuming that 20% of the administered activity reached systemic circulation and then exhibited the typical biodistribution for radiocolloids.

Dose to the fetus depends, of course, on the location of the melanoma. Only in the case of melanomas located rather close to the fetus (over the lower abdomen or back), is there a theoretical risk of exceeding 1 mSv [16.22].

16.2. RADIOGUIDED PARATHYROIDECTOMY

The protocols for radioguided parathyroidectomy differ for injection methods. Most investigators in the USA administer 740 MBq of 99mTc sestamibi 3 h before surgery, while in Europe (especially in Italy), only 37 MBq of ^{99m}Tc sestamibi is injected, 1–3 h before surgery.

16.2.1. Biodistribution

After intravenous administration, ^{99m}Tc sestamibi is rapidly cleared from the blood and taken up predominantly in muscle tissues (especially in the myocardium), liver and kidneys, with a smaller amount being concentrated in the salivary glands and thyroid. Other organs and tissues show a low uptake with a rather uniform distribution. No appreciable redistribution takes place from the myocardium, and there is no evidence of any in vivo metabolism of this radiopharmaceutical. The main pathway for excretion is via the hepatobiliary

system to the gastrointestinal tract, with some additional excretion taking place via the kidneys. Results of animal studies do not indicate any direct uptake and excretion via the gastrointestinal wall. Most of the injected activity is excreted within 48 h postadministration [16.23].

16.2.2. Radiation exposure of staff

Until now, it has only been possible to find a single article describing radiation exposures to the staff, considering the whole body of the patient as the radiation source [16.10]. The relevant data on estimated dose rates reported in Table 16.5 [16.10] consider various distances from the patient, while Table 16.6 [16.10] reports the actual exposure values for the staff considering the total length of surgery.

TABLE 16.5. DOSE RATES (MSV/H) EVALUATED AT VARIOUS DISTANCES FROM THE PATIENT DURING RADIOGUIDED PARATHYROIDECTOMY FOLLOWING ADMINISTRATION OF 740 MBq OF ^{99m}Tc SESTAMIBI

(Values in parenthesis are dose rates for the low dose protocol[a]: 37 MBq of ^{99m}Tc sestamibi) (reproduced from Ref. [16.10])

Distance	Side of lesion	Contralateral to lesion	Right abdomen	Left abdomen	From head
Close	60–70 (6.0)	50–60 (6.0)	100–120 (12)	50–60 (13)	9.0–10 (1.5)
50 cm	8.0–10 (1.0)	7.0–9.0 (0.8)	12–18 (1.5)	8.0 (1.5)	3.0 (0.8)
100 cm	3.0–5.0 (0.8)	3.0–5.0 (0.6)	4.0–5.0 (0.9)	3.0–4.0 (1.0)	1.2–2.0 (0.6)
150 cm	1.5–3.2 (0.5)	1.5–3.0 (0.5)	2.5 (0.5)	2.0 (0.7)	0.5–1.2 (0.5)
200 cm	0.4–1.4 (0.3)	0.5–1.2 (0.4)	1.5 (0.3)	1.5 (0.5)	0.3–0.5 (0.3)
>200 cm	0.2 (0.2)	0.2 (0.2)	0.2 (0.2)	0.2 (0.2)	0.2 (0.2)

[a] In the low dose protocol, surgery is performed sooner after administration of ^{99m}Tc sestamibi (typically 1 h post-injection) than in the full dose protocol (typically 3 h post-injection); at such earlier times, the contribution of tracer accumulation in the myocardium is relatively greater (left abdomen values) than that owing to accumulation in the hepatobiliary and gastrointestinal tract (right abdomen). Conversely, at later times post-injection (as in the typical full dose protocol), the contribution from the right abdomen is more important than from the left abdomen.

TABLE 16.6. RADIATION EXPOSURE TO STAFF DURING A TYPICAL PROCEDURE OF RADIOGUIDED PARATHYROIDECTOMY FOLLOWING ADMINISTRATION OF 740 MBq OF ^{99m}Tc SESTAMIBI

(Values in parenthesis are exposure values for the low dose protocol: 37 MBq of ^{99m}Tc sestamibi) (reproduced from Ref. [16.10])

Staff member	Radiation dose (μSv/procedure)
Anaesthesiologist	1.01–3.96 (1.11)
Senior surgeon	8.78–11.00 (1.14)
Assistant surgeon 1	7.6–10.00 (1.18)
Assistant surgeon 2	6.75–8.20 (0.79)
Nurse	3.64–8.00 (0.72)

16.2.3. Patient exposure

The effective dose to an adult patient is 9 μSv/MBq, and the effective doses to the fetus are 0.015 μGy/MBq in early pregnancy, 0.012 μGy/MBq at 3 month gestation, 0.008 μGy/MBq at 6 month gestation and 0.005 μGy/MBq at 9 month gestation.

16.3. POSITRON EMITTER BASED LOCALIZATION AND RADIOGUIDED SURGERY OF TUMOURS

[Fluorine-18]FDG is the positron emitting tracer that has more commonly been employed for radioguided surgery. This radiopharmaceutical is injected intravenously, with the operating protocols being somewhat different in terms of injected activities and time lapses between administration and surgery.

16.3.1. Biodistribution

The systemically administered radiopharmaceutical distributes throughout the entire body and its relative uptake in the tumour and surrounding normal tissue varies with time. While the optimal delay between administration and surgery has yet to be established, this parameter will depend on patient throughput in the nuclear medicine and surgery departments. Moreover, duration of surgery

may vary dramatically depending on location of the tumour. For these reasons, the amount of radioactivity present near the surgeon is very variable and also changes rapidly over time owing to the short half-life of ^{18}F (110 min).

16.3.2. Surgical staff exposure

Exposure data around patients have been measured or evaluated by many investigators. In particular, according to Heckathorne et al. [16.24], the equivalent dose rates per injected MBq at 0.5 m and 1 m from the patient at navel level, corresponding to the position of primary personnel (surgeon, assistant and scrub nurse) and of secondary personnel (anaesthesiologist and other surgical nurses), respectively, are given by:

$$D\ (\mu\mathrm{Sv}\cdot\mathrm{h}^{-1}\cdot\mathrm{MBq}^{-1}) = 0.194\mathrm{e}^{-0.4635t} \tag{16.2}$$

and

$$D(\mu\mathrm{Sv}\cdot\mathrm{h}^{-1}\cdot\mathrm{MBq}^{-1}) = 0.078\mathrm{e}^{-0.5137t} \tag{16.3}$$

where t is the time from injection in hours.

The radiation dose rates and exposures to surgeons, anaesthesiologists, assistants and scrub nurses measured in various studies are shown in Tables 16.7 [16.25–16.28] and 16.8 [16.24, 16.27–16.30].

16.4. NETs

In patients with NETs, real time intraoperative exploration using hand-held probes overcomes many of the limitations encountered with external imaging, thus allowing precise identification and localization of such tumours, including small sized and deeply located lesions that may escape scintigraphic detection. Therefore, application of these techniques reduces the rate of unsuccessful surgical explorations and enables more complete tumour resections. Although different tracers can be employed as an intraoperative guide for surgery (including radioiodinated MIBG and SST analogues labelled with the positron emitter ^{68}Ga), most of the clinical experience and the radiation protection assessments published so far have been based on the use of the commercially available radiopharmaceutical ^{111}In DTPA D-Phe^{1}-octreotide (OctreoScan).

TABLE 16.7. DOSE RATES TO THE STAFF DURING RADIOGUIDED SURGERY PROCEDURES BASED ON [^{18}F]FDG ADMINISTRATION

Reference	Dose rate (μSv/h) to:				
	Procedure length (h)	Surgeon's hands	Surgeon's torso	Anaesthesiologist	Nurse/resident
Piert et al. [16.25] (36–110 MBq injected immediately before surgery)	2–6.25 (2 cases)	—	2.5–8.6	0.8	—
Andersen et al. [16.26] (45 MBq injected 0–65 min before surgery)	2–3 (34 cases)	8.3 ± 1.0 (breast cancer) 12.8 ± 1.1 (melanoma) 35.9 ± 2.9 (gastrointestinal tract cancer)	7.5 ± 0.8 (breast cancer) 9.5 ± 1.0 (melanoma) 13.2 ± 1.1 (gastrointestinal tract cancer)	2.7 ± 0.4	—
Thermoluminescent dosimeters					
Andersen et al. [16.26] (45 MBq injected 0–65 min before surgery)	2–3 (25 cases)	—	12.4 ± 0.7 (breast cancer) 10.6 ± 0.7 (melanoma) 16.6 ± 1.0 (gastrointestinal tract cancer)	—	—

TABLE 16.7. DOSE RATES TO THE STAFF DURING RADIOGUIDED SURGERY PROCEDURES BASED ON [^{18}F]FDG ADMINISTRATION (cont.)

Reference	Dose rate (μSv/h) to:				
	Procedure length (h)	Surgeon's hands	Surgeon's torso	Anaesthesiologist	Nurse/resident
Electronic dosimeters					
Povosky et al. [16.27] (699 ± 181 MBq injected 180 ± 120 min before surgery)	235 ± 117 min (10 cases)	—	61 ± 57	49 ± 71	17 ± 17
Nalley et al. [16.28] (278 MBq injected approx. 5–5.3 h post-injection)	—	—	30 (63–54 MBq at surgery time)	2–1.6	7.5–5 (nurse) 24 (resident)
Nalley et al. [16.28] (281 MBq injected approx. 3–3.3 h post-injection)	—	—	53–47 (89–81 MBq at surgery time)	3.8–1.6	17–14 (nurse) 40–41 (resident)
Nalley et al. [16.28] (304 MBq injected from 3.4 h to 3.7 h post-injection)	—	—	20 (85–51 MBq at surgery time)	2–1.3	7.5–5 (nurse) 25 (resident)

TABLE 16.8. RADIATION EXPOSURES TO THE STAFF DURING RADIOGUIDED SURGERY PROCEDURES BASED ON [^{18}F]FDG ADMINISTRATION

Reference	Dose (μSv) to:				
	Procedure length (min)	Surgeon's hands	Surgeon's torso	Anaesthesiologist	Nurse/assistant
Kraeber-Bodéré et al. [16.29] (265 MBq injected 30 min before surgery)	—	90–270 (10 cases)	—	—	—
Piert et al. [16.30] (93–181 MBq immediately before surgery)	—	<300 (3 cases) 300 (1 case)	94–217	18–26	44–162 (assistant)
Povosky et al. [16.27] (699 ± 181 MBq injected 180 ± 120 min before surgery)	235 ± 117 (10 cases)	—	164 ± 135	119 ± 110	54 ± 60 (circulating nurse)
Nalley et al. [16.28] (278 MBq injected 4.9 h before surgery)	—	—	70	—	40 (resident)
Nalley et al. [16.28] (281 MBq injected 4.9 h before surgery)	—	—	40	—	50 (resident)

TABLE 16.8. RADIATION EXPOSURES TO THE STAFF DURING RADIOGUIDED SURGERY PROCEDURES BASED ON [^{18}F]FDG ADMINISTRATION (cont.)

Reference	Dose (μSv) to:				
	Procedure length (min)	Surgeon's hands	Surgeon's torso	Anaesthesiologist	Nurse/assistant
Nalley et al. [16.28] (304 MBq injected 4.9 h before surgery)	—	—	10	—	10 (resident)
Heckathorne et al. [16.24] (337 MBq injected)	94–150 (primary personnel 60–150 (secondary personnel)	—	16 (primary personnel)	11 (secondary personnel)	—
Heckathorne et al. [16.24] (370 MBq injected)	64–105 (primary personnel 36–117 (secondary personnel)	—	42 (primary personnel)	19 (secondary personnel)	—

16.4.1. Biodistribution

The biokinetic data on distribution of ^{111}In DTPA D-Phe^{1}-octreotide have originally been assessed in patients with carcinoid tumours or NETs of the gastrointestinal tract. Uptake in tumour tissue present in any given organ may therefore be included in the published organ uptake values. Upon intravenous administration, ^{111}In DTPA D-Phe^{1}-octreotide is assumed to be immediately taken up in the liver, spleen, kidneys and thyroid, while the rest is assumed to be homogeneously distributed in the remainder of the body. The measured retention values are best described by monoexponential or biexponential functions. The main route of excretion is via the kidneys, while less than 2% of injected activity is recovered in the faeces. Although some degradation seems to occur in vivo, most of the activity excreted in urine is still peptide bound, even 48 h post-injection. Excretion via the gastrointestinal tract is not included in the model because its contribution to the absorbed dose is negligible in normal circumstances. An observed excretion of 85% via urine after 24 h fits well with the model proposed [16.23].

16.4.2. Surgical staff exposure

Kurtaran et al. have evaluated the dose rates in various conditions derived from patients to whom ^{111}In DTPA Phe^{1}-octreotide had been administered for diagnostic purposes (mean injected activity of 140 ± 40 MBq) [16.31]. The data are shown in Table 16.9 [16.31], where the dose rates at 0.5 m, 1 m and 2 m distances from the patients are shown as a function of time post-injection.

For all three distances, the decline in dose rate was best described by the equation:

$$D(t) = D_0(0.74\mathrm{e}^{-ln\,2}t/T_1 + 0.26e^{-\ln 2}t/T_2)$$

where D_0 is the initial dose rate in μSv/h (see Table 16.9). The effective half-lives (T_1 = 2.94 h and T_2 = 65.2 h) and the physical half-life of ^{111}In (67.4 h) were utilized to calculate the biological half-lives (T_{biol}): T_{biol1} = 3.1 h and T_{biol2} = 83 d.

The biexponential pattern of decline of dose rates derived from patients following administration of this radiopharmaceutical has also been confirmed (although with different slope values) on a much higher scale of activities, i.e. those utilized for therapy with ^{111}In DTPA D-Phe^{1}-octreotide (6.3 ± 2.3 GBq) [16.32].

TABLE 16.9. INITIAL DOSE RATES (D_0) DERIVED FROM PATIENTS FOLLOWING ADMINISTRATION OF A DIAGNOSTIC ACTIVITY OF ^{111}In DTPA D-PHE^1-OCTREOTIDE AS A FUNCTION OF DISTANCE *(reproduced from Ref. [16.31])*

Distance (m)	D_0 (μSv/h)
0.5	6.61 ± 2.97
1	2.86 ± 1.22
2	1.14 ± 0.26

16.4.3. Patient exposure

The effective dose to an adult patient is 54 μSv/MBq, and the effective doses to the fetus are 0.082 μGy/MBq in early pregnancy, 0.060 μGy/MBq at 3 months' gestation, 0.035 μGy/MBq at 6 months' gestation and 0.031 μGy/MBq at 9 months' gestation.

16.5. EXEMPTED PRACTICES

Because most of the GOSTT procedures are performed using ^{99m}Tc labelled radiopharmaceuticals, their use can be considered as exempted practice when adhering to the recommendations listed in Table 1.1 of the Basic Safety Standards (BSS) [16.33]. Table 16.10 [16.33] lists the exemption levels for ^{99m}Tc and other radionuclides that can be of potential use in GOSTT procedures.

However, the exemption of radiological practices is established by national regulatory authorities, and therefore it may differ from country to country. The discussion in the following sections regards practices which are not exempted.

16.6. OCCUPATIONAL EXPOSURE

16.6.1. Staff exposure

As indicated in the sections above, staff occupational exposure can be considered to be quite low in general, taking into account all the considerations reported in Section 4.1. and some specific operational conditions: administered activities, surgical procedures and workloads.

TABLE 16.10. EXEMPTION LEVELS INDICATED IN REF. [16.33] FOR THE RADIONUCLIDES MOST COMMONLY EMPLOYED FOR GOSTT PROCEDURES

Nuclide[a]	Activity concentration (Bq/g)	Activity[b] (Bq)
Tc-99m	100	10^7
F-18	10	10^6
In-111	100	10^6
I-123	100	10^7
I-131	100	10^7

GOSTT: guided intraoperative scintigraphic tumour targeting.

[a] In the case of more than one radionuclide, the appropriate sum of the ratios of the activity or activity concentration of each radionuclide and the corresponding exempt activity or activity concentration are to be taken into account.

[b] Total activity of a given radionuclide present on the premises at any one time.

In the case of radioguided SLNB and ROLL procedures, the most common procedures with higher workloads, a rough conservative estimation can be performed by applying the following coefficients:

— Effective dose to the surgeon: 0.8 μSv per MBq present at the time of surgery;
— Equivalent dose to the surgeon's hands (skin): 3.2 μSv per MBq present at the time of surgery;
— Effective dose to the theatre nurse: 0.26 μSv per MBq present at the time of surgery;
— Effective dose to the pathologist: 0.2 μSv per MBq present at the time of surgery;
— Equivalent dose to the pathologist's hands (skin): 3.2 μSv per MBq present at the time of surgery.

16.6.2. Classification of working areas

The areas where a radiological practice is performed is to be classified from the point of view of the risk of exposure to ionizing radiation. Areas can

be classified as controlled or supervised according to the BSS, paras 3.88–3.92 [16.33]. A controlled area is any area:

> "in which specific measures for protection and safety are or could be required for:
>
> (a) Controlling exposures or preventing the spread of contamination in normal operation;
> (b) Preventing or limiting the likelihood and magnitude of exposures in anticipated operational occurrences and accident conditions."

A supervised area is "any area not already designated as a controlled area but for which occupational exposure conditions need to be kept under review, even though specific measures for protection and safety are not normally needed".

In general, the risks associated with non-exempted GOSTT procedures result in the classification of areas as supervised. Taking into account the nature and extent of radiation hazards in the classified areas, registrants and licensees will ideally:

— Delineate the classified areas by appropriate means;
— Display approved signs at appropriate access points to classified areas;
— Periodically review the conditions to determine any need for protective measures and safety provisions or changes to the boundaries of classified areas.

They will ideally also establish occupational protection and safety measures, including local rules and procedures that are appropriate for the classified areas.

16.6.3. Operating procedures and protective equipment

Standardized working procedures are to be formulated to minimize exposure from external radiation and contamination, and, in the event of contamination, to minimize its spread.

In GOSTT procedures, both the risk of external exposure and the contamination risk are usually quite low. Protective clothes used for protection from biological hazards are also adequate for contamination risk, and simple operating procedures, such as keeping the distance between the fingers and the radioactive substance as large as possible, are sufficient enough to reduce external radiation risks.

The attenuation of lead aprons for high energy γ rays (^{111}In, ^{18}F) is negligible, while γ rays emitted by ^{99m}Tc (140 keV) are attenuated by a factor of

approximately 2. In the latter case, it is a matter of judgement whether or not this dose reduction compensates for the effort of wearing an apron.

Only in the very rare cases where high activities are used and/or high workloads are present, is the need for handling radioactive specimens behind a protective shield and the need of equipment for contamination monitoring and washing facilities to be evaluated.

16.6.4. Monitoring

16.6.4.1. Individual monitoring

For any worker who is normally employed in a controlled area, or who occasionally works in a controlled area and may receive significant occupational exposure, individual monitoring is to be undertaken where appropriate, adequate and feasible. In cases where individual monitoring is inappropriate, inadequate or not feasible, the occupational exposure of the worker is to be assessed on the basis of the results of monitoring of the workplace and on information on the locations and durations of exposure of the worker.

For any worker who is regularly employed in a supervised area or who enters a controlled area only occasionally, individual monitoring is not be required, but the occupational exposure of the worker is to be assessed. This assessment is to be on the basis of the results of monitoring of the workplace or individual monitoring.

Although GOSTT operators do not usually require individual monitoring, the requirements stated in Ref. [16.34] paragraph 16.7. must be fulfilled, if deemed necessary.

16.6.4.2. Monitoring of the workplace

In controlled and supervised areas, a programme for monitoring the workplace, both for ambient dose equivalent and contamination levels, are to be established under the supervision, if so required by the regulatory authority, of a qualified expert and a radiation protection officer (Ref. [16.33] paras 3.96–3.98).

The nature and frequency of monitoring will depend on the possible levels of ambient dose equivalent and activity contamination, including their expected fluctuations and the likelihood and magnitude of potential exposures.

In controlled areas, contamination monitoring using a contamination monitor or wipe tests is to be carried out for all working surfaces, tools, equipment, personal clothing, shoes and any items removed from these areas.

16.7. MEDICAL EXPOSURE

Patient exposure to ionizing radiation for medical purposes must meet the two radiation protection fundamental principles of justification and optimization. Thus, the medical practitioners are to follow a justification procedure that is both documented and approved considering the efficacy, benefits and risks of the nuclear medicine procedure. In justifying the nuclear medicine procedure, relevant guidelines should be taken into account.

The medical practitioners who prescribe or conduct GOSTT procedures are to:

— Ensure that the exposure of patients be the minimum required to achieve the intended clinical objective;
— Take into account guidance levels if established.

If guidance levels are not defined by the national regulatory authority, indications given by relevant international guidelines should be considered.

Particular attention is to be given to the exposure of pregnant or lactating women and also to the performance, correct use and quality assurance of the equipment used for imaging and detection.

16.7.1. Pregnancy and lactation

The justification of nuclear medicine procedures in pregnant women requires special consideration. According to the ICRP [16.23], the risk to the fetus is considered negligible for procedures exposing a fetus to an equivalent dose less than 1 mSv.

In this respect, taking into account data reported in Section 16.1, during radioguided SLNB for breast cancer, the dose to the fetus is lower than 1 mSv, even for an injected activity of 100 MBq. In addition, in radioguided SLNB for malignant CM, the dose to the fetus will generally be below the 1 mSv limit. Only if the melanoma is located over the lower abdomen or back should the risk of exceeding 1 mSv be considered. In these cases, if a GOSTT procedure is not contraindicated in pregnant patients, it is preferable to use a same day protocol, enabling injection of a lower activity.

For GOSTT procedures with [^{18}F]FDG, ^{99m}Tc sestamibi and ^{111}In DTPA D-Phe^{1}-octreotide, as well as for any other procedure where there is a risk of exceeding 1 mSv, the advice of a qualified expert in nuclear medicine physics should be required to estimate fatal dose.

In lactating women, it is recommended that lactation be suspended for nursing mothers for 24 h after radiopharmaceutical administration of ^{99m}Tc and

^{18}F labelled tracers. Different specific indications will be given for other longer lived radioactive tracers.

16.7.2. Equipment and quality assurance

All radiation detectors must be checked and managed within a specific quality assurance programme. Surgeons are advised to work closely with their nuclear medicine colleagues and medical physicists in setting up quality control (QC) procedures. Recommendations for testing are:

— Upon purchase, tests of performance are advised to yield reference values for sensitivity, energy resolution and spatial resolution, to constitute a baseline for periodical checks.
— Before each use, a basic check of function and performance, determining count rate sensitivity to a long lived radioactive source and its energy spectrum.
— Visual inspection for damage, particularly cables and connectors.
— In the operating room, aiming the probe at the injection site can demonstrate that the probe is functioning; however, this is not a substitute for true QC, as even a 50% loss in sensitivity would not have any effect on the general response to the injection site.

Quality control of the gamma probe used to detect the SLN in the operating theatre should also be performed according to published protocols. At least two protocols have been published: the National Electrical Manufacturers Association protocol [16.35] and the protocol developed jointly by some Italian scientific associations [16.36], i.e. the Italian Association of Medical Physics, the Italian Association of Nuclear Medicine, the Italian Study Group on Radioguided Surgery and Immunoscintigraphy and the Italian National Task Force on Breast Cancer [16.37].

16.8. EXPOSURE OF THE GENERAL PUBLIC

Exposure of the general public from GOSTT procedures can be caused by the disposal of radioactive waste generated from these activities or by the radiation emitted by patients undergoing such procedures. Specific evaluations can be made for radioguided SLNB by taking into account the data reported in Section 16.1.

16.8.1. Radioactive waste

Radioactivity excreted by patients undergoing GOSTT procedures is very low and, similar to all other diagnostic nuclear medicine procedures, there is no need for collection of patient excreta, so ordinary toilets can be used.

The solid radioactive waste produced in GOSTT procedures is also limited to low activities of radionuclides with short half-lives. For this reason, appropriate delay of the release of the waste to allow for decay of the radioactive materials will reduce its environmental impact to a negligible level. The correct management of the waste produced from such procedures must therefore be evaluated, considering that such waste must be collected and disposed of after a sufficient time for the radionuclides that are present to fall below the values established by the IAEA publication Clearance of Materials Resulting from the Use of Radionuclides in Medicine, Industry and Research [16.38]. In the case of radionuclides used in GOSTT procedures, these values correspond to the values of radioactivity concentration indicated in Table 16.6, or in any case below the clearance values established by the national regulatory authority, if different. For radionuclides with shorter half-lives (e.g. ^{18}F), it may not be necessary to implement specific management of disposal of waste, whereas for radionuclides with longer half-lives, it is necessary to organize the collection of such waste and to store it in a special room until the radioactivity has decayed. In practice, it is the waste mainly due to ^{131}I or ^{111}In that requires special precautions.

16.8.2. Public exposure from patients

Radiation emission around patients undergoing GOSTT procedure is such that the cumulative dose at 1 m from the patient is much less than 0.1 mSv, which is a dose value considered safe enough to keep the maximum dose that could be received by another person due to external exposure from the patient a small fraction of the annual public dose limit.

REFERENCES TO CHAPTER 16

[16.1] FITZGIBBONS, P.L., LIVOLSI, V.A., Recommendations for handling radioactive specimens obtained by sentinel lymphadenectomy. Surgical Pathology Committee of the College of American Pathologists, and the Association of Directors of Anatomic and Surgical Pathology, Am. J. Surg. Pathol. **24** 11 (2000) 1549–1551.

[16.2] MICHEL, R., HOFER, C., Radiation safety precautions for sentinel lymph node procedures, Health Phys. **86** 2 (2004) S35–7.

[16.3] WADDINGTON, W.A., et al., Radiation safety of the sentinel lymph node technique in breast cancer, Eur. J. Nucl. Med. **27** (2000) 377–391.
[16.4] GENTILINI, O., et al., Safety of sentinel node biopsy in pregnant patients with breast cancer, Ann. Oncol. **15** (2004) 1348–1351.
[16.5] KLAUSEN, T.L., et al., Radiation doses to staff involved in sentinel node operations for breast cancer, Clin. Physiol. Funct. Imaging **25** (2005) 196–202.
[16.6] GLASS, E.C., ESSNER, R., GIULIANO, A.E., Sentinel node localization in breast cancer, Semin. Nucl. Med. **29** (1999) 57–68.
[16.7] CREMONESI, M., et al., Radiation protection in radioguided surgery of breast cancer, Nucl. Med. Commun. **20** (1999) 919–924.
[16.8] MOTTA, C., et al., Radioguided surgery of breast cancer: Radiation protection survey, Tumori **86** (2000) 372–374.
[16.9] BRENNER, W., et al., Radiation exposure to the personnel in the operating room and in the pathology due to SLN detection with Tc-99m-nanocolloid in breast cancer patients, Nuklearmed. **39** (2000) 142–145.
[16.10] BEKIŞ, R., et al., Exposure of surgical staff in surgical probe applications in radioguided parathyroidectomy, Eur. Arch. Otorhinolaryngol. **265** (2008) 1545–1548.
[16.11] MORTON, R., HORTON, P.W., PEET, D.J., KISSIN, M.W., Quantitative assessment of the radiation hazards and risks in sentinel node procedures, Br. J. Radiol. **76** (2003) 117–122.
[16.12] MARIANI, G., et al., Radioguided sentinel lymph node biopsy in malignant cutaneous melanoma, J. Nucl. Med. **43** (2002) 811–827.
[16.13] DELACROIX, D., GUERRE, J.P., LEBLANC, P., HICKMAN, C., "Radionuclide and radiation protection data handbook 2002", Radiation Protection Dosimetry, Vol. 98, Nuclear Technology (2002) 1–168.
[16.14] MINER, T.J., et al., Guidelines for the safe use of radioactive materials during localization and resection of the sentinel lymph node, Ann. Surg. Oncol. **6** (1999) 75–82.
[16.15] LAW, M., CHOW, L.W., KWONG, A., LAM, C.K., Sentinel lymph node technique for breast cancer: Radiation safety issues, Semin. Oncol. **31** (2004) 298–303.
[16.16] DE KANTER, A.Y., ARENDS, P.P., EGGERMONT, A.M., WIGGERS, T., Radiation protection for the sentinel node procedure in breast cancer, Eur. J. Surg. Oncol. **29** (2003) 396–399.
[16.17] SERA, T., et al., Sentinel node detection in malignant melanoma patients: Radiation safety considerations, Dermatol. Surg. **29** (2003) 141–145.
[16.18] NEJC, D., et al., Sentinel node biopsy in skin melanoma patients—measurements of absorbed doses of radiation to the hands of medical staff, J. Surg. Oncol. **93** (2006) 355–361.
[16.19] ALAZRAKI, N., GLASS, E.C., CASTRONOVO, F., VALDÉS OLMOS, R.A., PODOLOFF, D., Procedure guideline for lymphoscintigraphy and the use of intraoperative gamma probe for sentinel lymph node localization in melanoma of intermediate thickness 1.0, J. Nucl. Med. **43** (2002) 1414–1418.

[16.20] LAW, M., CHENG, K.C., WU, P.M., HO, W.Y., CHOW, L.W., Patient effective dose from sentinel lymph node lymphoscintigraphy in breast cancer: A study using a female humanoid phantom and thermoluminescent dosemeters, Br. J. Radiol. **76** (2003) 818–823.

[16.21] PANDIT-TASKAR, N., et al., Organ and fetal absorbed dose estimates from ^{99m}Tc-sulfur colloid lymphoscintigraphy and sentinel node localization in breast cancer patients, J. Nucl. Med. **47** (2006) 1202–1208.

[16.22] CHAKERA, A.H., et al., EANM-EORTC general recommendations for sentinel node diagnostics in melanoma, Eur. J. Nucl. Med. Mol. Imaging **36** (2009) 1713–1742.

[16.23] INTERNATIONAL COMMISSION ON RADIOLOGICAL PROTECTION, Radiation Dose to Patients from Radiopharmaceuticals (Addendum to ICRP Publication 53), Publication 80, Pergamon Press, Oxford and New York (1998).

[16.24] HECKATHORNE, E., DIMOCK, C., DAHLBOM, M., Radiation dose to surgical staff from positron-emitter-based localization and radiosurgery of tumors, Health Phys. **95** (2008) 220–226.

[16.25] PIERT, M., et al., Positron detection for the intraoperative localisation of cancer deposits, Eur. J. Nucl. Med. Mol. Imaging **34** (2007) 1534–1544.

[16.26] ANDERSEN, P.A., et al., Radiation exposure to surgical staff during F-18-FDG-guided cancer surgery, Eur. J. Nucl. Med. Mol. Imaging **35** (2008) 624–629.

[16.27] POVOSKI, S.P., et al., Comprehensive evaluation of occupational radiation exposure to intraoperative and perioperative personnel from ^{18}F-FDG radioguided surgical procedures, Eur. J. Nucl. Med. Mol. Imaging **35** (2008) 2026–2034.

[16.28] NALLEY, C., WIEBECK, K., BARTEL, T.B., BODENNER, D., STACK, B.C., Jr., Intraoperative radiation exposure with the use of ^{18}F-FDG-guided thyroid cancer surgery, Otolaryngol. Head Neck Surg. **142** (2010) 281–283.

[16.29] KRAEBER-BODÉRÉ, F., et al., Feasibility and benefit of fluorine 18-fluoro-2-deoxyglucose-guided surgery in the management of radioiodine-negative differentiated thyroid carcinoma metastases, Surgery **138** (2005) 1176–1182.

[16.30] PIERT, M., CAREY, J., CLINTHORNE, N., Probe-guided localization of cancer deposits using [^{18}F]fluorodeoxyglucose, Q. J. Nucl. Med. Mol. Imaging **52** (2008) 37–49.

[16.31] KURTARAN, A., et al., Radiation doses deriving from patients undergoing ^{111}In-DTPA-D-phe-1-octreotide scintigraphy, Eur. J. Nucl. Med. **24** (1997) 1298–1300.

[16.32] KONTOGEORGAKOS, D., et al., Optimization of doses received by the hospital staff and the members of the family of patients undergoing ^{111}In-DTPA-D-Phe^{1}-octreotide therapy, Radiat. Prot. Dosimetry **125** (2007) 403–406.

[16.33] EUROPEAN COMMISSION, FOOD AND AGRICULTURE ORGANIZATION OF THE UNITED NATIONS, INTERNATIONAL ATOMIC ENERGY AGENCY, INTERNATIONAL LABOUR ORGANIZATION, OECD NUCLEAR ENERGY AGENCY, PAN AMERICAN HEALTH ORGANIZATION, UNITED NATIONS ENVIRONMENT PROGRAMME, WORLD HEALTH ORGANIZATION, Radiation Protection and Safety of Radiation Sources: International Basic Safety Standards, IAEA Safety Standards Series No. GSR Part 3, IAEA, Vienna (2014).

[16.34] INTERNATIONAL ATOMIC ENERGY AGENCY, Applying Radiation Safety Standards in Nuclear Medicine, Safety Reports Series No. 40, IAEA, Vienna (2005).
[16.35] NATIONAL ELECTRICAL MANUFACTURERS ASSOCIATION, Performance Measurements and Quality Control Guidelines for Non-imaging Intraoperative Gamma Probes, NEMA, Rosslyn (2004).
[16.36] ASSOCIAZIONE ITALIANA DI FISICA IN MEDICINA, ASSOCIAZIONE ITALIANA DI MEDICINA NUCLEARE, GRUPPO ITALIANO PER LO STUDIO DELLA CHIRURGIA
[16.37] RADIOGUIDATA E DELL'IMMUNOSCINTIGRAFIA, FORZA OPERATIVA NAZIONALE SUL CARCINOMA MAMMARIO, Sonde Intraoperatorie per Chirurgia Radioguidata, Protocollo per il Controllo di Qualità (2001), http://www.fisicamedica.it/aifm/doc/Protocollo_sonde1.pdf
[16.38] INTERNATIONAL ATOMIC ENERGY AGENCY, Clearance of Materials Resulting from the Use of Radionuclides in Medicine, Industry and Research, IAEA-TECDOC-1000, IAEA, Vienna (1998).

CONTRIBUTORS TO DRAFTING AND REVIEW

Belcari, N.	University of Pisa, Italy
Bex, A.	Netherlands Cancer Institute, Netherlands
Biggi, E.	University of Pisa, Italy
Bisogni, G.	University of Pisa, Italy
Boni, G.	University of Pisa Medical School, Italy
Borsò, E.	University of Pisa, Italy
Brouwer, O.R.	Netherlands Cancer Institute, Netherlands
Cremonesi, M.	European Institute of Oncology, Italy
Del Guerra, A.	University of Pisa, Italy
Dondi, M.	International Atomic Energy Agency
Duatti, A.	International Atomic Energy Agency
Dubreuil, J.	CHU Lyon, France
El-Haj, N.	International Atomic Energy Agency
Erba, P.A.	University of Pisa, Italy
Ferrari, M.E.	European Institute of Oncology, Italy
Giammarile, F.	CHU Lyon, France
Graafland, N.M.	Netherlands Cancer Institute, Netherlands
Grosso, M.	University of Pisa, Italy
Horenblas, S.	Netherlands Cancer Institute, Netherlands
Klop, W.M.C.	Netherlands Cancer Institute, Netherlands
Lorenzoni, A.	University of Pisa Medical School, Italy
Manca, G.	University of Pisa Medical School, Italy
Mariani, G.	University of Pisa Medical School, Italy
Mazzarri, S.	University of Pisa Medical School, Italy

Meinhardt, W.	Netherlands Cancer Institute, Netherlands
Nieweg, O.E.	Netherlands Cancer Institute, Netherlands
Orsini, F.	University of Pisa Medical School, Italy
Paez, D.	International Atomic Energy Agency
Paredes, P.	Hospital Clinic of Barcelona, Spain
Pedroli, G.	European Institute of Oncology, Italy
Roca, I.	Hospital General Vall d'Hebron, Spain
Sabadell, D.	Hospital del Mar, Spain
Sandrucci, S.	University of Turin Medical School, Italy
Stokkel, M.	Netherlands Cancer Institute, Netherlands
Valdés Olmos, R.A.	Netherlands Cancer Institute, Netherlands
Vermeeren, L.	Netherlands Cancer Institute, Netherlands
Vidal-Sicart, S.	Hospital Clinic of Barcelona, Spain
Zaknun, J.J.	International Atomic Energy Agency

IAEA
International Atomic Energy Agency

No. 23

ORDERING LOCALLY

In the following countries, IAEA priced publications may be purchased from the sources listed below or from major local booksellers.

Orders for unpriced publications should be made directly to the IAEA. The contact details are given at the end of this list.

AUSTRALIA
DA Information Services
648 Whitehorse Road, Mitcham, VIC 3132, AUSTRALIA
Telephone: +61 3 9210 7777 • Fax: +61 3 9210 7788
Email: books@dadirect.com.au • Web site: http://www.dadirect.com.au

BELGIUM
Jean de Lannoy
Avenue du Roi 202, 1190 Brussels, BELGIUM
Telephone: +32 2 5384 308 • Fax: +32 2 5380 841
Email: jean.de.lannoy@euronet.be • Web site: http://www.jean-de-lannoy.be

CANADA
Renouf Publishing Co. Ltd.
5369 Canotek Road, Ottawa, ON K1J 9J3, CANADA
Telephone: +1 613 745 2665 • Fax: +1 643 745 7660
Email: order@renoufbooks.com • Web site: http://www.renoufbooks.com

Bernan Associates
4501 Forbes Blvd., Suite 200, Lanham, MD 20706-4391, USA
Telephone: +1 800 865 3457 • Fax: +1 800 865 3450
Email: orders@bernan.com • Web site: http://www.bernan.com

CZECH REPUBLIC
Suweco CZ, spol. S.r.o.
Klecakova 347, 180 21 Prague 9, CZECH REPUBLIC
Telephone: +420 242 459 202 • Fax: +420 242 459 203
Email: nakup@suweco.cz • Web site: http://www.suweco.cz

FINLAND
Akateeminen Kirjakauppa
PO Box 128 (Keskuskatu 1), 00101 Helsinki, FINLAND
Telephone: +358 9 121 41 • Fax: +358 9 121 4450
Email: akatilaus@akateeminen.com • Web site: http://www.akateeminen.com

FRANCE
Form-Edit
5 rue Janssen, PO Box 25, 75921 Paris CEDEX, FRANCE
Telephone: +33 1 42 01 49 49 • Fax: +33 1 42 01 90 90
Email: fabien.boucard@formedit.fr • Web site: http://www.formedit.fr

Lavoisier SAS
14 rue de Provigny, 94236 Cachan CEDEX, FRANCE
Telephone: +33 1 47 40 67 00 • Fax: +33 1 47 40 67 02
Email: livres@lavoisier.fr • Web site: http://www.lavoisier.fr

L'Appel du livre
99 rue de Charonne, 75011 Paris, FRANCE
Telephone: +33 1 43 07 50 80 • Fax: +33 1 43 07 50 80
Email: livres@appeldulivre.fr • Web site: http://www.appeldulivre.fr

GERMANY
Goethe Buchhandlung Teubig GmbH
Schweitzer Fachinformationen
Willstätterstrasse 15, 40549 Düsseldorf, GERMANY
Telephone: +49 (0) 211 49 8740 • Fax: +49 (0) 211 49 87428
Email: s.dehaan@schweitzer-online.de • Web site: http://www.goethebuch.de

HUNGARY
Librotrade Ltd., Book Import
PF 126, 1656 Budapest, HUNGARY
Telephone: +36 1 257 7777 • Fax: +36 1 257 7472
Email: books@librotrade.hu • Web site: http://www.librotrade.hu

INDIA

Allied Publishers

1st Floor, Dubash House, 15, J.N. Heredi Marg, Ballard Estate, Mumbai 400001, INDIA
Telephone: +91 22 2261 7926/27 • Fax: +91 22 2261 7928
Email: alliedpl@vsnl.com • Web site: http://www.alliedpublishers.com

Bookwell

3/79 Nirankari, Delhi 110009, INDIA
Telephone: +91 11 2760 1283/4536
Email: bkwell@nde.vsnl.net.in • Web site: http://www.bookwellindia.com

ITALY

Libreria Scientifica "AEIOU"

Via Vincenzo Maria Coronelli 6, 20146 Milan, ITALY
Telephone: +39 02 48 95 45 52 • Fax: +39 02 48 95 45 48
Email: info@libreriaaeiou.eu • Web site: http://www.libreriaaeiou.eu

JAPAN

Maruzen Co., Ltd.

1-9-18 Kaigan, Minato-ku, Tokyo 105-0022, JAPAN
Telephone: +81 3 6367 6047 • Fax: +81 3 6367 6160
Email: journal@maruzen.co.jp • Web site: http://maruzen.co.jp

NETHERLANDS

Martinus Nijhoff International

Koraalrood 50, Postbus 1853, 2700 CZ Zoetermeer, NETHERLANDS
Telephone: +31 793 684 400 • Fax: +31 793 615 698
Email: info@nijhoff.nl • Web site: http://www.nijhoff.nl

SLOVENIA

Cankarjeva Zalozba dd

Kopitarjeva 2, 1515 Ljubljana, SLOVENIA
Telephone: +386 1 432 31 44 • Fax: +386 1 230 14 35
Email: import.books@cankarjeva-z.si • Web site: http://www.mladinska.com/cankarjeva_zalozba

SPAIN

Diaz de Santos, S.A.

Librerias Bookshop • Departamento de pedidos
Calle Albasanz 2, esquina Hermanos Garcia Noblejas 21, 28037 Madrid, SPAIN
Telephone: +34 917 43 48 90 • Fax: +34 917 43 4023
Email: compras@diazdesantos.es • Web site: http://www.diazdesantos.es

UNITED KINGDOM

The Stationery Office Ltd. (TSO)

PO Box 29, Norwich, Norfolk, NR3 1PD, UNITED KINGDOM
Telephone: +44 870 600 5552
Email (orders): books.orders@tso.co.uk • (enquiries): book.enquiries@tso.co.uk • Web site: http://www.tso.co.uk

UNITED STATES OF AMERICA

Bernan Associates

4501 Forbes Blvd., Suite 200, Lanham, MD 20706-4391, USA
Telephone: +1 800 865 3457 • Fax: +1 800 865 3450
Email: orders@bernan.com • Web site: http://www.bernan.com

Renouf Publishing Co. Ltd.

812 Proctor Avenue, Ogdensburg, NY 13669, USA
Telephone: +1 888 551 7470 • Fax: +1 888 551 7471
Email: orders@renoufbooks.com • Web site: http://www.renoufbooks.com

United Nations

300 East 42nd Street, IN-919J, New York, NY 1001, USA
Telephone: +1 212 963 8302 • Fax: 1 212 963 3489
Email: publications@un.org • Web site: http://www.unp.un.org

Orders for both priced and unpriced publications may be addressed directly to:

IAEA Publishing Section, Marketing and Sales Unit, International Atomic Energy Agency
Vienna International Centre, PO Box 100, 1400 Vienna, Austria
Telephone: +43 1 2600 22529 or 22488 • Fax: +43 1 2600 29302
Email: sales.publications@iaea.org • Web site: http://www.iaea.org/books

14-30981

The objective of this publication is to provide an updated source for professionals using guided intra- or perioperative scintigraphic tumour targeting (GOSTT). It supports and facilitates both the clinical decision making process and the implementation of minimally invasive surgical procedures; the ultimate aim of both approaches is to improve the standard of health care received by patients with cancer. This publication provides an update on innovations in the use of radiopharmaceuticals for SLNM and SLNB, in combination with vital dyes, when appropriate, to facilitate the detection of sentinel lymph nodes. In addition, it provides an update on advances in the implementation of hybrid imaging technologies for the surgical management of patients with cancer in conjunction with intraoperative regional lymph node mapping. Experience with small-field scintigraphic imaging devices in the operating theatre is also presented.

IAEA HUMAN HEALTH SERIES

INTERNATIONAL ATOMIC ENERGY AGENCY
VIENNA
ISBN 978–92–0–102214–1
ISSN 2075–3772